Yeast-expression and molecular properties of human mitochondrial Uncoupling Protein 2

Margeoux Angelique Siscar Dela Rosa

Thesis submitted for the degree of Doctor of Philosophy

Norwich Medical School
Biomedical Research Centre
University of East Anglia, Norwich, UK

Date of submission: 31st December 2023

Declaration of Authorship

I declare that the contents of my thesis entitled "Yeast-expression and molecular properties of human mitochondrial Uncoupling Protein 2" are my original work, unless otherwise acknowledged, and have not been submitted for another degree in this or any other university. No parts of this research have been published prior to submission.

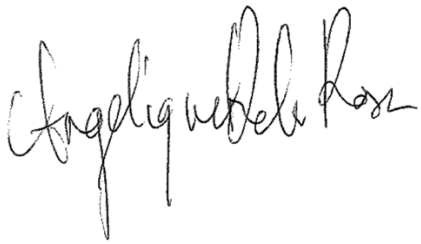

Margeoux Angelique Siscar Dela Rosa

Abstract

Uncoupling protein 2 (UCP2) is a mitochondrial carrier protein implicated in various pathophysiological conditions, such as diabetes and cancers. Its involvement in numerous dysregulated metabolic pathways make it an attractive target for therapeutic intervention. However, the exact function of the protein remains unclear. UCP2 has been proposed to function as an uncoupling protein to 'mildly uncouple' mitochondria mitigating the production of reactive oxygen species by mitochondria, or to transport 4-carbon metabolites across the mitochondrial inner membrane, which provides metabolic flexibility to the cell under conditions of nutrient stress. Mitochondrial carriers are inherently unstable, which makes them a particularly challenging class of membrane proteins to study. UCP2 is expressed in a variety of tissues, though at low abundance, where extraction from native sources is impractical. The heterologous expression of UCP2 in recombinant systems, such as bacteria, can produce misfolded protein, leading to incorrect conclusions on the protein's properties. To date, the biochemical function of UCP2 remains widely contested.

This work describes optimisation of human UCP2 protein expression in a protease-deficient *S. cerevisiae* strain, to yield folded protein suitable for extraction, purification and functional characterisation. It was observed that substitution of leucine at position 2 produced ~4-fold more UCP2 protein compared to WT protein. Quantification of UCP2 expression in yeast mitochondria indicates that this system produces ~20-fold more protein than native sources, with ~75% of protein produced extractable with non-ionic detergents, indicative of folded material. Purification attempts using a combination of ion exchange and covalent chromatography were able to enrich UCP2 in an intact form, but not purify the protein to homogeneity.

To probe the ligand binding properties of UCP2 without the need to purify, a novel thermostability assay, termed the "gel blot protein thermostability" assay, was developed using a polyethylene glycol-conjugated, maleimide-based thiol-reactive probe. The assay was able to successfully detect the pH-dependent binding of inhibitory nucleotides to human UCP1 in solubilised yeast mitochondrial membranes, through significant stabilising shift in relative protein thermostability.

Equivalent tests with UCP2 revealed that the protein is less stable than UCP1, where purine nucleotides do not induce any changes in stability, consistent with lack of any binding. These findings suggest that UCP2 is not regulated by these ligands and has different functional properties to UCP1, implying a distinct biochemical role.

Table of Contents

List of figures

List of tables

List of abbreviations

12MNG:	lauryl maltose neopentyl glycol
4HNE:	4-hydroxy-2-noneal
AAC:	ADP/ATP carrier
AAPH:	2,2'-azobis(2-methylpropionamidine) dihydrochloride
ADP:	adenosine diphosphate
AGC:	aspartate-glutamate carrier
AMPK:	adenosine monophosphate-activated protein kinase
AOM:	azoxymethane
ATP:	adenosine triphosphate
BAT:	brown adipose tissue
BCA:	bicinchoninic acid
BKA:	bongkrekic acid
BMI:	body mass index
BRET:	bioluminescence resonance energy transfer
BSA:	bovine serum albumin
β_3AR:	β3-adrenergic receptors
c-state:	cytoplasmic-open state
C4:	4-carbon
CAC:	colitis associated cancer
cAMP:	cyclic adenosine monophosphate
CATR:	carboxyatractyloside
CCCP:	carbonyl cyanide 3-chlorophenylhydrazone
CCL4:	chemokine CC motif ligand 4
CCL5:	chemokine CC motif ligand 5
$CD8^+$:	cluster of differentiation 8 positive
cDC1:	conventional type 1 dendritic cells
CPM:	7-Diethylamino-2-(4'-maleimidylphenyl)-4-methylcoumarin
CRC:	colorectal cancer
CXCL10:	C-X-C motif chemokine 10
CXCL9:	C-X-C motif chemokine 9
DC:	dendritic cell
DDM:	n-dodecyl-β-D-maltoside

DNP:	2,4-dinitrophenol
DOPC:	1,2-dioleoyl-sn-glycero-3-phosphocholine
Dox:	doxycycline
DPC:	dodecylphosphorylcholine
DSF:	differential scanning fluorimetry
DSS:	dextran sodium sulphate
ΔTm:	change in apparent protein melting temperature
DTT:	dithiothreitol
FCCP:	carbonyl cyanide-p-trifluoromethoxyphenylhydrazone
FRET:	fluorescence resonance energy transfer
GDP:	guanosine diphosphate
GLUT2:	glucose transporter 2
GPCR:	G-protein coupled receptor
GSIS:	glucose-stimulated insulin secretion
GTP:	guanosine triphosphate
HEK-293:	human embryonic kidney
HIF-1α:	hypoxia-inducible factor 1 alpha
IFNγ:	interferon gamma
IL-12:	interleukin 12
IL-1β:	interleukin 1 beta
IL-6:	interleukin 6
IM:	inner membrane
IMS:	intermembrane space
INS-1E:	insulinoma 1E cells
IPTG:	isopropyl-2-D-galactopyranoside
IRF5:	interferon regulatory factor 5
JNK:	Jun N-terminal kinase
K_{ATP}:	ATP-sensitive potassium channel
KO:	knockout
KRAS:	Kirsten rat sarcoma virus
LB:	lysogeny broth
LPS:	lipopolysaccharides
m-state:	matrix-open state

MAPK:	mitogen-activated protein kinase
NADH:	reduced nicotinamidine adenine dinucleotide
NADPH:	reduced nicotinamidine adenine dinucleotide phosphate
NK:	natural killer cell
Nluc:	Nanoluciferase
NMR:	nuclear magnetic resonance
NST:	non-shivering thermogenesis
PDAC:	pancreatic ductal adenocarcinoma
PEG:	polyethylene glycol
PEG-Mal-2K:	Poly(ethylene glycol) methyl ether maleimide conjugated to a 2 kDa adduct
PEG-Mal-5K:	Poly(ethylene glycol) methyl ether maleimide conjugated to a 5 kDa adduct
PET-CT:	positron emission tomography-computed tomography
PPAR:	peroxisome proliferator-activated receptor
PVDF:	polyvinylidene fluoride
Q-FT:	Q-flow through
RCR:	respiratory control ratio
ROS:	reactive oxygen species
S-FT:	S-flow through
SC-ura:	synthetic complete media devoid of uracil
SCM:	sulfo-cyanine3 maleimide
SDM:	site-directed mutagenesis
SDS:	sodium dodecyl sulphate
SEC:	size exclusion chromatography
SL+G:	selective lactate and glucose media
SMA:	styrene malic acid
SPQ:	6-methoxy-N-(3-sulfopropyl)quinolinium
T-ALL:	T acute lymphoblastic leukaemia
TCA:	tricarboxylic acid
TILs:	tumour infiltrating lymphocytes
T_m:	protein melting temperature
TME:	tumour microenvironment

TNF-α :	tumour necrosis factor alpha
TOCL:	tetraoleoyl cardiolipin
TPA:	thiopropyl agarose
TPS:	thiopropyl sepharose 6B
TX-100:	Triton X-100
UCP1:	uncoupling protein 1
UCP2:	uncoupling protein 2
UPS:	ubiquitin-proteasome system
WT:	wild-type
YP:	yeast peptone media
YPD:	yeast peptone media supplemented with 2% (w/v) glucose
YPL	yeast peptone media supplemented with 2% (v/v) lactate
YPR	yeast peptone media supplemented with 2% (w/v) raffinose

1. Introduction

1.1. Mitochondrial carriers and uncoupling proteins

Mitochondrial carriers are part of a large family of integral membrane proteins predominantly found in the inner membrane of mitochondria. Their collective role is to transport various substances, such as metabolites, ions or amino acids across the inner mitochondrial membrane. Translocation of these diverse molecules utilises a strict exchange mechanism (1). Amongst this family is the sub-family of proteins known as uncoupling proteins. The archetypal uncoupling protein 1 (UCP1), is responsible for catalysing proton leak across the inner mitochondrial membrane (2). UCP1 uncouples mitochondrial substrate oxidation from ATP synthesis as the protein provides an alternative pathway for protons to return to the mitochondrial matrix, enabling it to bypass ATP synthase. It is expressed in brown adipose tissue (3), where it facilitates the physiological process of non-shivering thermogenesis (NST) for thermoregulation in mammals (2).

The discovery of novel uncoupling proteins (UCP2-5) (4-8) has led many research groups to investigate if these related proteins are also capable of catalysing proton leak resulting in a thermogenic function (2, 9, 10) or if they are responsible for other biochemical roles (11, 12). UCP proteins are reported to play important roles in pathophysiological disorders, such as diabetes, cancer, obesity and neurodegenerative diseases (for reviews see: (13-16)).

1.2. Uncoupling Protein 1

UCP1 is a ~32 kDa monomeric protein (17-19) that is specifically expressed in the mitochondria of brown adipose tissue (BAT) (3, 20). The protein functions to transport protons from the mitochondrial intermembrane space (IMS) into the matrix, bypassing ATP synthase (2, 21). As a consequence, nutrient oxidation is uncoupled from ATP synthesis to release energy as heat instead of producing ATP. Heat produced in this manner facilitates the process of NST by BAT helping small eutherian (placental) mammals maintain body temperature (22-24). In humans, BAT depots were originally observed to decline after infancy (25) and were not thought to play a significant role in adults. Though, in the last 15 years, BAT depots have been

identified in human adults via the use of positron-emission tomographic and computed tomographic (PET-CT) scans (26), and found to correlate inversely with body mass index (BMI) and age, thereby highlighting a potential role of BAT in combatting obesity (26). The physiological role of UCP1 in BAT is very well characterised. A defining feature of UCP1-mediated uncoupling is activation by free fatty acids (27-30), which is inhibited by purine nucleotides (31-35). Following acute exposure to the cold, the brain triggers neuronal signals that activate β3 (β_3)-adrenergic receptors (β_3AR), a type of G-protein coupled receptors (GPCRs), in brown adipocytes. Upon β_3AR activation, the Gα subunit dissociates from the GPCR and activates adenylate cyclase, consequently increasing intracellular cAMP levels. Increased levels of cAMP activates protein kinase A, which in turn phosphorylates various enzymes including lipases and perilipin. Phosphorylation of hormone-sensitive lipase enables fatty acids to be released from triglyceride stores, whilst phosphorylation inhibits perilipin activity thereby enabling stored lipids to undergo lipolysis. Free fatty acids released into the cytosol directly activate UCP1, overcoming inhibition of the protein by purine nucleotides that bind at the cytosolic side, to switch on NST. Movement of protons through activated UCP1, rather than ATP synthase, dissipates the electrochemical proton gradient generated by the respiratory chain, releasing heat as a result, rather than generating ATP (2, 36, 37) (see **Figure 1.1**).

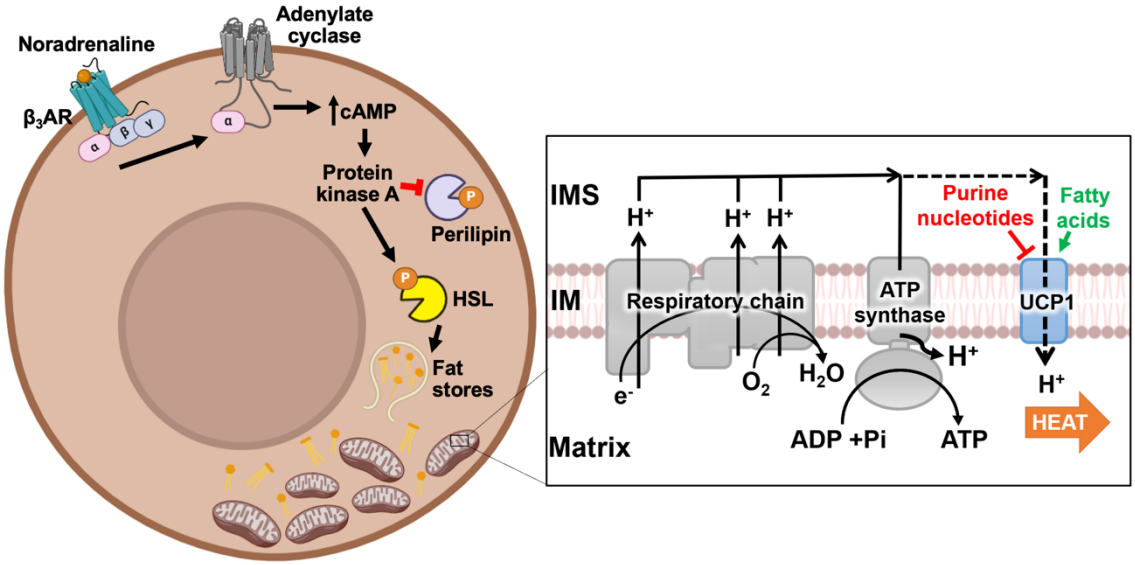

Figure 1.1: Schematic showing UCP1 activation in brown adipose tissue. *Following cold exposure, the brain sends signals via the sympathetic nervous system to trigger the release of noradrenaline from sympathetic neurones in innervated BAT. Noradrenaline binds to β_3AR located on the plasma membrane of brown adipocytes, leading to an intracellular signalling cascade. Following activation of β_3AR, the Gα subunit dissociates from activated receptors and acts on adenylate cyclase. Adenylate cyclase catalyses the conversion of ATP to cAMP, subsequently elevating intracellular cAMP levels. Increased cAMP acts on protein kinase A, which in turn phosphorylate perilipin, consequently preventing the action of lipid sequestration. Protein kinase A also phosphorylates hormone-sensitive lipase (HSL), which enables the liberation of free fatty acids from triglyceride stores. The release of free fatty acids into the cytosol enables their transport into the mitochondria, where they activate UCP1 to uncouple the mitochondrial membrane potential from oxidative phosphorylation (zoomed in panel). Heat is generated as a result of this proton leak, and it is responsible for NST in newborn humans (2, 36, 37).*

1.3. Uncoupling Protein 2

In 1997, Fleury and colleagues identified a novel gene positioned in a chromosomal region linked to obesity and hyperinsulinemia (4). The gene encoded for a mitochondrial carrier that had a 59% sequence homology to UCP1, hence, the resulting gene product was named uncoupling protein 2 (UCP2). UCP2 is a 33 kDa protein made up of 309 amino acid residues. The protein is localised to the

mitochondrial inner membrane and has conserved mitochondrial carrier family motifs (see section **1.5. Conserved structural features of mitochondrial carriers** for more details). Unlike UCP1, which is exclusively expressed in BAT (3), UCP2 is expressed in many different tissue and cell types, including lung, stomach, thymus, pancreatic β-cells, and bone marrow, with the highest expression levels observed in spleen mitochondria (38-40). UCP2 expression is also observed in various immune cells, including B cells, T cells, neutrophils and macrophages (41). Although UCP2 is expressed in many different cell types, its expression levels are at least two orders of magnitude lower than UCP1 expression in BAT mitochondria (38, 42). Unlike UCP1, which has a half-life of approximately 30 hours (43), UCP2 has a very short half-life of approximately one hour (40, 44, 45). This unusually short lifespan may be attributed to the protein degradation pathway that turns over UCP2 undergoes, which differs from UCP1 (46).

1.3.1. Proton Conductance

Since the discovery of UCP2, subsequent studies using isolated yeast (47, 48) and mammalian mitochondria (49-53), led to the initial conclusion that UCP2 can uncouple oxidative phosphorylation in the same way as UCP1. However, these results have been widely contested. For example, overexpression of UCPs in recombinant systems can lead to loss of mitochondrial membrane integrity as well as protein misfolding, which in turn can lead to improper insertion into the membrane. Hence protein overexpression can produce artefacts that appear to uncouple mitochondria (54-56).

Liposome proton flux assays have been used to assess proton transport activity of UCP2 (57-61), though the results have been conflicting. Some findings reported that UCP2, like UCP1, is capable of fatty-acid dependent H^+ transport, though protonophoric activity is only completely inhibited with millimolar concentrations of purine nucleotides (57, 61). Other studies also report that UCP2 proton leak activity can be mediated by polyunsaturated fatty acids, though activity could be inhibited by micromolar concentrations of purine nucleotide (60). However, others argue that a histidine pair (H145 and H147) present in hamster UCP1, but not in UCP2 and UCP3, is responsible for proton leak activity, with mutagenesis studies demonstrating a significant decrease in proton flux *in vitro* (62). However, respiratory

assays using isolated mitochondria (63) and HEK293 cells (64), demonstrate that this histidine pair motif is not important for proton conductance activity in UCP1. Consequently, studies using proteoliposomes were not able to clarify if UCP2 could transport protons like UCP1.

UCP proton conductance was claimed to require additional co-factors to restore proton transport activity in proteoliposome (65, 66) and isolated mitochondria systems (49, 50, 52, 53, 66-69). The first reported obligatory co-factor required for recombinant UCP1 activity was ubiquinone (coenzyme Q) (66). Echtay and colleagues claim that recombinant UCP1, UCP2 and UCP3 are able to mediate H^+ transport, but only in the presence of ubiquinone (65, 66), where free fatty acids are still required to activate UCP1 proton conductance (28). However, others have shown that ubiquinone does not affect UCP2 proton transport activity (58, 59, 70). Importantly, recombinant expression of UCP1 using mutant yeast strains that lack the ability to produce ubiquinone, demonstrate that the molecule is not an obligatory co-factor of UCP1 (71).

1.3.2. Regulator of ROS signalling

The mitochondrial respiratory chain is a significant producer of reactive oxygen species (ROS). UCP2 has been postulated to play a role in regulating mitochondrial ROS through the mechanism of mild uncoupling. The 'mild uncoupling hypothesis', proposed by Skulachev in 1996, proposes that uncoupling of mitochondria serves to maintain low levels of ROS, in order to mitigate detrimental effects of oxygen-derived radical molecules produced during high levels of oxidative phosphorylation (72).

The observation that UCP2 expression can be induced by oxidative stress (38), led to the proposition that superoxide-mediated proton leak by UCP2 directly controls reactive oxygen species generated by the respiratory chain. The antioxidant effect of mildly uncoupling mitochondria would relieve oxidative stress, but at the expense of ATP synthesis (73). To investigate this possibility, proton leak was measured in mitochondria isolated from pancreatic β-cells, kidney, and spleen tissue and was found to increase in the presence of an exogenous superoxide-producing system (xanthine and xanthine oxidase, which together generate superoxide radicals), and was attributed to UCP activity (52, 53). It was also later hypothesised that products of lipid peroxidation, brought on by oxidative damage, could also

activate UCPs. Such products include reactive alkenals and aldehydes (50, 74). As UCP1 was reported to be activated by retinoids (48, 75), it could be inferred that structurally related compounds resulting from lipid peroxidation could potentially induce UCP proton leak activity. In 2003, Echtay and colleagues proposed that superoxide and carbon-centered radical species, such as 2,2'-azobis(2-methylpropionamidine) dihydrochloride (AAPH) (69), induce phospholipid peroxidation, culminating in the production of reactive alkenals such as 4-hydroxy-2-nonenal (4HNE) (50), which activate UCPs. 4HNE is a highly cytotoxic aldehyde (76), that has been reported to cause cellular dysfunction through dysregulation of various process (77). Under conditions of oxidative stress, it has been reported that HNE concentrations can range from 10 μM to 5 mM; the upper limit of which is in excess of what would cause broad spectrum cytotoxic effects (77, 78). To study the effects of 4HNE in a physiologically relevant manner, proton leak experiments conducted on isolated mitochondria utilised 35 μM 4HNE (50), which is within the lower end of reported 4HNE range. 4HNE was reported to induce GDP-sensitive proton conductance in BAT, kidney and skeletal muscle mitochondria, indicating that 4HNE mediates mitochondrial uncoupling through UCPs (50). It must be highlighted that superoxide- (52, 68) and 4HNE-mediated (50, 79) uncoupling was only observed in the presence of fatty acids. For UCP1, 4HNE was later found not to be required for activation at all (80), which supports the idea that 4HNE is not required for uncoupling activity. While the data presented by Echtay and colleagues demonstrate that in the presence of exogenous superoxide and 4HNE, UCP2 can confer proton leak activity, many other groups have not been able to replicate these findings. Using the same experimental set-up in spleen mitochondria, Couplan and colleagues found that superoxide does not induce UCP2 uncoupling (81). Different groups have observed conflicting results with regards to UCP activation by reactive alkenals and particularly 4HNE (71, 81, 82), with Parker and colleagues suggesting that discrepancies in results could be attributed to differing experimental set-ups (83). Other investigations into HNE-induced uncoupling in skeletal muscle mitochondria suggested that a high membrane potential is required for UCP3-mediated uncoupling activity, which may not necessarily be physiologically relevant (83).

The conflicting data regarding UCP superoxide activation led to many questions regarding the physiological relevance of superoxide-induced uncoupling. Given that

UCP2 is expressed in cells involved in immune defence and that protein expression can be induced under conditions of oxidative stress (38, 41), the protein has been reasoned to play a role in regulating ROS. In innate immunity, neutrophils and macrophages employ the use of nitric oxide, superoxide and other reactive oxygen species in order to combat bacterial pathogens through the process of phagocytosis. These potent antimicrobials are contained within the phagolysosome. Release of these highly reactive molecules can be detrimental to the cell (84). UCP2 expression in both neutrophils and macrophages may be a mechanism to mitigate intracellular damage caused by uncontained phagolysosomes (85). There have been numerous experiments that support the idea that UCP2 may negatively modulate ROS levels, especially in the context of immunity. For example, when challenged with the brain parasite, *T. gondii*, macrophages isolated from UCP2 knockout (KO) mice eliminated more of the parasite compared to their wild-type (WT) counterparts (86). UCP2-deficient macrophages challenged with *S. typhimurium* also demonstrated high bactericidal activity compared to WT macrophages (86). In other studies, *L. donovani* was shown to upregulate UCP2 expression, thereby blunting macrophage-mediated immunity through attenuation of ROS production (87). The silencing of UCP2 in *L. donovani* infected macrophages correlated with an increase in ROS production and parasite clearance, through enhanced release of pro-inflammatory cytokines such as TNF-α and IL-12 (87). These findings highlight how UCP2 expression can diminish the innate immune response by attenuating ROS levels. Fine control of ROS production has been proposed to relate to the unusually short half-life of UCP2 *in vivo*, as the protein would need to be rapidly synthesised and degraded (44). Studies using spleen tissue from UCP2 KO mice exhibited higher levels of ROS and pro-inflammatory cytokines, such as IFNγ, IL-6 and IL-1β, following four days post infection with *L. monocytogenes* (41). The findings suggest that UCP2 may serve as a control mechanism to prevent overwhelming the immune response, not only through the modulation of ROS, but through subsequent signalling cascades which likely utilise ROS as signalling molecules for modulation of cytokine production (41, 88). One way the immune system may 'fine tune' UCP2 activity, is through modulation of the p38 and JNK signalling pathways. Following exposure to LPS, macrophages induced downregulation of UCP2 expression, which culminated in elevated ROS production, subsequently resulting in resistance to nitric oxide-induced apoptosis

(89). As well as potentially playing a role in ROS regulation in macrophages, UCP2 expression appears to regulate ROS levels in other cell types, including pancreatic β-cells (90-92) which will be discussed in the context of health and disease (see section **1.4.1. Potential role of UCP2 in diabetes**).

1.3.3. Alternative function of UCP2: metabolite transporter

In 2014, Vozza and colleagues proposed that UCP2 functions as a metabolite transporter, transporting 4-carbon TCA cycle metabolites out of the mitochondria (93). Using human hepatocarcinoma cells, which express high levels of UCP2 (94), it was demonstrated that UCP2 plays a regulatory role in glucose and glutamine oxidation, with UCP2-silenced cells showing a significant increase in mitochondrial membrane potential when grown in glucose, though a decrease in mitochondrial membrane potential is observed when cells were grown in glutamine (93), which is noteworthy given that glutamine acts as a translational up-regulator for UCP2 protein expression (95). Furthermore, UCP2-silenced mitochondria displayed significantly higher levels of Krebs cycle intermediates, when compared to WT mitochondria. Liposome uptake assays revealed that UCP2 specifically transported negatively charged molecules, such as malate, oxaloacetate, aspartate, malonate and sulphate in exchange for inorganic phosphate (93). Malate, malonate and phosphate are also known transport substrates of the dicarboxylate carrier (96-99). These results suggest that UCP2 is a mitochondrial carrier that is capable of transporting metabolites out of the mitochondria, thereby mediating glucose and glutamine oxidation by regulating the pool of Krebs cycle intermediates in the mitochondrial matrix (93).

1.4. UCP2 in health and disease

Since UCP2 is expressed in many diverse cell types, it is unsurprising that the protein has been implicated in many cellular pathways, especially those pertaining to ROS, ATP production and metabolic reprogramming (100-103). This section focuses on various areas in which there has been strong evidence to support UCP2 function in various (patho)physiologies and whether this protein could be a therapeutic target for the alleviation of various diseases.

1.4.1. Potential role of UCP2 in diabetes

The process of glucose-stimulated insulin secretion (GSIS) relies on the ATP/ADP ratio in pancreatic β-cells (104) (**Figure 1.2**). Maintenance of this ratio is dependent on the coupling efficiency of mitochondria (92). Given its expression in pancreatic β-cells (92, 105), coupled with the observation that the UCP2 gene being located within a chromosomal region associated with hyperinsulinemia and obesity (4), it is unsurprising that UCP2 has been implicated in playing a regulatory role in glucose and lipid metabolism (103). On this basis, various studies have investigated the role of UCP2 in diabetes.

Experiments comparing pancreatic islets from WT and UCP2-deficient mice revealed that UCP2-deficient islets exhibited higher intracellular ATP levels, consistent with improved mitochondrial coupling. In high glucose concentrations, UCP2-deficient islets secreted two- to three-fold more insulin, suggesting that UCP2 may suppress GSIS by mediating proton leak, thus reducing the ATP/ADP ratio (105), which is important for the GSIS signalling cascade (**Figure 1.2**). Moreover, it was observed that UCP2 expression in INS-1E insulinoma cells, a pancreatic β-cell model, dampens GSIS by mediating proton leak activity (92). In line with claims that UCP uncoupling activity was mediated by various co-factors, it was proposed that UCP2 uncoupling activity in pancreatic cells was superoxide-activated (106).

Under chronic hyperglycaemic conditions, WT pancreatic islets became desensitised to GSIS, whereas UCP2 KO islets maintained the same level of insulin secretion as normal glycaemic conditions. GSIS impairment could be rescued and enhanced in WT and UCP2 KO, respectively, following addition of manganese superoxide dismutase (106). Comparison of pancreatic islets obtained from WT and *ob/ob* mice, a model strain for diabetes and obesity (107), demonstrated higher levels of superoxide in *ob/ob* islets compared to islets from WT mice. Furthermore, islets harvested from UCP2-deficient *ob/ob* mice exhibited far higher levels of superoxide, almost three-fold more than that observed in WT *ob/ob* mice. From these findings, Krauss and colleagues suggest that UCP2 upregulation in *ob/ob* mice is vital for superoxide regulation (90, 91, 105), supporting the idea that UCP2-mediated uncoupling is regulated by superoxide activation in the context of pancreatic β-cells.

However, lack of reproducibility of superoxide-mediated effects (81) and the absence of fatty-acid activated UCP2 uncoupling activity in pancreatic β-cells (108), still calls into question the exact mechanism by which UCP2 dampens the GSIS response. Since pancreatic β-cell mitochondria can undergo high stress following postprandial stimulation (103), it is plausible that UCP2 acts to alleviate potential oxidative damage at the expense of ATP synthesis. The data presented suggests that UCP2 dampens first-phase insulin secretion in pancreatic β-cells (90, 105). Attenuation of GSIS highlights how UCP2 activity can potentially play a role in type II diabetes and obesity (109), though in low glucose concentrations, UCP2 may potentially function as a 4-carbon metabolite transporter that maintains cellular ATP/ADP ratio by providing metabolic flexibility to the cell through glutamine oxidation (93).

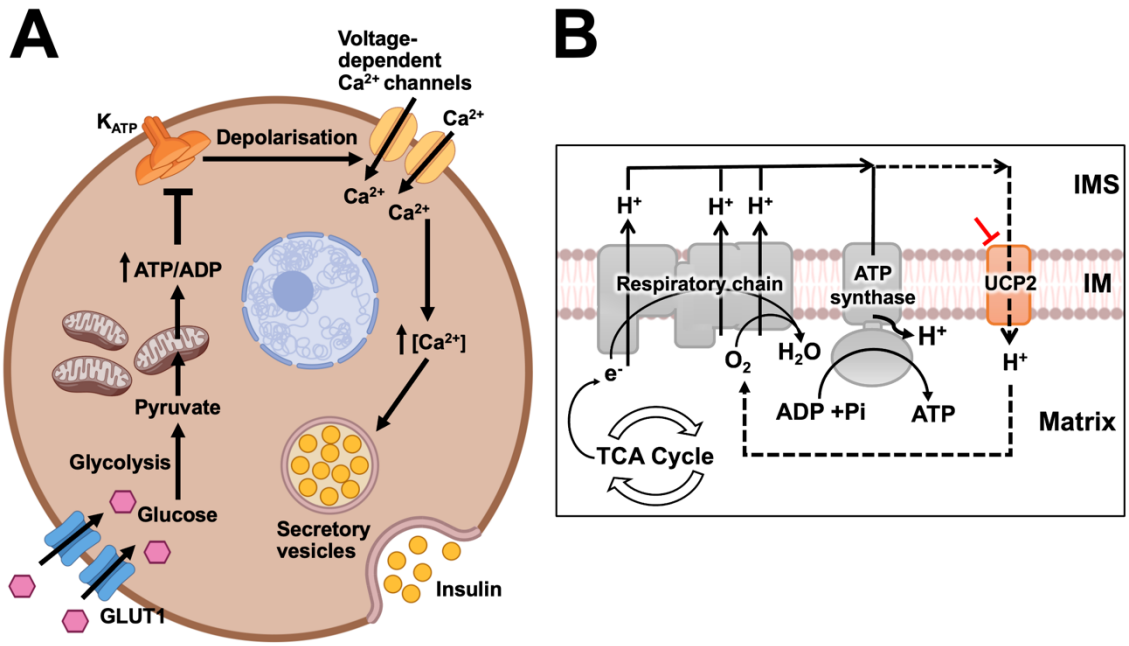

Figure 1.2: Schematic of glucose-stimulated insulin secretion (GSIS) in pancreatic β-cells. *(A) Following a meal, glucose is absorbed into pancreatic β-cells by GLUT transporters (GLUT1 in humans and GLUT2 in mouse (110)), where it enters glycolysis and is broken down to pyruvate. Pyruvate is transported into the mitochondria, where it is converted into acetyl-CoA, which then enters the TCA cycle, fuelling oxidative phosphorylation and generating ATP. Increased intracellular ATP binds to ATP-sensitive potassium channels, K_{ATP}, and inhibits the channel. Blocking of this ion channel results in membrane depolarisation. Consequently, depolarisation activates voltage-dependent calcium channels*

resulting in calcium influx into the cell. The subsequent increase in intracellular calcium enables insulin-containing secretory vesicles to fuse to the plasma membrane surface and release insulin into the bloodstream (104). B) Schematic of UCP2-mediated uncoupling and its proposed role in GSIS. Following a meal, elevated blood glucose levels cause an increase in the rate of respiration and ROS production in pancreatic β-cells. UCP2 is believed to mediate proton leak activity in pancreatic islets, consequently providing an alternative pathway for protons to travel back to the mitochondrial matrix at the expense of ATP synthesis (92). The increased proton leak across the mitochondrial inner membrane, should result in a decrease in proton motive force, leading to a reduction in ROS produced by the respiratory chain (90). This 'mild uncoupling' activity reduces the efficiency of the GSIS response as oxidative phosphorylation is not fully coupled and GSIS is reliant on alterations in ATP/ADP ratios for insulin release. In conditions where UCP2 is genetically knocked out or in pharmacologically inhibited conditions, GSIS is enhanced as protons can only cycle back into the mitochondrial matrix through ATP synthase (40, 105, 106).

1.4.2. The multi-faceted role of UCP2 in cancers

The role of UCP2 in cancer is enigmatic and appears to be context-dependent; whilst UCP2 expression in some cancers has been demonstrated to be detrimental for host cell survival (111-114), in others, it has also been shown to be beneficial for anti-tumour activity (115-119). This section provides notable examples where UCP2 is proposed to play a pivotal role in supporting cancer progression and how this relates to its proposed physiological roles as a C4 metabolite transporter or as a regulator of ROS.

In the context of melanomas, Cheng and colleagues demonstrated that induction of UCP2 expression promotes an anti-tumour microenvironment (115). Using transcriptomic analysis of melanoma patients, they found a positive correlation with high T cell immunity and *Ucp2* mRNA expression, which was strongly associated with pro-inflammatory chemokines responsible for the recruitment of dendritic cells (DCs) and T cells. Such chemokines include: CCL4, CCL5 and CXCL10, with the first two being chemical messengers for the recruitment of natural killer (NK) cells and leukocytes (120, 121). No correlation was found between these genes and other members of the UCP family, suggesting that T cell-mediated immunity was UCP2-

specific (115). Using doxycycline (Dox)-inducible melanoma cells with flag-tagged UCP2, it was demonstrated that UCP2 expression *in vivo* was demonstrated to enhance tumour infiltration by cytotoxic ($CD8^+$) T cells and NK cells. Using RAG and BATF3 KO mice, strains devoid of mature B and T cells (122) and $CD8^+$ dendritic cells (123), respectively, Cheng and colleagues proposed that UCP2-mediated immunity in melanoma was respectively, $CD8^+$ T cell and DC1-dependent. Their findings indicate that UCP2 overexpression shifts the cytokine milieu to an anti-tumour profile, by prompting the production of chemoattractant molecules such as CCL4, CCL5, as well as inflammatory cytokines such as CXCL9, CXCL10 and IFN-γ. The group postulate a mechanism by which UCP2 induction in melanoma supports an anti-tumour immune cycle through expression of interferon regulatory factor 5 (IRF5), summarised in **Figure 1.3**. Furthermore, pharmacological induction of UCP2 expression through the PPAR agonist, rosiglitazone, sensitises tumours that are resistant to immune checkpoint blockade, thus providing a potential avenue for therapeutic intervention (115).

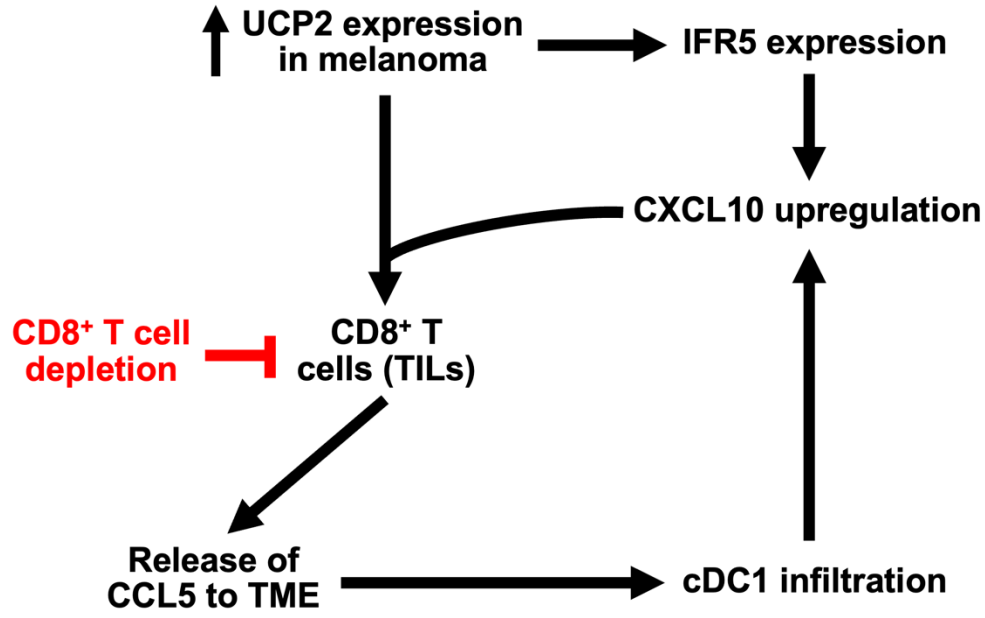

Figure 1.3: Schematic of the proposed mechanism by which UCP2 expression drives CD8+ T cell-cDC1-dependent immunity in melanomas. *Induced overexpression of UCP2 in melanoma cells upregulates IRF5 gene expression, which in turn stimulates the CXCL10 chemokine production. Secretion of CXCL10 into the tumour microenvironment (TME), promotes tumour infiltration by CD8+ T cells (specifically tumour infiltrating lymphocytes, TILs). Recruitment of TILs could lead to increased release of the chemokine, CCL5, which in turn recruits classical DCs (cDC1) to the TME. Tumour infiltration by cDC1 cells increases CXCL10 levels in the melanoma microenvironment. To support this proposed pathway, it was shown that CD8+ T cell depletion diminished CCL5 and CXCL10 levels, consequently downregulating cDC1 infiltration.*

In the context of colorectal cancer (CRC), Aguilar and colleagues deduced that loss of UCP2 expression increases a tumorigenic phenotype by altering metabolic pathways and redox homeostasis (116). Using azoxymethane (AOM)/dextran sodium sulphate (DSS)-treated mice to model colitis associated cancer (CAC) (124), UCP2 deletion was observed to increase the number tumours formed in the colon. Bioinformatic analyses of UCP2 KO tumours show altered expression levels of genes involved in cellular pathways pertaining to lipid, amino acid and carbohydrate metabolism as well as redox balance. Here, Aguilar et al. proposed that UCP2 loss causes a metabolic reprogramming of CRC tumours by diverting glycolysis-derived pyruvate from oxidative phosphorylation to fatty acid synthesis, enabling cell

proliferation through increased phospholipid production. Moreover, UCP2-deficient tumours exhibited a pro-oxidant state, through elevated levels of oxidised glutathione and depletion of NADPH levels, the latter being an important cofactor in ensuring glutathione reduction and fatty acid synthesis (116). Given the role of UCP2 as a potential C4 metabolite transporter that mediates glucose and glutamine oxidation through flux of TCA metabolites, alteration of endogenous UCP2 levels may alter normal metabolic pathways (118). Esteves and colleagues have demonstrated that UCP2 expression in cancer cells can lead to a metabolic shift, from a highly glycolytic phenotype, to one that is dependent on oxidative phosphorylation, with the shift due to increases in AMPK signalling and downregulated by hypoxia-inducible factor (HIF)-1α (117), which were also observed by Cheng and colleagues (115).

In pancreatic ductal adenocarcinoma (PDAC) cells, glutamine undergoes anabolism through a non-canonical pathway that feeds into the TCA cycle. This non-canonical pathway favours the use of cytoplasmic aspartate aminotransferase, GOT1, to convert glutamine-derived aspartate into oxaloacetate, which in turn is oxidised to malate by virtue of malate dehydrogenase and is reductively decarboxylated to generate pyruvate (126). Raho and colleagues proposed that in KRAS-positive mutants, UCP2 expression is essential in mediating aspartate efflux when cells were grown in glutamine (114). The group postulate that glutamine can be imported into mitochondria, through an alternatively spliced sodium-dependent, glutamine transporter (SLC1A5_var) (127), where the metabolite is catabolised in the mitochondrial matrix, with subsequent glutamine oxidation leading to aspartate removal from the mitochondria through UCP2 (114). UCP2-silencing decreased cell proliferation in KRAS-positive, but not KRAS WT PDAC cells, thereby highlighting the need for UCP2 to support dysregulated metabolism in KRAS-mutated cells. Metabolomic analyses of PDAC cells grown in glutamine suggest that loss of UCP2 in PDAC cells leads to the accumulation of glutamine-derived metabolites in the mitochondria, indicating that loss of UCP2 prevents the removal of TCA intermediates from the mitochondria, which in turn inhibits glutaminolysis (93, 114). Moreover, functional complementation assays using mutant yeast highlight that UCP2 may function synergistically with the glutamate-proton (Glu/H^+) symporter to

specifically efflux aspartate from the mitochondria (114), rather than the other negatively charged 4-carbon metabolites mentioned by Vozza and colleagues (93).

In the context of T acute lymphoblastic leukaemia (T-ALL), varying UCP2 expression levels were observed between two cell lines, HPB-ALL and Jurkat, with the former showing higher UCP2 expression (119). The study aimed to explore how UCP2 levels impact T-ALL cell proliferation and oxidative capacity. Respirometry analyses revealed that Jurkat cells primarily rely on glycolysis, whilst HPB-ALL cells with high UCP2 expression, favour oxidative phosphorylation. Glutamine deprivation or pharmacological inhibition of glutamine metabolism indicated that UCP2 expression in T-ALL cells is linked to intracellular glutamine levels and cell proliferation. UCP2 knockdown in HPB-ALL cells shifted their metabolism from oxidative phosphorylation to glycolysis, impacting respiration. The results indicate that UCP2 expression is tightly regulated by glutamine availability, and under glutamine-starved conditions, cells shift to a more glycolytic metabolism. The group proposed that in T-ALL cells that prefer oxidative phosphorylation, i.e. HPB-ALL, UCP2 operates as a malate transporter during glutamine oxidation (119).

Collectively, the findings covered in this section support multi-faceted roles of UCP2 within the cell, coupling redox balance with metabolic pathways. It must be noted that these findings highlight that the context in which UCP2 is expressed is an important factor that must be considered. There are many different ways cancer cells adapt to sustain growth, with the examples mentioned employing the use of deregulating cellular energetics and evading the immune response (128). Hence the type of cancer in which UCP2 is expressed is paramount in determining if this protein plays a tumorigenic or tumour suppressive role.

Since its discovery, UCP2 has been reported to catalyse proton leak in order to attenuate ROS levels in the process of ‘mild uncoupling’. However, more recent findings have indicated that the protein may be a metabolite transporter that removes 4-carbon metabolites from the mitochondria to provide metabolic flexibility to the cell. Given that UCP2 is expressed in a diverse range of cells (38-41), the physiological role of the protein remains unclear.

1.5. Conserved structural features of mitochondrial carriers

1.5.1. Structural characteristics based on structures of the ADP/ATP carrier

Sequence comparison of some of the first mitochondrial carrier proteins isolated from native tissues provided a base understanding of this family of membrane proteins (129-132). From these analyses, mitochondrial carriers were postulated to have a tripartite structure, owing to three tandemly repeated homologous domains (133).

The elucidation of a high-resolution structure of the ADP/ATP carrier (AAC) from bovine heart mitochondria (134) provided significant insight into the structure of mitochondrial carriers and has confirmed findings from preceding biochemical experiments. The first crystal structure of *Bos taurus* (Bt)AAC was resolved in the presence of a potent inhibitor, carboxyatractyloside (CATR), which locks the carrier in a "cytoplasmic-open" state, known as the 'c-state', as shown in **Figure 1.4A**. The monomeric structure of BtAAC comprises of six transmembrane α-helices that form a barrel structure. Two transmembrane helices form one domain, and in each domain odd- and even-numbered helices are connected by a matrix loop that contain short amphipathic α-helices that are parallel to the membrane surface. Odd-numbered helices contain a mitochondrial carrier signature motif Px[DE]xx[KR], where the proline residue facilitate a kink in the α-helix. Within the protein structure is an internal cavity that is lined with hydrophilic residues as well as a positively charged cluster which interacts with the phosphate moiety of ADP (134-136).

To understand the various requirements for substrate binding, Robinson and Kunji modelled protein sequences of characterised yeast mitochondrial carriers against the high-resolution structure of the BtAAC (136). Through comparative protein modelling, it was predicted that substrate binding occurs in the middle of the mitochondrial carrier and that three contact points within this pocket could coordinate substrate binding. The three contact points, located on the even-numbered helices, were postulated to distinguish different parts of a substrate. For example, the contact point on helix 2 was predicted to differentiate substrate based on its functional group, whilst the contact point on helix 6 is predicted to confer specificity through recognition of the variable group within the substrate (136). These observations are consistent with the three-fold pseudo-symmetrical structure of mitochondrial carriers and demonstrates how this family of transporters have

evolved to translocate a variety of substrates (139). Through their findings, Kunji and Robinson proposed that substrate binding induces a change in the protein conformation which enables substrate translocation across the inner mitochondrial membrane (136). This was later supported by high-resolution crystal structures of yeast AACs, in complex with CATR (140) in the c-state conformation and, later, in complex with bongkrekic acid (BKA), another potent inhibitor of AAC, revealing the 'matrix-open' (m-state) conformation of carriers (141).

The structures of yeast AAC in complex with CATR corroborate findings from the structure of BtAAC. As well as corroborating the formation of a matrix salt-bridge network that closes access to the central cavity at the matrix side, due to charged residues in the Px[DE]xx[KR] motif forming interdomain electrostatic interactions, the 'c-state' structure of yeast AAC also highlights highly conserved glutamine residues in proximity to this salt-bridge network. These glutamine residues hydrogen bond with charged residues of the signature motif, forming the 'Q brace'. This brace is believed to provide additional stability to the matrix salt-bridge network, when the carrier is in the 'c-state' (**Figure 1.4B**) (140). The AAC structure in complex with BKA revealed the m-state with the central cavity exposed to the mitochondrial matrix side of the membrane. Even-numbered helices contain the conserved mitochondrial carrier motif: [YF][DE]xx[KR], whereby charged residues within this motif interact electrostatically to form the cytoplasmic salt-bridge network, which closes the cytoplasmic side of the carrier. Highly conserved tyrosine residues in this motif act as the 'Y brace' by providing extra structural support to this salt-bridge network. Bulky and aromatic hydrophobic residues also add to this 'cytoplasmic gate' to block the carrier at the cytoplasmic side (**Figure 1.4B**) (141).

Mitochondrial carriers bind cardiolipin, a unique phospholipid of the mitochondrial inner membrane that is composed of two phosphatidic acid moieties connected by a glycerol backbone, at three positions, where it plays an important role in mitochondrial carrier function (**Figure 1.4A**) (142-144). In the carrier structures, the cardiolipin headgroups are observed to bind between matrix and even-numbered helices, providing structural support between the three domains (137, 145-147). In matrix helices, the cardiolipin headgroup interacts with a mitochondrial carrier conserved motif [YWF][KR]G, whilst the N-terminal end of even-numbered helices interact via a [YF]xG motif (145).

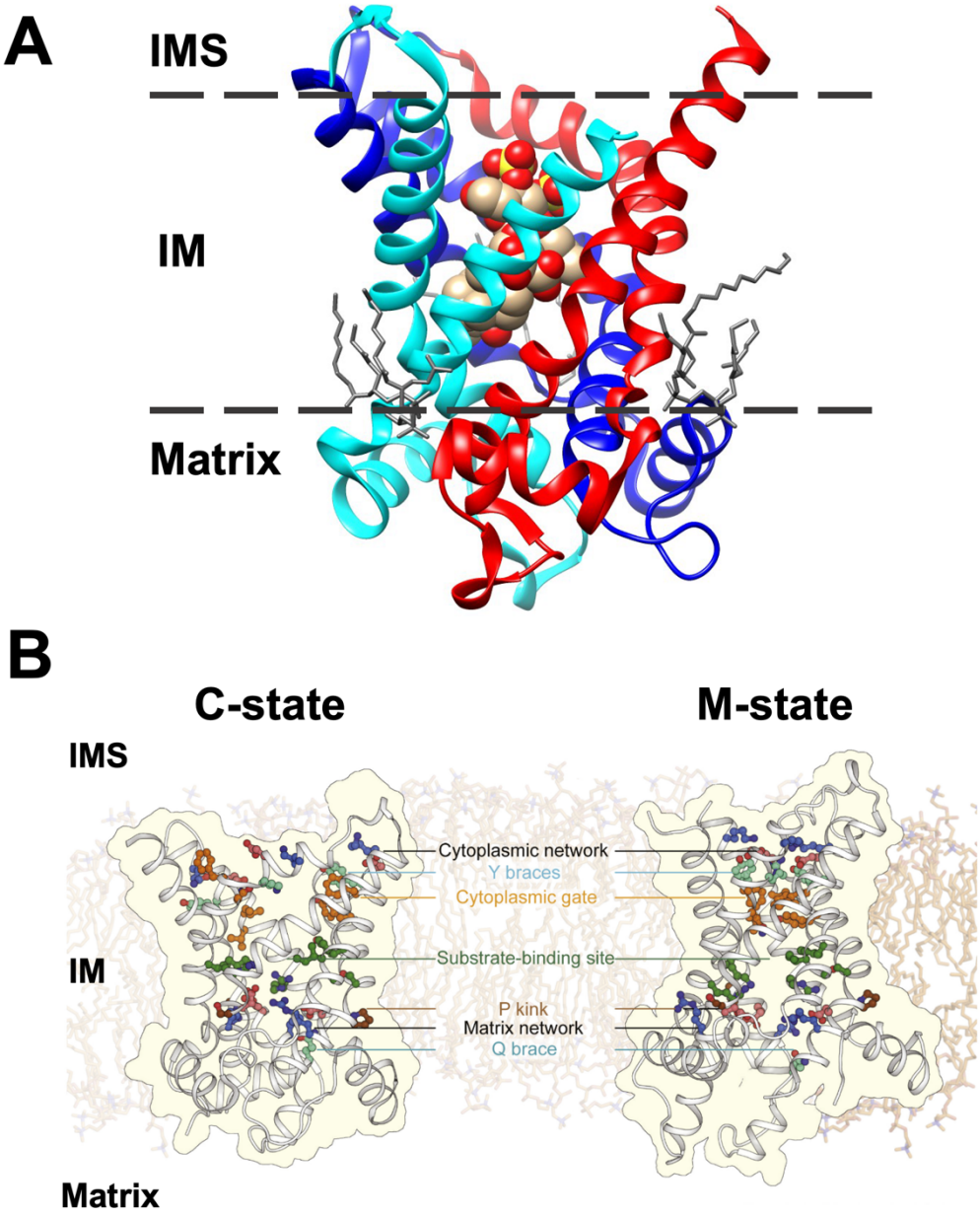

Figure 1.4: Structures of the ADP/ATP carrier in different conformations*. A) Protein structure of bovine AAC in complex with CATR elucidated by Pebay-Peyroula, et al. (2003) (PDB code: 1OKC) (137). Homologous repeats are depicted in as red, blue and cyan; cardiolipin molecules in shown in grey, whilst CATR is depicted as spheres located within the molecule. Structure was annotated using USCF Chimera. B) Schematic of yeast AAC in the c-state (CATR-inhibited) (PDB code: 4C9H) and m-state (BKA-inhibited) (PDB code: 6GCI). This schematic highlights the formation and dissociation of the two salt-bridge networks that are responsible for closing the carrier in its two different states. It also illustrates how these networks are stabilised by virtue of the Q brace and P kink (when in the c-state) and the Y brace and cytoplasmic gate (when in the m-state). This image is taken from Ruprecht & Kunji, 2020 (138).*

Through the resolved structures of AAC in the c-state and m-state conformation, it has been proposed that mitochondrial carriers translocate their respective substrates across the mitochondrial inner membrane via an alternate access mechanism (136, 139, 145, 148) (see **Figure 1.5**). In this process, mitochondrial carriers, poised in either in the c-state or m-state, bind a substrate within the central cavity, which induces a conformational change and transition of the carrier to the opposite state, to allow the release of the substrate on the other side of the membrane. In the case of AAC, ADP from the cytosol and mitochondrial IMS binds in the central cavity when the protein is in the c-state. The binding energy of ADP provides sufficient energy to break the matrix bonding network and transitions the carrier into the m-state, where the cytoplasmic bonding network forms instead and ADP is released into the mitochondrial matrix. With the substrate binding site accessible to the matrix conformation, matrix ATP binds to the central cavity, providing the energy to break, in this case, the cytoplasmic network of the protein and cycle it back into the c-state (98, 149-152). In the c-state, ATP is released into the mitochondrial IMS, thus the transport cycle can repeat (152). This mechanism of substrate transport constitutes a ping-pong mechanism, where substrates are translocated across the mitochondrial inner membrane in a sequential manner. In this model, one substrate binds to the carrier and is released prior to binding of the second substrate to the carrier (98, 151, 152).

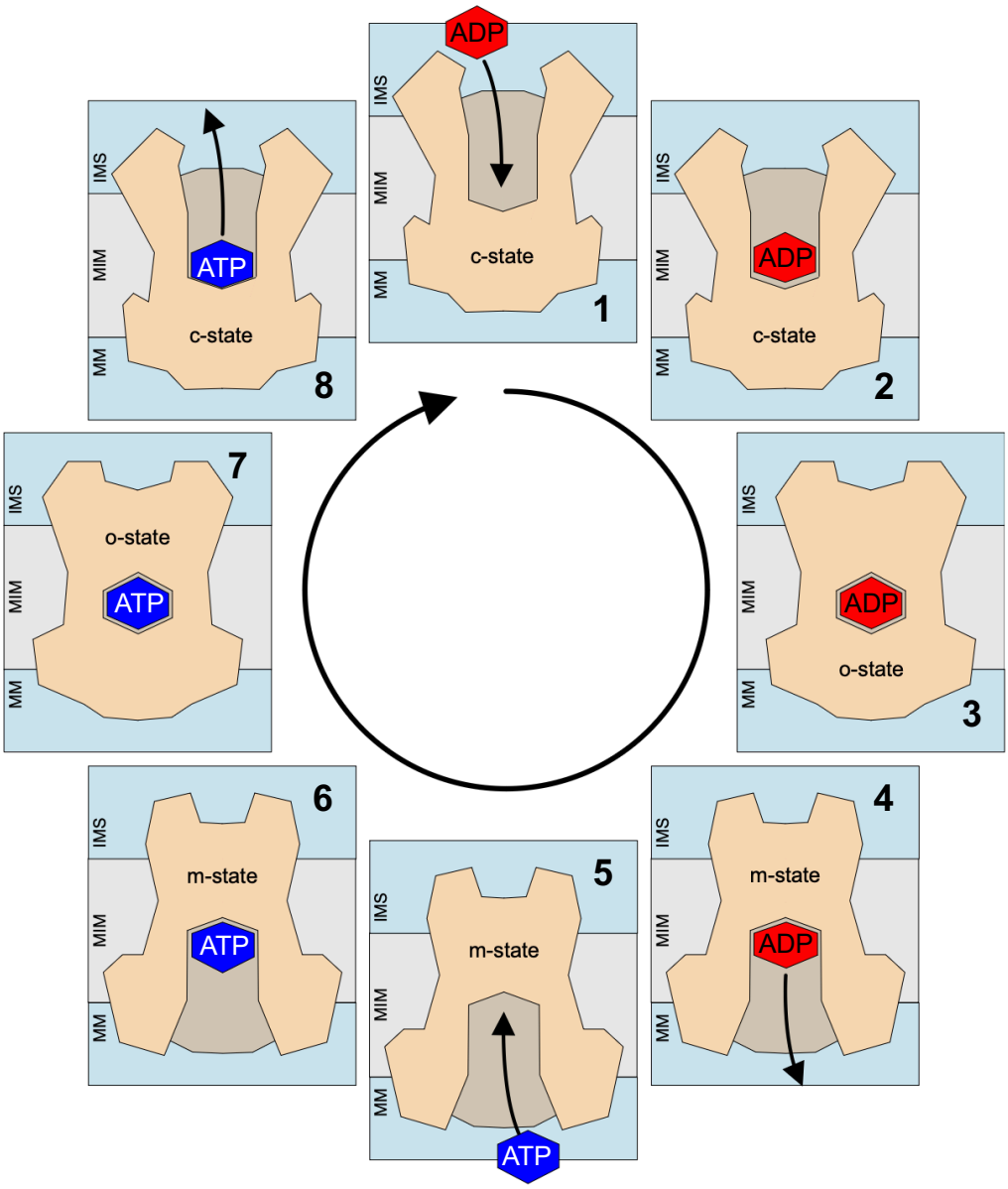

Figure 1.5: Schematic of proposed ping-pong mechanism of substrate transport by mitochondrial carriers (ADP/ATP carrier example). *The transport substrate (ADP) enters the mitochondrial carrier (AAC) from the IMS, binding to the substrate binding site located in the central cavity (steps 1-2). Substrate binding induces a conformation change in protein structure, to give rise to an occluded state (o-state), where the carrier is inaccessible to both the cytoplasm and the mitochondrial matrix (step 3), before fully transitioning to an m-state where the substrate binding site is open to only the matrix (step 4). With the protein accessible to the mitochondrial matrix, the cytosolic substrate is released (step 4), and a counter substrate from the matrix (ATP) can bind to the central cavity (step 5-6). The protein then undergoes the same process as described but in the opposite direction to translocate the second substrate to the IMS (steps 7-8). Image adapted from Cimadamore-Wertherin et al. (2024) (98).*

1.5.2. Resolved structures of UCP1

Recently, the first experimental structures of human UCP1 were elucidated in GTP-(153), ATP- and 2,4-dinitrophenol (DNP)-bound states as well as the carrier without a ligand bound (154). In all structures, UCP1 showed a pseudo symmetric 3-fold symmetry with three homologous domains comprising of two transmembrane helices, linked by a loop and small-matrix helix, consistent with most mitochondrial carriers (**Figure 1.6A**). The structures showed bound cardiolipin as expected, a lipid essential for mitochondrial protein structure and function (19, 155). The nucleotide-bound structures revealed an intermediate c-state-like structure, whereby the nucleotide is positioned with the phosphate groups facing towards the matrix salt-bridge network and the guanine moiety is poised towards the open intermembrane space of the protein (**Figure 1.6A**). The structures show that the phosphate moieties of the triphosphate nucleotides form extensive interactions between the matrix salt-bridge network and an arginine triplet (residues of the proposed substrate binding site (136, 139)), in the central cavity of the protein, thereby locking the protein a stable confirmation. In the GTP-bound state, the guanine group is observed to interact with residues towards the cytoplasmic side of the cavity, forming hydrogen bonds with asparagine residues as well as ionic interactions with charged residues (E191 and R92), stabilising the protein in an intermediate c-state (**Figure 1.6B**). Experimental structures of UCP1 in a DNP-bound and ligand-free state also show the protein in a cytoplasmic-open conformation (154).

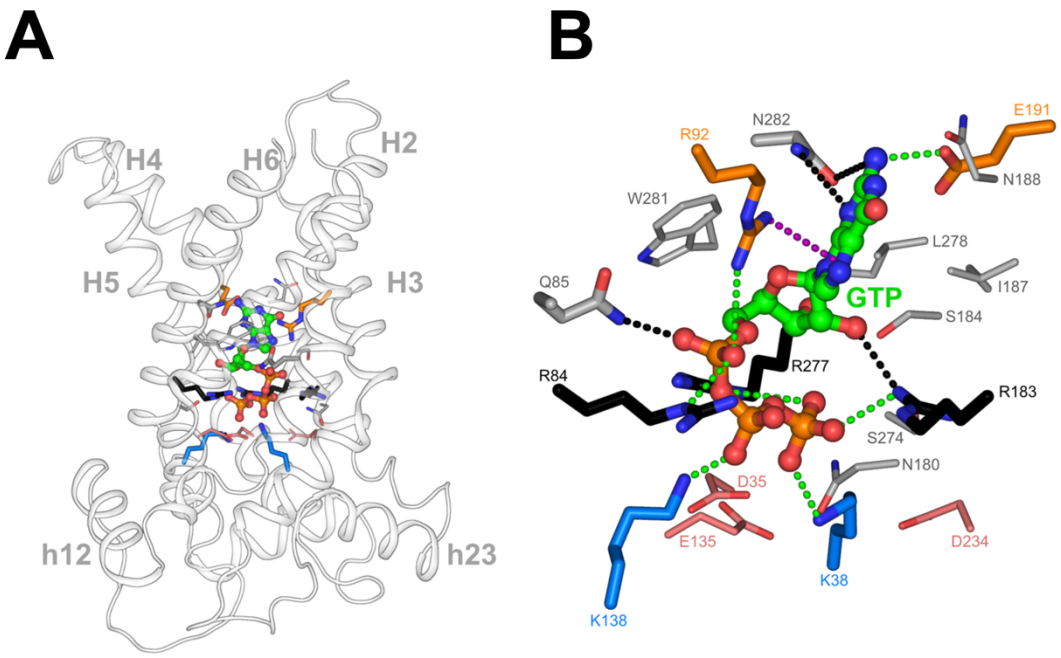

Figure 1.6: GTP-bound structure of human UCP1. *A) Lateral view of human UCP1 in a GTP-bound form. B) Close-up view of GTP and interacting residues. The arginine triplet is depicted in black; positively and negatively charged residues of the matrix salt-bridge network are shown in blue and red, respectively. Images were taken from Jones et al. 2023 (153).*

1.5.3. Resolved structure of UCP2

In 2011, a structure of mouse (Mm)UCP2 was reported using solution nuclear magnetic resonance (NMR) coupled with the technique of molecular fragment searching (156). In this study, recombinant UCP2 was expressed in a bacterial system and solubilised with the zwitterionic detergent, dodecylphosphocholine (DPC), prior to purification via a GDP-analogue column. Purification using this GDP-analogue column supposedly binds folded MmUCP2 (156). Fluorescence resonance energy transfer (FRET) experiments using DPC-solubilised UCP2 protein have reported binding of GDP with an apparent dissociation constant of ~5 μM (156). NMR analyses proposes that fatty acids bind to a peripheral site (between helices 1 and 6) within UCP2 to mediate proton conductance, with activation by fatty acids under allosteric control of GDP binding (157). However, the approach and methodologies used have led to the physiological relevance of the structure being questioned (155, 158-163). The main criticisms of the structure is the use of bacterial expression systems, which do not generate carrier in a folded state and the use of

DPC, a harsh ionic detergent, that does not maintain carrier proteins in an appropriately folded form (155, 158-162). Molecular dynamics simulations comparing the NMR structure of UCP2 with crystal structures of bovine AAC, demonstrate that the NMR-resolved structure is permeable to water (158, 159) and likely to be functionally irrelevant. Furthermore, the use of thermostability assays also highlight that whilst mitochondrial carriers may appear to be soluble in the presence of DPC, the protein is likely in an unfolded form (155).

1.6. General aims and objectives of the project

Due to its high sequence similarity with UCP1, it was proposed that UCP2 functions in a similar manner (4). Early biochemical characterisation of UCP2 was reported to facilitate proton leak in the presence of fatty acids, like that of UCP1, though instead of playing a thermogenic role, UCP2 was proposed to alleviate the production of ROS through 'mild uncoupling' (73). Investigations into proton transport activity in liposomes produced conflicting results, potentially owing to reconstitution of bacterially-expressed protein which are produced as inclusion bodies, but require refolding prior to liposome reconstitution (155, 158-163). Various studies probing into UCP2 proton transport have typically used purine nucleotides as a diagnostic for UCP2 proton transport activity (49, 50, 52, 53, 57-61, 65, 69, 70, 164), as well as a tool to select for folded UCP2 protein from bacterially-expressed systems (157). Emerging evidence suggests that UCP2 is a metabolite transporter that transports 4-carbon metabolites out of the mitochondria in order to provide metabolic flexibility to the cell (93, 114). The biochemical role of UCP2 is still unclear. Low abundance of UCP2 in native tissues (38, 40) makes isolation from native sources an impractical route for biochemical characterisation. The inherent instability of mitochondrial carrier proteins (155), has hampered efforts in elucidating the biochemical function of UCP2.

The overall aim of this project was to biochemically characterise UCP2 to clarify its functional properties. The objectives are:

1. To express intact human UCP2 in a yeast system for subsequent purification and study
2. To develop a purification strategy for UCP2 based on methods established for UCP1
3. To determine the molecular and functional properties of UCP2 and if they differ to UCP1. In particular, the ligand binding properties (e.g. purine nucleotide binding) and proton/metabolite transport properties of the protein

2. Materials and Methods

2.1. Bacteria and yeast strains

Chemically competent *E. coli* TOP10 cells were used for the generation of plasmid DNA. They were a kind gift from Professor Changjiang Dong (University of East Anglia). The chemically competent *E. coli* strain, C41 (DE3), which were generated for optimised membrane protein expression (165) were used for the overexpression of histidine-tagged UCP inclusion bodies. For protein expression of human UCP2, the protease-deficient *S. cerevisiae* strain, FGY217, was used. The FGY217 strain lacks the *Pep4* gene, which encodes for proteinase A (166), a protease required for the post-translational maturation of other vacuolar proteinases in *S. cerevisiae* (167). For protein expression trials of human UCP2, the WB12 *S. cerevisiae* strain was also used, which has disrupted *Aac2* and *Aac3* genes, making it deficient for these isoforms of AAC (168). The *S. cerevisiae* wild-type strain W303-1B was used for protein expression of human UCP1 protein as well as preliminary protein expression trials with human UCP2. With the exception of the TOP10 cells, all cell strains were obtained from the Mitochondrial Biology Unit, Cambridge.

Table 2.1. Composition of bacterial and yeast culture media

Media	Composition	Use
Escherichia coli		
LB broth (pH 7.0)	1% (w/v) tryptone 0.5% (w/v) yeast extract 1% (w/v) NaCl (pH corrected for with NaOH)	Propagation of *E. coli* cells devoid of an expression vector for the generation of competent *E. coli* cells
LB agar (pH 7.0)	Same composition as LB broth with additional 2% (w/v) agar	
LB broth/agar + ampicillin (pH 7.0)	Same composition as LB broth/agar with the addition of ampicillin following media	LB agar + ampicillin were used for colony selection following *E. coli* transformation.

	sterilisation to a final concentration of 100 µg/mL	LB broth + ampicillin were used to grow positive colonies in liquid culture.
SOC broth	2% (w/v) tryptone 0.5% (w/v) yeast extract 10 mM NaCl 2.5 mM KCl 10 mM $MgCl_2$ 10 mM $MgSO_4$ 20 mM glucose	Facilitate *E. coli* cell growth following heat-shock treatment during bacterial transformation of plasmid DNA
Saccharomyces cerevisiae		
Selective (SC-ura) media + glucose	0.67% (w/v) yeast nitrogen base 0.077% (w/v) CSM drop out: ura 2% (w/v) glucose	Propagation of *S. cerevisiae* cells transformed with a pYES2 vector
SC-ura + glucose agar	Same composition as SC-ura + glucose media with the addition of 2% (w/v) agar	Selective agar plates used for the selection of pYES2 positive transformants and for growth from glycerol stocks
Selective (SC-ura) lactate media + glucose (SL+G)	0.67% (w/v) yeast nitrogen base 0.077% (w/v) CSM drop out: ura 2% (v/v) DL-lactic acid 0.1% (v/v) glucose (pH corrected for with KOH)	Propagation of *S. cerevisiae* cells transformed with pYES2 vector, primarily used for UCP1 growth and expression
YPD media	1% (w/v) yeast extract 2% (w/v) peptone 2% (w/v) glucose	Growth medium for yeast transformation experiments

YPD agar	Same composition as YPD media with the addition of 2% (w/v) agar	Propagation of *S. cerevisiae* cells devoid of an expression plasmid for yeast transformation
YPD (0.75% (w/v) glucose) media	1% (w/v) yeast extract 2% (w/v) peptone 0.75% (v/w) glucose	Growth medium for FGY217 cells transformed with HsUCP2 construct
YPL media	1% (w/v) yeast extract 2% (w/v) peptone 3% (v/v) DL-lactic acid (pH corrected for with KOH)	Growth medium for W303-1B cells transformed with HsUCP1 construct
YPR media	1% (w/v) yeast extract 2% (w/v) peptone 2% (w/v) raffinose	Growth medium for WB12 cells transformed with HsUCP2 construct

2.2. Preparation of competent *E. coli* cells

Stocks of competent *E. coli* were prepared as described by Tang et al. (169). Briefly, competent *E. coli* (TOP10 or C41 (DE3)) cells devoid of antibiotic-resistant plasmid DNA were streaked onto an LB agar plate. A starter culture was produced by inoculation of a single colony into 5 mL LB media which was grown in a shaking incubator overnight at 37°C, 180 rpm. 1 mL of starter culture was inoculated into 100 mL pre-warmed LB media and grown for approximately 2 hours. When optical density (OD_{600}) reached between 0.4-0.5, cells were chilled on ice for 30 minutes and spun down at ~2000 x *g*, 10 minutes, 4°C. Pelleted cells were resuspended in 12.5 mL 100 mM $CaCl_2$ and 12.5 mL 40 mM $MgSO_4$ and incubated on ice for a further 30 minutes and then spun down as previously described. Pelleted cells were resuspended in 2.5 mL 100 mM $CaCl_2$ and 2.5 mL 40 mM $MgSO_4$ prior to the addition of glycerol (final concentration 10%). The final sample was divided into 100 µL aliquots, snap frozen in liquid nitrogen and stored in -80°C.

2.3. Constructs

2.3.1. Vectors for *S. cerevisiae* protein expression

Five human UCP2 expression constructs were generated for use in *S. cerevisiae*. A codon-optimised *Ucp2* gene (synthesised by Genscript) was ligated into a pYES2 plasmid using SacI and XbaI restriction sites. Gene expression is controlled by the presence of an inducible GAL1 promoter (170). Utilisation of the pYES2 vector to clone UCP2 proteins for recombinant protein expression were based on the general approach used for UCP1 (153, 171). Construct 1 containing an adenine-rich Kozak sequence ("CTCAAAAAATGT") with a codon encoding for a leucine at the second amino acid position was generated by Dr. Martin King (MRC Mitochondrial Biology Unit). Construct 2 containing the "CTCATAATGG" Kozak sequence with the native valine at position 2 was produced by Dr. Paul Crichton and Danielle Copeman (University of East Anglia). Constructs 3 and 4 were produced through overlapping PCR extension (see **section 2.4.1.** for details), see **Figure 2.1A** for schematic. A fifth construct consisting of a UCP1-like C-terminus was produced for the purposes of downstream purification efforts (see **Appendix 1.2** for construct sequence alignments). The pYES2 vector contains an ampicillin resistance gene and a *Ura3* gene, enabling colony selection following bacterial and yeast transformations, respectively.

2.3.2. Vectors for *E. coli* protein expression

To generate histidine-tagged inclusion bodies for the purposes of producing protein standards in Western blots, the yeast codon-optimised human *Ucp2* gene was cloned into the pMW172 expression vector (55, 56, 172). At the 5'-end of the gene, primers were designed to introduce an NdeI restriction site upstream of codons encoding for an N-terminal hexa-histidine tag and a short peptide linker sequence (encoding for the amino acids glutamate-leucine-isoleucine) which accounts for the SacI restriction site and Kozak sequence between the N-terminal histidine-tag and the start of the UCP gene. An EcoRI site was introduced at the 3'-end following 3 stop codons and the XbaI site produced for the pYES2 vector. The histidine-tagged gene construct was produced through overlapping PCR extension and subsequent restriction digestion and ligation reactions. The gene is downstream of a T7 promoter (**Figure 2.1B**), thus when the vector is transformed into the C41 (DE3) expression strain,

protein expression can be induced through T7 RNA polymerase which itself is regulated by the lacUV5 promoter. Hence, protein expression can be induced by activation of the lac promoter in the presence of the non-hydrolysable lactose analogue, isopropyl-2-D-galactopyranoside (IPTG) (173).

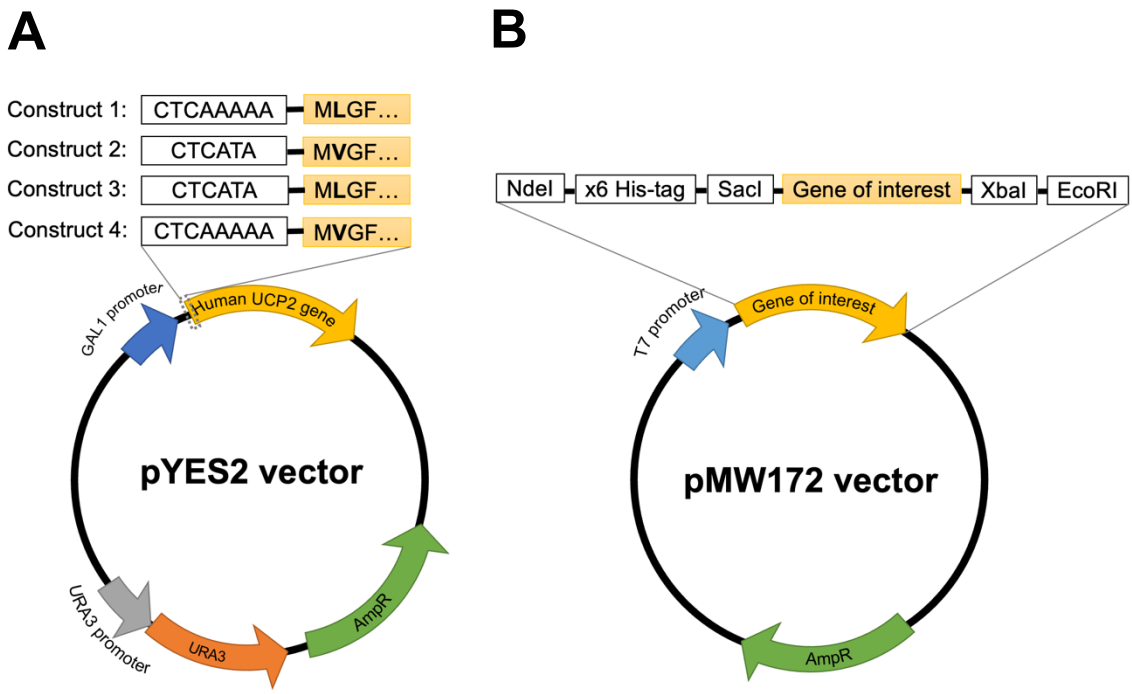

Figure 2.1: Schematic representation of the pYES2 and pMW172 expression vectors. *A) pYES2 vector containing the human Ucp2 gene. The schematic highlights differences between the 5'-region of the genes for constructs 1-4; the Kozak sequence preceding the start codon is defined in the white box, whilst the protein coding regions are shown in the yellow box, with alterations highlighted in bold. The gene is flanked by SacI and XbaI restriction sites at the 5'- and 3'-end respectively. The codon-optimised Ucp2 gene is downstream of the inducible GAL1 promoter. B) pMW172 vector containing a histidine-tagged gene cassette. The gene of interest is flanked by SacI and XbaI sites as with the pYES2 vector. An NdeI restriction site and codons encoding for a hexa-histidine tag was cloned into the 5'-end of the Ucp gene. Promoter regions are shown as blue arrows, the ampicillin resistance gene is shown as green arrows, the auxotrophic Ura3 selection marker is shown as an orange arrow in the pYES2 vector.*

2.4. Molecular biology

2.4.1. PCR amplification - generation of UCP2 constructs for *S. cerevisiae*

PCR amplification reactions were carried out using the KOD Hot Start DNA polymerase kit (Merck Chemicals Ltd.) following the manufacturer's instructions using thin-walled PCR tubes. Using construct 2 as the template DNA, oligonucleotide primers were designed either to alter the second amino acid from the native valine to leucine (construct 3) or to introduce an adenine-rich Kozak sequence (construct 4) (**Figure 2.1A**). All reactions were conducted using a thermocycler (Veriti 96-well thermal cycler, Applied Biosystems). Reaction mixtures and PCR amplification parameters are summarised in **Tables 2.2** and **2.3**, respectively.

2.4.2. Site-directed mutagenesis PCR – generation of histidine-tagged UCP constructs for *E. coli* inclusion body expression

Site-directed mutagenesis (SDM) primers were designed to remove an internal XbaI site within the coding region of the mouse *Ucp1* gene from the inherited pMW172 plasmid. SDM was conducted through QuikChange PCR (Agilent). SDM PCR reactions were conducted using a thermocycler (see **Table 2.4**), with the resulting products subject to incubation with DpnI at 37°C for an hour in order to digest the hemi-methylated parental DNA strand (174). Following removal of the internal XbaI site through SDM, overlapping PCR extension was conducted to incorporate an NdeI site and hexa-histidine tag to the 5'-end of codon-optimised human *Ucp2* gene and introduce an EcoRI site at the 3'-end of the gene (**Figure 2.1B**). PCR amplification reactions were carried using the KOD Hot Start DNA polymerase kits as described in **Tables 2.2** and **2.3**. Following PCR amplification PCR products were analysed by agarose gel electrophoresis. Primers used for molecular cloning are listed in **Appendix 1.3**.

Table 2.2: Composition of 50 µL PCR amplification reaction using the KOD Hot Start Polymerase kit

Reagent	Volume added (µL)	Final concentration
Ultra pure water (DNase free)	32	-
10x KOD buffer	5	1x
25 mM $MgSO_4$	3	1.5 mM
2 mM dNTPs	5	0.2 mM
10 µM forward primer	1.5	0.3 µM
10 µM reverse primer	1.5	0.3 µM
Template DNA (<10 ng/µL)	1	<0.2 ng/µL
KOD polymerase (1.0 U/µL)	1	1U

Table 2.3: Thermocycler settings for PCR amplification of *Ucp* genes into expression vectors

Number of cycles	Step	Temperature (°C)	Time
1	Denaturation	95	2 minutes
30	Denaturation	95	20 seconds
	Annealing	55	20 seconds
	Elongation	70	20 seconds
1	Elongation	70	1 minute

Table 2.4: Thermocycler settings for SDM PCR to remove an internal XbaI site from pMW172 vector

Number of cycles	Step	Temperature (°C)	Time
1	Denaturation	95	30 seconds
16	Denaturation	95	30 seconds
	Annealing	55	1 minute
	Elongation	72	4 minutes

2.4.3. Agarose gel electrophoresis

DNA fragments were visualised using agarose gel electrophoresis. 1% (w/v) agarose gels were cast using TAE buffer (40 mM Tris base; 20 mM acetic acid, 1 mM Na-EDTA) supplemented with 5 x 10^{-3} % (v/v) ethidium bromide. Samples were run at 75 V for an hour and visualised on either Bio-Rad Gel Doc EZ imager or ChemiDoc-IT®2 810 imager.

2.4.4. Restriction digestion

The vector and PCR products yielding bands of the correct size (>4000 bps and ~1200 bps, respectively) were digested either with SacI and XbaI for *Ucp2* gene insertion into the pYES2 vector, or with NdeI and EcoRI for the cloning of a histidine-tagged gene into the pMW172 vector. For each reaction, 5 µL of 10X FastDigest buffer (Thermo Fisher Scientific) was added to 40-50 µL DNA sample, prior to addition of FastDigest enzymes, with specified restriction enzymes used as stated above. Digestion reactions were incubated overnight at 37°C. Cut vectors were separated on a 1% (w/v) agarose gel, with the larger fragment excised from the gel and DNA purified using the QIAquick gel extraction kit as per manufacturer's instructions. PCR products were purified using the QIAquick PCR clean up kit as per manufacturer's instructions. DNA concentration was determined using the NanoDrop2000 spectrophotometer (Thermo Fisher Scientific). Production of a hexa-histidine tagged human UCP1 construct was generated by restriction digestion of the pMW172-histidine tagged plasmid using SacI and XbaI.

2.4.5. Ligation reactions of human UCP2 gene into pYES2

Following restriction digestion, gene inserts were cloned into digested vectors using T4 DNA ligase (400 U/µL), according to manufacturer's instructions. The human *Ucp2* gene was ligated into the pYES2 vector, whilst the insert encoding for hexa-histidine tagged UCP2 protein was ligated into the pMW172 vector. The human *Ucp1* gene was ligated into the pMW172 vector following the addition of the hexa-histidine tag. The 20 µL ligation reaction contained approximately 50 ng of vector to 25 ng insert with 1 U T4 ligase. Reactions were incubated at room temperature for 30 minutes prior to heat inactivation of the T4 ligase, which occurred at 65°C for 10 minutes.

2.4.6. *E. coli* transformation

For transformation into *E. coli*, 5 µL ligation product was added to 100 µL TOP10 cells, gently mixed and then incubated on ice for 30 minutes. Cells underwent heat shock treatment through a 60-second incubation at 42°C followed by a 2-minute incubation on ice. 900 µL SOC media was added to the cell mixture and then incubated in shaking incubator at 37°C, ~180 rpm for at least one hour. Following incubation, cells were pelleted and resuspended in 100 µL SOC media before being plated onto LB plates containing ampicillin for selection for transformants containing the desired plasmid.

2.4.7. Colony PCR

Colonies were picked from *E. coli* transformation plates and grown overnight at 37°C, ~180 rpm in LB media supplemented with ampicillin. For colony PCR, standard PCR amplification was conducted as previously mentioned (see **section 2.4.1** for details), with the main difference being that the template DNA was sourced from 1 µL of overnight cultures from picked colonies. Insert primers specific for the backbone vector were used to determine if ligation reactions were successful (see **Appendix 1.3** for primers). PCR reactions were carried out as previously described in **Tables 2.2** and **2.3**. Resulting PCR products were separated on 1% (w/v) agarose gels and potentially positive colonies were determined if bands of the correct size (~1200 bps) were visualised. Prior to sequencing, 0.5 mL of overnight cultures were taken, supplemented with glycerol (final concentration 30%) and flash frozen to generate glycerol stocks. Glycerol stocks were stored at -80°C until needed. Sequence-confirmed glycerol stocks were kept, whilst those harbouring additional mutations were discarded.

2.4.8. DNA sequencing

Plasmid DNA corresponding to colonies that gave a ~1200 bp band in analytical agarose gels were extracted from corresponding overnight cultures, using the QIA Quick Miniprep Spin Kit according to manufacturer's instructions. The generation of constructs were verified through Sanger sequencing courtesy of Source Bioscience UK Ltd. Sequences were analysed using mutli-alin. (http://multalin.toulouse.inra.fr)

against the predicted sequence based off primer design and from the codon-optimised gene sequence.

2.4.9. Transformation into expression vector – pYES2 plasmid into *S. cerevisiae*

Following sequence confirmation, pYES2 vectors containing the human *Ucp2* gene were transformed into *S. cerevisiae* through the lithium acetate method (175). FGY217 or WB12 cells were streaked onto YPD agar plates and grown for 4-5 days at 30°C. A single colony was inoculated into 10 mL YPD media and grown overnight at 30°C, 225 rpm. The following day, 2.4 mL of starter culture was inoculated into 50 mL pre-warmed YPD media and incubated for 4 hours at 30°C, 225 rpm. Following incubation, cells were pelleted (4200 x *g*, for 10 minutes at 4°C), then washed in ice-cold sterile water. Cells were pelleted as before and then resuspended in 0.5 mL ice-cold TE/Li-acetate solution (10 mM Tris HCl (pH 8.0), 1 mM EDTA, 100 mM lithium acetate). For each transformation reaction, 20 µL salmon sperm carrier DNA, 1 µg plasmid DNA and 100 µL yeast cells were combined and incubated at room temperature for 10 minutes. Samples were then resuspended in 0.5 mL ice-cold TE/Li-acetate solution supplemented with 40% (v/v) PEG 4000 before incubation at 30°C for 30 minutes. Cells then underwent heat-shock treatment by incubation at 42°C for 20 minutes. Cells were pelleted and resuspended in minimal volume (150 µL) sterile distilled water before being spread onto agar plates containing complete selective media lacking uracil (SC-ura), supplemented with 2% (w/v) glucose. Plates were left to grow at 30°C for 4-5 days.

2.4.10. Transformation into expression vector – pMW172 plasmid into C41 (DE3) *E. coli*

Sequence verified pMW172 plasmids encoding for histidine-tagged UCP protein were transformed into C41 (DE3) *E. coli* strain. Transformation into this bacterial expression strain follows the same protocol as previously described (see **section 2.4.6** for details), with the main difference being ~100 ng plasmid DNA is incubated with 100 µL competent C41 (DE3) cells.

2.5. Small-scale UCP2 protein expression and membrane isolation from *S. cerevisiae*

2.5.1. Protein expression trials

Glycerol stocks of *S. cerevisiae* cells containing the pYES2 plasmid with the *Ucp2* gene insert (construct 1-5) were streaked onto SC-ura agar plates containing 2% (w/v) glucose. Plates were incubated at 30°C for 3-4 days to allow for colony formation. Starter cultures were generated by inoculation of a single colony into 10 mL SC-ura + 2% (w/v) glucose media, prior to overnight incubation at 30°C, 225 rpm. The following day, the OD_{600} of overnight starters culture were measured, before being used to inoculate 50 mL pre-warmed media to a starting OD_{600} of 0.04. Cells were then grown at 30°C for approximately 6 to 17 hours. The large difference in time for growth prior to induction with galactose was due to testing different growth and expression protocols during optimisation screens (see **Chapter 3** for details). Following initial growth, a 10 mL sample was taken to provide a pre-induction read (t=0). Cultures were subsequently induced with galactose to a final concentration of 1%. For growth and protein expression using the WB12 strain, some conditions tested required cultures to be pelleted and resuspended in fresh yeast-peptone (YP) media supplemented with raffinose prior to induction with 1% (v/v) galactose. At various timepoints, cells were harvested (5000 x *g*, 4°C, 2 minutes), washed with ice cold sterile water and subjected to another low-speed spin (~900 x *g*, 1 minute). Cell pellets were snap frozen in liquid nitrogen prior to storage at -80°C. OD_{600} measurements were taken at each timepoint to monitor cell growth.

2.5.2. Isolation of mitochondrial membranes

Cells obtained from small-scale expression trials were washed with 1 mL breaking buffer (50 mM Tris HCl (pH 8.0), 0.65 M D-sorbitol, 5 mM Na-EDTA (pH 8.0), 5 mM aminocaproic acid, 5 mM benzamidine hydrochloride, 1 mM PMSF), spun down and then resuspended in 400 µL breaking buffer. Cells were homogenised by mechanical disruption using 0.6 g 500-micron glass beads with 1.5 mL Eppendorf tubes attached onto a horizontal multi-tube holder (SI-H524 attachment), mounted on a Vortex Genie 2 (Scientific Industries). Yeast cells were beaten at full power for 30 minutes at 4°C. Following homogenisation, the lid and bottom of the sample tubes were pierced, before being placed on top of 15 mL falcon tubes. Samples were

subjected to a brief low-speed spin (50 x *g,* 10 seconds) to pull down the resulting lysate. Samples were washed with 400 µL breaking buffer and spun down as before to rinse the glass beads of residual lysate. Following the second spin, the resulting lysate was centrifuged for 10 minutes at 5,000 x *g* at 4°C to pellet any unbroken cells and debris. The resulting supernatant was then transferred to clean tubes where they were subjected to a high-speed spin (21,000 x *g*) for 30 minutes at 4°C to pellet the mitochondrial membrane-containing fraction. The resulting supernatant was carefully aspirated and the pellet resuspended in 150 µL final buffer (50 mM Tris HCl (pH 8.0), 0.65 M D-sorbitol). Protein concentration was determined using the bicinchoninic acid method (176). Isolated mitochondrial membranes were snap frozen in liquid nitrogen and stored at -80°C.

2.6. Large-scale UCP protein expression in *S. cerevisiae*

2.6.1. UCP1 protein expression

Glycerol stocks of W303-1B cells transformed with human *Ucp1* (yeast codon-optimised) gene in the pYES2 vector were streaked onto SC-ura agar plates supplemented with 2% (w/v) glucose. Plates were incubated at 30°C for 3-4 days to allow for colony formation. UCP1 growth and protein expression was adapted as described in (177, 178). Pre-cultures were propagated through inoculation of a single colony into 10 mL SC-ura media supplemented with 2% (v/v) lactate and 0.1% (w/v) glucose (SL+G media) and grown overnight at 30°C, 225 rpm. The resulting pre-culture was then inoculated into 80 mL fresh SL+G media to produce a homogenous sub-culture and grown overnight as previously described. Sub-cultures were then inoculated into 1 L pre-warmed YPL media and grown overnight (30°C, 225 rpm) for 16 to 17 hours prior to induction of protein expression with galactose to a final concentration of 1%. Cells were further incubated for 6 hours to allow for human UCP1 protein expression, before being harvested by centrifugation (JLA 8.1000 rotor, 5000 x *g*, 10 minutes, 4°C). Cells were either processed immediately for mitochondrial isolation through enzymatic digestion (see **section 2.15.2**) or snap-frozen and stored in -80°C until needed for large-scale protein purification (see **section 2.10**).

2.6.2. UCP2 protein expression trials

Glycerol stocks of *S. cerevisiae*, either FGY217 or WB12 cells, were streaked onto SC-ura agar plates supplemented with 2% (w/v) glucose and incubated at 30°C for 3-4 days to allow for colony growth. Pre-cultures were propagated by inoculation of a single colony into 10 mL selective media, with samples grown overnight at 30°C, 225 rpm. Pre-cultures were then inoculated into 80-100 mL selective media for overnight growth at 30°C, 225 rpm. Starter cultures were inoculated into 1 L rich (YP) media and grown for 6-24 hours prior to induction with galactose (final concentration 1%). Cells were incubated for 6-22 hours at 30°C, 225 rpm and harvested by centrifugation (JLA 8.1000 rotor, 4500 rpm, 10 minutes, 4°C). The wide time scales provided for growth prior to and following induction by galactose was due to the growth/expression protocols tested (see **Chapter 3** for details). 10 mL cell culture samples were taken prior to induction and following harvesting to provide a readout for cell growth (through OD_{600}) as well as UCP2 protein expression through immunoblot analysis following small-scale membrane isolation. Cells grown for mitochondrial isolation through enzymatic digestion were used immediately and processed as described in **section 2.15.2**. Cells grown for detergent screening and protein purification were snap-frozen prior to storage at -80°C.

2.7. Large-scale isolation of crude mitochondrial membranes from *S. cerevisiae*

2.7.1. Cell lysis through mechanical disruption using a BeadBeater

Approximately 100 g of yeast cells were thawed and resuspended in ice-cold breaking buffer (100 mM Tris HCl (pH 8.0), 0.65 M D-sorbitol, 5 mM Na-EDTA (pH 8.0), 5 mM aminocaproic acid, 5 mM benzamidine HCl and 1 mM PMSF) in a total volume of 400 mL. Half the cell resuspension was decanted into a metal chamber containing 250 mL ice-cold 500-micron glass beads. The sample was mixed, and the contents topped up with breaking buffer to ensure minimal air in the system following addition of the rotor. The container was insulated with an ice water bath to ensure the temperature was kept at 0-4°C. Samples underwent mechanical disruption for 1 minute, followed by a minute break, for a total of 5 bead beats using the BeadBeater. The resulting homogenate was decanted into a pre-cooled beaker with beads subsequently washed 2-3 times with ice-cold breaking buffer. Lysing of yeast

cells using the BeadBeater was repeated as described for the second half of the cell resuspension buffer reusing the same beads.

2.7.2. Differential centrifugation

Pooled homogenates were transferred to JLA 16.250 Beckman tubes and centrifuged at 4,500 x *g*, for 20 minutes at 4°C. The resulting supernatant was subject to the same centrifugation step to fully remove residual whole cell contamination and cell debris. The resulting lysate was carefully aspirated, transferred to clean JLA 16.250 tubes, before being centrifuged at 28,000 x *g*, for 50 minutes at 4°C to pellet mitochondria. The resulting supernatant was discarded. The crude mitochondrial pellet was gently resuspended using a paintbrush, in minimal volume wash buffer (50 mM Tris-HCl (pH 8.0), 0.65 M D-sorbitol, 5 mM aminocaproic acid and 5 mM benzamidine HCl), before being transferred to JA 25.50 tubes. Samples were topped up with wash buffer and spun down at 28,000 x g for 50 minutes at 4°C to pellet the mitochondria-containing fraction. The supernatant was discarded, and the pellet resuspended as before. The sample was then transferred into clean JA 25.50 tubes, before undergoing the same centrifugation step. The resulting mitochondrial pellet was resuspended in minimal volume TBG buffer (10 mM Tris HCl (pH 8.0), 10% (v/v) glycerol, 500 µM PMSF), homogenised and assayed for protein concentration using the BCA method. Isolated mitochondrial membranes were snap frozen in liquid nitrogen and stored in -80°C.

2.8. Detergent screening for protein solubilisation

Crude mitochondrial membranes were thawed on ice from -80°C storage. To determine the folded state of the protein following yeast mitochondrial isolation, membranes were solubilised under different conditions using mild detergents, such as Triton X-100 (TX-100), dodecylmaltoside (DDM) and lauryl maltose neopentyl glycol (12MNG).

Initial solubilisation tests using mitochondrial membranes isolated from small-scale protein expression trials (as described in **section 2.5**), were conducted in different concentrations of detergent, with membranes being solubilised to give a final protein concentration of 2 mg/mL. The reaction mixtures were made up to a final volume of 150 µL, using either standard buffer (50 mM Tris HCl (pH 8.0), 0.65

M D-sorbitol) or salt/glycerol containing buffer (100 mM Tris HCl (pH 8.0), 10% (v/v) glycerol, 150 mM NaCl, supplemented with 1 protease inhibitor tablet (Roche)).

Preparative solubilisation tests were conducted using mitochondrial membranes from large-scale protein expression and isolated using the BeadBeater (as described in **section 2.7**). Membranes were solubilised at final concentration ranging from 2 mg/mL to 10 mg/mL with different detergent concentrations, to a total volume of 1 mL. In experiments where protein stability was tested at different pH, samples underwent buffer exchange via ultracentrifugation prior to solubilisation tests. Pelleted mitochondria were resuspended in new buffer (see **Table 2.5** for buffer compositions), before being solubilised with 0.5% (v/v) 12MNG or 0.5% (v/v) DDM at a protein concentration of 10 mg/mL, with reaction mixtures were made up to a total volume of 1 mL.

For both initial and preparative solubilisation trials, the detergent-membrane mixture was left to solubilise at 4°C for either 20 minutes or one hour. Following protein solubilisation, samples were transferred to ultracentrifuge tubes (TLA 100 and TLA 120.2 for initial (150 µL) and preparative (1 mL) solubilisation tests, respectively), and spun at high speed (~150,000 x *g*, for 20 minutes at 4°C) to pellet unfolded, insoluble material. Throughout the solubilisation procedure, SDS-PAGE samples were taken to determine protein solubility through immunoblot analysis. For details regarding the experimental parameters for protein solubilisation tests, see **Chapter 3** for exploratory solubilisation trials and **Chapter 4** for preparative solubilisation trials.

Table 2.5: Buffers used in preparative (1 mL) detergent screens

Buffer	Composition
bis-Tris buffer	20 mM bis-Tris (pH 6.0) 5 mM aminocaproic acid* 5 mM benzamidine HCl* 1 mM PMSF* 10% (v/v) glycerol
MES buffer	50 mM MES (pH 6.5) 5 mM aminocaproic acid* 5 mM benzamidine HCl* 1 mM PMSF* 10% (v/v) glycerol
Tris HCl buffer	20 mM Tris HCl (pH 8.0) 5 mM aminocaproic acid* 5 mM benzamidine HCl* 1 mM PMSF* 10% (v/v) glycerol
Piperazine buffer	20 mM Piperazine buffer (pH 9.6) 5 mM aminocaproic acid* 5 mM benzamidine HCl* 1 mM PMSF* 10% (v/v) glycerol *Reagent was added fresh on the day

2.9. Purification of UCP1 from native lamb BAT

Ovine UCP1 was purified from native sources using hydroxyapatite and thiol-reactive resins based on methods previously described (19, 179).

2.9.1. Preparation of the hydroxyapatite column

Approximately 7 g of hydroxyapatite (Bio-Rad 130-0420) was mixed and hydrated with 25 mL hydroxyapatite (HA) buffer (20 mM MOPS (pH 6.7), 20 mM Na_2SO_4, 0.16 mM EDTA) for an hour at room temperature. The hydrated slurry was packed into an empty 20 mL Bio-Rad PolyPrep column using a peristaltic pump (Minipuls pump attached with 'blue-blue' 1.65 mm PVC tubing) at a constant flow rate of ~0.7 mL/minute, to give a final volume of 15 mL. Following column packing, the top of the resin was closed by addition of a cotton frit. The column was kept at room temperature until required.

2.9.2. Isolation of mitochondrial carriers by hydroxyapatite

Lamb BAT was obtained from lambs that had died of natural causes during lambing season at local farms and was harvested by Dr. Paul Crichton. Tissue was stored in a liquid nitrogen dry store until mitochondrial isolation. BAT mitochondria were isolated by Dr. Paul Crichton and Danielle Copeman (University of East Anglia) as described in (19). Mitochondria were aliquoted into 100 mg stocks, snap frozen and stored liquid nitrogen dry store until needed. For isolation of *Ovis aries* (Oa)UCP1 protein, 100 mg of BAT mitochondria were thawed and supplemented with water to give a final volume of approximately 5 mL. Samples underwent ultracentrifugation using TLA 120.2 tubes at ~150,000 x *g* for 20 minutes at 4°C to pellet the mitochondrial membranes. The pellet was resuspended in HA buffer supplemented with TX-100 to give a final concentration of 3% and solubilised for 20 minutes at 4°C. Following solubilisation, samples underwent ultracentrifugation as previously described. The insoluble pellet was resuspended in 5 mL distilled water, with a sample being taken for SDS-PAGE. The supernatant containing solubilised protein was carefully aspirated and applied onto a pre-equilibrated hydroxyapatite column. The solubilised fraction was subject to a constant flow rate (0.7 mL/minute) and was chased with 0.5 mL HA buffer equilibrated to room temperature. The sample was left to incubate in the HA column at room temperature for 15 minutes to denature

contaminating mitochondrial carriers, such as AAC. The flow was then restarted with two sequential additions of 1 mL HA buffer, followed by ~10 mL. The first 10 mL eluate was discarded. The following 10 mL elution ('Post HA') fraction, enriched with OaUCP1, was collected on ice and snap frozen in liquid nitrogen. The 'Post HA' sample was stored at in a liquid nitrogen dry store until further use.

2.9.3. Preparation of thiol-reactive resin

300 mg of lysophilised thiolpropyl Sepharose 6B (T8387-Sigma) (TPS) was hydrated in an empty PD10 column with 10 mL de-gassed, distilled water and left rotating for 1 hour at 4°C. After rehydration, the resin was briefly centrifuged (500 x *g*, for 1 minute) to remove water.

2.9.4. Purification of ovine UCP1 using a thiol-reactive resin

The following purification procedure was conducted at 4°C. The 'Post HA' fraction containing TX-100-solubilised OaUCP1 protein was thawed on ice and supplemented with Tris HCl (pH 8.0) and EDTA (pH 8.0) to give final concentrations of 50 mM and 1 mM, respectively. The 'Post HA' fraction was then applied to the thiol-reactive resin and incubated, whilst rotating, for 1 hour at 4°C to allow binding of cysteine residues to the thiol-reactive resin through covalent chromatography. Following incubation with the thiol-reactive resin, the sample was allowed to flow through the resin by gravity flow. The PD10 column containing the thiol-reactive resin with bound proteins were attached onto a peristaltic pump (Minipuls pump attached with 'blue-blue' 1.65 mm PVC tubing), before being washed with 3 mL wash buffer 1 (20 mM Tris HCl (pH 8.0), 0.5% (v/v) 12MNG and 0.5 µg/mL (tetraoleoyl cardiolipin (18:1)) TOCL, 50 mM NaCl, 1 mM EDTA). A second frit was carefully added on top of the resin, then the sample was allowed to flow through the column, before two sequential 1 mL additions were applied. The resin was washed with a further 20 mL wash buffer 1 at a constant flow rate of ~2.5 mL/minute. The sample was subjected to a second wash with wash buffer 2 (20 mM Tris HCl (pH 8.0), 0.005% (v/v) 12MNG and 0.005 µg/mL TOCL, 50 mM NaCl, 1 mM EDTA) whereby an initial 3 mL of wash buffer 2 was added to rinse the column, followed by two sequential 1 mL chases. The sample was washed with 20 mL wash buffer 2 to reduce the detergent and lipid contents in the sample;

following this step the top frit was removed, the column was detached, and the resin subjected to a brief spin (500 x *g*, 30 seconds at 4°C) to remove residual buffer. The resin was subsequently resuspended in 1 mL elution buffer (wash buffer 2 supplemented with 150 mM dithiothreitol (DTT)) and left rotating at 4°C for 20 minutes. After incubation, the column was subjected to a brief spin as previously described. The first eluate ('E1') fraction was recovered and kept on ice. The resin was resuspended in an additional 0.8 mL elution buffer and subjected to another incubation at 4°C under gentle rotation. The second eluate ('E2') fraction was recovered following a brief centrifugation step (2000 x *g*, 1 minute, at 4°C) and kept on ice. Eluates were sequentially applied to a cold PD10 column pre-equilibrated with PD10 buffer (20 mM Tris HCl (pH 8.0), 0.005% (v/v) 12MNG and 0.005 µg/mL TOCL) and chased to give a final chase volume of 2.5 mL buffer. The resulting flow through was discarded. OaUCP1 was eluted from the column by three sequential additions of 0.833 mL of PD10 buffer. The resulting eluate was collected on ice. Protein concentration was determined through BCA assay. The sample was then snap-frozen and stored at -80°C until required for CPM thermostability assays.

2.10. Purification of recombinant human UCP1 protein

2.10.1. Alkali treatment of crude membranes

Alkali treatment of crude mitochondrial membranes were conducted as described by Lee et al. (2015) (19). Approximately 600 mg total mitochondrial membranes, containing human (Hs)UCP1 protein, were thawed from -80°C storage and homogenised using a Dounce homogeniser following resuspension in alkali buffer (100 mM Na_2CO_3 (pH 11.5), 1 mM EDTA). The homogenate was transferred into a pre-cooled beaker, before being topped up with alkali buffer to give a final ratio of 0.6 mL alkali buffer per milligram of membrane. The homogenate was left gently stirring at 4°C for 30 minutes for alkali treatment to remove peripheral membrane proteins (180). Samples were transferred to pre-cooled Type 45 Ti tubes for ultracentrifugation (200,000 x *g* for 40 minutes at 4°C) to pellet the mitochondrial membranes. The pellet was resuspended in alkali treatment wash buffer (20 mM Tris HCl (pH 8.0), 1 mM EDTA and 10% (v/v) glycerol) and homogenised as before. The sample underwent ultracentrifugation as previously described. The resulting pellet was resuspended in minimal volume 20 mM Tris HCl (pH 8.0) and

homogenised prior to determination of protein concentration by the BCA method. The final sample was snap frozen using liquid nitrogen and stored at -80°C until protein enrichment through ion exchange and covalent chromatography.

2.10.2. Removal of contaminating proteins using ion exchange chromatography

Alkali-treated HsUCP1-containing membranes were passed through ion exchange columns, S and Q as described by Lee et al. (2015) (19) with slight modifications. Briefly, 7-10 mg/mL HsUCP1 membranes were solubilised with 12MNG to a final concentration of 2%. Soluble and insoluble material was separated through centrifugation at 75,000 x *g* at 9°C for 50 minutes. The solubilised supernatant fraction was then passed through a pre-equilibrated S spin column (500 x *g* at 4°C) and chased with 2 mL 20 mM Tris HCl (pH 8.0). The resulting S-flow through ('S-FT') fraction was supplemented with 90 mM NaCl before being subsequently passed through a pre-equilibrated Q column. The resulting Q-flow through ('Q-FT') fraction either underwent covalent chromatography with TPS or was snap-frozen and stored in -80°C if purification could not be conducted in a single day. Following passage of the supernatant through both ion exchange spin columns, the resins were washed with 1 M NaCl. Eluted fractions resulting from the wash steps were taken for SDS-PAGE analysis and were named 'S-capture' and 'Q-capture', respectively.

2.10.3. Covalent chromatography using a thiol-reactive resin

Due to discontinued production of the TPS-6B resin, an alternative thiol-reactive resin was sourced, thiolpropyl agarose (TPA) (Stratech THIO-001A-CRE). For recombinant UCP purification using this resin, approximately 1 mL TPA hydrated slurry (equivalent to 300 mg of lyophilised TPS-6B) was spun down (500 x *g*, for 1 minute) to remove ethanol, prior to resuspension in 10 mL de-gassed, distilled water for an hour at 4°C under gentle rotation. The resin was briefly centrifuged to remove water prior to sample incubation.

Following removal of contaminants by ion exchange chromatography, the Q-FT fraction was supplemented with Tris HCl (pH 8.0), NaCl and EDTA to give final concentrations of 50 mM, 50 mM and 1 mM, respectively. Subsequently, the

supplemented Q-FT was mixed with the hydrated TPS or TPA resin in a 50 mL falcon tube and was left rotating for 1 hour in the cold room to enable covalent chromatography of cysteine residues to the thiol reactive resin. After incubation in the cold room, the sample was passed through an ice-cold empty PD10 column by gravity flow. The column was then washed with 100 mL ice-cold TP wash buffer (50 mM Tris HCl (pH 8.0), 50 mM NaCl, 1 mM EDTA, 0.05% (v/v) 12MNG and 0.05 µg/mL TOCL). Residual buffer was removed by a brief centrifugation at 500 x *g* for 1 minute at 4°C. To elute covalently bound proteins, 0.9-1 mL TP elution buffer (TP wash buffer dissolved with 150 mM DTT) was applied onto the closed PD10 column, containing the thiol resin, before being incubated in the cold room for 20 minutes, whilst rotating. Protein was eluted through centrifugation (500 x *g*, for 1 minute at 4°C) and the eluted fraction measured. Another 0.9-1 mL TP elution buffer was applied onto the resin, before being incubated for another 15 minutes to elute proteins that remained bound to the resin. Elution was conducted via centrifugation as previously described and both fractions were pooled to produce the TP elution fraction.

Excess DTT was removed from samples either using a PD10 column or through a Superdex 200 10/300 size exclusion column, pre-equilibrated with TP wash buffer or with SEC elution buffer (10 mM Tris HCl (pH 8.0), 50 mM NaCl, 0.01% (v/v) 12MNG and 0.01 µg/mL TOCL), respectively. Where a PD10 column was used for DTT removal, eluates were applied to column as described in the purification strategy of native OaUCP1 (see **section 2.9.4**). Eluates were sequentially applied to the column and chased to give a final volume of 2.5 mL. The initial flow through was discarded. The UCP1 enriched fraction was subsequently eluted from the column by three sequential additions of 0.833 mL of TP wash buffer. The resulting eluate was collected on ice. When size exclusion chromatography using a Superdex column was conducted for the purification of recombinant UCP protein, the 1.8-2 mL eluate was concentrated to approximately 0.5 mL. The concentrated sample was clarified through a high-speed spin (16,000 x *g* for 10 minutes at 4°C) to pellet aggregates before sample application onto the AKTA Pure. Samples subjected to size exclusion chromatography (SEC), were passed through Superdex 200 10/300 column, at a flow rate of 0.5 mL/minute at 4°C, with fractions dispensed as 0.5 mL

fractions. Fractions corresponding to a second peak (approximate elution volume of 11-12 mL) in the chromatogram were collected and pooled to give the final purified sample. Protein concentration was determined through BCA assay. The sample was then snap-frozen and stored at -80°C.

2.11. Purification of recombinant human UCP2 protein

To optimise human (Hs)UCP2 purification, several conditions were tested. The purification strategy utilised was as described by Lee and colleagues (19), whereby crude mitochondrial membranes were subjected to an alkali treatment prior to contaminant removal by ion exchange spin columns. Subsequently UCP2 protein was separated via covalent chromatography using a thiol-reactive tag.

2.11.1. Ultracentrifugation of crude membranes

Crude total mitochondrial membranes, obtained from large-scale membrane isolation, were thawed from -80°C storage and mixed using a Dounce homogeniser. Membranes that were to undergo buffer exchange into buffers of different pH were topped up with the appropriate buffer, prior to ultracentrifugation at 200,000 x *g* for 45 minutes at 4°C (see **Table 2.5** for composition of different buffers). Pelleted membranes were resuspended with the same buffer and spun as described to ensure that samples were resuspended in different pH. The resulting pellet was resuspended in minimal volume buffer, homogenised and protein concentration was determined using the BCA assay. Ultracentrifuged membranes were immediately used for protein purification following protein quantification by BCA.

2.11.2. Removal of contaminating proteins using ion exchange chromatography

Processed HsUCP2-containing membranes were transferred to 50 mL tubes, with the addition of detergent to give a final concentration of 0.5%. Membranes derived from FGY217 yeast were solubilised in 12MNG, whilst WB12-derived membranes were solubilised in DDM. Alkali-treated membranes were also supplemented with protease inhibitors, 5 mM aminocaproic acid, 5 mM benzamidine HCl, 1 mM PMSF to inhibit proteolysis throughout the preparation. Membranes were left rotating at 4°C for 20 minutes for membrane protein extraction using mild detergents.

Following protein solubilisation, the unfolded material was separated by subjecting the sample to a high-speed spin. FGY217-derived samples were transferred into pre-cooled JA 25.50 tubes and spun for 50 minutes at 75,000 x *g* at 9°C, whilst WB12-derived samples were transferred into pre-cooled Type 70 Ti polycarbonate tubes and spun for 25 minutes at 75,000 x *g* at 4°C. The insoluble pellet fraction containing unfolded protein, was resuspended in distilled water with a sample taken for SDS-PAGE analysis; FGY21-derived and WB12-derived pellets were resuspended in 30 mL and 10 mL water, respectively. The supernatant containing solubilised protein was recovered, then passed through a pre-equilibrated Vivaspin S Maxi column through a slow spin (500 x *g* at 4°C). After complete passage of the solubilised sample, the sample was chased with 5 mL buffer supplemented with 0.5% detergent to wash the S resin, subsequently yielding the S-FT sample. This fraction was then applied onto a pre-equilibrated Vivaspin Q Maxi column and centrifuged as before. Following complete passage of the S-FT, 5 mL buffer with 0.5% detergent was chased to give the Q-FT fraction. Where samples were resuspended in highly alkaline pH, namely over pH 8.0, the Q-FT samples was titrated down to pH 8.0 using Tris-HCl (pH 6.8) in a drop-wise manner. For details regarding the different conditions tested for the purification of recombinant human UCP2, see **Chapter 4**.

2.11.3. Enrichment of human UCP2 using a thiol reactive resin

Enrichment of human UCP2 was conducted as described in **section 2.10.3**.

2.12. Purification of denatured histidine-tagged UCP proteins

2.12.1. Expression and isolation of histidine-tagged UCP inclusion bodies

To generate histidine-tagged UCP proteins, UCP inclusion bodies were expressed in and isolated from C41 (DE3) cells as previously described by Stuart et al. (56) and Echtay et al. (1999) (181). A glycerol stock scraping of C41 (DE3) cells containing pMW172 constructs encoding for an N-terminal histidine-tagged UCP protein were inoculated into 100 mL LB media supplemented with ampicillin (final concentration 100 µg/mL). Cultures were grown overnight at 37°C, 250 rpm. 1 L pre-warmed LB media in 2 L flasks, supplemented with ampicillin (final concentration 100 µg/mL) were inoculated with overnight culture to a starting OD_{600} of 0.2. Cells were

incubated at 37°C for approximately 50 minutes until OD_{600} reached 0.5-0.6, at which protein expression was induced by 1 mM IPTG (final concentration). Cells were grown for 2 hours at 37°C to allow for sufficient protein production, before being harvested (12,000 x *g*, for 15 minutes at 4°C). Cells were rinsed with ice-cold solution A (50 mM Tris HCl (pH 8.0), 25% (w/v) sucrose), then homogenised using a glass Dounce homogeniser to give a total volume of 20 mL. Resuspended samples were supplemented with 5 mg lysozyme, then incubated for 30 minutes at 37°C, 180 rpm. Following lysozyme digestion, the sample was supplemented with 2 mL 10% (v/v) TX-100, 200 µL 500 mM PMSF and 2 mL 0.18 M EDTA, before sonication. Whilst the samples were on ice, sonication was conducted (using a Soniprep 150 Plus ultrasonic disintegrator, MSE), with 30 seconds on half power, followed by a 30 second rest, for a total of 6 minutes. Samples were transferred to JA 25.50 tubes for centrifugation at 43,000 x *g*, for 15 minutes at 4°C to pellet inclusion bodies. For all centrifugation steps (43,000 x *g*, for 15 minutes at 4°C), deceleration rate of the sample was reduced to enable maximal yield of inclusion body pellets. The resulting pellet was resuspended in 10 mL solution B (1 M urea, 1 % (v/v) TX-100, 0.1% (v/v) β-mercaptoethanol, 1 mM PMSF), homogenised, sonicated and centrifuged as previously described. Resuspension in solution B was repeated and the pellet processed. The resulting pellet was then resuspended in 20 mL solution C (20 mM Tris HCl (pH 8.0), 1 mM EDTA, 10 mM β-mercaptoethanol and 0.5% (v/v) TX-100) prior to homogenisation, sonication and centrifugation. Pelleted inclusion bodies were then washed in solution D (50 mM Tris HCl (pH 8.0), 0.1 mM β-mercaptoethanol), homogenised and centrifuged as before. The final pellet was then resuspended in 10 mL solution D, homogenised and transferred to 50 mL tubes before being centrifuged at 15,500 x *g* for 15 minutes at 4°C. Inclusion body pellets were snap-frozen and stored at -20°C.

2.12.2. Purification of histidine-tagged UCP proteins

Purification of histidine-tagged UCP proteins following inclusion body isolation from C41 (DE3) cells was achieved through Ni-NTA affinity chromatography. Purification of inclusion bodies was based on the Ni-NTA Superflow protocol by Qiagen, under denaturing conditions. Isolated inclusion bodies were thawed before resuspension in 10 mL lysis buffer (100 mM Tris HCl (pH 8.0), 8 M urea, 100 mM

NaH_2PO_4). The resuspension was homogenised using a Dounce homogeniser before centrifugation (15,500 x *g*, 10 minutes at 4°C) to pellet insoluble material and particulates. The clarified supernatant was then filtered, using syringe filters with 0.2-0.45 μm pore sizes to further remove any particulates, with sample taken for SDS-PAGE analysis. The clarified, filtered lysate was then applied onto a 1 mL Ni-NTA Superflow cartridge, pre-equilibrated with lysis buffer. Sample was passed through the column at a flow rate of 1 mL/minute using a peristaltic pump (Minipuls pump attached with 'blue-blue' 1.65 mm PVC tubing). The resulting flow-through was collected and a sample taken to give a readout for the unbound flow through ('FT') fraction. The column was subsequently washed with 10 mL wash buffer (100 mM Tris HCl (pH 6.3), 8 M urea, 100 mM NaH_2PO_4) to remove non-specifically bound contaminants; the resulting eluate produced the 'Wash' fraction. Histidine-tagged proteins were eluted from the column with 10 mL elution buffer (100 mM Tris HCl (pH 4.5), 8 M urea, 100 mM NaH_2PO_4), thereby giving the 'Elution' fraction.

Subsequent buffer exchange to remove contaminating urea was achieved through a combination of centrifugal filtration using Vivaspin concentrators with molecular weight cut offs (MWCO) at either 10,000 Da (for histidine-tagged UCP2 protein) or 30,000 Da (for histidine-tagged UCP1 protein), followed by a final desalting step using a PD10 column. To remove the bulk urea, the Ni-NTA column elution fraction was applied onto a 20 mL Vivaspin concentrator, pre-equilibrated with resuspension buffer 1 (20 mM Tris HCl (pH 8.0), 2% (w/v) sarkosyl). The elution fraction was spun at 8000 x *g*, at 4°C until the final volume in the reservoir reached 1 mL. The concentrated eluate was then resuspended and mixed with resuspension buffer 1 giving total volume of 10 mL. The diluted eluate was then subjected to the same spin step, until the volume reached 1 mL, whereby a sample, labelled 'Spin 1', was taken for SDS-PAGE analysis. The sample was then topped up with resuspension buffer 2 (20 mM Tris HCl (pH 8.0), 0.5% (w/v) sarkosyl) to a total volume of 10 mL and spun as previously stated, until the sample was concentrated 1 mL, with a 'Spin 2' sample was taken for SDS-PAGE analysis. Using a PD10 column pre-equilibrated with resuspension buffer 2, residual urea was removed by passing the 1 mL sample through the desalting column, followed by three sequential chases with 0.5 mL resuspension buffer 2. The resulting flow through was discarded. Purified inclusion

bodies were eluted from the column with three sequential additions of 0.833 mL resuspension buffer 2 to give a final volume of 2.5 mL. The final purified sample was assayed for protein concentration using the BCA assay, with the final protein concentration determined using bovine serum albumin (BSA) standards diluted in both sterile distilled water and resuspension buffer 2 to account for absorbance interferences from sarkosyl. Samples taken throughout the Ni-NTA purification protocol were loaded on SDS-PAGE gels for Coomassie staining and immunoblot analysis to determine protein purity.

2.13. Detection of proteins through SDS-PAGE

SDS-PAGE gel samples taken from various experiments were diluted in 3x gel loading buffer (150 mM Tris HCl (pH 6.8), 30% (v/v) glycerol, 6% (v/v) SDS, 3 mM EDTA, 0.03% (v/v) bromophenol blue, 3% (v/v) β-mercaptoethanol) prior to loading onto pre-cast 4-15% Mini PROTEAN TGX polyacrylamide gels (182). Samples were separated with SDS running buffer (25 mM Tris, 192 mM glycine, 0.1% (w/v) SDS) for approximately 30-50 minutes with the current fixed to 20-30 mA per gel. Protein bands were visualised using either InstantBlue Coomassie stain or ReadyBlue Coomassie stain.

2.14. Detection of specific proteins through immunoblot analysis

SDS-PAGE gels containing separated protein samples were transferred onto activated polyvinylidene difluoride (PVDF) membranes by the wet transfer method (183). PVDF membranes were activated with 100% methanol for approximately 30 seconds. Transfers were run at 4°C for 1 hour at a fixed voltage (100 V) using transfer buffer (25 mM Tris, 192 mM glycine, 20% (v/v) methanol). Transfers were conducted with gentle stirring, in the presence of an ice block in the transfer tank to prevent hotspots during the transfer. Following the transfer, blots were briefly rinsed with TBS-T buffer (20 mM Tris (pH 7.4), 150 mM NaCl, 0.1% (v/v) Tween-20), before being incubated for an hour with blocking buffer (5% (w/v) semi-skimmed milk diluted in TBS-T buffer) at room temperature under gentle agitation. Following blocking of non-specific proteins, primary antibody was incubated overnight at 4°C to detect the protein of interest. Horseradish peroxidase (HRP)-conjugated secondary

antibodies were incubated for an hour at room temperature. After each incubation with antibodies, membranes were briefly rinsed three times and then washed three times for three minutes using TBS-T buffer. Antibody solutions were diluted in blocking buffer. Primary antibodies were utilised with the following dilution factors: rabbit 'anti-UCP2' (Millipore 144-157) 1:2000-1:8000; rabbit 'anti-UCP1' (Sigma U6382) 1:5000-1:20,000; rabbit 'anti-UCP1' (Abcam 155117) 1:5000-1:10,000; chicken 'anti-AAC' (AgriSera, custom manufactured) 1:10,000. The UCP1 antibody from Sigma (U6382) was used to track UCP1 expression in native and recombinant yeast systems, whilst the UCP1 antibody from Abcam (155117) was used to for UCP1 protein quantification using inclusion body standards. Secondary horseradish peroxidase (HRP) antibodies were applied using the following dilution factors: goat 'anti-rabbit HRP' (Millipore AP123P) 1:20,000 and 1:5000-1:20,000 against UCP2 and UCP1, respectively; rabbit 'anti-chicken HRP' (Sigma A9046) 1:10,000 against AAC. The signal on blots were developed through enhanced chemiluminescence using the Amersham ECL kit and visualised either on a ChemiDoc XRS+ Gel Imaging system (182), G:Box Chemi-XRQ system (GeneSys) or ChemiDoc MP Imaging system (182).

2.15. Isolation of mitochondria

2.15.1. Isolation of spleen mitochondria from wild-type mice

Mitochondria was isolated from spleen tissue from WT mice (C57BL/6 genotype) (184) to serve as a positive control for Western blot analysis, due to the high relative abundance of UCP2 expression in this tissue (38, 185). Spleen mitochondria was isolated as outlined by Pecqueur et al. (38). Briefly, spleen tissue was isolated and washed with STE buffer (250 mM sucrose, 10 mM Tris-HCl (pH 7.5), 1 mM Na-EDTA), before homogenisation through a Dounce homogeniser with isolation buffer (STE buffer supplemented with 5 mg/mL BSA, 1 mM benzamidine HCl and 0.1 mM PMSF), at a ratio of 5 mL buffer per gram of spleen tissue. The resulting homogenate was then subjected to a low-speed spin (750 x *g* for 10 minutes at 4°C) to remove tissue debris and nuclei. Following centrifugation, the supernatant was filtered through a cell strainer (with a 70 µm cut-off) before being subjected to a high-speed spin (10,000 x *g* for 10 minutes at 4°C) to pellet the mitochondria-enriched fraction. The resulting supernatant was discarded whilst the pelleted mitochondrial

fraction resuspended in isolation buffer using a paintbrush, prior to centrifugation as previously described. After the second high-speed spin, the pelleted mitochondrial fraction was resuspended in minimal volume STE buffer before protein determination through the BCA method. SDS-PAGE gel samples were taken for Western blot analysis. Remaining samples were flash frozen in liquid nitrogen and stored at -80°C until further use.

2.15.2. Isolation of intact mitochondria from *S. cerevisiae*

After harvesting freshly grown cells expressing either HsUCP1 or HsUCP2 protein and the equivalent uninduced controls, respiring yeast cells were subjected to enzymatic digestion by the snail gut enzyme, Zymolyase (AMSBIO 120491), for the isolation of intact, coupled mitochondria for oxygen consumption assays. The following procedure was adapted from (186).

Approximately 20-40 g yeast cells were washed with ambient sterile distilled water, spun down (2,500 x *g* for 5 minutes) and then resuspended in pre-warmed alkaline solution (100 mM Tris SO_4 (pH 9.4), 10 mM DTT) at an approximate ratio of 2 mL alkaline solution per gram of wet cell pellet. Alkaline resuspensions were transferred to sterile flasks and incubated at 30°C under gentle shaking (~80 rpm) to soften the cell wall and ensure it was more susceptible to digestion by Zymolyase (187). W303-1B UCP1 preparations were incubated for 20 minutes, whilst FGY217 UCP2 preparations were incubated for one hour. Due to the long growth time required for UCP2 protein expression, FGY217 cells were incubated in alkaline solution for longer (up to an hour) to ensure disruption of the alkali-sensitive glycopeptide linkages between β1,6-glucan polymers and yeast cell wall proteins (188, 189).

Following incubation, cells were pelleted as before and washed twice in pre-warmed spheroplast buffer (20 mM Tris HCl (pH 7.4), 1 mM EDTA, 1.2 M sorbitol). Subsequently cells were resuspended in 100 mL spheroplast buffer and then transferred to sterile flasks. Samples were taken from both induced and uninduced conditions to check the degree of cell wall digestion by Zymolyase; samples taken in the absence of Zymolyase provided an undigested control. Yeast cell wall digestion was monitored by combining 10 µL yeast cell suspension with 990 µL sterile distilled water and measuring OD_{600}. With increasing cell wall degradation over time, OD_{600}

should decrease as the sample becomes less turbid due to osmotic disruption of spheroplasts in water. Cells were incubated at 30°C under gentle agitation (~80 rpm), in the presence of Zymolyase at a ratio of 5 mg enzyme per gram of wet cell pellet for a maximum of one hour to avoid non-specific digestion by Zymolyase. Samples were taken from each flask every 5 minutes, read three times in a spectrophotometer to determine an average OD_{600} value to determine the degree of cell wall digestion. A decrease in OD_{600} ranging from 60-90% from the undigested control was deemed sufficient for downstream homogenisation (190).

Following sufficient cell wall digestion by Zymolyase, spheroplasts were pelleted at 2000 x *g* for 5 minutes at 4°C, prior resuspension in ice-cold homogenisation buffer (20 mM MOPS-KOH (pH 7.2), 1 mM EDTA, 0.6 M sorbitol, 0.2% (w/v) defatted BSA, 5 mM aminocaproic acid, 5 mM benzamidine HCl and 1 mM PMSF) at a ratio of 5 mL buffer per gram of wet cell pellet. Spheroplasts were washed twice with homogenisation buffer prior to gentle homogenisation. Samples were decanted into pre-chilled Dounce homogenisers and carefully homogenised by 15-30 slow, gentle strokes using a tight-fitting pestle, to ensure the integrity of the mitochondrial membrane. Subsequent homogenates were decanted to pre-chilled 50 mL falcon tubes and centrifuged at 2500 x *g* for 5 minutes at 4°C to pellet cell debris. The resulting supernatant was carefully aspirated, transferred to clean 50 mL falcon tubes, and then subjected to the same spin to remove any whole cell contamination from the mitochondria-containing fraction. The aspiration and centrifugation step were repeated to ensure maximal removal of contaminating whole cells from the sample. The mitochondria-containing supernatant fractions were transferred to clean falcon tubes and subjected to high-speed centrifugation (12,000 x *g*, for 10 minutes at 4°C) to pellet mitochondria. The resulting supernatant was discarded. Using a paintbrush, the pellet containing the mitochondrial fraction was initially resuspended in minimal volume ice-cold SEM buffer (20 mM MOPS-KOH (pH 7.2), 1 mM EDTA, 0.6 M sorbitol), before being washed in a total volume of 45 mL buffer to remove contaminating BSA. The sample underwent another high-speed spin as previously stated, to pellet mitochondria. The supernatant was discarded, and the pellet fraction was resuspended in minimal volume (~500 µL) of SEM buffer. Mitochondrial protein concentration was determined using the BCA method prior to respiratory assays.

2.16. Respiratory assays using isolated mitochondria

Intact mitochondria isolated by enzymatic digestion were subsequently used for respiratory assays to determine oxygen consumption rates in the presence of known UCP1 ligands.

2.16.1. Preparation of the oxygen electrode

Respiratory assays were conducted using a Clarke-type oxygen electrode, Oxytherm+ (Hansatech, Norfolk). The electrode was set up as per manufacturer's instructions. The electrode was set up one day before the respiratory assays were to be conducted, with the electrode left polarised and stirring overnight at room temperature. Electrode calibration was conducted on the same day as respiratory assays, using the 'air saturated water' method. Briefly, sterile distilled water, pre-equilibrated to experimental temperature (30°C), was inserted into the electrode chamber to establish an 'airline' value for oxygen content within the chamber. Once an 'airline' value was determined, sodium dithionite was added to the chamber to establish anaerobiosis within the chamber. Due to inconsistencies with electrode response times following overnight polarisation, the electrode was subjected to anaerobic conditions using sodium dithionite prior to respiratory assays to ensure efficient electrode response times. Electrode responsiveness was considered sufficient when the time taken for the chamber to reach anaerobiosis, following dithionite addition, was less than one minute from the resting 'airline' value.

2.16.2. Experimental set up

Oxygen consumption assays were conducted at 30°C with the stirrer speed set at 50. For each run, 1.5 mL electrode buffer (20 mM MOPS-KOH (pH 7.2), 0.5 mM EDTA, 0.6 M sorbitol, 2 mM $MgCl_2$, 10 mM K_2HPO_4, 0.1% (w/v) BSA) was applied into the oxygen electrode chamber and sealed. Upon reaching a stable value for oxygen content, isolated mitochondrial suspension was pipetted into the chamber giving a final concentration of 0.5 mg/mL mitochondrial protein. The chamber was immediately sealed, and a new baseline oxygen value was determined following addition of mitochondria. Respiratory effectors were added into the to the chamber using Hamilton syringes (see **Table 2.6** for list of effectors added).

Table 2.6: Effectors used in respiratory assays using isolated mitochondria

Effector	Working concentrations	Reason for addition
NADH	3 mM	Respiratory substrate for yeast mitochondria; acts through external NADH dehydrogenases
Succinate	10 mM	Respiratory substrate that is oxidised by complex II
ADP	200 µM	Enables state 3 respiration in the presence of respiratory substrate
FCCP	1 mM	Chemical uncoupler – allows for maximal respiration of mitochondria
CATR	1.5 µM	Inhibitor of AAC – used to detect proton leak mediated through AAC
GDP	100 µM	Inhibitor of UCP1 – used to detect UCP1-mediated proton leak
Oleic acid	6 µM	Activator of UCP1 – used to activate UCP1-mediated proton leak
Oligomycin	1 µg/mL	Inhibitor of ATP synthase – used to detect proton leak through through ATP synthase

2.16.2. Analysis

Oxygen consumption traces were obtained using the OxyTrace+ software (version 1.0.48). Respiratory rates in the presence of ligands were taken in a 10 second window, when oxygen consumption rates in the chamber reached near steady-states. Respiratory rates were normalised to mitochondrial protein load. Respiratory control ratios were calculated by dividing the uncoupled rate (i.e. in the presence of NADH and FCCP) with the rate of substrate alone (i.e. in the presence of NADH) (55).

2.17. SPQ charge flux assays

2.17.1. Sample preparation

Lipid mixtures containing 1,2-dioleoyl-sn-glycero-3-phosphocholine (18:1 DOPC) and tetraoleyl (18:1) cardiolipin (TOCL) were dried to 10 mg aliquots (9.5 mg DOPC with 0.5 mg TOCL) by nitrogen gas. Dried lipids were redissolved in 100% methanol

to remove any residual chloroform and dried by nitrogen gas. Lipid mixtures were stored at -20°C until needed.

For proteoliposome formation, liposome mixtures were resuspended in 'Internal buffer' (30 mM TEA-TES (pH 7.5), 100 mM K^+ (PO_4) (pH 7.5), 0.5 mM (TEA)EDTA (pH 7.5)) and mixed to ensure lipid resuspension. SPQ dye and purified protein samples (either recombinant HsUCP1 or HsUCP2) were sequentially added to the mixture at a final concentration of 2 mM and 20 µg load, respectively. For liposome formation, samples were left rotating at 4°C, with 8 successive additions of Biobeads (4 x 30 mg followed by 4 x 60 mg) applied to the mixture to remove excess detergent. Mixtures were left rotating overnight prior to charge flux assays.

Following overnight rotation at 4°C, liposomes were applied onto a Bio-Rad spin column (Bio-Rad 732-6204) for Biobead removal by centrifugation (~100 x *g*, 30 seconds). To ensure removal of endogenous fatty acids in the proteoliposome mixture, methyl-β-cyclodextrin was added to the resulting eluate to a final concentration of 40 mM and left to incubate on ice for 30 minutes. Samples were then applied onto a cold PD10 column, pre-equilibrated with external buffer (30 mM TEA-TES (pH 7.5), 100 mM TEA^+ (PO_4) (pH 7.5), 0.5 mM (TEA)EDTA (pH 7.5)), and subsequently chased with external buffer to a final volume of 2.8 mL. Liposomes were eluted by 2 consecutive additions of 700 µL external buffer, with liposomes collected as two separate fractions.

2.17.2. Liposome experiments

In a quartz cuvette, 425 µL external buffer and 75 µL liposome samples were resuspended, before being applied into a Cary Eclipse fluorimeter (Agilent). SPQ fluorescence was measured at 334/443nm. In each test, 2.5 µM valinomycin was added following 40 seconds to generate a membrane potential, followed by 2 µM CCCP at 100 seconds to reveal the capacity of the liposomes.

To obtain the internal volume of the liposomes to determine the quantity of proton transfer in rate calculations, liposomes were diluted with external buffer and solubilised with 0.24% (v/v) TX-100. Sequential additions (4-5) of 1 µM SPQ were applied, providing fluorescence readout that could be plotted onto a calibration curve.

To obtain the proton calibration to determine changes in TES^- quenching relative to fluorescence signal, 75 µL liposome samples were resuspended with 425 µL internal buffer and 20 µM nigericin. Sequential additions of 1 M H_2SO_4 was added to the cuvette until the fluorescence signal plateaued.

2.17.3. Data analysis

For proton calibration, Stern-Volmer plots (1/F over $\delta[H^+]$) (191) were produced to normalise for changes in fluorescence with TES^- quenching against H_2SO_4 concentration. Data obtained from the fluorimeter was normalised to fluorescence using these plots. Fluorescence signals obtained from internal capacity runs were plotted as a function of SPQ concentration.

Proton transport rates were estimated by fitting the fluorescence signal obtained following valinomycin signal, using the exponential function 'Plateau followed by one phase association' in GraphPad Prism (version 8), between 40 seconds (the point in valinomycin addition) and 100 seconds (the point of CCCP addition).

2.18. CPM thermostability assays

To determine ligand binding properties of purified proteins, CPM thermostability assays were conducted as described by Crichton et al. (2015) (155), which were developed from those described by Alexandrov and colleagues (192). The thiol-sensitive dye, 7-Diethylamino-3-(4'-Maleimidophenyl)-4-Methylcoumarin (CPM) was used as probe. CPM is intrinsically weakly fluorescent, however its fluorescence intensity increases when reacted with cysteine residues (193).

2.18.1 Preparation of CPM dye

CPM dye was dissolved in DMSO at 5 mg/mL and stored at -80°C until use. For use in thermostability tests, the CPM stock was diluted in assay buffer (20 mM HEPES (pH 7.5), 0.1% (v/v) 12MNG) in a 1:50 dilution, giving the CPM buffer. For each round of thermostability runs, CPM buffer was made fresh prior to use.

2.18.2. Experimental set-up

For each reaction, 2 µg purified protein was resuspended in assay buffer to give a total reaction volume of 50 µL following the addition of 5 µL CPM buffer. Under

standard conditions, experiments were conducted at pH 7.5, with the assay buffer consisting of 20 mM HEPES (pH 7.5), 0.1% (v/v) 12MNG. With HsUCP1 purine nucleotide titration experiments, where experiments were conducted at pH 6.0, the assay buffer was made up using 20 mM bis-Tris (pH 6.0), 0.1% (v/v) 12MNG. In the presence of ligands, the additional volume required for ligand addition would be subtracted from the volume of assay buffer required. The addition of ligands was also used to indirectly determine the quality of the purified protein sample, especially with regards to HsUCP2 purifications. Ligands tested include: CATR, GDP, ADP and aspartate (see **Table 2.7** for rationale). Components were mixed in thin-walled PCR tubes placed on an ice-cold metal plinth, mixed and left to incubate on ice for 10 minutes. Following incubation, tubes were placed in the Rotor-Gene 2plex HRM cycler (Qiagen), where samples are subjected to a gradual temperature ramp from 25-90°C whilst changes in CPM fluorescence were monitored. Increases in temperature results in the denaturation of protein in the sample, exposing internal cysteine residues and enabling the CPM dye to react to form a fluorescent adduct, thereby leading to an increase in fluorescence signal. Using built-in analysis software, an apparent 'melting' temperature was obtained from the derivative profile of the fluorescence signal profile. The apparent melting temperature obtained provides an indicator of relative protein stability.

Table 2.7: Ligands tested in the CPM thermostability assays

Ligand	**Working concentrations**	**Target protein (Effect on protein thermostability)**
CATR	1 mM	ADP/ATP carrier (Stabilising)
GDP	0.1 μM – 1 mM (log titre)	UCP1 (Stabilising)
ADP	0.1 μM – 1 mM (log titre)	
Aspartate	1 mM	HsUCP2 (*Stabilising)

*In the presence of cardiolipin, a stabilising shift should be observed with proposed UCP2 transport substrates (194, 195).

2.19. Gel blot protein thermostability assay

To determine ligand binding properties of proteins from impure samples, the gel blot protein thermostability assay was developed. This novel technique relies on the use of Western blotting and utilises the thiol-reactive reagent, poly(ethylene glycol) methyl ether maleimide conjugated to 2 kilodalton species (PEG-Maleimide-2K), as a probe. Provided that the protein of interest presents solvent-exposed cysteine residues, the detection of folded protein material can be visualised and quantified when coupled with a temperature ramp.

2.19.1. Sample preparation

Mitochondrial membranes obtained from large-scale membrane isolation preparations were thawed on ice, resuspended in either 20 mM bis-Tris (pH 6.0) or 20 mM HEPES (pH 7.5) buffer at a final concentration of 0.5 mg/mL, before being solubilised with 0.1% DDM or 0.1% 12MNG. Membranes were then either left untreated or were treated with 1 mM ligand. With untreated ('no ligand') samples, buffer was added to match the volume added in treated samples. Membranes were briefly vortexed to mix, before being dispensed into 25 µl aliquots in 200 µl thin-walled PCR tubes. Prior to the temperature gradient, all PCR tubes were subjected to a brief spin to ensure that the reaction mixture was at the bottom of the tube. Following the brief spin, samples were stored on a metal plinth on ice to ensure that samples were kept cold until the temperature ramp.

2.19.2. Experimental set-up

For the gel blot protein thermostability assay, a Veriti 96-well thermal cycler (Applied Biosystems), was programmed to cycle in a way that allowed samples to be incubated for 5 minutes at 4°C prior to a transient increase in temperature for 5 seconds, before cooling back to 4°C for another 5 minutes (see **Figure 2.2** for visualisation of sample additions). The graphical interface of this PCR machine displays the live timings of thermal cycles, thereby enabling for application of reagents at the desired times as well as the addition and the removal of samples from the machine following temperature treatment and incubation with PEG-Maleimide-2K.

At the start of the assay, the first set of PCR tubes were placed in the PCR machine, set at 4°C. Using a multi-channel pipette, PEG-Maleimide-2K was simultaneously added to the tubes 5 minutes prior to a 5 second temperature spike (see "+PEG-Mal-2K" downward arrow in **Figure 2.2**). Tubes were left to incubate with a working concentration of 0.5 mM PEG-Maleimide-2K, 5 minutes before and 5 minutes after the transient increase in temperature. Following the 5 minutes incubation with PEG-Maleimide-2K post temperature spike, samples were quenched with DTT (1 mM final concentration) to stop maleimide reacting further with protein thiols and immediately removed from the machine (upward arrow in **Figure 2.2**). Shortly after the temperature spike from the previous sample, tubes for the next temperature spike were inserted into the PCR machine and incubated at 4°C for 5 minutes (see **Figure 2.2** for details). This process is repeated until all the desired temperatures have been tested. The temperature range tested were 30-80°C and 5-65°C for HsUCP1- and HsUCP2-containing membranes, respectively, with temperature spikes sequentially increasing by 5°C intervals. In each set, one sample was quenched with DTT, thereby serving as the 'unlabelled' PEG-Maleimide-2K-free control. Following the assay, samples were supplemented with 3x gel loading buffer, before being run on an SDS-PAGE gel for the purposes of Western blotting. All blots obtained for the gel blot protein thermostability assay were visualised on the G:Box Chemi-XRQ GeneSys system, using the GeneSys software (version 1.5.7.0). Blots were imaged at 1-minute intervals for a total of 5 or 8 minutes for HsUCP1-containing membranes and HsUCP2-containing membranes, respectively.

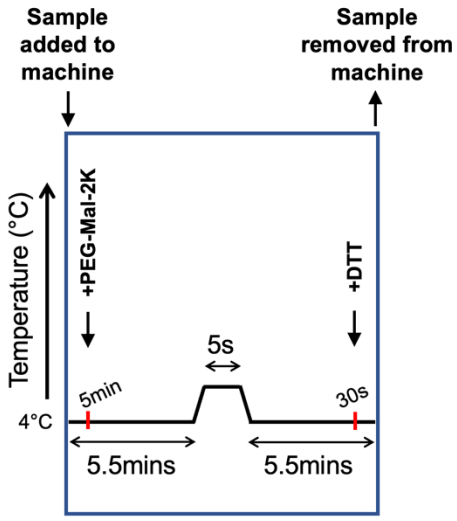

Figure 2.2: Schematic of gel blot protein thermostability assay method using a Veriti 96-well thermal cycler. *Visualisation of thermal cycling method programmed in a Veriti 96-well PCR machine. The programme is set at 4°C for 5 minutes 30 seconds, followed by a 5 second temperature spike which is succeeded by another 5 minutes 30 seconds at 4°C. At each given temperature, PCR tubes are inserted into the thermal cycler when the temperature is set at 4°C. PEG-Maleimide-2K is added to the samples at the 5-minute mark (downward arrow ↓). Samples are then subjected to a pre-determined temperature spike for 5 seconds, before returning to 4°C for another 5-minute incubation with PEG-Maleimide-2K following the transient increase in temperature. After approximately 10 minutes overall incubation with PEG-Maleimide-2K, samples are quenched with DTT and removed from the PCR machine at the 30 second mark (upward arrow ↑). During the 5-minute incubation period following the temperature spike of the preceding sample, samples that will be subjected to the next temperature spike are applied to the PCR machine at the 5-minute mark as previously described. This procedure is repeated for all the samples until all the desired temperatures have been tested.*

2.19.3. Data Analysis

To generate an apparent protein melting temperature, Western blots were subjected to densitometric analysis, with the normalised data modelled to a version of the Boltzmann sigmoidal equation to show protein unfolding.

Densitometric analysis of chemiluminescent images generated following 5 minutes exposure were conducted using ImageJ. For each lane, peaks representative of

protein signals for the 'unlabelled' (33 kDa) and 'PEGylated' (>33 kDa) protein samples were delineated to quantify signal intensity. The total fraction of folded protein for each lane was calculated as the sum of the signal intensity for the unlabelled and PEGylated readouts (see **Figure 2.3**). To produce a protein 'melting' profile, the fraction of folded protein for each lane was normalised to the average signal intensity of the first two PEGylated lanes (**Equation 1**). These first two lanes with sample held at the lowest temperatures, were taken to represent folded protein. Two lanes were used rather than one to reduce the impact of error deviation from just one lane (e.g. a loading error) when carried across the data through to normalisation. This method of normalisation also controls for potential errors between datasets that are difficult to control, such as discrepancies in transfer efficiency between Western blots. Furthermore, the use of the first two PEGylated lanes ensures that the data is normalised to folded protein in the sample rather than the total signal obtained from the "unlabelled" lane, as this may contain unfolded material (see **Figure 2.3** for clarification on data analysis pipeline).

Equation 1:

$$Fraction\ folded\ protein = \frac{Signal\ intensity\ per\ lane}{(Signal\ intensities\ of\ first\ 2\ PEGylated\ lanes)/2}$$

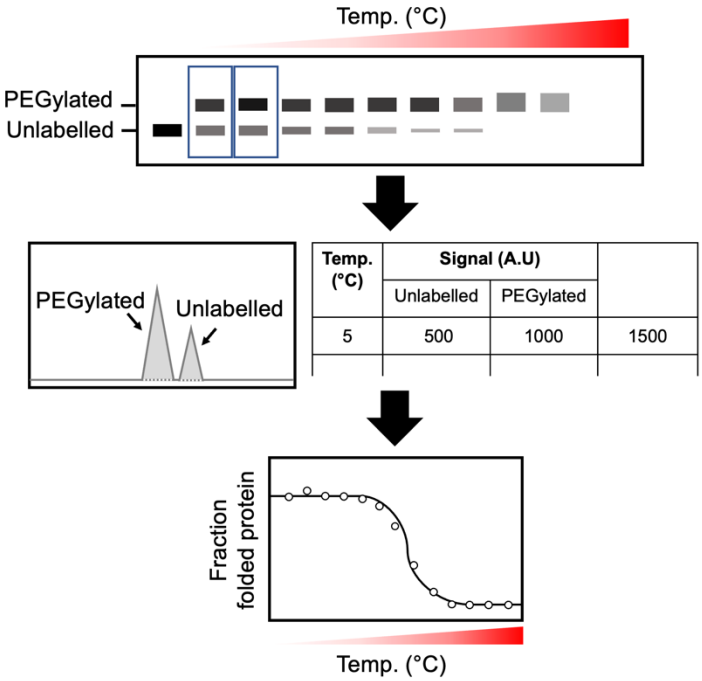

Figure 2.3: Data analysis pipeline of gel blot protein thermostability assay following Western blot visualisation. *Chemiluminescent images of the gel blot protein thermostability assay samples generated following 5 minutes exposure were analysed on ImageJ. Lanes were highlighted using the rectangular selection tool, with histograms displaying the relative protein signal intensity being presented as peaks. Peaks corresponding to the signal intensity of unlabelled and PEGylated protein species at each given temperature (represented by one lane) were outlined, ensuring that the bottom of the peaks were aligned to the baseline signal. Using the magic wand tool to quantify the area under the curve, raw values can be extracted from the histograms and collated in Excel, where the fraction of folded protein can be calculated. The fraction of folded at each given temperature is then normalised to the average signal intensity of the first two PEGylated lanes (in this schematic, lanes 2 and 3). Normalised data is then inputted into GraphPad Prism and fitted onto an adapted Boltzmann sigmoidal curve (**Equation 2**), from which an apparent protein melting temperature can be obtained.*

Normalised readouts were plotted as a function of temperature in GraphPad prism. The observed trends were modelled onto an "inverted" Boltzmann sigmoidal curve (**Equation 2**). The Boltzmann equation has been applied in differential scanning fluorimetry (DSF) to determine protein thermostability. In DSF, the fluorescence signal transitions from a low to a high signal intensity (196), as is observed in CPM thermostability assays, as the fluorescence signal is indicative of the cysteine residues

reacting with the fluorophore, hence the increase in fluorescence. In the case of the gel blot protein thermostability assay, a disappearance in signal is observed, hence the normalised data is fitted onto an "inverted" Boltzmann sigmoidal curve, modelled from dose-response curves with 4 parameters (197):

Equation 2:

$$Apparent\ Tm\ (°C) = \frac{Top + (Bottom - Top)}{(1 + (\frac{x}{Tm})^{Slope})}$$

where the 'Top' value is defined as the maximum y value, 'Bottom' is the minimum y value and 'slope' is the gradient of the curve. Through this equation an apparent protein melting temperature generated as the T_m value, which is defined as the x value given at the midpoint value of y.

3. Expression of human Uncoupling Protein 2 in *S. cerevisiae* mitochondria

3.1. Introduction

Since the discovery of the UCP1 homologues (UCP2-5) (4-8), many researchers have questioned the function of these proteins. Whilst the physiological role of UCP1 in brown adipose tissue is very well characterised (36), the role of UCP2 remains widely contested (110, 198). A significant issue that has hampered past efforts to study UCP2 function, is its limited abundance (38, 185) and stability (41, 46) in native tissues. Whilst some mitochondrial carriers more abundantly expressed in native sources have been successfully isolated for the purposes of structural (137) and functional analyses (17, 179, 199, 200), this is an impractical avenue for the isolation and purification of UCP2 protein. Hence, the use of heterologous expression systems is required to produce enough protein for purification efforts (201).

Bacterial expression systems have routinely been used for heterologous overexpression of membrane proteins, owing to their practicality and the high protein yields, with *E. coli* being the most used bacterium for recombinant protein expression (202). Production of mitochondrial carriers in *E. coli* systems, tends to generate unfolded inclusion bodies (203-206), with high levels of the expressed protein proving lethal to the host cell (165). The use of specifically engineered bacterial strains (C41 (DE3) and C43 (DE3)), tolerant of membrane protein overexpression (165), have been utilised in the study of mitochondrial carrier proteins. In such experiments, where mitochondrial carriers are generated as inclusion bodies, protein is purified and refolded prior to reconstitution into liposomes for metabolite transport studies (93, 203, 207-210). Other types of bacteria have also been utilised in membrane protein production, including the Gram-positive bacterium, *L. lactis* (211). Expression of functional eukaryotic membrane proteins has been demonstrated using *L. lactis* (212), including various mitochondrial carriers, such as the ADP/ATP carrier (AAC), the dicarboxylate carrier (54), the GDP/GTP carrier (213) and the human mitochondrial citrate carrier (214); though in some cases expression levels of mitochondrial carriers in *L. lactis* did not correlate with activity

(211). Previous unpublished work has demonstrated that expression of UCPs, including human UCP2, in *L. lactis* did not necessarily yield folded protein (215). Whilst bacterial systems have proven suitable for the expression of many soluble proteins and some membrane proteins (165, 216), it has been demonstrated by numerous researchers that mitochondrial carrier material generated in *E. coli* is extractable in widely used zwitterionic detergents, such as DPC, but in an incorrectly folded form (155, 158-162). Consequently, expression of UCP2 in bacterial systems has led to misinterpretations regarding the protein's structural and functional properties (163).

An avenue used to overcome the generation of misfolded membrane proteins is by using recombinant protein expression in eukaryotic systems, such as yeast. Utilisation of yeast expression systems have been successful in the expression of mammalian membrane proteins (217, 218). Various mitochondrial carriers have successfully been expressed in yeast in a functional form, including AAC (141, 145, 147, 152), the ATP-Mg/phosphate carrier (219), the mitochondrial pyruvate carrier (220, 221) and the oxodicarboxylate carrier (222). UCPs have also been expressed in yeast (55, 56, 93, 114, 153, 177, 178, 223, 224), with various studies utilising pYES2 inducible expression systems to control for recombinant protein expression (55, 56, 93, 114, 153, 177, 178, 223, 224), whilst others have demonstrated the generation of functional protein through functional complementation experiments (114). Whilst UCPs have been expressed in yeast, protein overproduction has been reported to produce expression artefacts which have led to conflicting conclusions about the function of these proteins (54-56, 225).

This chapter describes the development and optimisation of a yeast expression system to produce intact UCP2 protein for subsequent purification efforts and functional studies.

3.2. Aims

1. To develop and optimise a recombinant yeast expression system capable of producing practical amounts of UCP2 protein for downstream protein purification studies.
2. To verify that the protein produced in this recombinant system is appropriately folded by solubilisation tests in the presence of mild detergents.

3.3. Results

3.3.1. Small-scale UCP2 expression trials based on a UCP1 expression protocol

To produce UCP2 protein in yeast, a pYES2 expression vector system (170) was used where UCP2 gene expression is controlled by a galactose-inducible promoter. The vectors used included a codon-optimised UCP2 gene with a Kozak translation initiation consensus sequence at the 5'-end for protein expression in yeast.

For initial protein expression trials, two variants of the UCP2 construct were tested, where notable differences occur in the 5'-region of the UCP2 gene. Construct 1, created by Dr. Martin King (MRC Mitochondrial Biology Unit), consists of an adenine-rich Kozak sequence ("CTCAAAAAATGT") and substitutes the second amino acid from the native valine to leucine. Adenine-rich Kozak sequences are common in the mRNA of highly expressed genes in yeast (226), which may enhance gene expression through the formation of unstructured regions encouraging ribosomal binding and translation (227). Alteration of the second amino acid to leucine from the native valine was a constraint to retain relevant restriction sites for potential cloning into *L. lactis* expression vectors (145). Construct 2, produced by Dr. Paul Crichton and Danielle Copeman (University of East Anglia), includes a shorter Kozak sequence ("CTCATAATGG"), which has proven successful for UCP1 expression (171), and retains the full wild type UCP2 amino acid sequence (see **Figure 3.2** for schematic). UCP2-containing expression vectors were transformed into two yeast strains: the wild-type, W303-1B, and the protease-deficient, FGY217. Whilst the W303-1B strain has been routinely used for mitochondrial carrier protein

expression (55, 56, 93, 114, 153, 177, 178, 223, 224), the FGY217 strain was screened due to its efficacy in expressing membrane proteins (228).

Small-scale growth and protein expression trials were based on UCP1 expression protocols outlined by Arechaga et al. (177) and Echtay et al. (178), whereby overnight cultures were propagated in selective lactate media supplemented with low glucose (SL+G) prior to inoculation into 50 mL YPL growth media. Cultures were grown overnight for approximately 16-17 hours (OD_{600} 4-5) at 30°C, prior to induction of protein expression with 1% galactose. Cells were grown for a maximum of 8 hours, with samples taken at two-hour intervals to provide a readout for cell growth and protein expression (see **Figure 3.1A** for schematic). Exploratory growth trials demonstrated that WT yeast did not grow well in overnight cultures or in growth media supplemented with lactate (see **Appendix Table 2.1**), hence the protease-deficient strain was used for all the UCP2 expression trials mentioned throughout this work, unless otherwise stated.

The OD_{600} of 50 mL FGY217 cultures, increased following protein induction, indicating continued cell growth and that UCP2 expression does not affect host cell viability (**Figure 3.1B**). UCP2 protein expression was determined through Western blot analysis of isolated mitochondrial membrane fractions. Initial attempts to detect UCP2 at varying times after induction using the anti-UCP2 Abcam probe (ab97931) without high background were unsuccessful (**Figure 3.1D** and **Appendix Figure 2.1**), though clear visualisation of UCP2 in Western blots was achieved with the Millipore antibody (Millipore 144-157) (**Figure 3.1C**). A reason for differences in protein visualisation could be due to the epitope in which the antibodies have been raised against; the Abcam anti-UCP2 probe targets a highly hydrophobic region of the protein (residues 250-309) (229), which may be inaccessible following denaturation by SDS-PAGE, whereas the Millipore antibody recognises matrix loop residues (230), which could arguably be more accessible as the residues would be more polar in nature and may disfavour interactions with the hydrophobic transmembrane domain of the protein. Use of the Millipore UCP2 antibody revealed signals consistent with the successful production of UCP2 in yeast mitochondria, but with a clear difference in protein expression between the constructs tested. Based on densitometric analysis, construct 1 shows an almost 4-fold increase in protein expression compared to construct 2 following four hours expression. Importantly, for

both constructs, samples taken from the uninduced (0 hour) cells show no UCP2 protein signal in blots, prior to galactose addition, as would be expected in this galactose-inducible UCP2 expression system. Whilst 30 μg of mitochondria isolated from mouse spleen, which have the highest detectable amounts of UCP2 (185), was used as a positive control, it did not show a UCP2 signal following 5 minutes exposure time (final lane in **Figures 3.1C-D**). The absence of UCP2 signal from isolated spleen mitochondria may relate to differences protein expression and the limited detection range of the blots, where the recombinant system contains greater amounts of UCP2 protein compared to native tissue. Importantly, the Millipore antibody and expression pattern validates UCP2 protein production in our inducible system, hence it is used for the detection of UCP2 protein in subsequent immunoblots.

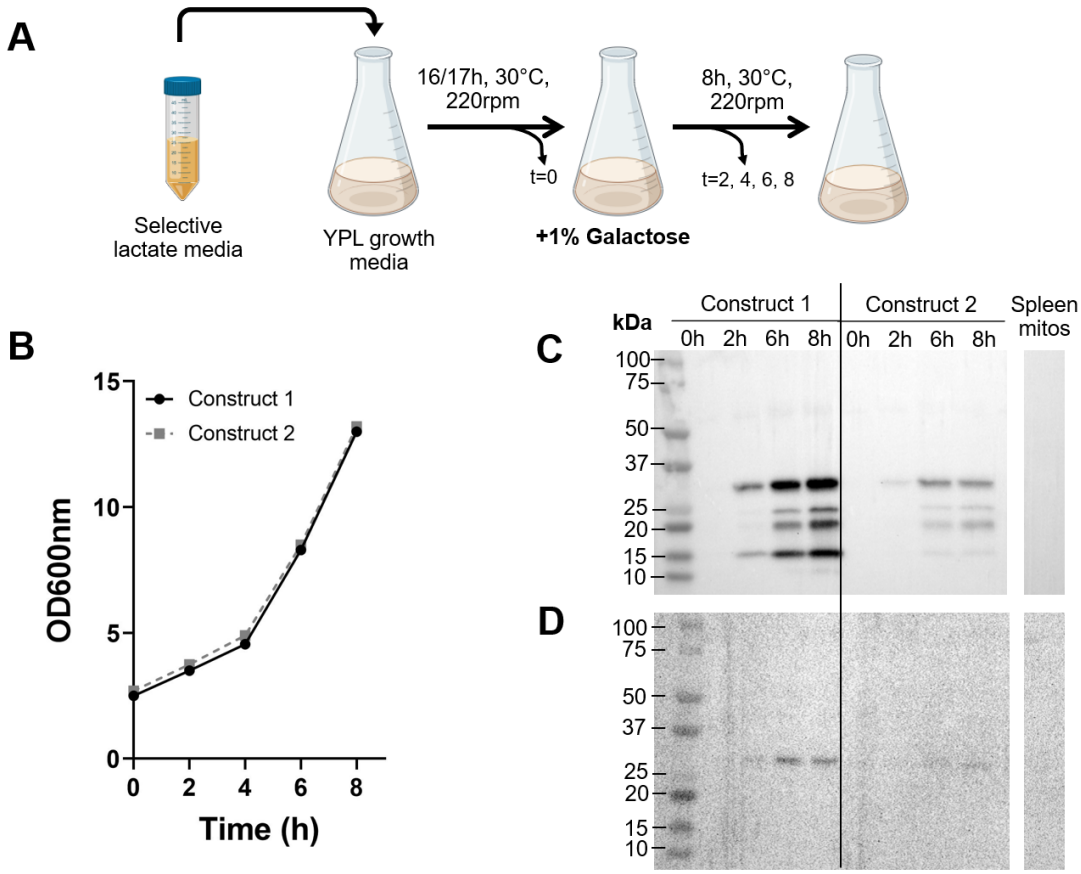

Figure 3.1: Initial HsUCP2 protein expression trials using a UCP1-based expression protocol. *A) Schematic of small-scale (50 mL) protein expression trials based on UCP1 expression protocols (177, 178). Illustrations obtained from BioRender. B) Growth of FGY217 HsUCP2 cells transformed with constructs 1 and 2 following induction of protein expression by 1% (v/v) galactose (time = 0h). Growth was monitored by OD_{600} of cultures harvested at 2-hour intervals. C-D) Western blots of UCP2 expression trials probed with the Millipore (144-157) (C) or Abcam (ab97931) (D) antibody. For immunoblot analysis, 10 µg yeast mitochondrial membranes were loaded and 30 µg spleen mitochondria was used to serve as a positive control given its high relative abundance of UCP2 protein from native sources (185). Times indicated above lanes indicate to the time cells were harvested following protein induction by galactose (0h).*

To determine which difference in construct 1 was likely responsible for increased protein expression observed, one of the two main differences from construct 1 was systematically introduced into construct 2, to generate two new constructs. The production of construct 3 substitutes the second amino acid from valine to leucine,

whilst pairing it with an adenine-depleted ("CTCATAATGT") Kozak sequence. Conversely, construct 4, introduces an adenine-rich ("CTCAAAAAATGG") Kozak sequence upstream of the fully WT UCP2 coding region (see **Figure 3.2** for schematic and **Appendix 1.2** for sequencing alignment data).

Further small-scale (50 mL) protein expression trials using *S. cerevisiae* cells transformed with either constructs 1, 2, 3 and 4 were conducted simultaneously as previously described. Comparative immunoblot analysis revealed increased UCP2 protein production from membranes derived from cells transformed with constructs 1 and 3 specifically (**Figure 3.2**). Both these constructs share the substitution of the second amino acid to leucine, thereby highlighting how a subtle alteration in the N-terminal end of the protein leads to increased protein expression (231). Subsequently, FGY217 cells transformed with either construct 1 or construct 3, referred to as "high-expressing" constructs, were carried forward for further experiments.

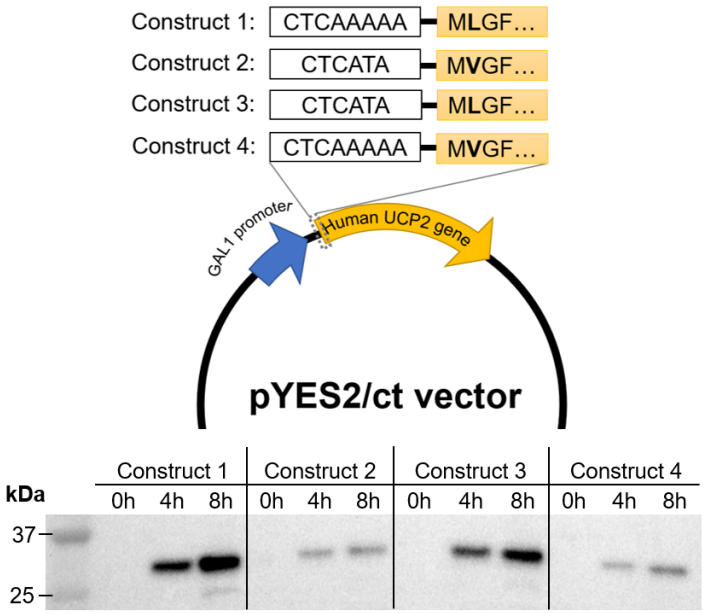

Figure 3.2: Differential levels of UCP2 protein expression from four different constructs. *Schematic of the pYES2 construct highlighting differences between constructs 1-4, around the translation site of the HsUCP2 gene. Western blot comparing UCP2 protein expression from mitochondrial membranes derived from FGY217 cells transformed with one of four constructs, as indicated (bottom). 10 µg yeast mitochondrial membranes were loaded into each lane; time above lanes indicate the time cells were harvested, with 0 hours (0h) representing cells harvested prior to galactose induction.*

3.3.2. Solubilisation trials

To determine if protein produced using the FGY217 recombinant system was folded, solubilisation trials were conducted with non-ionic, mild detergents such as TX-100, DDM and 12MNG. These detergents were tested as they can solubilise and retain UCP1 and other mitochondrial carriers in a folded state but are unlikely to be harsh enough to solubilise unfolded protein (19, 155, 179, 232). As such, solubilisation tests using these detergents can report on the folded state of the protein whereby folded and unfolded material can be separated following high-speed centrifugation, and the UCP2 content in the respective supernatant and pellet fractions, quantified.

In tests, UCP2 produced using both "high-expressing" constructs did not solubilise well in 1% TX-100, where little or no UCP2 protein could be extracted in the supernatant (see supernatant (S) lane, **Figure 3.3**). At lower TX-100 concentration (0.3%), higher amounts of UCP2 (~20%) appeared to be soluble but only for construct 1 (not 3) (**Figure 3.3**). In comparison, consistently higher levels of UCP2 could be extracted using 1% 12MNG, where ~25% of the total UCP2 protein could be extracted from the membrane, regardless of which construct was used for expression (**Figure 3.3**). This is consistent with the observation that maltose neopentyl glycol type detergents have been successful in solubilising intact eukaryotic membrane proteins in a stable form (233-236), including UCP1 from native (19) and recombinant sources (153, 237).

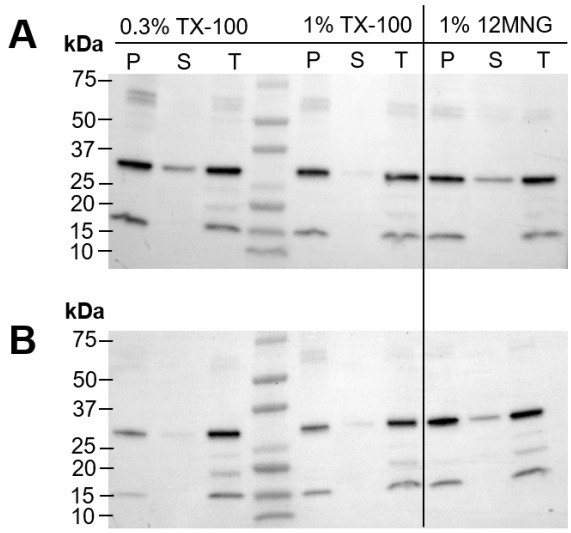

Figure 3.3: Initial solubilisation screens conducted with UCP2. *Western blots of solubilisation tests conducted with TX-100 and 12MNG using mitochondria extracted from "high-expressing constructs", construct 1 (A) and construct 3 (B). Samples are loaded as a fraction of the total volume and labelled as: T - total protein; S – solubilised supernatant; P – insoluble pellet.*

Various other parameters, such as buffer composition, detergent type, and detergent concentration were tested to determine if extraction of intact UCP2 from mitochondrial membranes could be improved. Two buffers were tested to determine if components such as salt and glycerol could aid UCP2 solubilisation. As 12MNG was successful in extracting UCP2 protein from membranes, the related detergent, DDM, a mild, non-ionic detergent that has been used in the solubilisation of various eukaryotic membrane proteins (238, 239), including the AAC (141, 147), was also tested. The detergent concentration was also increased to establish if this was a limiting factor.

Minimal differences were observed when membranes from "high-expressing constructs" were solubilised with 12MNG or DDM (see **Figure 3.4** (construct 1 results) and **Appendix Figure 2.2** (construct 3 results)), suggesting that either detergent is equally effective for further solubilisation screens. It was found that similar levels of UCP2 could be extracted from membranes using 2% and 4% 12MNG (**Figure 3.4B** and **Appendix Figure 2.2B**), suggesting maximal extraction had been achieved at 2%. Introduction of salt and glycerol in the buffer, only appeared to reduce the fraction of UCP2 solubilised by detergent (see pellet (P)

fractions, under 'Solubilisation buffer' conditions in **Figure 3.4A** and **Appendix Figure 2.2A**). Salt and glycerol are used in preparative solubilisations where higher protein concentrations are ~10 mg/mL; addition of these components in small-scale (150 µL) solubilisation tests where protein concentration is 5-fold less (2 mg/mL) could have negatively affected extraction of intact UCP2 from membranes, hence the lower signals seen in the solubilised supernatant fractions. Overall, these results indicate that at least one third of UCP2 protein produced in this recombinant system can be extracted from mitochondrial membranes using mild detergents in a form that would be suitable for downstream functional characterisation.

Subsequently, larger-scale UCP2 expression tests were conducted to support protein production. Construct 1 was chosen as the default for larger-scale expression as initial immunoblots demonstrated that UCP2 protein generated using this construct produced marginally higher levels of UCP2 protein (**Figure 3.2**).

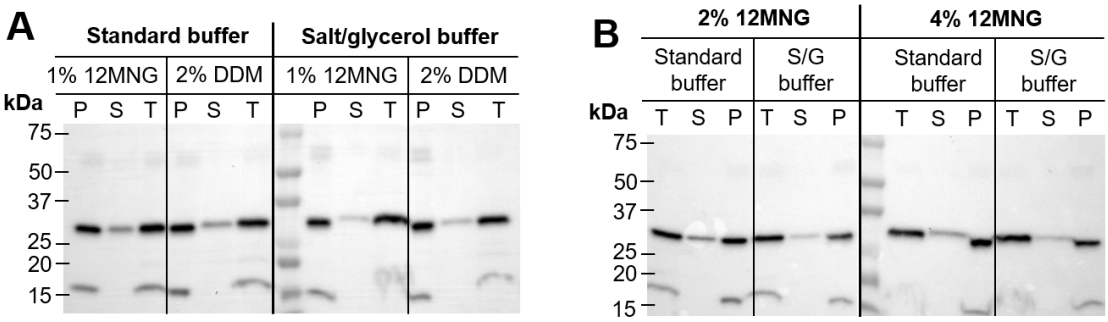

Figure 3.4: Investigating UCP2 solubility under different solubilisation conditions. *A-B) Western blots of (construct 1-expressed) UCP2 solubilisation fractions, following extraction with mild, non-ionic detergents, 12MNG and DDM. Samples were resuspended either in 'standard buffer' (50 mM Tris HCl (pH 8.0), 0.65 M D-sorbitol) or 'salt/glycerol buffer' (100 mM Tris HCl (pH 8.0), 10% glycerol, 150 mM NaCl supplemented with a protease inhibitor tablet) as denoted above lanes ('salt/glycerol buffer' is abbreviated to 'S/G buffer' in B). Samples are loaded as a fraction of the total volume and labelled as: T - total protein; S – solubilised supernatant; P – insoluble pellet.*

3.3.3. Expression trials based on an FGY217 strain-tailored expression protocol

Small-scale expression tests were progressed to larger scale to assess if UCP2 production was sufficient for downstream purification. Initial larger-scale (1 litre)

UCP2 expression attempts, using the previously outlined UCP1 expression protocol, demonstrated that FGY217 growth on lactate was economically impractical for the purposes of protein purification. In 12 litres of culture, approximately 30 g of cell pellet was obtained, thereby averaging 2.5 g cell pellet/L culture. In contrast, human UCP1 (HsUCP1) expression in W303-1B cells produced economically feasible amounts of cell pellet per litre flask (averaging 25 g cell pellet/L culture) (171), which suggests that growth on lactate may be limiting for the protease-deficient strain.

Further protein expression optimisation screens were inspired by a protocol outlined by Drew and colleagues, which details a method for screening membrane protein expression in *Pep4* deleted yeast strains, such as FGY217 (228). In this protocol, FGY217 cells are seeded from plates into a selective (SC-ura) starter media supplemented with 2% glucose before being inoculated into SC-ura growth media containing 0.1% glucose, to a starting OD_{600} of 0.12. Cells are cultured to an OD_{600} ~0.6, at which point protein expression is induced with 2% galactose for 22 hours at 30°C (see **Figure 3.5A** for schematic). To see if intact UCP2 expression and overall biomass could be improved, the Drew et al. (2008) protocol (228) was attempted with several variables included to aid optimisation. The following conditions were investigated: starter and growth media composition, galactose concentration and growth temperature following induction in small-scale (10 mL) trials (see **Figure 3.5A** for variables altered). Starter media refers to the selective media in which single colonies are propagated and grown in before protein expression; different glucose concentrations were tested to determine if glucose concentration in starter media affected protein expression. Growth media describes the media in which overnight starter cultures are inoculated into and where protein expression occurs. SC-ura media was used to replicate conditions outlined by Drew et al. (228), while the use of YPD or YPL as growth media were also tested to determine if rich media, albeit lacking plasmid selection pressure, could increase overall cell biomass and UCP2 production. Two galactose concentrations were tested to determine if 2% was required as outlined by Drew and colleagues (228). Reducing the temperature following induction was also assessed for its potential to increase the quality of UCP2 protein produced.

Propagation of cells in starter media supplemented with low or high concentrations of glucose showed no obvious trend with regards to cell growth (**Figure 3.5B)**. Cells cultured in SC-ura growth media generally grew to lower densities than cells cultured in rich (YP) growth media (**Figure 3.5B**). Whilst cells cultured in SC-ura growth media demonstrated a minor temperature- and galactose-dependent increase in growth, equivalent trends relating to the specific changes observed with cells cultured in YPD (0.1%) glucose or YPL media were less clear (**Figure 3.5B**). Minimal differences were observed in UCP2 protein expression in cells grown in rich (YP) media (**Figure 3.5D** and **3.5E**), regardless of the glucose concentration in the starter culture. However, protein expression of cells grown in SC-ura media demonstrated a drastic decrease in UCP2 production when propagated in 2% glucose starter culture (**Figure 3.5C**). Moreover, cells incubated in SC-ura growth media, in general, demonstrated higher UCP2 expression when grown at 30°C (**Figure 3.5C**), which was independent of the galactose concentration used for protein induction. Trends observed in selective media could be attributed to the notion that selective media has predefined amounts of components, whereas the exact nutrients in yeast extract-peptone (YP) based media are variable which could be one reason why no obvious trend in UCP2 protein expression when grown in rich media (240). In this small-scale expression screen, it was found that cells incubated at 30°C following galactose induction demonstrated higher levels of UCP2 protein compared to those incubated at 25°C following protein induction. This is consistent with the fact that at higher temperatures, there would be higher rates of translation hence increased levels of protein production (241). UCP2 protein expression was largely unaffected by the increase in galactose concentration, demonstrating that 1% galactose is sufficient for the purposes of protein induction and is not limiting. Therefore, subsequent expression trials will utilise 1% galactose for protein induction, with cells cultured at 30°C.

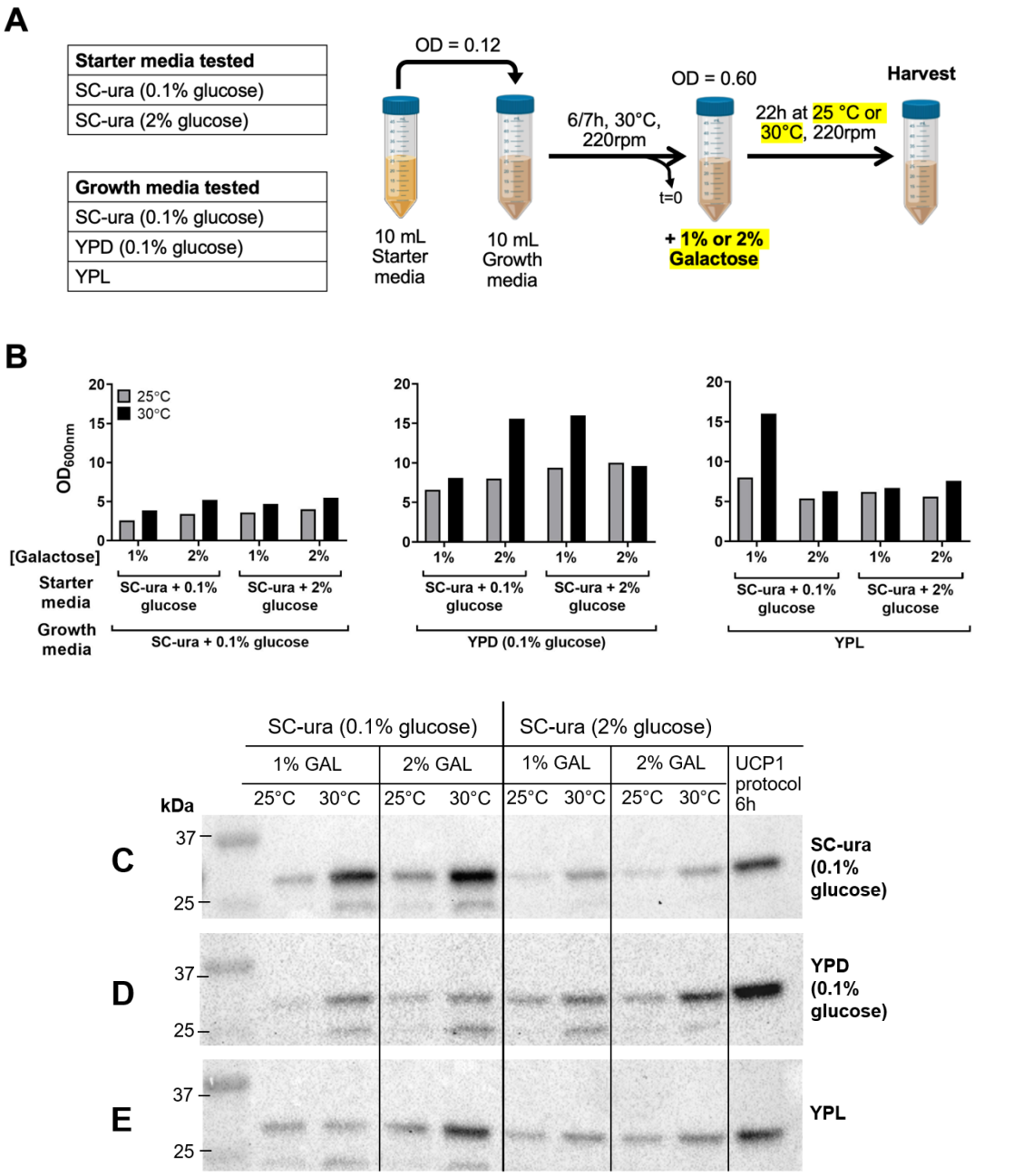

Figure 3.5: Small-scale (10 mL) expression trials based on an expression protocol tailored for protease-deficient yeast strains. *A) Schematic of small-scale (10 mL) protein expression trials based off a membrane protein expression protocol outlined by Drew et al. (228). Differences in selective and growth media are summarised in tables, whilst differences in galactose concentration and induction temperatures are highlighted in yellow. Illustrations were supplied courtesy of BioRender. B) FGY217 cell growth determined through* OD_{600} *measurements following 22 hours induction in varying conditions. Samples were propagated in selective (SC-ura) media containing either low (0.1%) or high (2%) glucose, before being*

inoculated into either growth media: SC-ura (0.1% (w/v) glucose), YPD (0.1% (w/v) glucose) or YPL. Samples were incubated at 30°C until induction of protein expression with either 1% or 2% galactose. Subsequently samples were incubated at either 25°C (grey bars) or 30°C (black bars) following induction and harvested after 22 hours. UCP2 protein expression at 22 hours was determined by Western blots, with cultures cultivated either in SC-ura (0.1% (w/v) glucose) (C), YPD (0.1% (w/v) glucose) (D) or YPL media (E). UCP2 protein expressed using the previously outlined UCP1 protocol were loaded to compare relative protein levels between expression methods ('UCP1 protocol 6h' lane). In each lane, 10 µg yeast mitochondrial membranes were loaded. Small-scale (10 mL) expression trials were conducted once to screen UCP2 protein expression.

The results from the small-scale (10 mL) expression screen suggest that UCP2 production using a strain-tailored expression protocol (228), generally produced less protein than the original UCP1-based protocols (177, 178) (**Figure 3.5C-E**). Whilst cells grown at UCP2 protein expression grown at 30°C in SC-ura media demonstrated similar levels as the UCP1 based protocol (**Figure 3.5C**), it is unlikely sufficient biomass would be attained in larger-scale growth trials as cells grown in selective media grew to much lower densities than cells cultures in YPD or YPL media (**Figure 3.5B**).

3.3.4. Large-scale UCP2 expression optimisation trials

Following small-scale protein expression screens utilising the Drew method (228), large-scale trials were conducted to determine if sufficient biomass for the purposes of protein purification. Here, "sufficient biomass" is defined as obtaining a cell pellet of equal to or greater than 10 g/L of growth culture. To compare UCP2 protein between each expression method, mitochondrial membranes derived from cells grown using the UCP1 expression protocol were included in Western blot analyses.

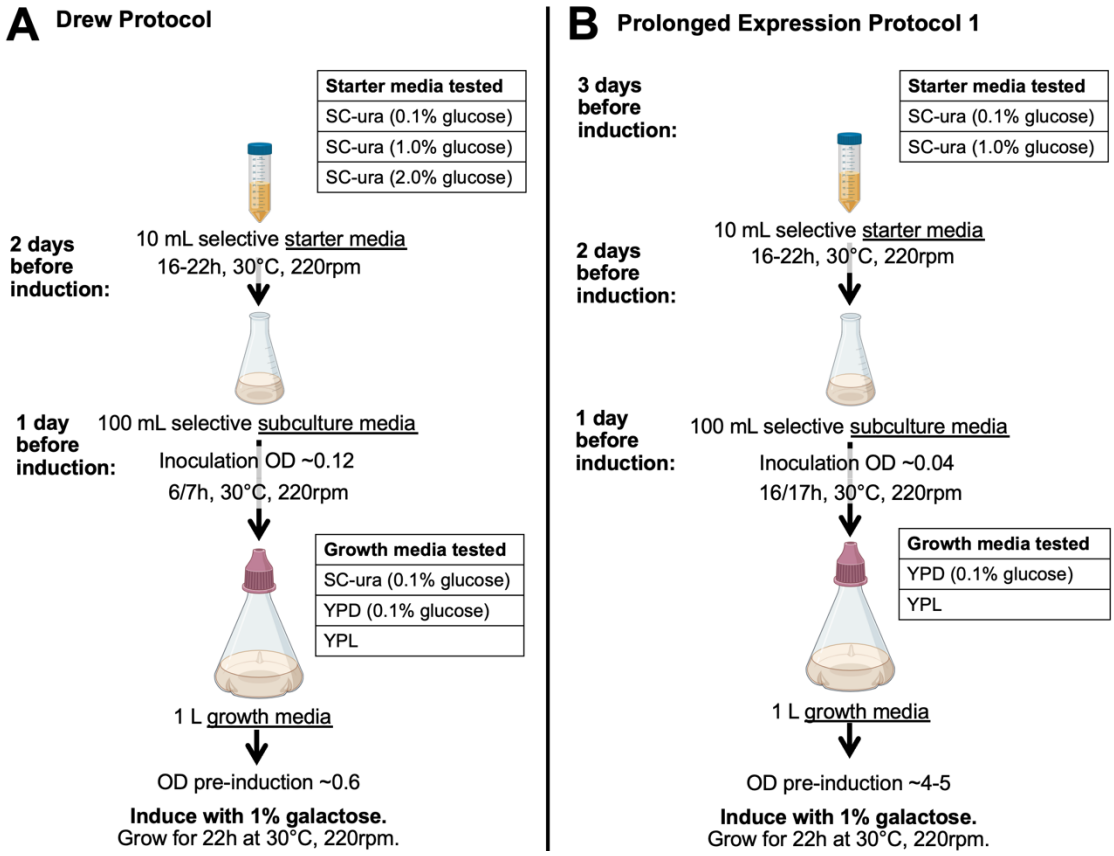

Figure 3.6: Schematics of large-scale expression protocols tested for the optimisation of large-scale UCP2 protein expression. *A) Diagram describing protein expression by Drew et al. (2008) (228). B) Diagram outlining "Prolonged expression protocol 1", a blend of UCP1-based protocols and the Drew protocol. Conditions that were modified in each large-scale expression protocol are summarised in the relevant tables. Illustrations were supplied courtesy of BioRender.*

3.3.4.1. Drew expression protocol

To determine if the Drew protocol was a viable route for larger-scale (1 L) protein expression, screens were conducted. As illustrated in **Figure 3.6A**, a single yeast colony is propagated in 10 mL selective starter media overnight, prior to inoculation into 100 mL subcultures of the same media. Following overnight growth, the subcultures are inoculated into 1 L growth media to a starting OD ~0.12, grown until OD reaches 0.6 (~6/7 hours), at which point galactose is added. Cells are harvested following 22 hours of protein induction at 30°C.

In preliminary screens, cells were propagated in 2% glucose selective starter/subcultures to ensure sufficient growth prior to inoculation in various 1 L

growth media. Cultures grown in selective (SC-ura) 1 L growth media supplemented with 0.1% glucose demonstrated limited growth, producing less than 10 g cell pellet/L culture (**Appendix Figure 2.3A**). Lack of cell growth is likely due to the restricted nutrients available in selective media (240). In contrast, sufficient biomass (>10 g cell pellet/L culture) could be achieved when cells were grown in rich media respiring on either low (0.1%) glucose or lactate (**Appendix Figure 2.3A**). However, UCP2 expression using the Drew protocol showed decreased expression levels compared to the UCP1 expression protocol (**Appendix Figure 2.3B**), which align with results obtained from the 10 mL expression screens (see '30°C' lanes under 'SC-ura (2% glucose) in **Figure 3.5C-E**). Reduced levels of UCP2 expression may be attributed to remaining glucose in the culture, which inhibits the GAL1 promoter of the pYES2 system (242, 243). Based on these preliminary larger-scale tests, the use of selective media as growth media was not economically viable for further protein expression efforts as cell growth and protein expression was limited with the Drew protocol.

Whilst increasing protein expression time in rich media supplemented with glucose or lactate addressed biomass concerns, UCP2 expression was reduced compared to the original UCP1 protocol. Therefore, subsequent large-scale expression screens were conducted to assess whether reducing glucose concentration in the starter/subculture media could enhance UCP2 protein expression. In these experiments, cells were propagated in SC-ura starter media supplemented with either 0.1% or 1% glucose, prior to inoculation into 1 L rich growth media containing lactate (YPL) or glucose (YPD (0.1% glucose)), as outlined in **Figure 3.6A**. Sufficient biomass could be obtained when grown in either YPD (0.1% glucose) or YPL, irrespective of the glucose concentration in the starter media (**Figure 3.7A**). However, a clear difference in UCP2 protein expression was observed, which was dependent on the available carbon source in the growth media. Cultures grown in glucose demonstrated minimal UCP2 protein production when compared to their lactate-respiring counterparts (**Figure 3.7B**). Moreover, cultures grown in YPL, as described by Drew and colleagues, showed comparable levels of UCP2 expression to those grown as outlined in the UCP1 protocol. This result was not observed in the small-scale expression trials, therefore suggesting discrepancies between small and

large-scale protein expression screens, which could arguably be attributed to lag times in cell growth (244).

Collectively, the results show that by culturing cells in YP media at 30°C, inducing protein induction with 1% galactose and extending protein expression time in YP media from 6 hours to 22 hours addresses the issue of insufficient biomass yields observed in the UCP1-based protocol. However, in most conditions tested, UCP2 protein expression is severely hampered. Use of YPL as growth media in the Drew protocol was a possible route for large-scale protein expression as improved biomass could be obtained and the levels of UCP2 produced were comparable with levels observed using the UCP1 expression protocol.

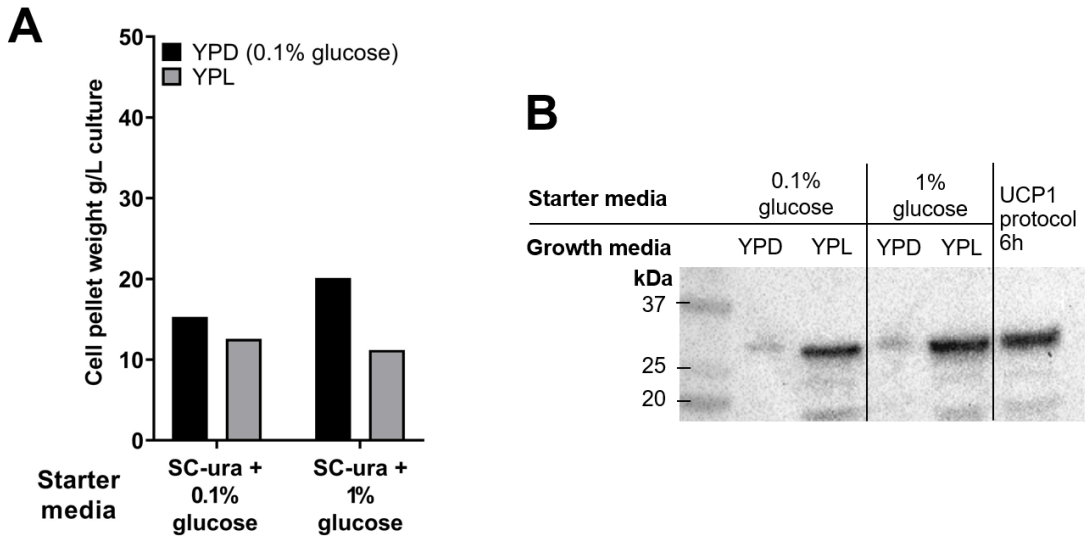

Figure 3.7: Large-scale expression trial using the Drew protocol (228). *A) Cell pellet weights obtained per litre of culture following 22 hours protein expression. Cells were cultivated either in 1 L YPD (0.1% (w/v) glucose) (black bars) or YPL (grey bars) growth media. B) Western blot quantifying UCP2 expression following 22 hours induction; in each lane, 10 µg yeast mitochondrial membranes were loaded, with membranes isolated from cells grown using the UCP1 protocol loaded for comparison ('UCP1 protocol 6h' lane). Large-scale (1 L) expression trials were conducted once to determine which conditions would be sufficient to increase starting biomass.*

3.3.4.2. Prolonged expression protocol 1

Optimisation of the Drew expression protocol, in particular cultivation of cells at 30°C in yeast-peptone extract media and extended protein expression with 1%

galactose, improved cell pellet yields, though initial solubilisation tests indicated that the level of protein extracted from membranes was suboptimal (see Drew protocol blot in **Appendix Figure 2.4**). To investigate whether UCP2 expression could be enhanced by prolonging overall culture growth time, a hybrid protocol ("Prolonged expression protocol 1") was developed, which incorporated aspects from both the UCP1 protocol (177, 178) and the Drew protocol (228). As outlined in **Figure 3.6B**, a single colony is propagated in 10 mL selective starter media overnight (16-22 hours) before subculture into 100 mL of the same media. Subcultures are added into 1 L growth media at a lower density (OD ~0.04) to allow for an extended growth period (~16/17 hours following inoculation), where galactose induction occurs once cells have reached much higher densities (OD values of 4-5) as with the UCP1 expression protocols (177, 178). Cells are then harvested following a further 22 hours of protein induction at 30°C, similar to the Drew expression protocol (228) in **Figure 3.6A**.

Combinations of selective starter culture (containing 0.1% or 1% glucose) and 1 L growth media (YPD (0.1% glucose) or YPL) were tested to assess UCP2 protein expression. In all conditions, >10 g of cell pellet/L could be obtained for the purposes of downstream purification efforts (**Figure 3.8A**) and, surprisingly, cultures propagated in 0.1% glucose starter media and YPD 0.1% glucose growth media demonstrating the highest cell pellet yield (~35 g of cell pellet/L, **Figure 3.8A**). Furthermore, the YPD/low glucose conditions with higher biomass yield, gave UCP2 expression levels that were comparable to levels observed in the UCP1 protocol (**Figure 3.8B**). Interestingly, prolonged respiration on lactate proved detrimental to UCP2 expression as illustrated by the notable level of degradation products following 22 hours of growth (**Figure 3.8B**), which supports the observation that growth on lactate may be unfavourable for FGY217 growth (245).

A variation of the prolonged expression protocol was tested to determine if biomass and UCP2 protein yields could be further enhanced. In the "Prolonged expression protocol 2", cultures underwent 34 hours growth in 100 mL selective sub media to ensure depletion of residual glucose in the media, thereby minimising variable galactose repression in the 1 L growth media. High levels of cell pellet (>25 g /L culture) could be obtained in all conditions except low glucose/YPD (see **Appendix Figure 2.5A and B**), contrary to previous observations in "Prolonged

expression protocol 1", which demonstrated the highest biomass yield (~35 g of cell pellet/L). Prolonged growth in subculture was detrimental to protein quality as indicated by increased protein degradation product and a lack of signal observed at 33 kDa, the size of intact monomeric UCP2 (see **Appendix Figure 2.5C**). The results suggest that extending growth time in selective subculture did not enhance UCP2 production, indicating that mature yeast cells may be prone to a high degree of protein degradation through necrosis pathways (246).

Blending aspects of the UCP1 and the Drew expression protocols to produce "Prolonged expression protocol 1", revealed potential options to express UCP2 protein for large-scale (1 L) protein purification efforts. The use of YPD (0.1% glucose) as growth media was a viable avenue for large-scale protein expression as practical amounts of cell pellet could be obtained (all >10 g/L of growth culture), whilst maintaining UCP2 expression levels observed with the UCP1 expression protocol.

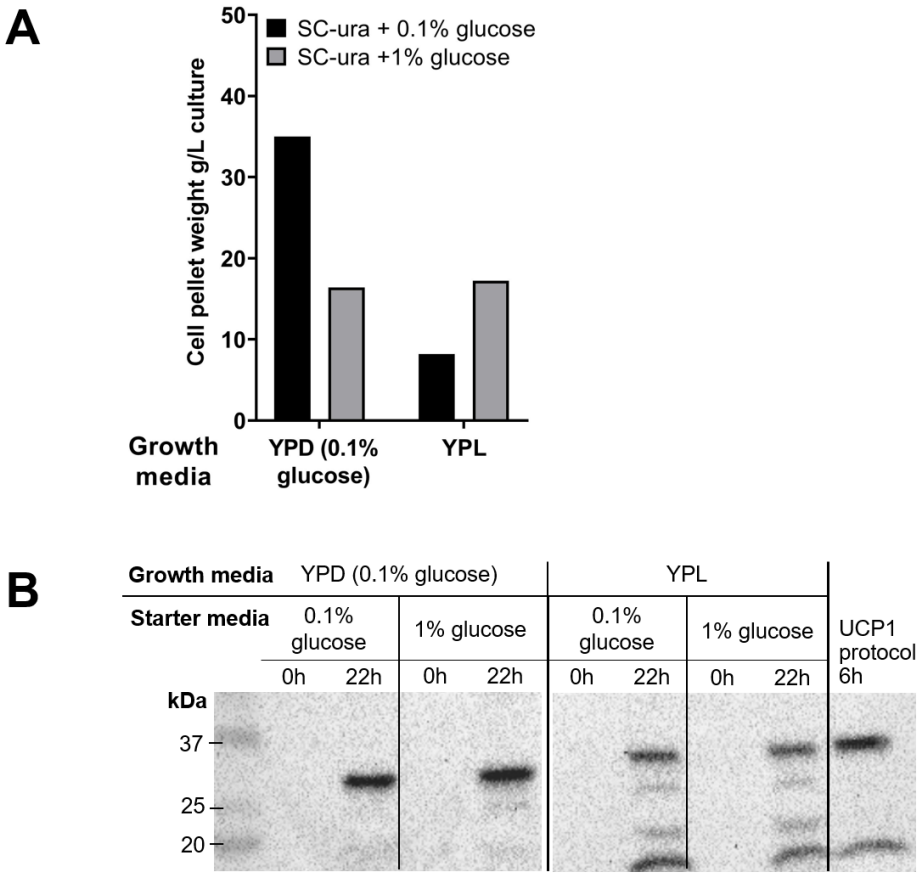

Figure 3.8: Large-scale expression trial of cells grown using "Prolonged expression protocol 1". *A) Cell pellet weights obtained per litre of culture following 22 hours protein expression. Cells are propagated in selective media (SC-ura) containing either 0.1% (w/v) glucose (black bars) or 1% (w/v) glucose (grey bars), before further cultivation either in 1 L YPD (0.1% (w/v) glucose) or YPL growth media. B) Western blot quantifying UCP2 expression at the point of protein induction (0h) and following 22 hours protein expression; each lane is loaded with 10 μg yeast mitochondrial membranes, membranes derived from cells grown using the UCP1 protocol were loaded for comparison ('UCP1 protocol 6h' lane). This large-scale (1 L) expression trial was conducted once to determine if the described conditions would be sufficient to increase yeast cell pellet yields.*

3.3.4.3. Titration of glucose into YP media

Given that the optimal biomass yield and UCP2 expression combinations found using the "prolonged expression protocol 1" were most likely related to glucose utilisation and the threshold of its subsequent removal, further large-scale expression screens were carried out, with glucose systematically varied in YPD growth media to

enhance UCP2 expression further. Cultures were propagated in selective starter media containing low (0.1% glucose), before being inoculated into YP media with various higher concentrations of glucose (0.1% to 1.0% as summarised in the table in **Figure 3.9A**). Cell incubation time was also extended from 16/17 hours to 24 hours to allow for increased glucose utilisation prior to galactose addition. Cells were harvested following 22 hours protein expression (see **Figure 3.9A** for schematic).

Cultures grown in rich media supplemented with a glucose concentration above 0.25% demonstrated sufficient levels of cell growth (>10 g/L culture), as evidenced by high average cell pellet yields per litre of culture (**Figure 3.9B**). Increasing glucose concentration is beneficial for maximising cell pellet yields, though it may potentially affect UCP2 protein expression as it is under the control of a GAL1 promoter, which is repressed in the presence of glucose (242). Intriguingly, with increasing levels of glucose there was an increase in UCP2 protein expression, with expression levels peaking at 0.75% glucose (**Figure 3.9C**). Moreover, UCP2 protein expression at 0.75% glucose matched levels observed using the UCP1 expression protocol (**Figure 3.9C**), though the appearance of some UCP2 degradation products (<33 kDa) were also noted, following prolonged growth (**Figure 3.9C**). At 1% glucose, there is variation in UCP2 expression, as illustrated by the difference in signal intensities in the last two lanes in **Figure 3.9C**, representative of mitochondrial membranes isolated from two separate 1 L growth cultures. Variation in protein expression is likely attributed to excess glucose repressing the GAL1 promoter (242, 243).

This large-scale expression screen was conducted with duplicates, showing consistent results in both protein expression and biomass yield. The findings show that sufficient biomass and UCP2 protein expression could be obtained when cells were cultured in rich media containing 0.75% glucose. Hence, growth in 0.75% glucose was taken forward for standard large-scale (1 L) UCP2 protein expression and shall be referred throughout as “Prolonged expression protocol 3”.

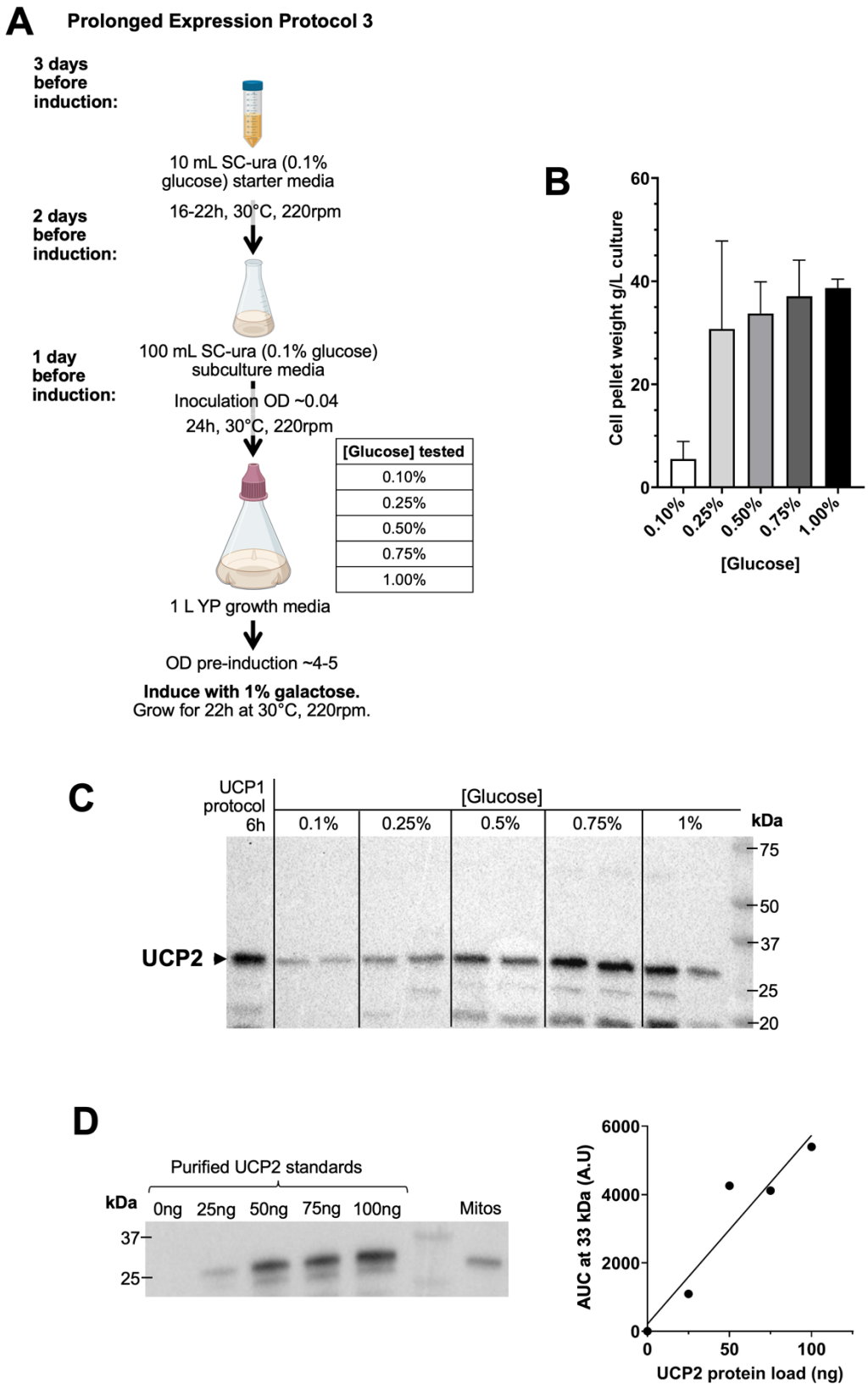

Figure 3.9: Large-scale UCP2 expression trial titrating glucose in the growth media. *A) Schematic of large-scale expression protocol tested for the optimisation of large-scale UCP2 protein expression. B) Average cell pellet weights obtained per litre of culture following 22 hours protein expression in YP media containing different glucose concentrations. Error bar shows the*

S.E.M of 2 replicates. C) Western blot of UCP2 expression in the glucose titration expression trials. In each lane, 10 µg yeast mitochondrial membranes were loaded, with the UCP2 protein expressed using the UCP1 based protocol loaded as a reference to compare relative protein levels in each condition ('UCP1 protocol 6h' lane). D) Quantification Western blot of UCP2 expression (grown in 0.75% glucose) using purified histidine-tagged UCP2 inclusion bodies as protein standards (left). The signal obtained from 10 µg yeast mitochondrial membranes expressing UCP2 was interpolated against a UCP2 standard curve (right).

3.3.5. Quantification of UCP2 protein in recombinant expression system

To quantify the amount of UCP2 protein expressed in yeast mitochondria in absolute terms, histidine-tagged unfolded UCP2 inclusion bodies were produced in *E. coli* and purified to homogeneity to use as protein standards for Western blot quantification (see **section 2.12** and **Appendix 1.4** section for inclusion body purification). Densitometric analysis indicated that UCP2 generated using "Prolonged expression protocol 3" constitutes approximately ~0.4% of mitochondrial membrane protein (**Figure 3.9D**), which is 20-fold more than the amount quantified in spleen mitochondria, the highest UCP2-expressing tissue (38, 185).

3.3.6. Solubilisation tests of membranes from "Prolonged expression protocol 3"

Small-scale (150 µl) solubilisation screens were inconsistent in reporting the amount of folded UCP2 protein extracted from mitochondrial membranes, evidenced by irreproducible signals in the supernatant fractions (**Appendix Figure 2.6**). Irreproducibility in results led to concerns regarding the experimental set-up as the method relies on ultracentrifugation using tiny (TLA 100.2) tubes to separate folded and unfolded material, which poses technical challenges that may lead to inconsistencies observed in Western blots. Therefore, to obtain a more reliable and representative readout for intact UCP2 protein, preparative solubilisation screens were conducted, which mimic conditions of a large-scale solubilisation. Here, "preparative" is defined by the nature of the membrane sample and the scale at which the solubilisation trial is conducted.

In preparative solubilisation tests, mitochondrial membranes were obtained using large-scale membrane isolation methods which involves five 1-minute pulses of mechanical disruption of cells at temperatures below 4°C using a Beadbeater (see

section 2.7 for details), which differs from small-scale membrane isolations as cells are mechanically disrupted on a vortex for 30 minutes at 4°C (see **section 2.5.2** for details). The difference in membrane isolation methods suits the scale of the preparation; small-scale membrane isolations, which typically yield low protein concentrations due to limited starting material, are routinely used to inform on protein expression and small-scale (150 µl) solubilisation tests. Large-scale membrane isolations are preparative in nature, yielding highly concentrated (>15 mg/mL) membrane samples (171), that are used for downstream purification efforts, where in most cases, the subsequent step is solubilisation. To mimic conditions of a large-scale solubilisation, "preparative" solubilisation tests were conducted where the reaction volume was scaled to 1 mL with the total protein concentration used for solubilisation fixed to 10 mg/mL. Detergent concentration and solubilisation time were investigated to determine if there was a difference in UCP2 solubility and if various parameters could be optimised prior to protein purification.

In general, it was observed that at least 75% of UCP2 protein produced in the recombinant system could be extracted from mitochondrial membranes at 0.5%, 1% and 2% 12MNG and DDM (**Figure 3.10**). Extending the solubilisation time did not appear to improve the level of UCP2 protein extracted from membranes (**Figure 3.10**), suggesting that time is not a limiting factor in protein solubilisation. Overall, the results demonstrate that preparative (1 mL) solubilisation tests showed consistent estimates for the UCP2 signal in the supernatant and pellet fractions, providing a more reliable indicator of intact UCP2 that may be extracted. Taken together, it was decided that large-scale solubilisation would be conducted using 0.5% detergent for 20 minutes to minimise protein unfolding during downstream processing, such as protein purification.

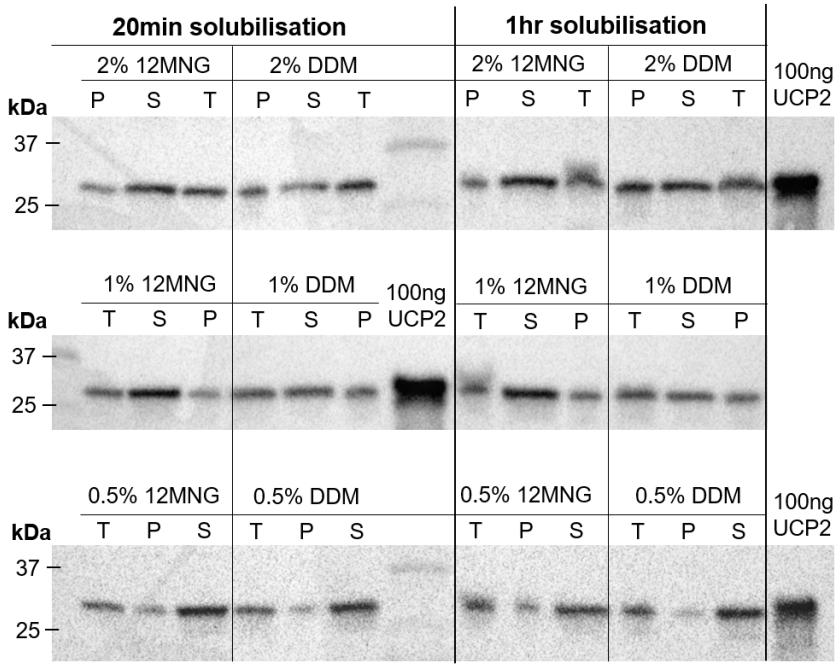

Figure 3.10: Preparative solubilisation screens. *Western blots of preparative (1 mL) solubilisation screens. Membranes were isolated from cells grown in large-scale 1 L cultures and were solubilised in 0.5%, 1% or 2% (v/v) detergent for either 20 minutes or 1 hour (as indicated). 100 ng purified UCP2 inclusion bodies are used as a control between blots. Samples are loaded as a fraction of the total volume and are denoted as T – total proteins; S – solubilised supernatant; P – insoluble pellet.*

3.4. Discussion

The results presented in chapter 3 describe the optimisation of an expression protocol capable of producing intact UCP2 protein in *S. cerevisiae* mitochondria. Using a glucose-dependent prolonged expression protocol, it was shown that UCP2 protein could be expressed in the FGY217 yeast strain, to levels higher than in native sources (185), yielding practical amounts of biomass for protein purification efforts. Furthermore, ~75% of recombinantly expressed protein could be extracted from yeast mitochondrial membranes in the presence of mild detergents, such as 12MNG and DDM, consistent with the characteristics of folded mitochondrial carrier protein (155, 158-163).

3.4.1. Increased protein expression by changes in the N-terminus

The studies presented here reveal that a significant increase in human UCP2 expression in yeast occurs when leucine was at position 2, rather than specific use of an adenine-rich Kozak sequence. Recent proteomic analysis in *S. cerevisiae*, demonstrates that mitochondrially-targeted proteins show a bias for bulky hydrophobic residues at position 2, with leucine being the most prevalent at this position (231). It is hypothesised that leucine at position 2 prevents cleavage of the initiator methionine, thereby enabling N-acetylation. The role of N-terminal acetylation in protein degradation and stability seems context-dependent, though it is proposed that acetylation may aid in organelle-targeted protein import through favourable hydrophobic interactions between the protein and organelle membranes (247). Interestingly, when valine is substituted for the native leucine at position 2 in yeast-expressed rat aldehyde dehydrogenase, decreased protein expression was observed (248), consistent with the trends presented here with UCP2. Whilst the exact mechanism relating to increased protein expression is not fully understood, this finding demonstrates how a simple change in the second amino acid can enhance recombinant mitochondrial protein expression in yeast, which may be utilised for other recombinant proteins.

3.4.2. FGY217 on different carbon sources

Initial small-scale (50 mL) expression trials, utilising a UCP1-based expression protocol, were important in determining UCP2 protein production in the protease-deficient yeast strain, however proved to be an impractical route for large-scale (1 L) cultures for the purposes of protein purification. Utilisation of lactate by FGY217 may have led to insufficient biomass, as previous studies have indicated that growth on a non-fermentable carbon source, such as lactate, can induce mitophagy in the W303-1B yeast strain when subjected to conditions of nutrient stress (245). In yeast, autophagy is achieved by trafficking organelles to the vacuole (249), where protein degradation occurs through proteolytic activity of vacuolar proteases, such as proteinase A, an enzyme required for maturation of several vacuolar proteases (167). Proteinase A is encoded for by the *Pep4* gene, of which the FGY217 strain lacks. Deficiencies in cellular protein degradation has been reported to limit cell growth under nutrient stress conditions (250), which could be a reason for the limited biomass obtained following overnight growth on lactate and after 6 hours protein

induction with galactose. Growth on lactate using the method outlined by Drew and colleagues (approximately 6-7 hours growth on lactate prior to induction with galactose for 22 hours) demonstrated appreciable levels of cell growth, so it could be rationalised that FGY217 cells sustained prolonged growth on galactose rather than lactate. Bouillaud and colleagues have demonstrated that W303 yeast seeded on selective agar plates supplemented with galactose form colonies following 48 hours growth (251). These finding supports the notion that yeast cells are capable of prolonged growth on galactose.

Following numerous large-scale optimisation screens, it was interesting to find that prolonged growth on 0.75% glucose was capable of matching UCP2 expression levels as observed in the UCP1-based expression protocol. Given that UCP2 expression is under the control of a GAL1 promoter, which is repressed in the presence of glucose (242, 243), the observation that UCP2 increased with increasing glucose seemed counterintuitive. It has been shown that activation of the GAL pathway is sensitive to the ratio of external glucose and galactose concentrations, mainly through competitive import of glucose and galactose by hexose transporters (252). Subsequently, it has been postulated that growing yeast in mixtures of glucose and galactose can "prime" cells to utilise galactose following glucose depletion, thereby mitigating diauxic lag growth (253). It could be argued that cultures grown in low (0.1-0.25%) glucose concentrations may exhaust glucose prior to galactose addition, thereby resulting in a slower growth rate, due to a longer lag phase where the cells are undergoing a metabolic switch to galactose utilisation. This delayed lag phase could be a reason for lower UCP2 protein expression. Cultures grown in higher glucose concentrations are likely to contain residual levels of glucose at the point of protein induction. In these conditions, cells are likely to respire primarily on glucose, but may also be utilising added galactose to a lesser degree. Hence, at high glucose conditions, cells exhibit greater growth as cells proliferate faster in glucose-rich media, but are also able to switch from glucose to metabolise galactose at a much later time in the protein induction period, where protein expression is less likely to be repressed.

The purpose of expressing recombinant UCP2 is to clarify its function as it remains widely contested, though one hypothesis is that the protein acts as a 4-carbon metabolite transporter (93) that provides metabolic flexibility to the cell under conditions of stress (114, 119). Recombinant expression of functional UCP2 protein

has been demonstrated in oleate-dependent media in yeast mutants, where UCP2 compensates for aspartate/glutamate activity in AGC1 knockout yeast (114). This method of recombinant UCP2 expression was not pursued due to time constraints and potential challenges associated with generating knockout mutants in the wild-type (W303-1B) strain, which exhibited unsuccessful yeast growth in preliminary growth and protein expression trials. Raho and colleagues quantify recombinant UCP2 protein expression relative to loading controls (114), though the specific proportion of UCP2 within mitochondrial membrane proteins remains unknown. Hence, for expression screens using the method by Raho and colleagues (114), quantifying UCP2 protein expression in absolute terms would be essential to assess its practicality for protein purification. Furthermore, the issue of ensuring that sufficient levels of biomass (>10 g cell pellet/L culture) would also need to be addressed, especially when producing protein for downstream protein purification.

3.4.3. Avenues for protein purification based on UCP2 protein solubility

The use of hydroxyapatite chromatography, which has been used to isolate mitochondrial carriers from native sources, such as AAC (254) and UCP1 (179), is reliant on the use of TX-100 to extract carrier proteins in a functional form (232). In the context of UCP1 purification, hydroxyapatite chromatography can also be utilised in conjunction with thiol-reactive chemistry to purify UCP1 protein from an enriched sample, since UCP1 has a cysteine residue at the C-terminal end of the protein which acts as an intrinsic tag, (see (19)). The important inclusion of an immobilisation step allows for buffer-exchange and removal of contaminants, in which TX-100 detergent can be swapped out for more mild stabilising detergents, such as DDM and 12MNG (19, 155). Since UCP2 was seen to be predominantly insoluble when extracted with TX-100 in preliminary small-scale (150 µl) solubilisation screens, the use of TX-100 was excluded in subsequent tests as 12MNG and DDM were observed to extract more folded material. For this reason, the use of hydroxyapatite chromatography will not be explored in downstream purification efforts.

Recombinant expression of untagged UCP1 protein in yeast has generated intact protein (62, 65, 153, 178, 255-257), which can be purified through the use of a bespoke purification strategy (153, 171). The ‘S,Q and TP’ method, originally developed for the purification of UCP1 from native sources (19), is compatible with

stabilising detergents, such as 12MNG or DDM, which is beneficial as it removes the need for a detergent-exchange step and also allows efficient extraction of intact UCP2 protein from mitochondrial membranes. Hence this purification strategy will be used as a base for UCP2 purification efforts.

4. Enrichment of human Uncoupling protein 2 from *S. cerevisiae*

4.1. Introduction

Purification of proteins relies on separating proteins based on their molecular properties, such as net charge, hydrophobicity or size (258). Conditions for purification often require optimisation to obtain high yields of functional protein. Compared to soluble proteins, the purification of membrane proteins is particularly challenging (259, 260). Integral membrane proteins are amphipathic in nature, consisting of a hydrophobic transmembrane core embedded within the lipid bilayer and hydrophilic surfaces where the protein interacts with the aqueous environment. The structure and function of integral membrane proteins are influenced by the physiochemical properties of the lipid bilayer (261). Extraction of membrane proteins are often achieved by detergents (262), though alternative methods, such as the use of styrene malic acid polymers (SMAs) (263-267) and lipid nanodiscs (268-270) have also been used for the study of membrane proteins and membrane protein complexes. Careful consideration is required, especially with detergent selection, when isolating functional membrane proteins as purification strategies need to accommodate the addition of solubilisation agents (271).

With the rise of recombinant expression systems, proteins can be engineered to incorporate purification tags for selective binding in affinity chromatography, to allow for a high degree of protein purification (271). However, prior to routine use of heterologous expression systems and genetically modified constructs, membrane protein purification from native sources was achieved through other chromatographic methods, such ion exchange (272, 273), ligand-affinity (274) and antibody-affinity (275). Hydroxyapatite, a resin composed of calcium and phosphate ions (276), has been used in the purification of DNA (277) and proteins (278), including native mitochondrial carrier proteins for structural (137, 199) and biochemical analysis (17, 179, 200). In later years, the production of mitochondrial carrier proteins has been carried out using various expression systems (see **Chapter 3** for an overview). In *E. coli* systems, histidine-tagged mitochondrial carriers, produced

as inclusion bodies, were purified through nickel affinity chromatography with unfolded material 'refolded' through an Amberlite column (93, 203, 209, 210, 279, 280). Recombinant UCP protein expression in *L. lactis* and *S. cerevisiae* suggested that the addition of purification tags yielded poor expression levels in these systems and generated misfolded material (215). Several studies have indicated that UCP proteins can produce misfolded protein artefacts in yeast (55, 56) or *E. coli* systems (163). Subsequently, a bespoke strategy used for the purification of native lamb UCP1 (OaUCP1) was developed, which utilises ion exchange chromatography or hydroxyapatite to remove contaminants, with a subsequent purification step dependent on a thiol-reactive resin to immobilise OaUCP1 via a cysteine residue towards the C-terminus, thereby acting as an intrinsic tag (19). This step allows for further removal of contaminants, especially non-proteinaceous ones, including excess detergent and lipid, which can impact on downstream analysis (19). Use of the thiol-reactive chemistry has been successful in the purification of yeast-expressed recombinant UCP1 (153, 171).

The efforts outlined in this chapter focuses on the optimisation of protein purification using the strategy outlined by Lee and colleagues for native OaUCP1 (19), avoiding the need for added protein tags and risk of producing misfolded UCP2 protein. In the method outlined, OaUCP1 is purified to apparent homogeneity, by thiol-reactive chemistry, by virtue of a cysteine residue near the C-terminus. Here, it was postulated that HsUCP2 protein produced using the recombinant yeast system (see **Chapter 3** for UCP2 expression) could be isolated in the same way as it also possesses a cysteine residue towards the C-terminus.

4.2. Aim

To purify UCP2 protein to from yeast mitochondrial membranes in a folded form for biochemical characterisation.

4.3. Results

A significant proportion (>75%) of recombinantly expressed UCP2 protein was observed to be folded when treated with 0.5% 12MNG following 20 minutes

solubilisation (see **section 3.3.6**), hence this condition was used for subsequent large-scale solubilisations, which is the first step in membrane protein purification strategies following cell lysis (271).

4.3.1. Ion exchange chromatography

In the purification strategy outlined by Lee et al. (2015) (19), the first step following solubilisation involves ion exchange chromatography, which acts to remove contaminating proteins, allowing UCP1 to pass through via negative chromatography (see **Figure 4.3** for an adapted schematic). The use of ion exchange resins can be used to purify proteins based on the overall charge of protein, which can be altered based on the pH of the buffer (281). Preliminary investigations were conducted to determine if ion exchange chromatography could be used to purify or enrich UCP2 protein.

To investigate if ion exchange chromatography could be used to facilitate purification of UCP2 protein, it was important to determine if protein stability was affected by pH. Accordingly, preparative (1 mL) solubilisation tests were conducted to check UCP2 solubility and protein stability. In these solubilisation trials, UCP2-containing membranes were subject to high-speed centrifugation to pellet the mitochondrial fraction, before being resuspended in buffers of varying pH, with solubilisation trials conducted immediately after buffer exchange (see **section 2.8** for details). A majority (>90%) of the total (T) UCP2 protein was observed to be soluble at pH 8.0 and pH 9.6, as shown by the high signal intensity in the solubilised supernatant (S) fraction compared to what remained in the pellet (P) in Western blots (**Figure 4.1A**). At low pH (pH 6.0 and pH 6.5), only 25-50% of protein could be solubilised, suggesting that UCP2 protein is less stable at acidic pH (**Figure 4.1A**).

Since purification experiments can be long and arduous, the ability to split the method would be more practical. Hence, solubilisation screens were also performed on buffer-exchanged membranes that had undergone cryo-storage to assess the impact of buffer pH after snap-freezing and storage in -80°C. Interestingly, the apparent instability of UCP2 in acidic pH was further exacerbated following -80°C storage, as little or no UCP2 signal was observed in the solubilised supernatant (S) fractions, specifically at lower pH only (6.0 and 6.5) (**Figure 4.1B**). The effect of

UCP2 instability at low pH is more pronounced when compared with samples that were immediately solubilised following buffer exchange into different pH (comparison of immediately (I) and frozen (F) solubilised fractions in **Figure 4.1C**). Whilst a majority of UCP2 protein could be solubilised under mild alkaline conditions, less intact UCP2 protein was present when samples were subjected to a snap-freeze and thaw cycle, compared to those that were immediately solubilised (comparison of immediately (I) and frozen (F) solubilised fractions in **Figure 4.1C**).

Results from these preparative solubilisation trials indicate that UCP2 is more stable in alkaline pH and suggest that resuspension in acidic pH is detrimental to protein stability. The results also show that subjecting membranes to a freeze-thaw cycle drastically reduces the amount of folded UCP2 protein in membranes, suggesting that future purification strategies that require buffer exchange and solubilisation steps should be conducted on the same day as the downstream purification to maximise folded protein yields.

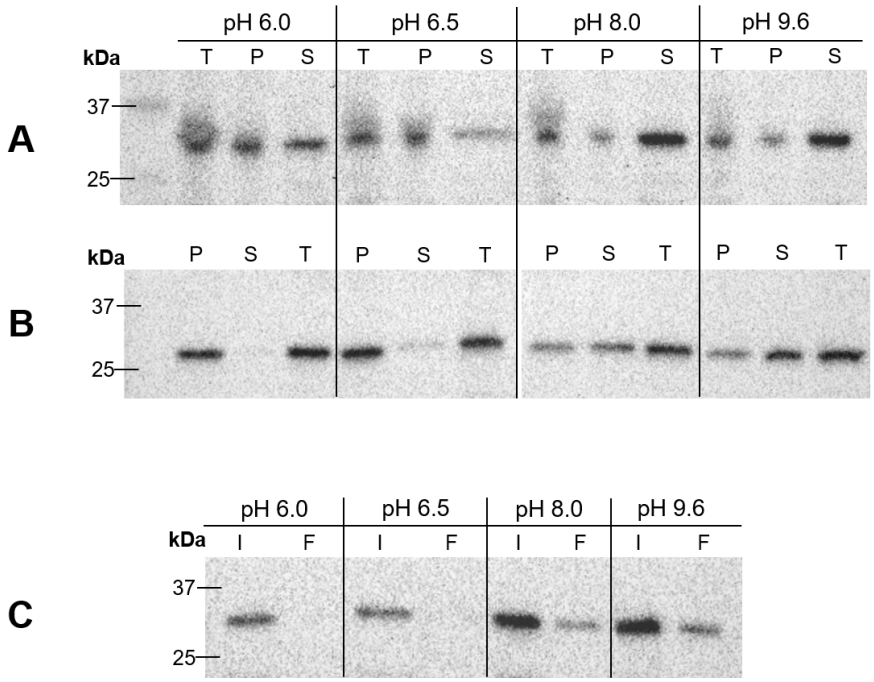

Figure 4.1: UCP2 solubility in different pH*. A-B) Western blots of fractions taken from preparative solubilisation trials conducted immediately after buffer exchange (A) or following cryo-storage of buffer-exchanged membranes (B). UCP2-containing membranes were buffer-exchanged into either 20 mM bis-Tris (pH 6.0), 50 mM MES (pH 6.5), 20 mM Tris HCl (pH 8.0) or 20 mM piperazine (pH 9.6). Samples are described as the 'total proteins' – T; 'solubilised supernatant' – S and the 'insoluble pellet' – P. C) Western blot comparing the solubilised supernatant fractions from both solubilisation trials. Solubilised supernatant fractions were obtained from trials that underwent immediate solubilisation following buffer exchange – I or membranes that underwent buffer exchange following a snap-freeze and thaw cycle – F. For all blots, samples were loaded as a proportion of the sample volume.*

4.3.1.1. UCP2 binding trials to S-, Q- or TPS-resins

Following assessment of UCP2 protein stability at different pH, investigations were carried out to assess the binding of UCP2 onto ion exchange columns and possible purification strategies. Anionic (methyl sulfonate (S)) and cationic (quaternary ammonium (Q)) spin columns were utilised for rapid assessment of UCP2 binding capabilities onto these ion exchange columns.

In binding trials, detergent-solubilised mitochondrial membrane fractions, prepared at different pH (6.0, 8.0 and 9.6) as described above, were applied to S- and Q-spin columns. To establish if UCP2 could be eluted from ion exchange columns in a

folded form, the columns were subjected to washes containing increasing amounts of NaCl, as well as a harsh "strip" (1% SDS and 1 M NaOH for S- and Q-columns, respectively) to ensure any unfolded material is eluted from the column. In these experiments, UCP2-containing membranes were resuspended in pH 8.0 and pH 9.6 as the protein was observed to be stable under these conditions. Although UCP2 was observed to be unstable at pH 6.0, binding trials were conducted at this pH to determine if it was at all possible to enrich for UCP2 protein using either ion exchange column.

At pH 8.0 and pH 9.6, it was discerned that UCP2 does not bind to either S or Q columns as UCP2 is only observed in the 'flow through' fractions in Western blots (**Figure 4.2B and 4.2C**). At both these pH values it was observed that the Q-column had a purifying effect as it removed contaminating proteins, evidenced by the total protein signals in the Coomassie-stained gel in the presence of 100 mM, 250 mM and 1 M NaCl (see "Q-Wash" fractions in Coomassie-stained gels in **Figure 4.2B and 4.2C**). Conversely, this purifying effect was not observed with the S-column as there is a lack of protein signal in any of the fractions following the "S-Flow through" (see "S-Wash" fractions in Coomassie-stained gels **Figure 4.2B and 4.2C**), which implies that a vast majority of mitochondrial membrane proteins, including AAC (see AAC in 'flow through' fractions detected by Western blots in **Figure 4.2B and 4.2C**), do not bind to the S column at pH 8.0 and pH 9.6, and are negatively charged at alkaline pH. At pH 6.0 it was observed that few proteins bind to the S-spin column (see "S-Wash" fractions in Coomassie-stained gels **Figure 4.2A**). It was observed that at pH 6.0, UCP2 binds to the S column and can only be eluted under denaturing conditions, which may imply that the protein precipitated onto the column (see "S-Wash 3" and "S-Strip" lanes Western blot in **Figure 4.2A**). These preliminary findings suggest that UCP2 is unstable at pH 6.0 and that purification strategies would be inefficient at acidic pH. Given that UCP2 is stable in mild alkaline pH, purification strategies will focus on these pH values.

The solubilised supernatant fraction was also applied to the thiol-reactive resin, thiopropyl Sepharose 6b (TPS), to determine if UCP2 could bind to the resin in a redox-dependent manner, like that of UCP1, and thus be utilised in the S+Q purification strategy as outlined by Lee and colleagues (19). HsUCP1 has a cysteine residue near its C-terminus at position 305, which likely binds to the resin enabling

purification by covalent chromatography. HsUCP2 also has a cysteine towards the C-terminus at position 302, however this residue is followed by seven amino acid residues, unlike HsUCP1 (4). Preliminary tests with TPS shows that UCP2 can bind to the resin in a redox-sensitive manner, though the signal observed in the elution fraction in the Western blot was not equivalent to the total folded protein incubated with the resin (see Western blot in **Appendix Figure 3.1**).

The findings obtained in the binding trials show that ion exchange chromatography alone is not a feasible avenue to purify UCP2. Notably, UCP2 was observed to bind to the cationic exchanger (S column) at pH 6.0, though it was not possible to elute the protein under naturing conditions. At alkaline pH, where UCP2 was observed to be stable, the protein could not be immobilised by either cationic or anionic exchange columns. However, the results indicate a potential use of ion exchange chromatography to remove contaminants, hence its use in combination with other methods, such as covalent chromatography as described by Lee et al. (19) was explored in purification trials.

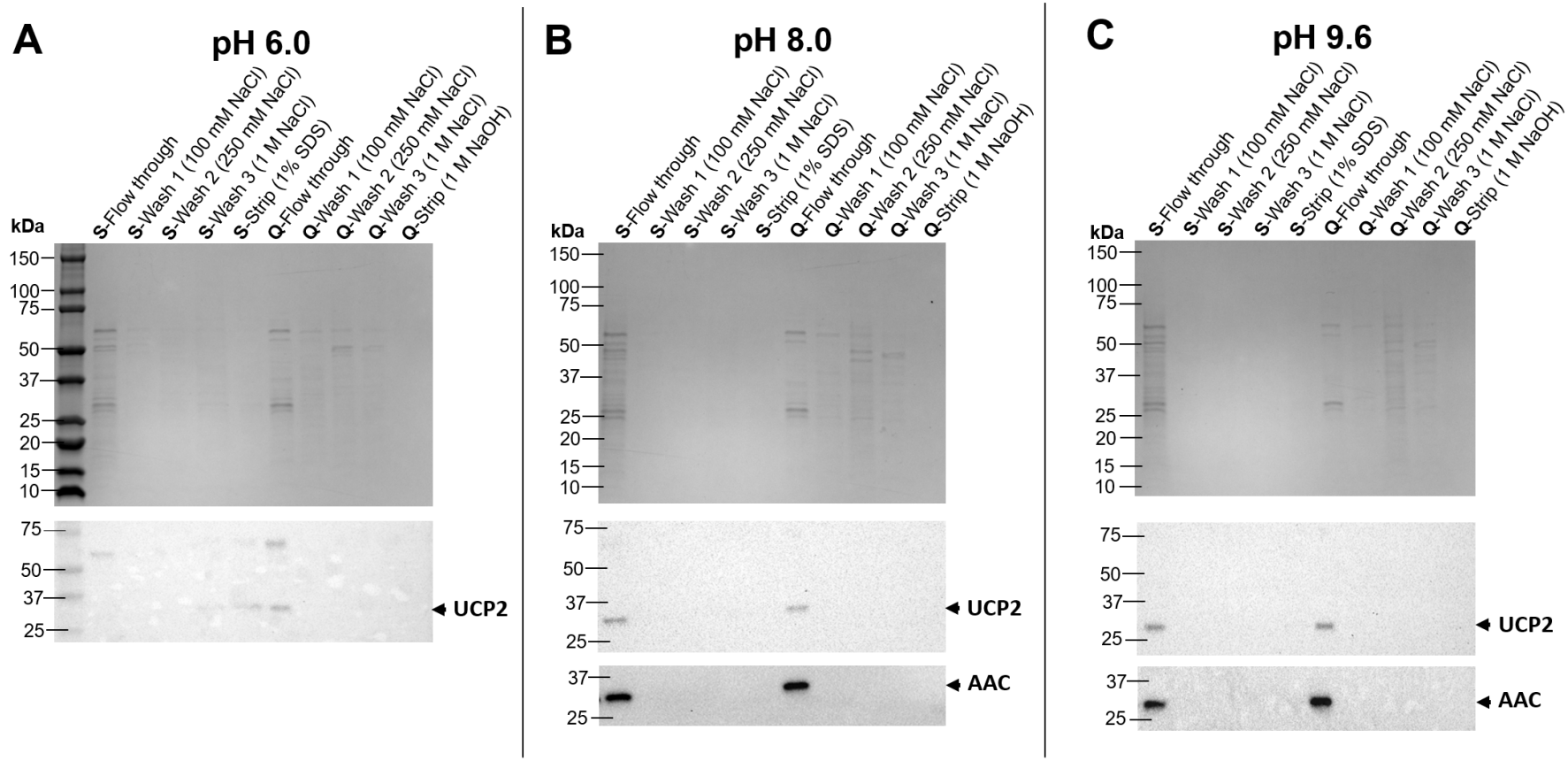

Figure 4.2: UCP2 binding onto S- or Q- columns*. A-C) Coomassie-stained gels (top panels) and Western blots (bottom panels) of samples taken from S- or Q-binding trials. Samples were resuspended in either 20 mM bis-Tris (pH 6.0) (A), 20 mM Tris-HCl (pH 8.0) (B) or 20 mM piperazine (pH 9.6) (C). The 'Flow through' fractions represent the portion of supernatant that passes through the spin column following a low-speed spin. After application of the supernatant, the columns are washed with 100 mM NaCl ("Wash-1"), followed by a subsequent 250 mM NaCl wash ("Wash 2") and a final 1 M NaCl wash ("Wash 3"). The S- and Q-columns were then 'stripped' (with 1% (v/v) SDS and 1 M NaOH, respectively) to ensure the removal of aggregated material on the column. Fractions prefixed with 'S' and 'Q' represent samples passed through the S- and Q-spin columns, respectively. Samples are loaded as a fraction of the total volume. Western blots track UCP2 or AAC protein as indicated.*

4.3.2. S+Q Purifications

The findings obtained in the binding trials suggest that UCP2 shows similar characteristics to UCP1 as it passes through both S- and Q-spin columns at slightly alkaline pH and can, in principle, bind to a thiol-reactive resin in a redox-dependent manner. Consequently, purification attempts were conducted to establish if intact UCP2 purification could be achieved through the combined use of these resins as described by Lee and colleagues (2015) (19) (see **Figure 4.3** for purification schematic).

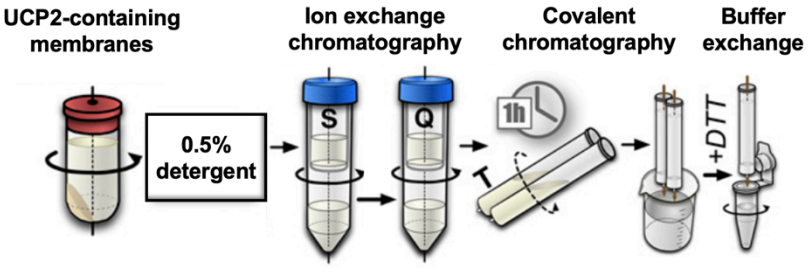

Variations in membrane treatment:
Alkaline treatment (pH 11.3)
Buffer-exchange by ultracentrifugation (pH 8.0)
Buffer-exchange by ultracentrifugation (pH 9.6)
Pre-treatment with 1 mM ADP* (pH 8.0) *during preceding membrane isolation step
WB12-derived membranes

Figure 4.3: Schematic of HsUCP2 purification using the S+Q TP method as outlined by Lee et al. (19). *UCP2-containing membranes are subjected to different treatments (summarised in table) before solubilisation with 0.5% detergent. The folded supernatant fraction is sequentially passed through S- and Q-spin columns prior to incubation with thiol-reactive resin (T). Covalently bound proteins are eluted with 150 mM DTT, with final samples subjected to buffer exchange using a PD10 column or a size exclusion column. Image was adapted from Lee et al. (2015) (19).*

4.3.2.1. Purification of UCP2 using harsh alkali-treated membranes

Given that HsUCP2 is stable in mild alkaline pH, it was reasoned that it may remain intact during a high alkaline wash treatment of mitochondria as described in the purification strategy by Lee et al. (2015) (19). In these experiments, 'crude' total mitochondrial membranes were subjected to incubation with sodium carbonate (pH 11.5) for 30 minutes prior to solubilisation. The supernatant fraction containing folded

protein is then passed through an S-spin column, of which the resulting flow through fraction is applied onto a Q-spin column, with the subsequent flow through incubated with thiol-reactive resin (see **Figure 4.3** for purification schematic).

It was observed that a large portion of protein could be solubilised in the presence of 0.5% 12MNG following treatment at pH 11.5, including UCP2 (see supernatant fraction **Figure 4.4A and 4.4B** (top panel)). Whilst the S- and Q-columns exert a purifying effect by immobilising contaminants (see "S-Capture" and "Q-Capture" fractions in Coomassie-stained gels in **Figure 4.4A**), the Coomassie-stained gel reveals that most of the proteins are lost in the TPA flow through ("TPA-Flow through" fraction (**Figure 4.4A**)). Elution of thiol-reactive proteins from the TPA resin results in a single band on the Coomassie-stained gel ("TPA-Elution" fraction (**Figure 4.4A**)) corresponding to the typical size of most mitochondrial carriers (203, 282), which is retained following buffer exchange on a PD10 column. When specifically probed by Western blot analysis, a large amount of UCP2 is solubilised and passes through both ion exchange columns as previously observed at milder alkaline pH (see 'S-Flow through' and 'Q-Flow through' fractions in **Figure 4.2B and 4.2C**). However, most of the UCP2 protein is lost in the TPA flow through fraction (UCP2 (top panel) Western blot **Figure 4.4B**), suggesting that cysteines, including C302, may be inaccessible to the thiol-reactive resin. When probed against AAC, this carrier was seen to track with UCP2, with a large portion lost in the TPA flow through, though some AAC protein binds to the resin and is present after elution and DTT removal (see 'Post PD10' fraction, in AAC Western blot **Figure 4.4B** (bottom panel)).

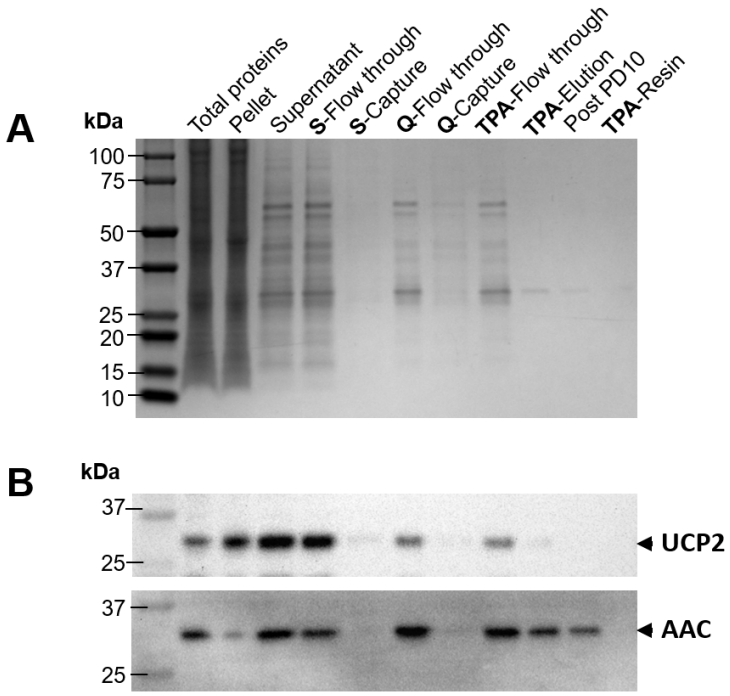

Figure 4.4: S+Q TPA purification using alkali-treated membranes*. Coomassie-stained gel (A) and Western blots (B) tracking HsUCP2 and AAC, as indicated, in S+Q TPA purification of enriched (alkali-treated) membranes. Total proteins are representative of the total alkali-treated membranes, with the folded supernatant and unfolded pellet fractions separated by a high-speed spin. The supernatant is sequentially passed through S- and Q-columns, prior to incubation with thiol-reactive resin (thiopropyl agarose – TPA) for covalent chromatography. Bound proteins are eluted with DTT ('TPA-Elution') and samples are buffer-exchanged using a PD10 column (resulting eluate is denoted as 'Post PD10'). 'Flow through' fractions are representative of samples passed through the S, Q and TPA columns, whilst the 'Capture' fractions represent samples immobilised by the ion exchange columns and eluted with 1 M NaCl. Gel samples are fractionally loaded as a proportion to the sample volume.*

Since most UCP2 protein purifications were conducted in a single day, thermostability assays using the thiol-reactive, coumarin-based dye, CPM, were utilised after obtaining the final purified sample. The CPM thermostability assay is a protein unfolding assay (192) that provides an indication of protein stability of cysteine-containing proteins in the absence or presence of various ligands (155, 194, 195, 283, 284). In this assay, the weakly fluorescent thiol-sensitive dye, CPM (285), is applied to a purified protein sample and reacts with accessible cysteine residues to generate a fluorescent adduct. As an increase in temperature is applied to the sample, an increase

in fluorescent signal is observed, as CPM reacts with cysteine residues buried in the protein as they become solvent-exposed due to heat-induced unfolding (192). Purified, monodispersed folded protein is expected to show a sigmoidal increase in signal as the protein population transitions from a folded to unfolded state (see top panel of **Figure 4.5A**). The peak generated in profiles showing the first derivative (dF/dT) of the fluorescence signal can be used to describe an apparent protein melting temperature ('T_m') as a practical marker of relative protein stability (155, 283) (see bottom panel of **Figure 4.5A**). As well as reporting on the general integrity of a protein sample, the assay can also be used to detect protein-ligand binding via the associated shifts in thermal stability due to net bonding changes in the protein (155, 194, 195, 283, 284) (**Figure 4.5A**). For UCP1, purine nucleotide inhibitors have been found to induce an increase in T_m, whereas fatty acid activators and related compounds that have been observed to induce UCP1 proton leak activity, are reported to induce a decrease in T_m (153, 155, 284).

Here, the CPM protein thermal shift assay was used to assess the composition and integrity of the final samples from UCP2 purification attempts. Carboxyatractyloside (CATR), a well-known inhibitor of AAC (286), was tested to detect contamination of functional AAC protein in the preparations. Guanosine diphosphate (GDP), an inhibitor of UCP1 (31-35) was used to detect UCP1-like stabilising shifts (in OaUCP1 controls (see **Appendix Figure 3.2**) and HsUCP1 tests – see **section 5.4.1** for further examples (153, 155, 284)), in HsUCP2 purified samples, should it bind purine dinucleotides as some have claimed (52, 53, 57, 60, 61, 67, 156, 205, 287). Aspartate was also tested as it is a proposed transport substrate of UCP2 (93, 114).

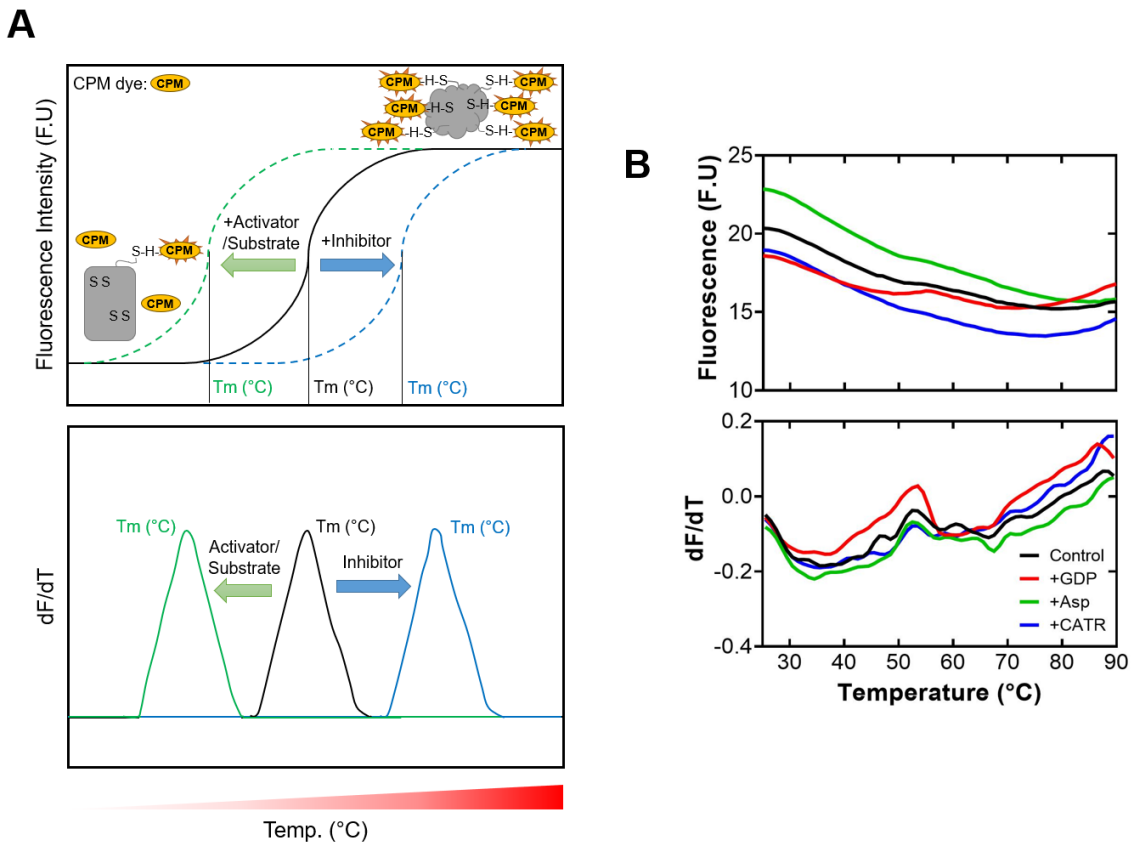

Figure 4.5: Principles of the CPM thermostability assay*. A) Diagrammatic representation of expected fluorescence (top) and first derivative (bottom) profiles of folded protein denaturation in the CPM assay. In fluorescence profiles, the starting fluorescence is low as CPM cannot access and react with protein-buried cysteine residues in the folded state. Upon protein unfolding the fluorescence increases as cysteine residues become solvent exposed and react with CPM, giving a characteristic sigmoidal profile (top panel). An apparent protein melting temperature ('T_m') can be gained from the peaks in the first derivative profile (bottom panel). Protein is represented by a grey square (folded state) and a grey cloud (unfolded state); unreacted CPM dye is represented as a yellow oval, whilst thiol-reacted CPM is represented as a yellow oval encircled with orange spikes. B) Fluorescence signal (top) and derivative (bottom) traces from CPM thermostability assays using 2 µg of the final purified sample (derived from alkali-treated membranes), prepared as outlined in* ***Figure 4.3****, in the absence or presence of 1 mM CATR, 1 mM GDP or 1 mM aspartate. Native OaUCP1 was used as a control in CPM assay runs (see* ***Appendix Figure 3.2A****).*

CPM assay tests conducted with alkali-treated samples purified using methods outlined in **Figure 4.3**, do not show a typical sigmoidal transition in fluorescence signal, suggesting that most proteins in the final sample are unfolded (**Figure 4.5B**);

similar fluorescence profiles have been observed with thermally denatured proteins (155, 192). Furthermore, there are no thermal shifts detected in the presence of CATR, GDP or aspartate, which indicates a lack of folded AAC and no indication of folded UCP2 protein in the final purified sample. In contrast, the fluorescence signal obtained with native OaUCP1 controls started at a much higher fluorescence value compared to HsUCP2 purified samples (see **Appendix Figure 3.2A**), which could be attributed to solvent-exposed cysteine residues in the OaUCP1 folded state, not present in HsUCP2 (284). The signal also showed a typical sigmoidal increase indicative of folded protein, where the associated peak in the derivative profile shifted to higher values with added GDP, consistent with nucleotide binding and functional characteristics of UCP1 (155) (see **Appendix Figure 3.2**).

The final yield of purified protein obtained from the purification was minimal, with 190 µg purified protein produced from approximately 320 mg alkali-treated membranes, which in turn was enriched from approximately 760 mg of mitochondrial membranes (see **Appendix Table 3.1**). As such, methods of Lee and colleagues (19), as described, was not feasible for purifying recombinant UCP2 protein as it generates only micromolar amounts of protein (representing only 0.03% of starting mitochondrial membranes), most of which is likely to be unfolded.

4.3.2.2. Purification of UCP2 in mild alkaline buffer

As initial purification attempts were not successful, the next logical step was to investigate if removing the harsh alkaline (pH 11.5) treatment prior to S+Q could give better yields. Therefore, the purification protocol (19) was adapted, with total membranes resuspended in 20 mM Tris HCl (pH 8.0) or 20 mM Piperazine (pH 9.6) buffer instead of the harsh alkali treatment (**Figure 4.3**; ultracentrifugation was used for the purposes of buffer exchange). This amended purification was otherwise conducted as outlined in **Figure 4.3**, but with the "Q-flow through" samples at pH 9.6 also being titrated down to pH 8.0 prior to incubation with the thiol reactive resin, as reactivity is pH sensitive and less efficient above pH 8.0 (288).

Comparison of purification profiles of membranes subjected to a harsh alkali treatment (**Figure 4.4A**) with membranes resuspended in mild alkali buffers (Coomassie-stained gels in **Figure 4.6**), shows that more protein, including UCP2, was soluble when membranes were not pre-treated with sodium carbonate/pH 11.5

conditions (see supernatant fractions in **Figure 4.4**, for harsh alkali-treatment, and **Figure 4.6**, for mild conditions). The purifying effect of the thiol-reactive resin is observed for both alkali-treated and mildly treated membranes (see "TPA-Flow through"/"TPS-Flow through" fractions in **Figure 4.4** and **Figure 4.6**, respectively), as most contaminating proteins are removed in the flow through of these samples. In both conditions, a prominent Coomassie signal following elution from the TPS resin is observed (see "TPS-Elution" fractions in Coomassie-stained gels in **Figure 4.6**); the size of this single band is consistent with the size of most mitochondrial carriers (203, 282). When blotted for UCP2, protein was observed to pass through both S- and Q-columns at pH 8.0 and pH 9.6 (UCP2 blots in **Figure 4.6**), consistent with results obtained in the binding trials (see UCP2 blots in **Figure 4.2B and 4.2C**). Moreover, relatively strong signals can be observed in the "TPS-Elution" fraction and subsequent steps, therefore implying that UCP2 can be purified under mild conditions (UCP2 blots, **Figure 4.6**). However, when probed against AAC, it is also observed in the same fractions as UCP2, thereby indicating AAC protein contamination (AAC blots, **Figure 4.6**), as well as potential contamination of other mitochondrial carriers, in the final sample.

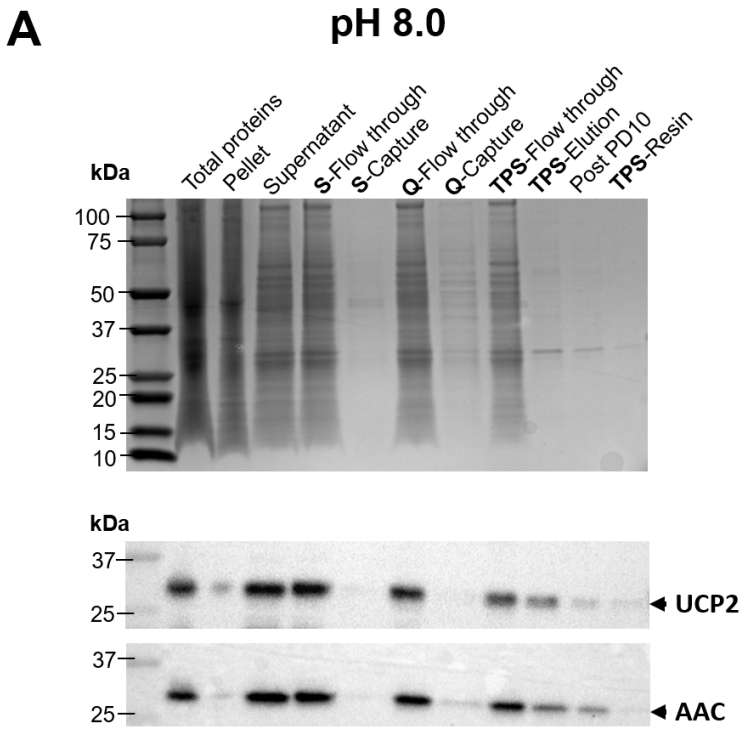

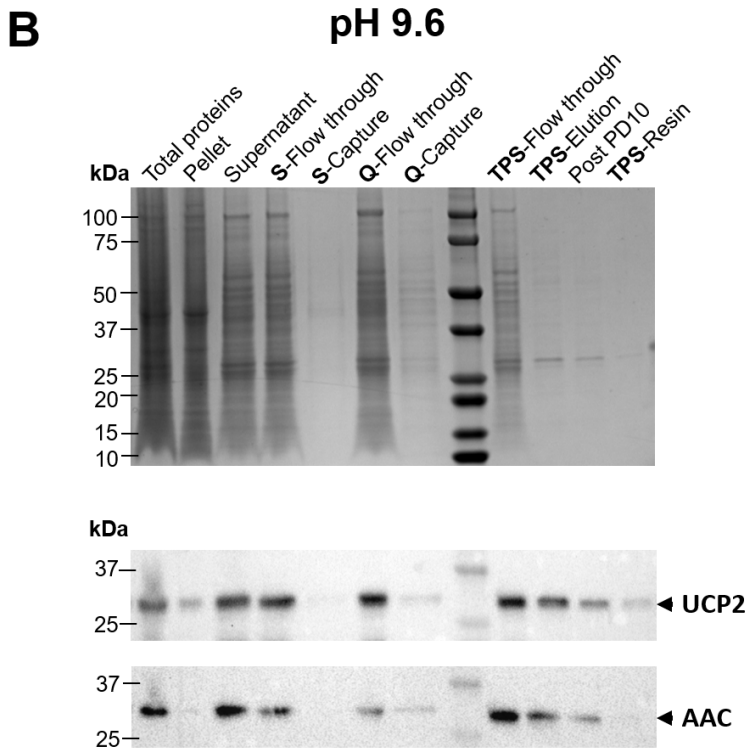

Figure 4.6: S+Q TPS purification using ultracentrifuged membranes resuspended in mild alkali buffers. *A-B) Coomassie-stained gel (top panels) and Western blots (bottom panels) tracking HsUCP2 or ScAAC, as indicated, during purification using adapted S+Q TPS methods (19). To aid purification of folded HsUCP2 protein, mitochondrial membranes are resuspended in either 20 mM Tris HCl (pH 8.0) (A) or 20 mM piperazine (pH 9.6) during ion exchange chromatography, rather than subjecting mitochondrial membranes to a harsh alkali pre-treatment. Gel samples are loaded by fractional load, proportional to the sample volume.*

Final PD10 eluates were subjected to the CPM thermostability assay to assess the purity of the final protein samples as described previously (see **Figure 4.5A**). Whilst the initial starting fluorescence of samples solubilised at pH 8.0 were relatively similar (**Figure 4.7A**, top panel), it was interesting to observe that samples originally resuspended in piperazine (pH 9.6) demonstrated variable levels of starting fluorescence (**Figure 4.7B**, top panel). It has been previously shown that the maleimide-based reaction with CPM and protein thiols is pH-sensitive, with the reaction being faster at alkaline pH (192). However, the pH of the piperazine-resuspended sample is titrated down to pH 8.0 prior to incubation with TPS, indicating that the piperazine-based buffer, rather than pH, could contribute to the differences in starting fluorescence observed in the CPM assays. It has been reported

that fluorescent probes produced from a piperazine-coumarin scaffold shows increased fluorescence signal following reaction with thiol groups (289). Given that CPM is a coumarin-based thiol-reactive dye, it may be possible that CPM reacts with piperazine inadvertently increasing the fluorescence intensity of the samples prior to the CPM assay.

Unlike purified samples from the alkali-enriched purification, protein samples purified under mild conditions show a sigmoidal transition in CPM fluorescence traces (top panels in **Figure 4.7**), suggesting that intact protein was obtained following purification under these mild conditions. However, the derivative profile obtained from each fluorescence trace revealed a broad peak spanning a wide temperature range (bottom panels in **Figure 4.7**), suggesting that the signal obtained is likely a mix of different protein contributions to the apparent protein melting temperature. In the presence of CATR, GDP and aspartate, no discernible thermal shift is observed (bottom panels in **Figure 4.7**), which could indicate either the absence of folded AAC and UCP2 protein, respectively, or that the collective melting temperature of proteins in the final purified sample masks any thermal shifts attributable to a single protein. These findings suggest that the purified sample is a heterogenous mixture, and the melting temperatures obtained are the average of all of cysteine-containing proteins in the final sample.

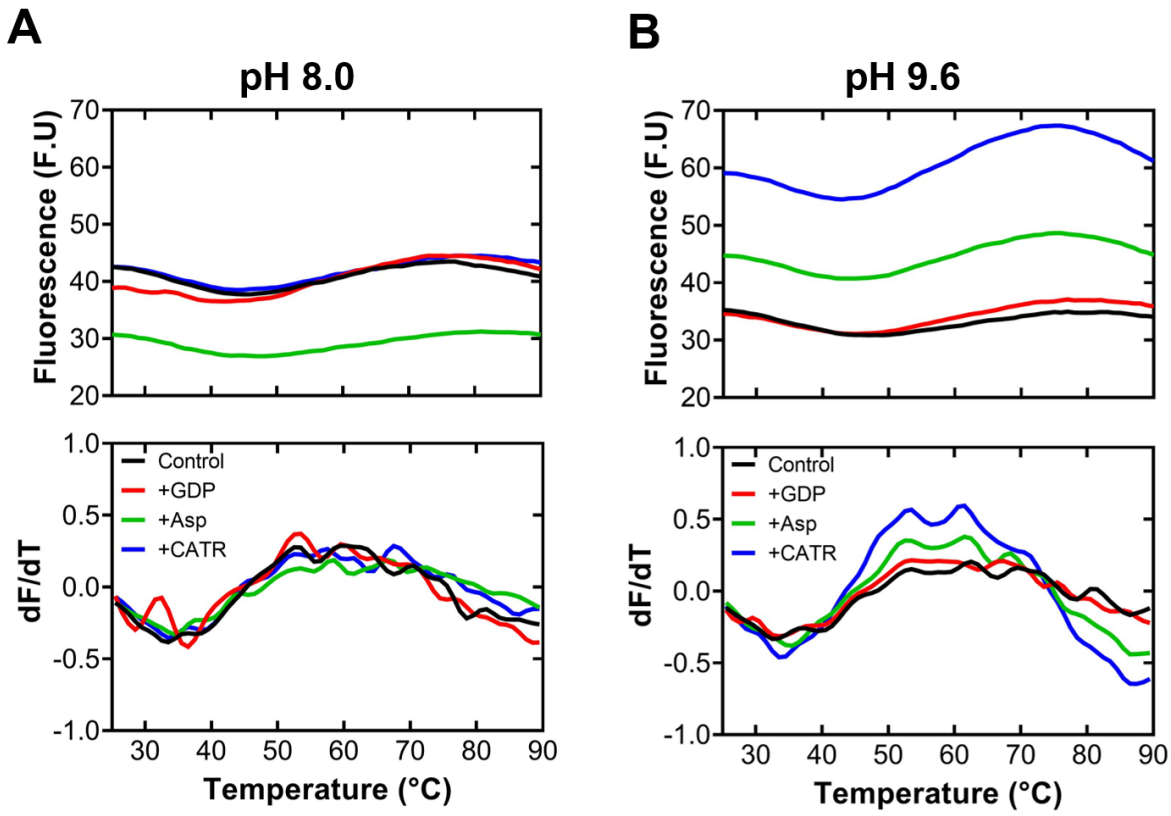

Figure 4.7: Assessment of final samples from UCP2 purification attempts with milder pH conditions using the CPM thermostability assay. *Fluorescence signals (top) and corresponding derivative (bottom) traces from CPM thermostability assays using the final purified samples, derived from membranes that were initially resuspended in 20 mM Tris HCl (pH 8.0) (A) or 20 mM piperazine (pH 9.6) (B) for the purposes of ion exchange chromatography. Thermostability assays were conducted at pH 7.5 (as standard protocol), using 2 µg of purified protein in the absence or presence of 1 mM CATR, 1 mM GDP and 1 mM aspartate to detect AAC- and UCP2-dependent thermal shifts. Native OaUCP1 was used as a control (see* ***Appendix Figure 3.2B-C****).*

Size exclusion chromatography (SEC) of purified intact mitochondrial carriers shows that they are monomeric with masses of ~70 to 130 kDa or more, made up largely by associated detergent and lipid (98, 290), with functional OaUCP1 eluting similarly with a mass of ~127 kDa (19). To assess whether UCP2 protein remained intact following the purification process, final samples from purification attempts were applied onto a Superdex 200 Increase 10/300 gel filtration column, with a prior ~2-fold concentration of samples using spin filter columns in some cases. The SEC chromatograms of samples obtained using pH 8.0 and pH 9.6 (both lacking the harsh

alkali treatment) and concentrated before loading onto the column show similar profiles, with a prominent peak at an elution of ~8 mL, corresponding to the void volume that likely contains misfolded protein aggregates, followed by a second peak at ~11 mL, which likely represents folded mitochondrial carrier in detergent-lipid micelles (**Figure 4.8**; (19, 98, 290)). The concentrated samples demonstrated twice as much absorbance compared to non-concentrated samples (see **Appendix Figure 3.3**), indicative of twice as much protein present, relating to the higher concentration and amount loaded. Western blot analysis of SEC fractions revealed the presence of UCP2 associated with the ~11 mL carrier peak (see Western blots in **Figure 4.8** and **Appendix Figure 3.3**), but only for samples prepared using pH 8.0 and not pH 9.6 during ion exchange chromatography. UCP2 signal could be detected in void fractions when little or no carrier peak signal was detected, but also at later elution volumes as a degraded peptide (~10-15 kDa) in all cases (**Figure 4.8** and **Appendix Figure 3.3**). Therefore, the use of only pH 8.0 in place of the alkali-treatment is likely to facilitate purification of intact UCP2, when purifying using the S, Q, TP method.

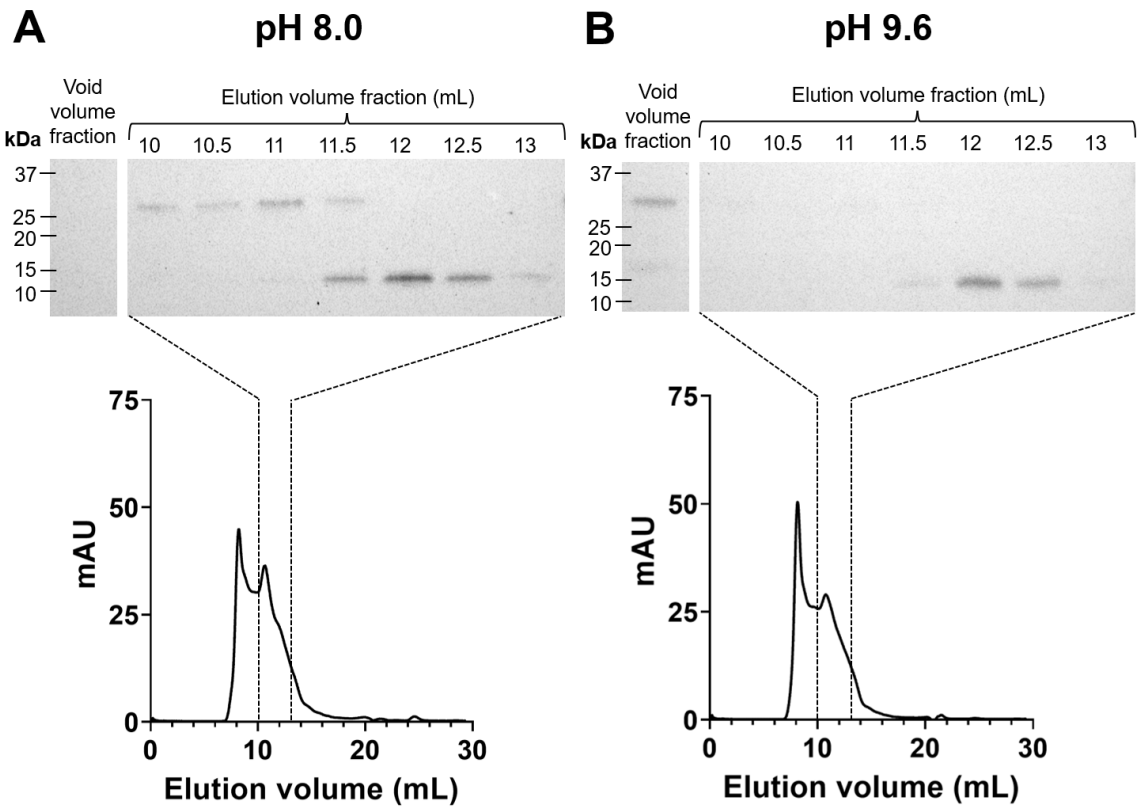

Figure 4.8: Determining HsUCP2 quality through size exclusion chromatography. *A-B) Chromatograms (bottom panels) of size exclusion tests using 2-fold concentrated eluates from post PD10 samples from purifications using membranes that were initially resuspended in 20 mM Tris HCl (pH 8.0) (A) or 20 mM piperazine (pH 9.6) (B) for the purposes of ion exchange chromatography. SEC runs were conducted at pH 8.0. Western blots (top panel) taken from corresponding SEC runs; lanes are labelled to match the elution volume from which the fractions were taken; the void peak was taken at 9 mL elution volume. Samples are loaded in proportion to the fraction volume collected by the AKTA.*

Whilst solubilisation screens showed UCP2 to be soluble at pH 9.6 (**Figure 4.1**), no intact protein was observed following sample application onto a SEC column, suggesting that UCP2 does not tolerate purification at >pH 8.0. Arguably, the need to titrate the Q-flow through sample from pH 9.6 to pH 8.0, for the purposes of covalent chromatography with the thiol-reactive resin, could also be a reason for the lack of intact folded protein signal, as addition of acidic buffer (Tris HCl (pH 6.8)) may have been detrimental to UCP2 protein stability following partial purification by ion exchange columns. Prior to SEC analysis, post PD10 eluates from purifications involving sample resuspension in pH 8.0 and pH 9.6 for ion exchange

chromatography, were quantified and found to contain similar, relatively high amounts of protein, ~3-3.25 mg (~15-fold more than alkali-treated membranes, see **Appendix Table 3.1**). The high protein yield obtained prior to SEC, supports the notion that the final purified sample is likely to be intact, but comprised of mixed protein populations, with a heterogenous mix of protein populations, as implied from the CPM assay data (**Figure 4.7**).

The data indicates that when purified under mild conditions, the final purified sample is likely contaminated with other mitochondrial carrier proteins. The most abundant carrier in yeast, and detected contaminant is AAC, of which there are three isoforms in yeast (145). One strategy that was explored to reduce AAC contamination in the final purified sample was to include ADP throughout the isolation methods. ADP is reported to destabilise solubilised AAC in the absence of lipids (155), interacting as a transport substrate, which may help remove the carrier during purification through induction of different conformational states, whilst at the same time the purine nucleotide may stabilise HsUCP2, assuming it can bind in the same way as it does to HsUCP1 (52, 53, 57, 60, 61, 67, 156, 205, 287). When tested, the purification profile observed resembled the profile obtained in the absence of ADP in mild conditions (at pH 8.0, without the alkali treatment step), with a strong protein band observed in Coomassie-stained gels at ~33 kDa at the TPA elution step (**Appendix Figure 3.4A**). However, purification using ADP pre-treated membranes showed more binding of UCP2 to the TPA resin (see UCP2 Western blot in **Appendix Figure 3.4B**, compared with **Figure 4.6A**). Whilst AAC also tracks with UCP2 in the ADP pre-treated condition, more protein is lost in the TPA flow through (AAC Western blot in **Appendix Figure 3.4B**, compared with **Figure 4.6A**). Even so, results obtained from CPM thermostability assays suggests that the dominating protein species present in the final purified sample is likely unfolded as the fluorescence profiles fails to display the expected increases and sigmoidal transition with increasing temperature (**Appendix Figure 3.4C**).

From the data gathered, it is clear that UCP2 protein can be enriched from mitochondrial fractions under mild conditions, though a large portion (>60%) of protein is lost due to lack of binding to the thiol-reactive resin. To maximise UCP2 protein binding capacity onto the TPS resin, a construct mimicking the C-terminal residues of UCP1 was produced ("construct 5"), which specifically replaces the

terminal three residues of HsUCP2 with cysteine-alanine-threonine (see **Appendix Figure 1.1** for sequence alignment of construct 5). Given that UCP1 protein can be purified through the cysteine 305 residue towards the C-terminus, it was hypothesised that adding this 'tag' would increase covalent binding of UCP2 to the thiol-reactive resin. Small-scale (50 mL) expression trials of construct 5 demonstrated that comparable levels of UCP2 protein were generated compared to construct 1 following 22 hours protein induction (**Appendix Figure 3.5A**), whilst 1 mL-scale solubilisation tests show that similarly high levels of intact UCP2 can be extracted from mitochondrial membranes (**Appendix Figure 3.5B**, compared to **Figure 3.10** (**Chapter 3**)). Subsequent UCP2 expression and purification attempts using construct 5 with 'tagged' UCP2 were conducted as before using mild pH 8.0 conditions in place of the alkali treatment. The resulting purification profile was found to be comparable to the equivalent profile obtained using non-tagged UCP2, though more protein is captured by the ion exchange columns (Coomassie-stained gel in **Figure 4.9A** compared to **Figure 4.6A**). Consequently, the TPS resin had a less purifying effect on protein purification (Coomassie-stained gel in **Figure 4.9A**). Surprisingly, less UCP2 protein was observed to bind to the thiol-reactive resin (Western blot in **Figure 4.9A**), despite the additional cysteine residue engineered in towards the C-terminus. When applied to a SEC column, a dominant peak and shoulder was observed at 10-12 mL elution volume, potentially representing mitochondrial carrier proteins. However, the significant loss of UCP2 in the earlier stages of the purification suggested these are likely other carriers and that alternative approaches would be needed.

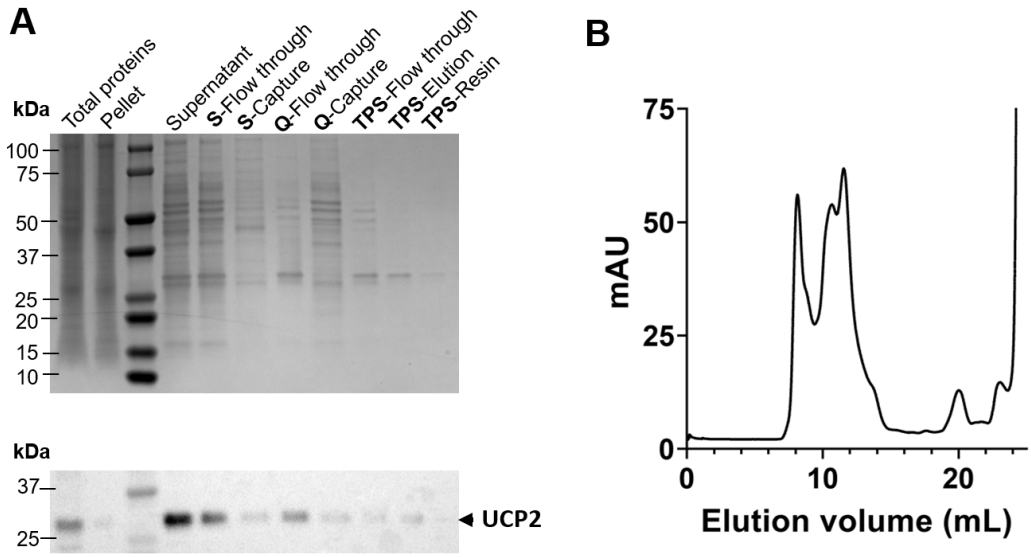

Figure 4.9: S+Q TPS purification using construct 5 (HsUCP2 variant with a UCP1-like C-terminus). *A) Coomassie-stained gel (top panel) and Western blots (bottom panel) tracking HsUCP2 protein. Gel samples are loaded by fractional load, proportional to the sample volume. B) Chromatogram of size exclusion runs using a 5-fold concentrated PD10 eluate.*

4.3.3. Expression of UCP2 in the AAC-deficient yeast strain to mitigate AAC contamination

Western blot analyses indicated that AAC is present in the final preparation when attempting to purify UCP2. As the most abundant carrier, and a type that is particularly unstable when solubilised and isolated (155), AAC may be present as a dominant contaminant in the final sample. To circumvent the problem of AAC contamination, the use of an AAC-deficient (WB12) strain of yeast was explored to express and purify recombinant human UCP2.

4.3.3.1. HsUCP2 expression in the WB12 strain

To establish if recombinant UCP2 expression was viable in the WB12 strain, small-scale (50 mL) expression screens were conducted to determine if modifications of established growth and expression protocols could produce intact UCP2 protein. In particular, the use of glucose and raffinose (291) were tested as alternative carbon sources, where in the case of glucose cells are not dependent on mitochondrial respiration in the AAC-deficient yeast strain. It was observed that UCP2 expression in the WB12 strain using prolonged expression protocol 3 (outlined in **Chapter 3, section 3.3.4.3**) did not produce similar levels of expression to the FGY217 strain (see

Appendix Figure 3.6). UCP2 protein production in the WB12 strain was only comparable to expression levels in the protease-deficient, FGY217 strain, when WB12 cells were grown in low glucose media (YPD 0.75% glucose) for 16/17 hours before resuspension into raffinose-containing (YPR) media (**Figure 4.10B**). Upon resuspension into YPR, galactose was added to induce protein expression for 22 hours (see **Figure 4.10A** for small-scale (50 mL) schematic). Growth and expression in low glucose media alone did not yield any protein expression in WB12 strain (see **Appendix Figure 3.7**), highlighting the need to change the carbon source from glucose to raffinose prior to protein induction. UCP2 protein production in glucose/raffinose media was consistent between small-scale (50 mL) and large-scale (1 L) cultures (**Figure 4.10C**). Whilst high levels of UCP2 protein could be expressed in the AAC deficient strain, solubilisation screens revealed that the generated protein was almost all present in a non-extractable, likely unfolded form, as shown by intense signals in the insoluble pellet fraction (**Figure 4.10D**). This outcome may be a consequence of prolonged expression in the AAC-deficient strain.

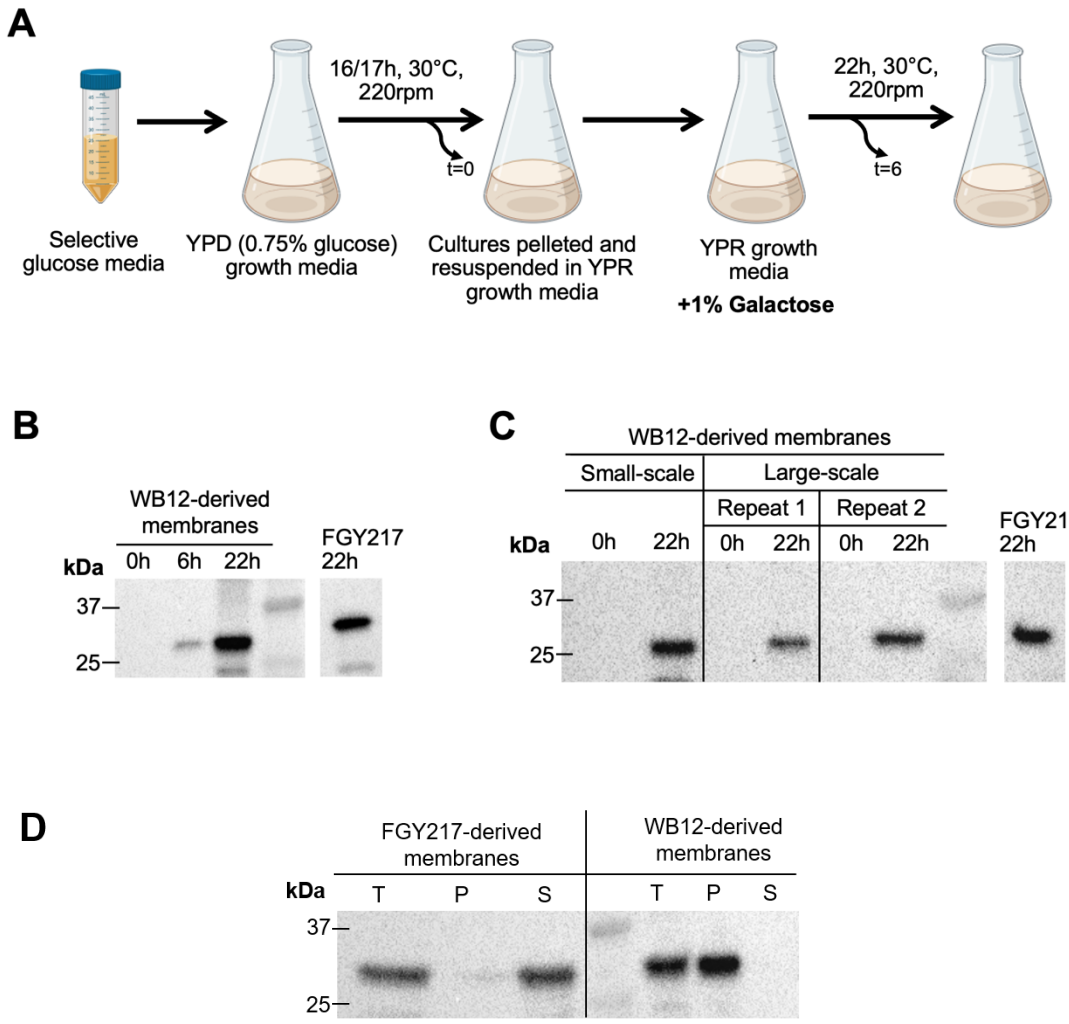

Figure 4.10: HsUCP2 expression in the WB12 yeast strain. *A) Schematic of small-scale WB12 expression screen following an adapted UCP1 expression protocol (177, 178), whereby cells were cultured in 50 mL YPD (0.75% glucose) media for overnight (16/17 hours) growth, pelleted and resuspended in raffinose (YPR) growth media prior to 22 hour protein induction with 1% galactose. B-C) HsUCP2 protein production in the WB12 strain was compared to protein production in the FGY217 strain in 50 mL small-scale (B) and 1 L large-scale (C) expression trials following 22 hours growth through Western blot analysis. In each lane, 10 µg mitochondrial membranes were loaded. Times above the lanes represent the hour at which samples were taken following induction with 1% galactose, with '0h' representing the time prior to galactose addition. D) The quality of the recombinant UCP2 protein produced in the WB12 strain was determined through solubilisation tests, with fractions obtained from a parallel solubilisation screen conducted using FGY217 membranes loaded as a control. Fractions are loaded proportional to the total volume; solubilisation fractions are described as the 'total proteins' – T; 'solubilised supernatant' – S and the 'insoluble pellet' – P.*

To determine if reducing the expression time could improve the amount of intact protein generated, protein expression was systematically varied between 6 and 22 hours (see **Figure 4.11A** for small-scale (50 mL) schematic). Decreasing protein expression time to 10 hours in the WB12 strain retained similar levels of HsUCP2 protein expression using the FGY217 expression system (**Figure 4.11B**), though it was observed that only a very small amount (<10%) of protein could be solubilised in the presence of mild detergent (see **Figure 4.11C**). Though minimal levels of folded UCP2 protein could be extracted from WB12 mitochondrial membranes, it was observed that DDM was able to solubilise slightly higher amounts of protein than 12MNG. Therefore, to maximise the amount of folded protein extracted from WB12 membranes, the use of DDM was taken forward for subsequent large-scale solubilisations.

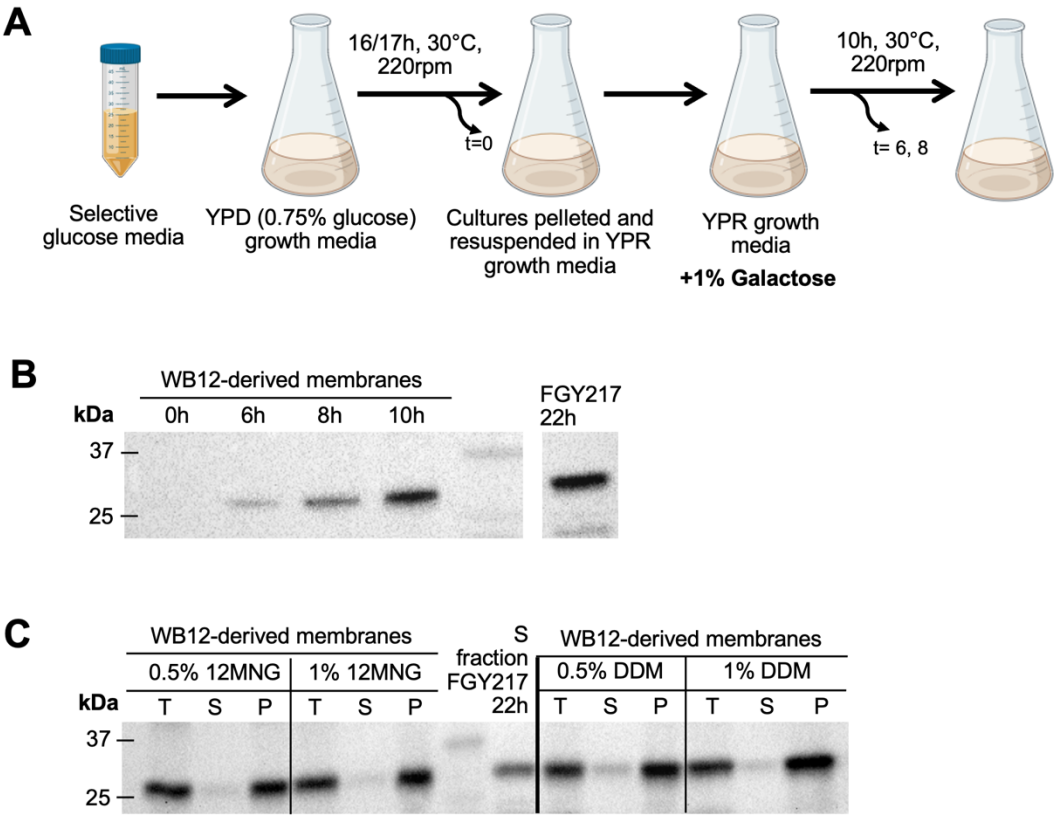

Figure 4.11: Reducing protein induction time in the WB12 strain to improve protein solubility. *A) Schematic of small-scale WB12 expression screen following an adapted UCP1 expression protocol (177, 178); cells were cultured in 50 mL YPD (0.75% glucose) media for overnight (16/17 hours) growth, pelleted and resuspended in raffinose (YPR) growth media prior to 10 hour induction with 1% galactose. B) Western blot of WB12 membranes from small-scale expression, times above the lanes represent the timepoint cells were harvested. 10 µg mitochondrial membranes were loaded into each lane. Mitochondrial membranes isolated from FGY217 cells were loaded for comparison of protein expression ('FGY217 22h' lane). C) Fractions obtained from 1 mL-scale solubilisation trials, using WB12 membranes induced for 10 hours following the outlined expression protocol. The 'S fraction FGY217 22h' is representative of a solubilised fraction using FGY217 membranes grown using prolonged expression protocol 3. Fractions are loaded as proportional to the total volume; solubilisation fractions are described as the 'total proteins' – T; 'solubilised supernatant' – S and the 'insoluble pellet' – P.*

4.3.3.2. S+Q TPA purification of HsUCP2 derived from WB12 membranes

To ascertain if UCP2 protein expression using the WB12 strain was a viable option for generating recombinant protein fit for downstream biochemical characterisation, purification was conducted using WB12 membranes that were subjected to 10 hours

protein induction. In this iteration of the S+Q TPA purification protocol, WB12-derived mitochondrial membranes were solubilised in 0.5% DDM, prior to sequential passage through S and Q columns and subsequent incubation with thiol-reactive resin (see **Figure 4.3** for schematic).

High levels of total protein were solubilised and passed through ion exchange columns, though no band could be observed after elution of covalently bound proteins (Coomassie-stained gel in **Figure 4.12A** (top panel)). When probed for UCP2, a significant proportion of protein is unfolded, with less than 10% of UCP2 protein produced in WB12 cells extracted in a folded form (see UCP2 Western blot in **Figure 4.12A** (middle panel)), consistent with previous solubilisation screens (**Figure 4.11C**). Whilst UCP2 protein is seen to pass both ion exchange columns, no UCP2 protein could be detected after the TPA steps though a signal could be observed in the 2 µg load lane (see UCP2 Western blot **Figure 4.12A**), suggesting that the amount of protein bound onto the TPA resin is undetectable or potentially masked by the signal intensity obtained from the total protein lane. When blotted against AAC, no signal is observed throughout the purification profile, thus confirming the use of the WB12 strain as a way of circumventing AAC contamination (see AAC Western blot in **Figure 4.12B** (bottom panel)). The lack of a protein signal in the Coomassie-stained gel between 25-37 kDa, which would correspond to the size of most mitochondrial carriers (203, 282), suggests that the final purified sample is likely a heterogenous mixture of other proteins, enriched in the absence of carriers. Despite the lack of a dominant 33 kDa band, thermostability assays were conducted to determine the quality of protein produced and if a protein melting temperature could be obtained.

The fluorescence signal obtained in CPM assays (**Figure 4.12B**) do not show a clear transition from low to high fluorescence, suggesting cysteine accessibility is already maximal in the protein population before heating. Interestingly, the fluorescence signal did not decrease with increasing temperature as shown with previous CPM assays conducted using purified samples from other purifications outlined in this chapter. Similar fluorescence profiles featuring a 'flatline' in fluorescence units have been observed with native OaUCP1 and *E. coli*-generated UCP1 protein solubilised in harsh detergents, such as DPC, where carriers are not in an appropriately folded state (155, 192).

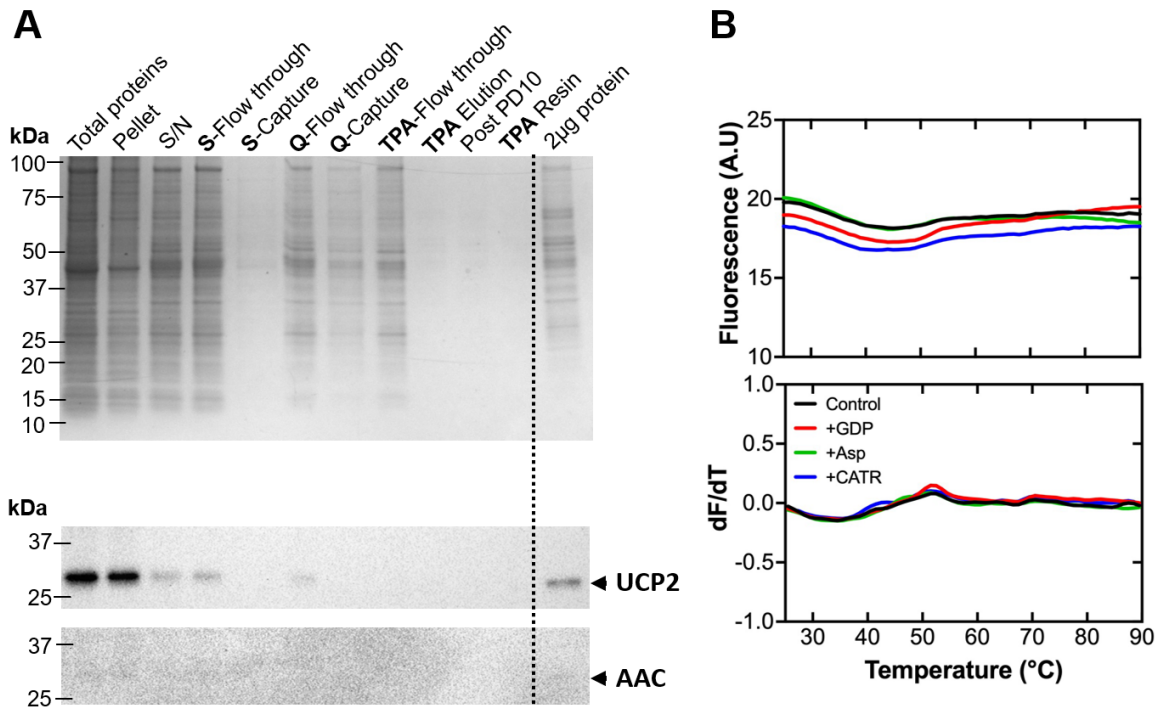

Figure 4.12: S+Q TPA purification of HsUCP2 protein from WB12 membranes. *A) Coomassie-stained gel (top panel) and Western blots tracking UCP2 and AAC protein (middle and bottom panels, respectively) throughout an S+Q TPA purification of WB12 mitochondrial membranes. Gel samples are loaded in proportion to the total sample volume, except for the final lane, where 2 µg of the final purified sample was loaded. B) Fluorescence (top) and derivative (bottom) traces from CPM assay runs using 2 µg purified protein obtained from WB12 purification. Native OaUCP1 was used as a control for thermostability assays (see* ***Appendix Figure 3.2E****).*

Under mild conditions, ~1.5 mg of protein could be obtained from WB12 mitochondrial membranes, accounting for ~0.79% of the total membranes used (**Appendix Table 3.1**). Although this percentage was relatively high compared to other purifications used (see 'Protein purified per mg membrane' column in **Appendix Table 3.1**), the results presented clearly show that protein expression of UCP2 using the WB12 strain was impractical for UCP2 protein expression and purification as protein generated using this strain yielded predominantly unfolded material, with the final sample unlikely to be enriched for recombinant UCP2.

4.4. Discussion

The purpose of these studies was to determine if recombinantly expressed HsUCP2 protein generated in our heterologous yeast expression system could be purified using core methods established for UCP1. The findings demonstrate that under mild conditions, UCP2 protein can be enriched from mitochondrial membranes, using adapted and optimised protocols. Whilst it was not possible to purify recombinant human UCP2 to homogeneity using the S+Q and TP approach, other purification strategies that were not explored in the context of this work could be investigated to determine if it is possible to purify intact human UCP2.

4.4.1. Enrichment of UCP2 protein by S+Q TP purification method

The use of a bespoke purification strategy, originally developed for the purification of OaUCP1 from native lamb tissue (19), was unable to purify the closely related HsUCP2 protein to homogeneity, in a folded and functional form. It could be argued that protein purification from native tissue may behave differently compared to protein purification from recombinant systems. However, the S+Q TP method has been utilised to successfully purify yeast-expressed UCP1 protein (153, 171), therefore suggesting that the inability to purify UCP2 could be due to fundamental differences in the molecular properties of the proteins. Human UCP1 is composed of 307 amino acids, with a C-terminal cysteine residue at position 305, whereas human UCP2 consists of 309 amino acids, with a C-terminal cysteine residue at position 302 (4). The slight variation in the position of the cysteine residue between the two proteins could be the reason why purification by covalent chromatography was unsuccessful. Whilst the cysteine residue in human UCP1 is followed by two small amino acids (alanine and threonine), the cysteine residue in human UCP2 is succeeded by seven amino acids, two of which are charged (arginine at position 305 and glutamate at position 306) and two of which are bulky hydrophobic residues (proline and phenylalanine at positions 308 and 309, respectively). Potential steric hindrance caused by amino acids following the cysteine 302, could be why UCP2 could not be purified using thiol-reactive chemistry. A UCP2 mutant harbouring a UCP1-like cysteine towards the C-terminus was produced, though it was unclear if this protein remained folded following the purification methods used.

Purification profiles using membranes derived from the protease-deficient strain show an enrichment at ~33 kDa, the size of most mitochondrial carriers (203, 282),

though most of these samples are likely to be contaminated with other carrier proteins. Results from most CPM assays involving UCP2 purified samples do not show a characteristic sigmoidal transition from low to high fluorescence, indicative of unfolded protein species dominating the final sample. These findings suggest that UCP2 could be more unstable than UCP1 as the protein cannot be purified using the same methods.

4.4.2. Human UCP2 expression in the AAC-deficient yeast strain

To circumvent the issue of AAC contamination in the final purified sample, the use of an AAC-deficient strain was utilised. Unfortunately, recombinant expression of UCP2 in the WB12 strain yielded predominantly unfolded protein. In contrast, HsUCP1 expressed in WB12 yeast was not only purified using the S+Q and TPS protocol but was found to be folded and functionally active (Dr. Camila Cotrim and Danielle Copeman, unpublished data). Interestingly, when a marsupial variant of UCP1 (*Monodelphis domestica* UCP1) was expressed in the WB12 strain, the purified sample was observed to be unfolded (Dr. Camila Cotrim, unpublished data), suggesting that the marsupial UCP1 may be more like mammalian UCP2 than to human (eutherian) UCP1. Differences in the quality of the UCP protein produced in the WB12 strain could be attributed to the functional properties of the protein, suggesting that human UCP1 expression in the WB12 strain does not affect the host cell viability, whereas expression of human UCP2 and marsupial UCP1 was unfavourable as most of the protein expressed was unfolded. These observations may further indicate that UCP2 is very unstable compared to UCP1, and if misfolded in the WB12 strain, is likely to be degraded in the AAC-deficient, yet protease-containing strain. These findings suggest that subtle differences between the physiochemical properties of UCP1 and UCP2 indicate these proteins are functionally distinct, despite the 59% protein sequence homology.

4.4.3. Suggestions for future UCP2 purification efforts

The efforts in this chapter show attempts to purify UCP2 protein from recombinant systems in the absence of purification tags, relying on solvent-exposed cysteine residues to act as an intrinsic tag. These efforts were based on unpublished observations that recombinant expression of tagged UCP1 protein was poor and failed to generate folded material (215). However, recent literature has demonstrated that

yeast- (153) and mammalian- (237) expressed UCP1 protein could be purified using N-terminal histidine- and streptavidin-tags, respectively. Furthermore, tagged UCP1 protein could be purified to a high level of purity sufficient for structural purposes. Subtle differences in the respective expression systems used may therefore be critical. One avenue that could be investigated for future UCP2 purification efforts, is to determine if affinity chromatography can be used to purify UCP2 to homogeneity, now with the use of the protease-deficient yeast strain, which has shown some success for generating intact UCP2. Based on data from UCP2 protein expression optimisation screens (see **Chapter 3** for details), engineering a purification tag at the C-terminus of the protein may be beneficial, as addition of an N-terminal tag may potentially affect the improved protein expression that was observed following change of the second amino acid to leucine.

5. Functional characterisation of human Uncoupling protein 2 produced in *S. cerevisiae*

5.1. Introduction

Since the discovery of the *Ucp2* gene, the product of which has a 59% protein sequence similarity to UCP1 (4), the function of the UCP2 protein has been the subject of much debate (198, 292, 293). It is well established that UCP1, which is highly expressed in BAT mitochondria, catalyses proton leak to uncouple oxidative phosphorylation and generate heat in the physiological process of non-shivering thermogenesis (2, 9, 10). UCP1 activity is regulated by interacting ligands: fatty acids, which activate the protein (2, 21, 27) and purine nucleotides, which bind and inhibit the carrier from the cytosolic side (31, 33, 34, 294). Unlike UCP1, which is almost predominantly expressed in BAT and beige tissue (3, 295), UCP2 is expressed at far lower magnitudes and in a variety of different tissues and cell types (38, 41, 42, 185), such as pancreatic β-cells (90, 105, 185) and immune cells (41, 42). Along with other UCP1 homologs, UCP2 was proposed to catalyse proton leak to 'mildly uncouple' the mitochondria to reduce the production of ROS by mitochondria and associated oxidative stress, rather than playing a thermogenic role like UCP1 (296). Studies using pancreatic β-cells, demonstrated that UCP2 expression dampens glucose-stimulated insulin secretion (GSIS) (90, 92, 105), a process that is sensitive to ATP/ADP ratios (104). Hence, removal of UCP2 from pancreatic β-cells was proposed to enhance GSIS by improving mitochondrial coupling (90, 92, 105). In neutrophils and macrophages, cells that utilise ROS to clear pathogens and express UCP2 (84), it was found that UCP2-deficient cells were more effective in clearing bacteria and parasites (86-88), potentially through elevated levels of ROS production. As such, these findings supported the possibility that UCP2 may function to uncouple mitochondria to prevent the formation of ROS.

Various studies with isolated mitochondria have reported that UCP2 mediates uncoupling of mitochondria in a GDP-sensitive manner (51), with proton leak induced by fatty acids, and augmented by various co-factors, such as ubiquinone (49, 65, 66), superoxide (52, 53, 69) and the reactive alkenal, 4-hydroxy-2-nonenal (4HNE)

(50, 69, 79). Though findings reporting UCP2 uncoupling activity in isolated mitochondria have been widely contested. In yeast mitochondria, general protein expression can cause artefactual uncoupling due to loss of mitochondrial membrane integrity (55), whilst independent experiments from various lab groups could not replicate UCP2 uncoupling activity, and associated claims relating to ubiquinone (71), superoxide (81) or 4HNE (81, 82, 297). Hence, it remains unclear whether or not UCP1 homologs conduct protons in a similar manner to UCP1. More recent studies have suggested that UCP2 is a 4-carbon metabolite transporter that functions through an antiporter exchange mechanism (93, 114, 119), like other carriers, which provides metabolic flexibility in cells, particularly during the utilization of glutamine (93, 114, 116, 119, 298). Even so, it remains unclear if proton transport is coupled to 4-carbon metabolite transport activity or if an independent proton leak activity is facilitated by UCP2.

The question of whether UCP2 uncouples mitochondria remains widely controversial (293, 299), though a key characteristic of UCP1 that is also claimed to occur for UCP2, owing to its high sequence similarity, is the protein's ability to bind purine nucleotides. Studies using *E. coli*-expressed UCP2 protein report that UCP2 does bind purine nucleotides and include claims of a nucleotide-bound UCP2 structure solved by NMR (57, 156, 204, 205, 300). Notably, several studies use purine nucleotides as a diagnostic for UCP2-dependent leak activity (49, 50, 52, 53, 65, 66, 74, 164, 205, 301, 302). Liposome reconstitution studies of *E. coli*-produced UCP2, report that millimolar concentrations of purine nucleotides are required to inhibit UCP2 activity (57, 93), which is distinct from UCP1, which only requires micromolar amounts to inhibit UCP1 activity (57). Most studies reporting on the nucleotide binding properties of UCP2 are based on bacterially-expressed protein (57, 156, 204-206, 300), which is reliant on 'refolding' using ionic detergents (203). The use of these detergents has called into question conclusions drawn from such studies (155, 158-162). Therefore, it remains unclear if UCP2 binds purine nucleotides in the same way as UCP1.

This chapter summarises experiments undertaken to clarify the functional properties of UCP2, including the development of a novel assay that reports on ligand binding to solubilised UCP protein without the need to purify.

5.2. Aims

1. To clarify if UCP2 can conduct protons like that of UCP1, using proteoliposomes and isolated mitochondria.
2. To determine if UCP2 binds purine nucleotides in a similar manner to that of UCP1, where purine nucleotide binding increases protein stability, particularly at low pH.

5.3. Results – Investigation into HsUCP2 proton conductance activity

5.3.1. Proton transport assays

Chapter 4 demonstrates that UCP2 could not be purified to homogeneity using methods established for the purification of UCP1. Despite this, investigation into proton conductance activity of HsUCP2 was conducted through trials to reconstitute the final purified samples into liposomes. Given that previous studies have indicated successful liposomal reconstitution of some UCP2 protein from solubilised mitochondrial fractions (93), it was rationalised that semi-purified protein samples could also be reconstituted into liposomes to provide insight into the protein's proton transport activity.

In proteoliposomes, proton flux can be monitored through changes in the fluorescent dye, SPQ, which is quenched by the anions of buffers, such as TES^- as well as PO_4^- but not the protonated forms (191). During protein reconstitution, SPQ is entrapped into liposomes, along with a high concentration of potassium salts (100 mM K(TES/PO_4) relative to outside. Following liposome formation, liposomes are exchanged into buffers devoid of potassium with components otherwise matched using TEA-salts, and no SPQ dye (see **Appendix Figure 4.1** for schematic). In the experimental set-up, starting fluorescence is low as SPQ is quenched by the TES^- anion. Upon addition of the potassium ionophore, valinomycin, K^+ ions specifically flow down their chemical gradient across the lipid membrane to generate a charge gradient, positive outside, negative inside. This membrane potential, in turn, provides a driving force for protons to enter the liposome. The presence of active UCP1, or other proton leak routes, results in proton influx that can be monitored by increases in SPQ fluorescence, which occurs due to the decrease in TES^- anion concentration from protonation and associated quenching. Addition of the protonophore, CCCP, as a

control, allows for protons to rapidly move and equilibrate across the liposomal membranes, and reveal the total proton transport capacity of the liposomes (see **Appendix Figure 4.1A** for schematic). Preliminary data with liposomes generated using UCP2 samples purified under mild conditions showed minimal levels of proton transport, which was 100-fold less than rates observed with reconstituted HsUCP1 controls (see **Figure 5.1A** for rates and **Appendix Figure 4.1B** for traces). Quantification of UCP2 reconstituted into the liposomes using purified inclusion body standards did not detect any protein in the final sample in the 0 to 40 ng protein range (**Figure 5.1B**), though a very faint band could be detected when the proteoliposome sample is blotted in the absence of UCP2 protein standards (**Appendix Figure 4.2**), suggesting that UCP2 is either present in the picogram range or is not reconstituted into the liposomes at all. Due to time constraints, this line of investigation was not explored further.

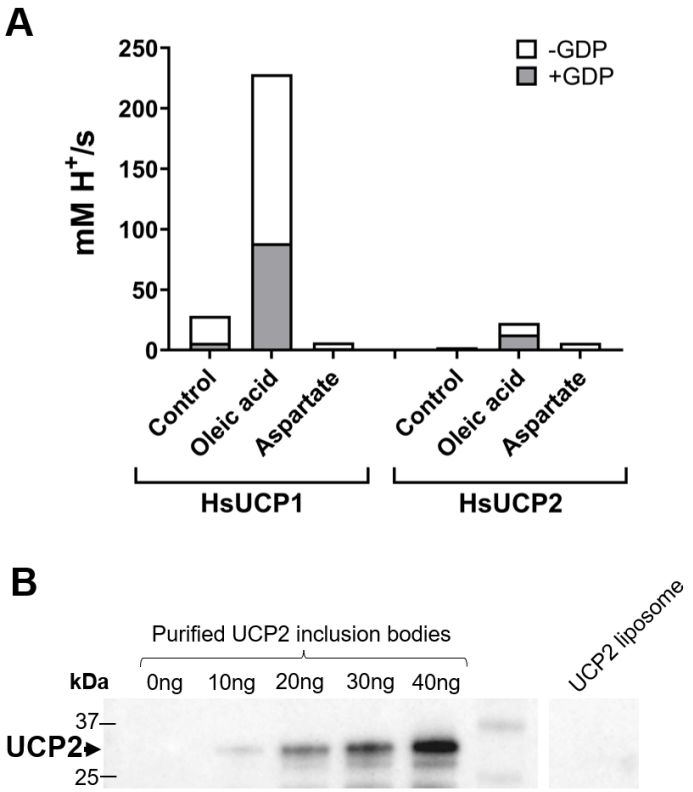

Figure 5.1: Investigating UCP2 proton transport activity using liposomes. *A) Proton flux rates of UCP1 and UCP2 liposomes treated with oleic acid, a known UCP1 activator, and aspartate, which is reported to be a transport substrate of UCP2 that is potentially exported from mitochondria in exchange for Pi/H^+ (93, 114). B) Quantification Western blot of UCP2 liposomes using protein standards generated as bacterial inclusion bodies; ~0.28 µg protein was loaded onto gel (liposome sample), assuming 100% reconstitution efficiency.*

5.3.2. Oxygen consumption assays using isolated mitochondria

Preliminary investigations to detect UCP2 proton flux activity were unsuccessful in liposome assays. Subsequent avenues in exploring UCP2 proton leak was investigated through oxygen consumption assays using isolated yeast mitochondria. Using a Clark-type oxygen electrode, oxygen consumption of isolated mitochondria can be measured following the addition of respiratory substrates such as NADH or succinate. Upon mitochondrial substrate addition, mitochondria undergo state 2 respiration, establishing a proton electrochemical gradient across the mitochondrial inner membrane. Addition of ADP enables state 3 respiration, whereby mitochondria generate ATP until the ADP is exhausted, at which point they enter state 4. Respiratory rates are dependent on proton leak pathways, particularly when other routes of proton re-entry into the matrix, e.g. via the ATP synthase during ADP phosphorylation, are not active (e.g. during state 2 and state 4 respiration). Addition of protonophores, like FCCP, allows protons to permeate across the mitochondrial inner membrane into the matrix, dissipating the proton gradient and relieving back pressure on the respiratory chain, leading to maximal oxygen consumption rates (110). Mitochondrial coupling can be quantified through a respiratory control ratio (RCR), which traditionally is the ratio of respiratory rates supporting ATP synthesis and proton leak (state 3) to those that are limited by proton leak activity alone (110). In yeast, an equivalent RCR metric can be calculated by dividing the oxygen consumption rate gained in the presence of a respiratory substrate and a protonophore (uncoupled state) by the rate obtained in the presence of respiratory substrate alone (state 2 respiration) (55). Accordingly, the presence of high proton leak rates results in low RCR values. To determine if UCP2 can uncouple mitochondria in a similar manner to that of UCP1, oxygen consumption and RCR values were gained for mitochondria isolated from yeast induced to express UCP1 or UCP2, or from respective uninduced controls. For UCP1 control tests, it was found that RCR values were no different between induced and uninduced mitochondria (see **Table 5.1** and **Appendix Table 4.1**) (303), and no obvious differences in respiratory rates could be observed between UCP1 induced and uninduced mitochondria suggesting that heterologous expression of UCP1 (~2% of mitochondrial protein) did not necessarily affect expression of mitochondrial respiratory enzymes (**Appendix Figure 4.3** and **Appendix Figure 4.4**).

Preliminary tests conducted in the presence of fatty acids and GDP demonstrated no significant difference in oxygen consumption rates between UCP1-containing and uninduced mitochondria (**Appendix Figure 4.5A**). Preliminary respiratory assays were also conducted with mitochondria induced to express UCP2 or from matched uninduced controls. In these mitochondria, oxygen consumption rates were observed to be far lower compared to equivalent UCP1 tests, particularly the UCP2-containing mitochondria (**Appendix Figure 4.5B)**. The difference in oxygen consumption rates could be due to the differences between the W303-1B and FGY217 yeast strains or it could be due to differences in how the yeast were grown for recombinant protein induction. Due to issues with cell growth/low mitochondrial yields, differences in UCP protein expression levels, limited resolution of the methods, inability to observe clear changes relating to proton leak induced by UCP1 controls and potential differences in the wider respiratory behaviour of the different strains used in these tests, it was decided that this method of detecting proton leak would not allow for appropriate comparison between proteins and assessment of UCP2.

Table 5.1: Table showing the mean RCR values for HsUCP1 and HsUCP2 containing yeast mitochondria.

	UCP1		**UCP2**	
	Uninduced	Induced	Uninduced	Induced
Mean RCR:	1.5	1.8	2.0	1.7
S.E.M:	0.31	0.16	0.06	0.09
p-value:	0.46		0.02	
Significance?	ns		*	

*RCR values were calculated by dividing the oxygen consumption rate obtained in the uncoupled state (i.e. in the presence of NADH and FCCP), by the rate obtained in state 2 respiration (i.e. with NADH alone) (55). Error is presented as S.E.M of 4-5 experiments. Statistical analysis between uninduced and induced mitochondria was conducted using t-tests, *p<0.05. See* ***Appendix Table 4.1*** *for individual RCR values obtained.*

5.4. Results – Investigation into HsUCP2 purine nucleotide binding

Chapter 4 documents various attempts to purify UCP2 using adapted methods established for UCP1 and the associated challenges. A purified preparation would allow application of valuable ligand binding assays, e.g. by the CPM thermostability assay, as has been performed using UCP1 (155, 284). Given that UCP2 could not be purified to homogeneity, alternative methods of probing ligand binding properties of UCP2 were explored, particularly to assess purine nucleotide binding, which is well-characterised for UCP1.

5.4.1. Development of a gel blot-based protein thermostability assay to probe the ligand binding properties of membrane proteins

To develop a novel assay capable of probing ligand binding properties of membrane proteins in samples without purification, the same core principles of the CPM protein-ligand binding thermostability assay were utilised, i.e. the monitoring of cysteine residue-accessibility changes to track thermal denaturation thresholds. The CPM assay is well-suited to studying purified membrane proteins, which require detergent compatibility, and has been used to successfully assess ligand binding to several carriers (147, 153, 155, 194, 219, 221, 284, 304). Use of the assay has shown that well-established ligands of UCP1, fatty acid activators (2, 21) and purine nucleotide inhibitors (31, 305), induce distinct shifts in UCP1 stability thresholds, destabilising and stabilising the protein, respectively (155, 284).

For assay development, purine nucleotide inhibitors were used to detect protein thermal stability shifts; UCP1 shows a higher affinity for nucleotide binding at acidic pH (29, 200, 306, 307), which is reflected in relatively large increases in protein stability observed at low pH (153, 155). To recapitulate the pH-sensitivity of nucleotide binding, CPM assays were conducted at pH 6.0 and pH 7.5, using purified human (Hs)UCP1 in the presence of purine diphosphate nucleotides, GDP and ADP. Logarithmic variation of nucleotide concentrations was conducted to resolve concentration-dependent shifts in binding. A prominent concentration-dependent stabilisation of UCP1 protein could be observed for both nucleotides, as demonstrated by incremental shifts in fluorescence and first derivative signals obtained from CPM assays (**Figure 5.2A**), which was far less prominent at pH 7.5 (**Figure 5.2B**). UCP1 stabilisation was emphasised at acidic pH, where as low as 10 μM concentrations of

GDP and ADP induced a clear stabilising effect at pH 6.0 (by ~10°C) with little effect at pH 7.5 (**Figure 5.2C**, **Appendix Table 4.2** and **Appendix Table 4.3**). At 1 mM nucleotide, a ~20°C increase in apparent T_m at pH 6.0 and ~13°C increase at pH 7.5 could be observed for each nucleotide (**Figure 5.2C**, **Appendix Table 4.2** and **Appendix Table 4.3**). The effect of ligand binding can be expressed as a change in apparent protein melting temperature from the control ("no ligand") condition, denoted as the delta T_m (ΔT_m). When ΔT_m is plotted as a function of the nucleotide concentration, a clear difference in protein stability can be observed at acidic and near neutral pH (**Figure 5.3**). ADP demonstrated a slightly higher degree of protein stabilisation compared to GDP in acidic pH, as shown by higher T_ms at each respective nucleotide concentration (**Figure 5.3**, **Appendix Table 4.2** and **Appendix Table 4.3**). When plotted on a linear scale, the protein stability increase at pH 6.0 appeared to saturate at >100 μM nucleotide (**Figure 5.3A**), whereas at pH 7.5, a saturating effect was not observed in the range used (up to 1 mM) (**Figure 5.3A**). The high stabilisation induced at lower pH is more clearly observed in the logarithmic plots, with thermostability showing a biphasic curve, likely representative of saturated binding (**Figure 5.3B**).

The results presented are consistent with previous observations in the literature, which highlight the pH dependence of nucleotide binding to UCP1 (29, 33, 153, 155, 308). UCP1 protein stability increased in a concentration-dependent manner, with 1 mM nucleotide showing the highest degree of protein stabilisation in the CPM assay, displaying 10°C to 20°C increases in apparent protein T_m, at pH 7.5 and pH 6.0 respectively.

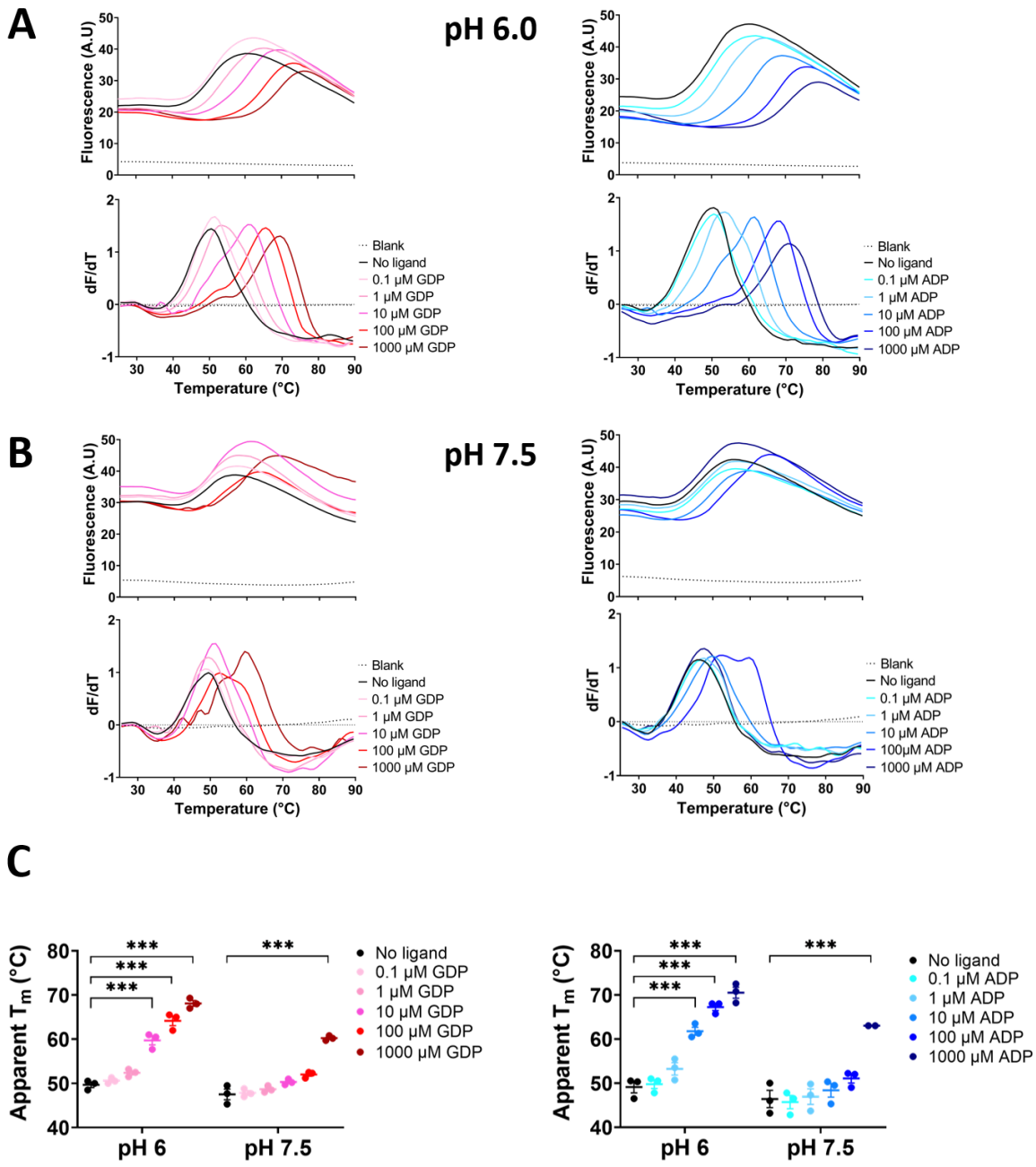

Figure 5.2: Shifts in HsUCP1 thermostability with increasing purine nucleotide concentration. *A-B) Representative thermal denaturation profiles (top panels) and corresponding first derivative profiles (bottom panels) of CPM thermostability assays using purified HsUCP1 protein with logarithmic concentrations of purine nucleotides. Experiments were conducted at pH 6.0 (A) or at pH 7.5 (B) in the presence of 0.1% 12MNG in the assay buffer. For each run, 2 µg purified HsUCP1 protein was used, except in blank runs. C) Scatterplots comparing the average apparent protein T_m at a given nucleotide concentration at pH 6.0 or pH 7.5. Individual points show the apparent T_m obtained for each run, with the bar representing the mean apparent T_m and error bars showing the S.E.M of three experiments.*

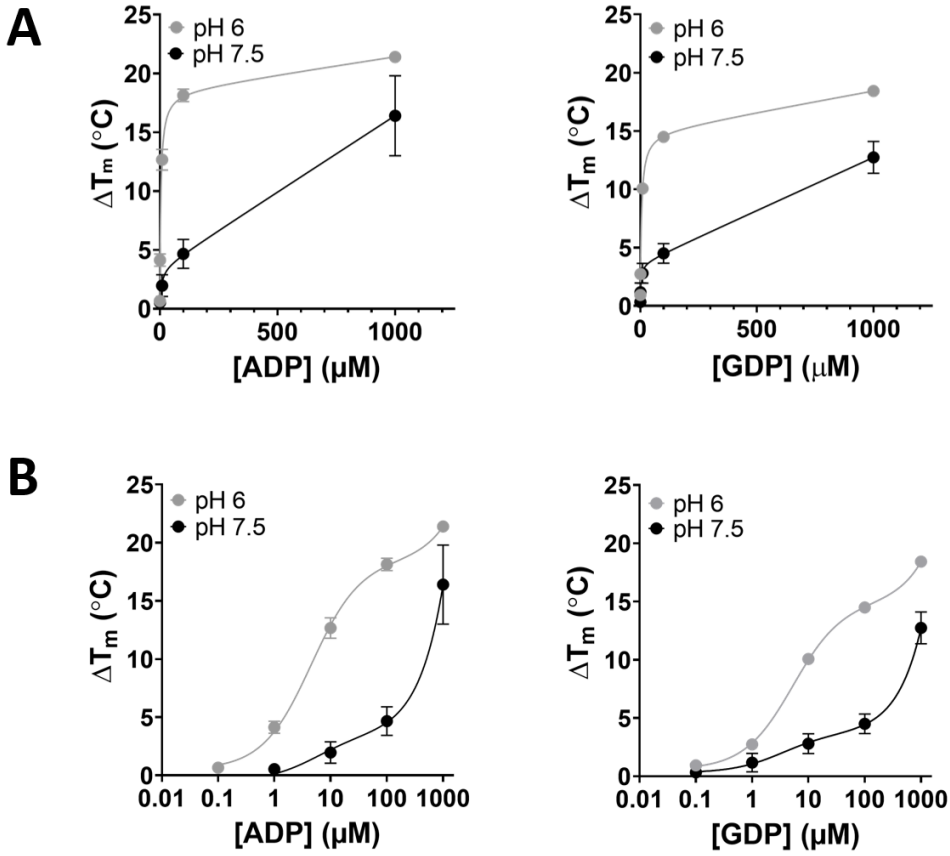

Figure 5.3: HsUCP1 thermostability as a function of nucleotide concentration. *Changes in UCP1 protein thermostability (ΔT_m) plotted on linear (A) and logarithmic (B) graphs as a function of increasing GDP (left) or ADP (right) concentration at pH 6.0 (gray line) and pH 7.5 (black line). Values are expressed as the mean, with error shown as S.E.M of three experiments. Points were fitted in GraphPad Prism, using the 'One-site - Total binding' model to account for the fact that the CPM assay cannot account for non-specific binding with increasing ligand concentration.*

5.4.2. Characterisation of PEG-Maleimide reagents for protein labelling

The CPM assay relies on the use of a maleimide-based thiol-reactive probe as a means of detecting protein thermal shifts in purified samples. In the context of proteins, maleimide is a useful tool for labelling as the maleimide moiety selectively reacts with cysteine residues through thiol-Michael addition reactions, whereby the electron-deficient carbon double bond in the cyclic imide ring undergoes nucleophilic attack by the cysteine sulfhydryl side chain, forming a stable thiosuccinimide linkage (309, 310) (**Appendix Figure 4.6**). Given that CPM can successfully detect thermal shifts of purified UCP1 protein (155, 284), other maleimide reagents were researched as

potential probes. PEG-maleimide species have been shown to react with cysteine residues in mitochondrial carriers to shift the molecular weight of the protein in PAGE analysis (219), and have the potential to allow tracking of cysteine accessibility of proteins without purification through application of immunoblot detection. Commercial PEG-maleimides are available that react to form 2- or 5-kilodalton covalently-linked adducts at protein thiols (referred to as PEG-Mal-2K and PEG-Mal-5K, respectively). Labelling with these maleimide reagents should, in theory, result in molecular weight shifts based on the number of cysteine residues in the protein, corresponding to the addition of the 2- or 5-kilodalton adduct.

For assay development, UCP1 was used to allow observed trends in protein thermostability to be checked against data obtained with the CPM thermostability assay. It was decided that PEG-Mal-2K would be taken forward for testing given its success in detecting cysteine accessibility in the ATP-Mg/Pi carrier (219). To mimic the CPM assay, a method was developed that coupled the PEG-Mal-2K reaction with a temperature ramp to incrementally test protein stability at different temperatures, in order to gain profiles on changes in cysteine accessibility and thresholds of unfolding. In these experiments, a thermal cycler was programmed to pre-incubate the samples with PEG-Mal-2K for 5 minutes at 4°C, followed by a transient (5 second) incubation at a chosen temperature, before samples are cooled back to 4°C and incubated for a further 5 minutes to allow PEG-Mal-2K to react with any exposed cysteine residues. The reaction was subsequently quenched with the addition of the reducing agent, DTT (see **Methods, section 2.19.2** for further details). The process of thermal cycling was repeated several times over a wide temperature range (30°C to 80°C, at 5°C intervals for UCP1 samples). To detect nucleotide-induced shifts in UCP1 stability, trials using PEG-Mal-2K were initially conducted at pH 6.0 where the nucleotide binding is most pronounced (33, 153, 155, 308), but where the maleimide reaction is slower and could become limiting (see **Appendix Figure 4.7**; (311)).

Initial thermostability trials using HsUCP1 mitochondrial membranes in the absence of any ligand, illustrated that at least one cysteine residue was PEGylated at all temperatures where the protein was tested and detected. However, a disappearance in the UCP1 signal with increasing temperature was observed (see top blot **Figure 5.4**), which was not expected as SDS-denatured samples still produced a signal in blots (see **Appendix Figure 4.8**). Interestingly, the presence of protein signal coincides with the approximate temperatures in which UCP1 is observed to be folded in the CPM

assay (see **Figure 5.2A**), whilst the absence of signal correlates with temperatures in which UCP1 is thermally denatured in CPM assays (**Figure 5.4**, top blot). Therefore, to confirm if the disappearance of the signal observed in the presence of PEG-Mal-2K correlated with the denaturation temperature of UCP1, solubilised mitochondria were subjected to the same thermostability procedure, though in the absence of PEG-Mal-2K, and where high-speed centrifugation was used to separate folded from unfolded material. Signals in Western blots probing for folded protein that remained soluble in the supernatant fraction illustrates similar trends in UCP1 protein thermostability, with signals observed at temperatures where protein is likely to be folded (**Figure 5.4**, middle blot). There are some discrepancies at what exact temperature the UCP1 signal is lost between PEG-Mal-2K-treated and centrifuge-separated samples, though this could relate to differences in sample processing following temperature treatment (**Figure 5.4**, top and middle blots). Importantly, total fractions of samples subjected to thermostability assays in the absence of PEG-Mal-2K, i.e. before ultracentrifugation, shows a signal at all temperatures, consistent with normal Western blotting following protein separation by SDS-PAGE (**Figure 5.4**, bottom blot). These findings suggest that PEG-Mal-2K used in these protocols can separate folded from unfolded UCP1 and can potentially be used to monitor the folded state of the protein, as signals on Western blots correlate with temperatures at which UCP1 is observed to be thermostable based on CPM thermostability assays.

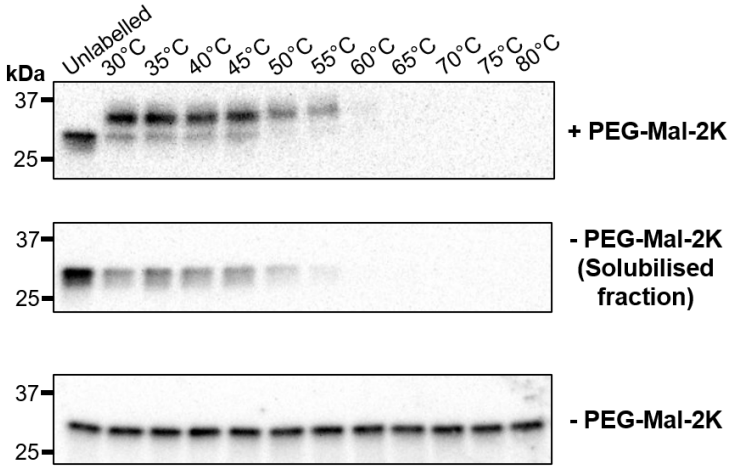

Figure 5.4: Control experiments of the gel blot protein thermostability assay. *Western blots of 0.1% DDM detergent-solubilised mitochondrial membrane samples treated with a temperature ramp, with experiments conducted in the presence (top blot) and absence (middle and bottom blots) of PEG-Mal-2K. In the absence of PEG-Mal-2K, heat-treated mitochondrial membranes were either subjected to a high-speed spin to separate out the folded and unfolded material, with the solubilised supernatant fraction, containing folded protein being taken for Western blot analysis (middle blot); or samples were just loaded onto the gel following addition of gel loading buffer (bottom blot). Experiments were conducted in 20 mM bis-Tris (pH 6.0). The incubation temperature of samples is indicated, with the "Unlabelled" lane representative of samples incubated at 4°C; ~3.3 µg of isolated mitochondria was loaded into each lane. Images displayed are unprocessed chemiluminescent images.*

Through densitometric analysis, it was observed that when the combined signal for unlabelled (~33 kDa) and PEGylated (>33 kDa) protein species per lane was plotted as a function of temperature, the data could be fitted onto a sigmoidal curve that gives a high starting plateau, representative of folded protein signal, and finishes at 0, corresponding to the lack of signal produced by thermally denatured UCP1 (see **Figure 5.5** for schematic and **Appendix Figure 4.9**). Since values obtained from the densitometry signals are prone to variation in arbitrary units (i.e. variations in overall blot to blot intensity), Western blots were normalised to the average protein signal of the first two lanes containing PEG-Mal-2K, as these lanes are representative of folded protein signal where the temperatures used are unlikely to be sufficient to denature the protein. Normalisation to the first two PEGylated lanes accounts for variables such as discrepancies in transfer efficiency between Western blots (see **Appendix Figure**

4.9B). The normalised profile is characteristic of a Boltzmann transition (196), though instead of transitioning from low to high, as is seen in CPM assays, the curve is inverted and transitions from high to low. When fitted onto a "inverted" Boltzmann sigmoidal curve, an apparent protein melting temperature can be interpolated (see **Figure 5.5** for schematic and **Methods, section 2.19.3** for further details). Since this thermostability assay is dependent on Western blots for visualisation, one variable that may influence the apparent protein T_ms generated is the effect of blot exposure time, as prolonged exposure time usually correlates with the signal intensity (312, 313). With the exception of one repeat, normalised data to fractional changes across each blot, did not show substantial (>5°C) differences in the apparent protein T_ms after 1- and 5-minutes exposure (**Appendix Table 4.4**). Thus, to ensure standardisation of calculated apparent melting temperatures, blots developed for 5 minutes were used for densitometric analysis.

Taken together, the results presented in this section demonstrate that when coupled with a temperature ramp, PEG-Mal-2K can be purposed as a potential probe capable of reporting on the folded state of cysteine-containing proteins. Signals obtained in Western blot analyses correlate well with temperatures at which UCP1 is likely to be folded, based on results from the CPM thermostability assay, whilst the disappearance of protein signal correlates with temperatures at which UCP1 is unfolded, consistent with CPM assay results. Moreover, when the protein signals are plotted as a function of temperature, an inverted Boltzmann curve can be modelled through the points and an apparent protein melting temperature can be obtained. This novel assay shall be referred to as the "gel blot protein thermostability assay", thereby encompassing all the key elements required for its function as a thermostability assay.

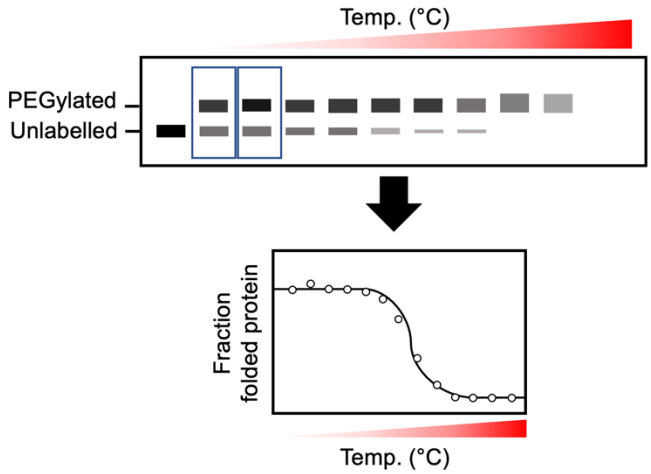

Figure 5.5: Schematic summarising data analysis of Western blots obtained from gel blot protein thermostability assays. *Chemiluminescent images obtained from gel blot protein thermostability assay experiments were subjected to densitometric analysis, with the area of interest encompassing both the unlabelled (~33 kDa) and PEGylated (>33 kDa) as shown (top panel). Values obtained from densitometry were normalised to the average signal of the first two lanes containing PEG-Mal-2K as these fractions likely represent folded protein, given that samples are incubated at temperatures that would be considered thermostable for the protein of interest. Data points are subsequently plotted as a function of temperature, where an inverted Boltzmann sigmoidal curve can be fitted to obtain an apparent protein T_m. The resulting "inverted Boltzmann curve" represents a thermal denaturation curve for the gel blot protein thermostability assay.*

5.4.3. Application of the gel blot protein thermostability assay to detect ligand binding properties of UCPs

The use of PEG-Mal-2K to detect thermal denaturation of proteins in Western blots show clear trends in HsUCP1 signals, with the presence and disappearance of protein signals correlating with folded and unfolded states of the protein, respectively, the results of which are corroborated by fluorescence signals observed in the CPM thermostability assay (see **section 5.4.1**).

5.4.3.1. Detection of stabilising interactions between UCP1 and purine nucleotides

To determine if the gel blot protein thermostability assay can detect stabilising trends in protein thermostability in the presence of inhibitors, as with the CPM assay (155, 194, 221, 304), experiments using HsUCP1-containing mitochondria were conducted

with purine nucleotides, GDP and ADP. Purine nucleotide diphosphates were tested to compare melting temperatures obtained from the gel blot protein thermostability assay, with results from the CPM assay. The CPM assay can detect 1°C resolution changes in fluorescence, thereby providing readouts for protein melting temperature with micromolar concentration of nucleotides, with 1 mM nucleotide demonstrating the highest degree of protein stabilisation (see **Figure 5.2C** and **Figure 5.3**). In contrast, the gel blot protein thermostability assay has a much lower resolution (5°C) as samples are incubated at individual temperatures, representing the discrete data points that can be fitted on an inverted Boltzmann curve from which apparent protein T_ms can be produced. Therefore, to assess if pH-sensitive UCP1-dependent thermal shifts could be observed in the gel blot protein thermostability assay, experiments were conducted at pH 6.0 and pH 7.5 in the presence of 1 mM nucleotide, as this concentration induced increases in protein melting temperatures of ~20°C and ~10°C, respectively, according to the CPM assay (see **Figure 5.2C** and **Figure 5.3**). Consistent with preliminary experiments, in the absence of ligand, a gradual decrease in protein signal was observed with increasing temperature, with 50% of the signal lost at ~50-55°C (**Figure 5.6**, top blot and **Appendix Figure 4.10**), with thermal denaturation curves producing average apparent protein T_ms of ~50°C and ~53°C at pH 6.0 and pH 7.5, respectively (see **Figure 5.8A** (top panel) and **5.8B**, for thermal denaturation profiles and apparent T_ms, respectively). In the presence of purine nucleotides, a clear difference was observed in Western blots, where the protein signal, indicative of folded protein, was sustained up to 70°C-80°C (**Figure 5.6**, middle and bottom blots; see **Appendix Figure 4.10** for replicates), with clear shifts in protein thermostability observed in the Boltzmann curves (**Figure 5.8A**, top panels). Interpolated T_ms obtained from the gel blot protein thermostability assay are similar to values generated from the CPM assay using UCP1 purified protein (see **Appendix Tables 4.2** and **4.3** (1000 μM condition) and **Appendix Table 4.5**, for CPM assay and gel blot protein thermostability assay results respectively) (155); though the effect of pH on nucleotide binding was not as pronounced, with only moderate differences (~3°C to 4°C) in apparent protein T_ms observed between pH 6.0 and pH 7.5 (**Figure 5.8B**). Interestingly, ADP exerted a slightly more stabilising effect compared to GDP at each respective pH, as demonstrated by higher T_m values (**Figure 5.8B**). Apparent UCP1 protein T_ms generated from the gel blot protein thermostability assay are 5°C-

10°C higher than values obtained from the CPM thermostability assay. In both assays, samples include 0.1% detergent, with the gel blot protein thermostability assay utilising DDM, whilst the CPM assay uses 12MNG, the latter of which has a more stabilising effect on mitochondrial carriers (155). Hence, the increase in apparent T_m obtained from the gel blot protein thermostability assay is likely attributed to the higher amount of stabilising lipids, such as cardiolipin (155), which is likely at a relatively high concentration with these detergent-solubilised mitochondrial membrane samples, but minimal in the CPM thermostability assay with purified protein.

The results generated demonstrate a proof-of-concept that the gel blot protein thermostability assay can detect ligand binding interactions without the need for protein purification.

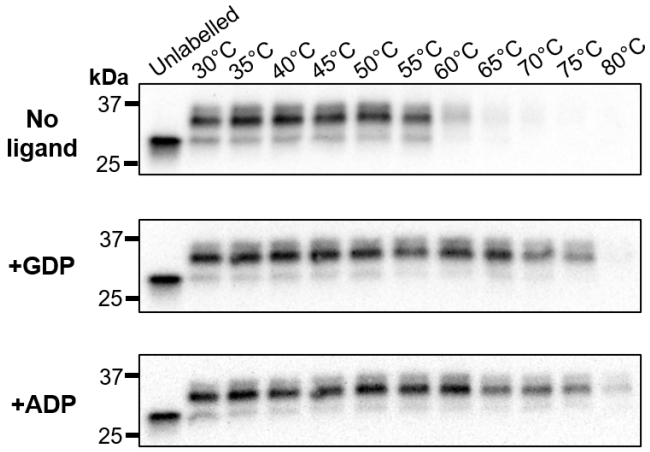

Figure 5.6: Representative blots of the gel blot protein thermostability assay conducted with HsUCP1 samples. *Western blots of UCP1-containing mitochondrial samples, solubilised with 0.1% DDM, in absence or presence of 1 mM GDP or 1 mM ADP, as indicated. Blots show results for experiments conducted in 20 mM bis-Tris (pH 6.0). The incubation temperature of the samples is indicated above lanes, with the "Unlabelled" lane representative of samples incubated at 4°C in the absence of PEG-Mal-2K; ~3.3 µg of isolated mitochondria was loaded into each lane. Images displayed are unprocessed chemiluminescent images.*

5.4.3.2. Initial gel blot protein thermostability assay experiments with UCP2

The gel blot protein thermostability shift assay demonstrates that the binding of UCP1 inhibitors, such as GDP and ADP, which lock the protein into a more stable

confirmation (153, 237), can be detected using HsUCP1-containing mitochondrial membranes.

Since the gel blot protein thermostability assay successfully detects purine nucleotides binding to UCP1, through stabilising shifts in protein thermostability, it was used to address the question of whether or not human UCP2 can bind purine nucleotides in a similar way. Initial UCP2 gel blot protein thermostability assay experiments were conducted as outlined for UCP1, whereby mitochondrial membranes are solubilised with 0.1% DDM and samples subjected to a transient temperature spike with temperatures ranging from 30°C to 80°C. Initial results using HsUCP2-containing membranes show weak signals in Western blots in the presence of PEG-Mal-2K, suggesting that the protein is unfolded from 40°C (**Appendix Figure 4.11**). In membranes, UCP2 also showed some ~55 kDa species, both in the "Unlabelled" (PEG-Mal-2K free) and PEG-Mal-2K treated samples, despite the presence of DTT in the loading buffer (**Appendix Figure 4.11**) and was not always observed in past blots (see **Chapter 3**, **Figure 3.9C** and **Chapter 4**, **Figure 4.2**). The ~55 kDa species may represent covalent homo- or hetero-protein associations, e.g. related to protein degradation pathways (45), and/or *in vitro* processing artefacts, and along with other higher molecular weight signals were excluded from densitometric analysis. As such, only the signal associated with monomeric UCP2 and PEG-2K-labelled species were included for data processing. As the signal for folded UCP2 protein was lost after two data points (30°C and 35°C) (**Appendix Figure 4.11**), UCP2 samples were tested using a lower temperature range (5°C-65°C) in order to establish a baseline signal for folded protein in the presence of PEG-Mal-2K. Whilst a readout could be observed at 5°C-65°C, the signals generated for PEG-Mal-2K treated samples were faint compared to the unlabelled control, which made densitometry analysis very difficult (**Appendix Figure 4.12**). Given that addition of PEG-Mal-2K is used to detect folded protein, the unlabelled lane is representative of the total amount of UCP2 in mitochondrial membranes, irrespective of the folded state of the protein. Results from initial experiments with DDM-solubilised membranes, suggest that over half of the total protein appears to be unfolded at 5°C, which would be inconsistent with observations from previous solubilisation screens that show >75% UCP2 solubilisation in the presence of 0.5% DDM when protein concentration is at 10 mg/mL (see **Chapter 3**, **section 3.3.6**). Use of 12MNG, rather than DDM for membrane solubilisation resulted in a higher signal intensity for UCP2 protein in the presence of

PEG-Mal-2K, suggesting that 12MNG is more stabilising than DDM (**Appendix Figure 4.12**). Consequently, 12MNG was used to solubilise the UCP2-containing membranes for the gel blot protein thermostability assay. These preliminary results indicate that UCP2 is very unstable compared to UCP1 and other mitochondrial carriers (98, 147, 155, 219, 220), as a lower temperature range was required to obtain a signal for folded protein, with 12MNG exerting a more stabilising effect than DDM.

5.4.4. Nucleotide binding properties of HsUCP2

As described, various parameters, such as temperature range and the detergent used for solubilisation, were adjusted from conditions established for UCP1, to detect the presence of folded UCP2 protein. Accordingly, UCP2 gel blot protein thermostability assays using 12MNG-solubilised membranes were conducted in the presence of 1 mM nucleotides, at pH 6.0 and pH 7.5, sampling a temperature range of 5°C to 65°C to ensure a baseline signal for folded protein could be obtained. Qualitatively, Western blot signals obtained for UCP2 demonstrated similar patterns in protein stability, regardless of nucleotide addition (**Figure 5.7** and **Appendix Figure 4.13**). In the absence of ligands, UCP2 was observed to be far more unstable compared to UCP1, as shown by differences in the thermal denaturation profiles (**Figure 5.8A**), with mean T_ms of ~37°C and ~40°C observed at pH 6.0 and pH 7.5, respectively (**Figure 5.8B** and **Appendix Table 4.6**). The differences in T_ms aligns with observations in chapter 4, that UCP2 is less stable at low pH, as shown by less folded protein in the soluble supernatant fractions (see **Chapter 4**, **section 4.3.1**). Thermal denaturation profiles show that in the presence of 1 mM nucleotides, no significant shifts in protein thermostability could be observed at either pH 6.0 or pH 7.5 (**Figure 5.8**), which is in line with patterns seen in Western blots (**Figure 5.7**). These data indicate that human UCP2 does not bind nucleotides like human UCP1, where nucleotide binding exerts a strong stabilising effect on the protein (153, 237).

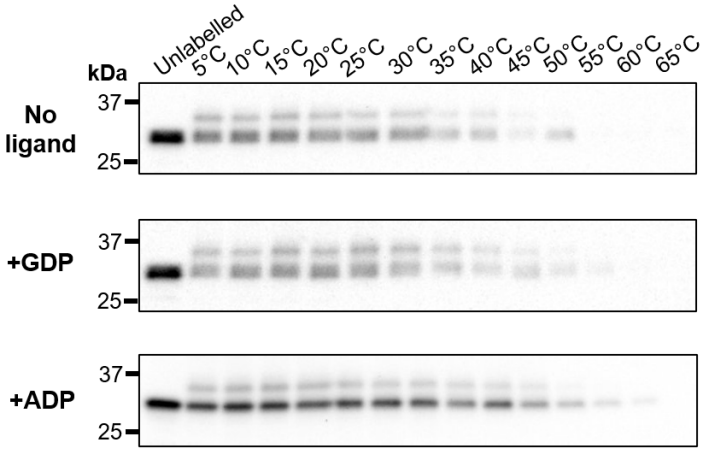

Figure 5.7: Representative blots of the gel blot protein thermostability assay conducted with HsUCP2 samples. *Western blots of UCP2-containing mitochondrial membrane samples, solubilised with 0.1% 12MNG. Experiments were conducted in 20 mM bis-Tris (pH 6.0), in absence or presence of 1 mM GDP or 1 mM ADP, as indicated. The incubation temperature of samples is indicated above lanes, with the "Unlabelled" lane representative of samples incubated at 4°C in the absence of PEG-Mal-2K; ~3.3 µg of isolated mitochondria was loaded into each lane. Images displayed are unprocessed chemiluminescent images.*

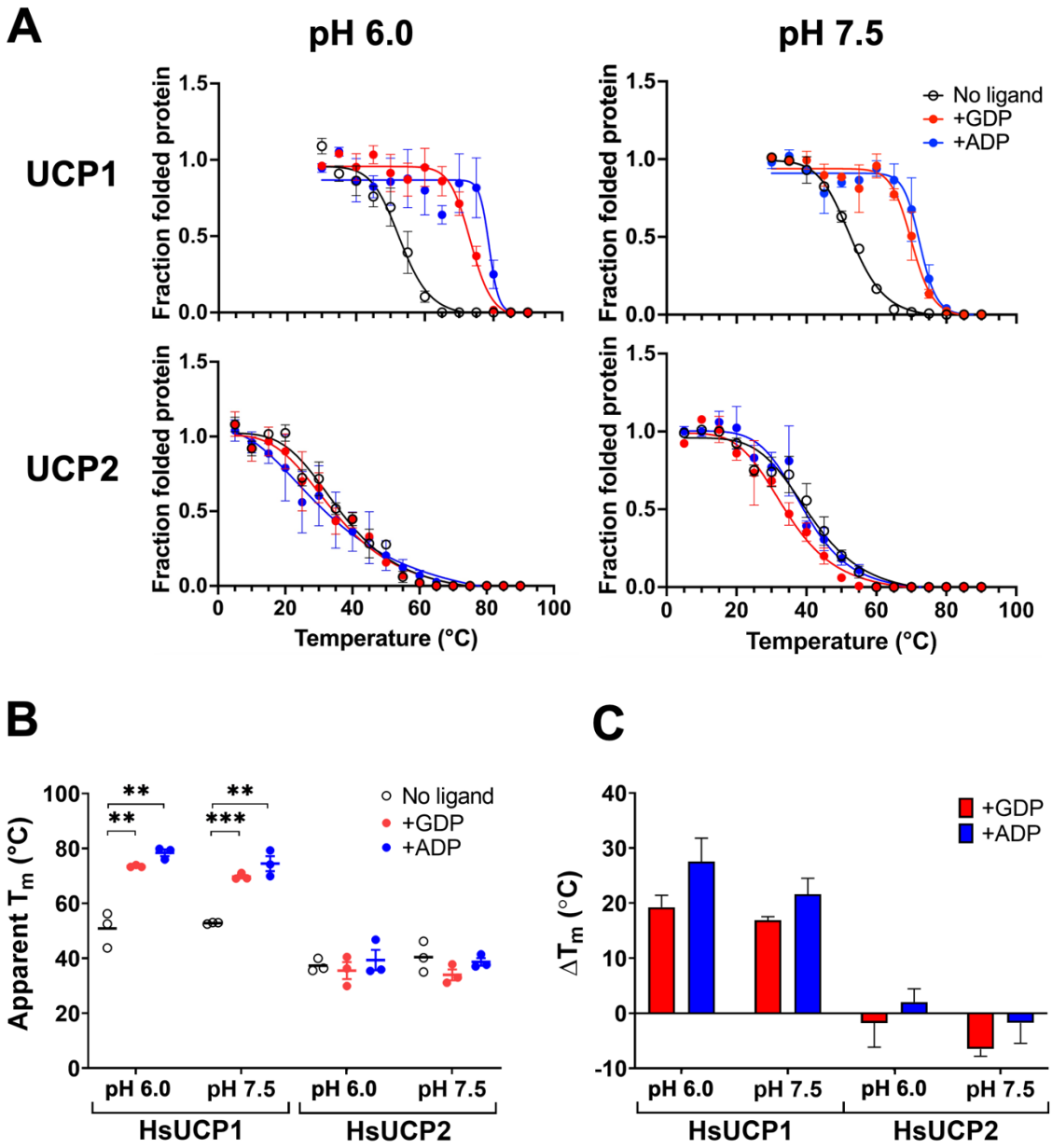

Figure 5.8: Comparison of gel blot protein thermostability assay data from UCP1 and UCP2 samples. *A) Thermal denaturation profiles generated from gel blot protein thermostability assay experiments using HsUCP1- (top panel) and HsUCP2-containing (bottom panel) mitochondrial membranes in the absence or presence of 1 mM GDP or 1 mM ADP, as indicated, at pH 6.0 (left) or pH 7.5 (right). HsUCP1-containing samples were solubilised with 0.1% DDM, whilst HsUCP2-containing samples were solubilised with 0.1% 12MNG. Curves are modelled using an inverted Boltzmann equation, with values displayed as the mean of three replicates. Error bars represent the S.E.M of three replicates. B) Scatterplot summarising the average apparent protein T_m of HsUCP1 and HsUCP2 obtained from gel blot protein thermostability assay experiments, in the absence or presence of 1 mM GDP or 1 mM ADP at pH 6.0 or pH 7.5, as indicated. Individual points show protein T_ms obtained per replicate, middle bar shows the mean T_m of*

*three experiments, with error bars showing the S.E.M. Statistical analysis performed using a Student's t-test (*p<0.05, **p<0.005, ***p<0.001). C) Changes in HsUCP1 and HsUCP2 protein T_m (ΔT_m) in the presence of nucleotides at pH 6.0 and pH 7.5. ΔT_ms were calculated by subtracting interpolated T_m in the presence of ligand from the interpolated T_m in the no ligand condition. Error bars are shown as the S.E.M.*

Human UCP2 shares the major structural features that have been identified to be important for nucleotide binding with UCP1. However, results obtained from the gel blot protein thermostability assay indicate that UCP2 does not bind purine nucleotides in the same way as that of human UCP1. Cryo-EM structures of human UCP1 locked with GTP (153) and ATP (237) demonstrate that UCP1 is in a cytoplasmic-open (c-state) confirmation, where purine nucleotides bind in the central cavity, with multiple salt bridge and hydrogen bond interactions with conserved amino acid residues. The symmetry related arginine triplet (R84, R183, R277), equivalent to the substrate recognition points in other carriers (139), predominantly coordinates the phosphate moieties of purine nucleotides, but also the ribose group which hydrogen bonds to the α-phosphate, the interaction of which is supported by Q85. Residues N282 and E191 make hydrogen bond and salt bridge interactions with the base, supported by R92, which interacts with the ring structure through a cation-π interaction. Moreover, K39 and K138, which partake in forming the matrix salt bridge network that closes the cavity at the matrix side, form salt bridges with the γ- and β-phosphates, respectively. Other hydrophobic residues, such as W281, have also been shown to be important for nucleotide binding (153, 314). Importantly, all of these residues are conserved across in UCP2 (and UCP3) (**Appendix Figure 4.14**), suggesting other, potentially more subtle, differences are responsible for the lack of purine nucleotide binding observed here.

5.5. Discussion

The results presented in chapter 5 describes the avenues taken to functionally characterise human uncoupling protein 2. Results obtained from liposomal reconstitution of samples taken from purification attempts and oxygen consumption assays on HsUCP2-containing yeast mitochondria did not clarify the question of whether UCP2 conducts protons in the same way as UCP1. Whilst the question of UCP2 proton conductance is still left unresolved, the development of a new

thermostability assay capable of probing ligand binding properties of proteins suggests that human UCP2 does not bind purine nucleotides in the same way as UCP1 as it did not induce protein stabilisation.

5.5.1. Gel blot protein thermostability assay development

5.5.1.1. Advantages and limitations of the gel blot protein thermostability assay

The studies presented here show the development of a maleimide-based thermostability assay capable of probing ligand binding properties of proteins in impure samples. The ability to probe into thermostability of protein samples in heterogenous mixtures allows for the characterisation of proteins without the need to purify proteins, making the assay potentially applicable to many different systems where protein material is scarce or where it is difficult to isolate the protein in a stable, folded state, as was the case for UCP2. One caveat of this new technique is that it is dependent on efficient and specific antibody binding to detect the protein of interest, also subsequently ensuring that protein epitopes are not occluded by the addition of the PEG-Mal-2K adduct. Given that PEG-Mal-2K is thiol-reactive, it is highly reliant on the latency of cysteine residue accessibility in the protein to detect protein unfolding, and so will not be useful for proteins devoid of cysteine residues.

5.5.1.2. Mechanism of action

A critical attribute of the gel blot protein thermostability assay is the apparent ability to distinguish folded protein from thermally denatured protein. It was interesting to see that when proteins were chemically unfolded by SDS, prior to sample incubation with PEG-Mal-2K and treatment to high temperatures, a protein signal was observed in blots, despite being denatured with heat as well, compared to using heat alone. Since the presence of signal correlates with folded protein in the gel blot protein thermostability assay, it was unclear why such different results were obtained when the protein was unfolded using SDS vs. heat. A possible explanation for this observation could be attributed to interference from SDS prior to PEG-Mal-2K addition to the samples. SDS is an ionic denaturant that is routinely used in protein electrophoresis analysis, functioning by coating proteins in negative charge, thereby allowing for protein separation based on molecular mass (315). Addition of SDS to samples prior to heat treatment, likely prevents PEG-protein aggregation, by ensuring that the protein is solubilised and can migrate down the gel like conventional SDS-PAGE. Thermal denaturation of proteins in the presence of PEG-Mal-2K, but in the

absence of SDS, likely results in unfolded protein aggregates, which prevents the protein species from entering the gel. Given that PEG-Maleimide can be used as a cross-linker in various hydrogels (316), it is possible that PEG-Mal-2K exacerbates the formation of protein aggregates to the extent that addition of SDS later (in the gel loading buffer) does not recover a signal. Consequently, a gradual disappearance in protein signal on blots is observed as a function of temperature.

5.5.1.3. Further applications of the gel blot protein thermostability assay

In the context of this work, the gel blot protein thermostability assay was conducted using human UCP1 and UCP2, both of which are mitochondrial inner membrane proteins, containing 8 and 6 cysteine residues, respectively. With increasing temperature, a gradual loss of protein signal is observed, though based on the number of PEGylated protein species, only two cysteine residues are observed to react at each given temperature. In the context of other proteins, which have less cysteine residues, it would be interesting to see if a maximum of two cysteine residues are also observed. The gel blot protein thermostability assay also demonstrated that UCP1-containing membranes incubated with purine nucleotides show stabilising shifts in Western blots, which can be quantified to produce protein melting temperatures, with values close to that obtained by the well-established CPM thermostability assay (155). It would be interesting to utilise this assay to detect protein thermal shifts in the presence of reported transport substrates of UCP2, such as aspartate (93) as well as reported inhibitors such as genipin (317) and various chromane derivatives (318). Furthermore, the gel blot protein thermostability assay could be utilised to probe into ligand binding properties of proteins from native tissues, thereby potentially circumventing the need to express recombinant proteins altogether. Given the challenging nature of membrane protein purification, this novel assay has the potential to study ligand binding properties of other eukaryotic membrane proteins, such as GPCRs (319), which may also be unstable in various recombinant expression systems (320).

5.5.2. UCP2 does not bind purine nucleotides in the same way as UCP1

Through the development of the gel blot protein thermostability assay, it was observed that the addition of purine nucleotides did not induce stabilising interactions with human UCP2, as was observed for human UCP1. The results suggests that UCP2 does not bind purine nucleotides in a similar manner to that of UCP1, despite having

all the key residues observed to interact with purine nucleotides (4). The results suggest that subtle deviations in conserved amino acid residues may be responsible for the differences observed in purine nucleotide binding properties of UCP1 and UCP2.

In the matrix salt-bridge network, HsUCP1 has a glutamate at position 135 (E135), whilst in HsUCP2 the corresponding residue is aspartate (D138) (**Appendix Figure 4.14**). Through respiratory assays conducted with isolated yeast mitochondria, Jiménez-Jiménez and colleagues report a 64% decrease in palmitate-induced respiration in the presence of GDP with a UCP1 mutant where glutamate is substituted for aspartate (UCP1_E135D) (63). The difference in nucleotide-sensitive, fatty-acid induced respiration between the UCP1 and UCP1_E135D is significant, indicating that substitution of glutamate to aspartate negatively affects purine nucleotide binding (63). Jones and colleagues, propose that E135 in HsUCP1 may be involved in co-ordinating a proton to support nucleotide binding to UCP1 (153). The shorter side chain in D138 in HsUCP2 may interrupt this function and prevent nucleotide binding. Furthermore, a shorter residue may result in a tighter matrix network, subsequently bringing helices closer together, which may compromise the ability of nucleotides to fit into the cavity.

In the nucleotide-bound structure, various hydrophobic residues in the central cavity have the potential to form interactions with guanine moiety of the nucleotide (153, 154). Molecular dynamic simulations of rat UCP1, propose a triplet of hydrophobic residues (F88, I187, W281 – rat UCP1 numbering) important in nucleotide binding to UCP1 (314). In HsUCP2, valine is found at the equivalent position (V189), whereas in HsUCP1 isoleucine is conserved (I187) (**Appendix Figure 4.14**). Mutation of I187 to alanine has been shown to significantly reduce GDP-mediated inhibition (314). Therefore, the subtle change to valine in UCP2, may contribute for the lack of binding. However, homology models of energy-minimised UCP2, demonstrate that the HsUCP2, can form the similar interactions with GTP as human UCP1 when poised in the c-state (see **Figure 5.9**).

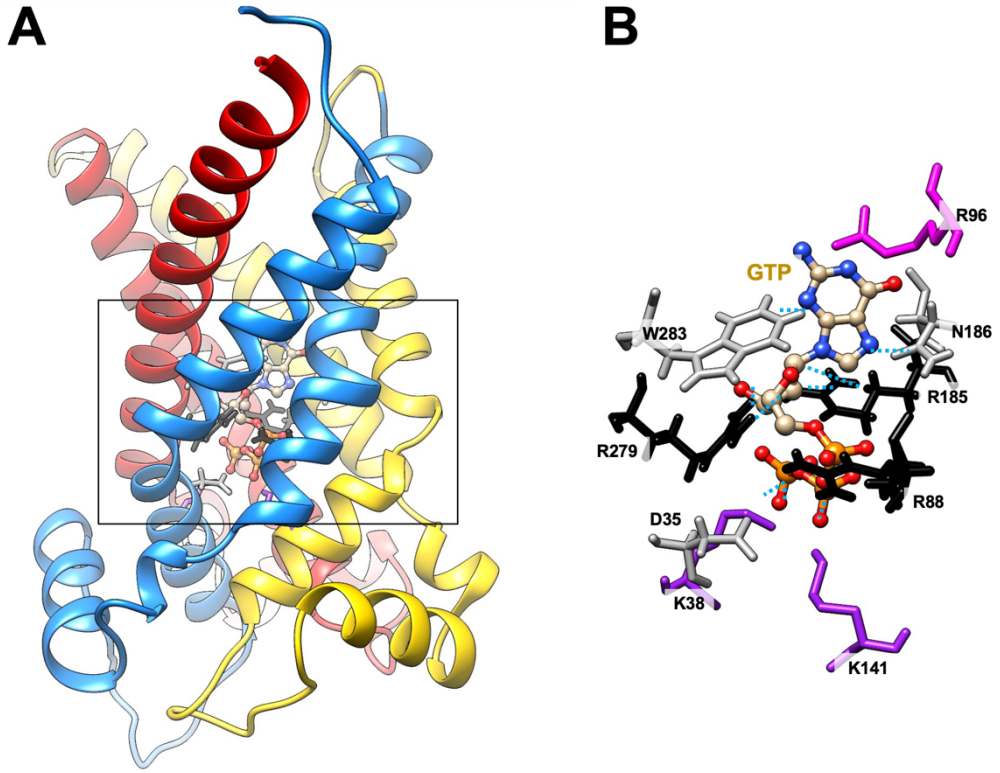

Figure 5.9: Potential interactions of human UCP2 with GTP in a c-state conformation. *A) Lateral view of human UCP2 in the cytoplasmic-open (c-state) conformation modelled using the resolved cryo-EM structure (PDB: 8G8W) (153), with a GTP molecule modelled in the substrate binding site. The three domains are depicted in blue, yellow and red. B) Close-up view of residues observed to interact with GTP inside the binding cavity. Matrix salt-bridge residues are depicted in purple, arginine triplet residues shown in black, R96 (part of the cytoplasmic insulator residues) in magenta and all other residues in gray. Residues that may form potential bonds with GTP are shown through blue dotted lines. Models were made using the Modeller interface in UCSF Chimera (321, 322) and energy-minimised in the GalaxyRefine2 server (323). Potential interactions (observed through the Clash/Contact tool in Chimera) and depicted as a blue dotted line.*

Another argument, for why purine nucleotides do not induce stabilising interactions could be that UCP2 may favour an m-state conformation. In the primary cytoplasmic salt-bridge network, HsUCP2 has a lysine at position 100 (K100), whereas in HsUCP1 the equivalent residue is glutamine (Q100). Removal of this charged residue in HsUCP1 results in a weaker cytoplasmic salt-bridge network as the glutamine cannot form ionic interactions with D196. In HsUCP2, residues of the cytoplasmic salt-bridge network are all able to form salt-bridge interactions between all helices, highlighting

that the primary cytoplasmic network is likely stronger in HsUCP2 than HsUCP1. Furthermore, the existence of charged residues one turn of the helix above the primary cytoplasmic salt-bridge network, suggest a possibility of a secondary salt-bridge network that may further the strengthen the carrier in an m-state conformation (171). Both HsUCP1 and HsUCP2 can form ionic interactions, i.e. K116-E200 and R119-D202, respectively, which may serve to increase the overall bonding of the cytoplasmic network. Taken together, these differences in key residues in the primary and secondary cytoplasmic networks of HsUCP2, suggest that the protein may be more stable in an m-state conformation, relative to HsUCP1. Though exactly how these differences relate to nucleotide binding is not clear. In an energy-minimised matrix-open (m-state) model of UCP2, potential interdomain interactions between the arginine triplet and negative residues of the matrix-salt bridge network have been observed, which may serve to further strengthen the m-state conformation (see **Figure 5.10**). Given that the arginine triplet and the matrix salt-bridge network are seen to interact with nucleotides (153, 154), it could be rationalised that purine nucleotides may preferentially bind in the c-state conformation, thus lack of purine nucleotide binding observed with UCP2 could be due to the protein's inability to reside in the c-state conformation. Whilst not definitive, the m-state model provides a potential rationale for why human UCP2 does not bind purine nucleotides in a similar manner to that of human UCP1, as multiple interactions within the protein potentially keep it locked in the m-state, which may explain the experimental data obtained from the gel blot protein thermostability assays. Interestingly, inhibition of UCP2 (93) and UCP3 (280) activity by 10 μM BKA, an inhibitor known to lock AAC in an m-state conformation (141), demonstrated ~50% reduction in metabolite transport activity. These findings may suggest that these UCP homologues potentially prefer an m-state conformation as low concentrations of BKA are required to inhibit protein activity.

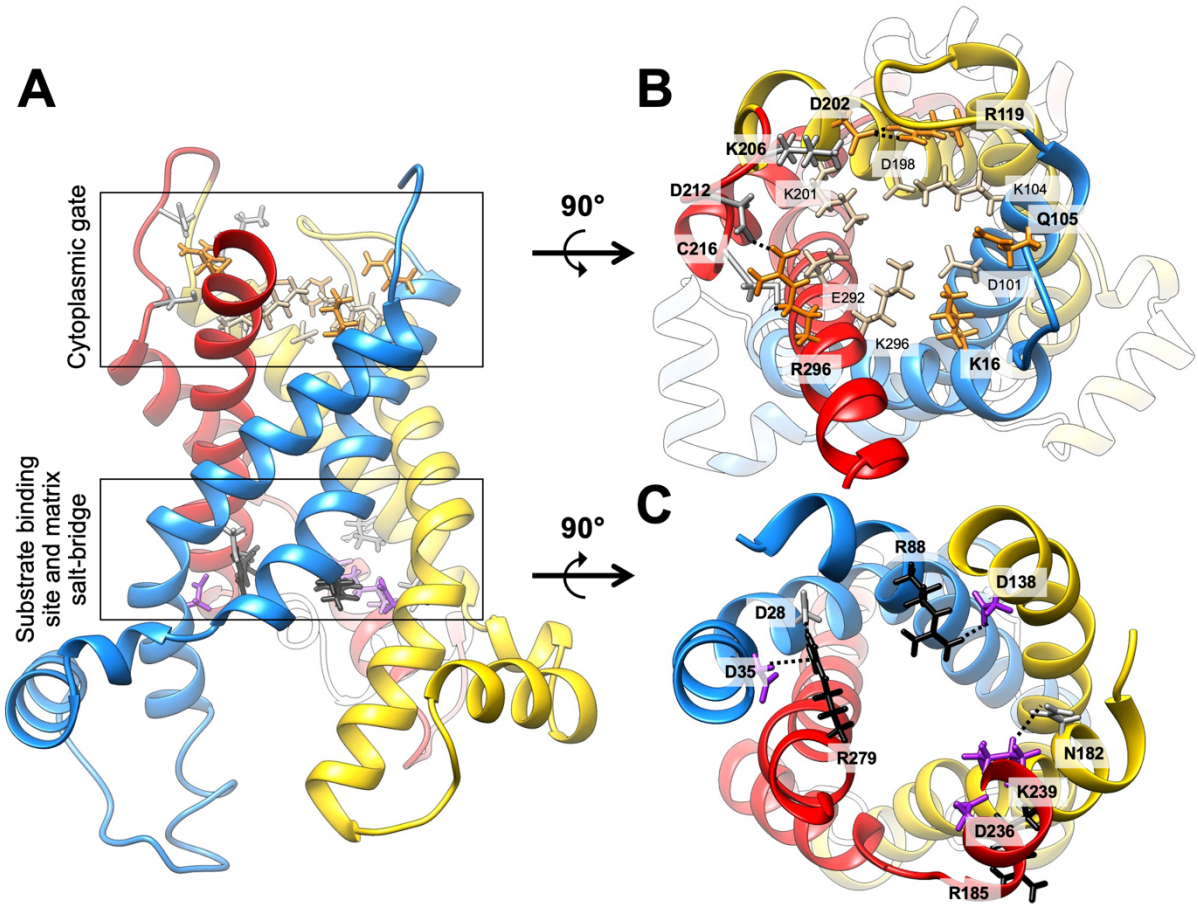

Figure 5.10: Potential interactions of human UCP2 in the m-state conformation. *A) Lateral view of human UCP2 in the matrix-open (m-state) conformation modelled using the TtAAC BKA-inhibited structure (PDB: 6GCI) (141), highlighting potential interactions in the cytoplasmic salt-bridge network and matrix salt-bridge network. The three domains are depicted in blue, yellow and red. B) Top-down view of the cytoplasmic gate, consisting of the primary salt-bridge network (tan) and the secondary salt-bridge network (depicted in orange and labelled in bold). Residues that may form potential bonds with the secondary cytoplasmic salt-bridge are shown in gray and labelled in bold. C) Bottom-up view of potential interdomain interactions formed between the arginine triplet and residues of the matrix salt-bridge network. Residues involved in potential interdomain interactions are shown as sticks, with the arginine triplet depicted in black, matrix salt-bridge network residues are shown in purple and residues observed to form additional interdomain contacts in gray. Models were made using the Modeller interface in UCSF Chimera (321, 322) and energy-minimised in the GalaxyRefine2 server (323). Potential interactions (observed through the Clash/Contact tool in Chimera) and depicted as a black dotted line.*

6. Discussion

6.1. Chapter 3 - Key findings

The low abundance of UCP2 in native sources (38, 185) makes purification of the protein from tissues impractical. Therefore, the use of bacterial and yeast expression systems has been utilised to study the function of UCP homologues. Early literature suggested that UCP homologues are capable of proton transfer activity (47, 48, 57, 58, 60, 61), in the presence of various activators, such as ubiquinone (49, 66), superoxide (52, 53, 69) and lipid peroxidation products (50, 74) though the findings are widely debated (71, 80-83).

Bacterial expression systems produce misfolded carrier protein, which require 'refolding' prior to biochemical characterisation using ionic detergents (203). Though soluble in ionic detergents, bacterially-expressed proteins are likely to be an incorrectly folded form (155, 158-162), as was previously observed for UCP2 (163). Yeast expression systems have been utilised to study proton leak activities of UCPs, though uncoupling artefacts have been observed due to protein overexpression (55, 56). In order to biochemically characterise UCP2 protein activity in isolation, a yeast expression system was optimised to ensure relatively high levels of recombinant protein expression for the purposes of protein purification. Chapter 3 shows that recombinant expression of uncoupling protein 2 in the protease-deficient (*Pep4* deletion) yeast strain, FGY217, allowed for UCP2 production to levels 20-fold higher than native sources (38, 185), with at least 75% of the protein generated found to be intact following extraction with mild non-ionic detergents, such as DDM and 12MNG.

Previous work has reported that recombinant UCP2 can be expressed in the wild-type (W303-1B), yeast strain for the purposes of respiratory assays (48, 54-56, 81, 255). With the exception of Stuart and colleagues (56), it is unknown to what degree UCP2 was expressed in yeast mitochondrial membranes in a correctly folded and functional form. Through functional complementation studies, Raho and colleagues have shown functional UCP2 expression in AGC1 knockout strains of yeast, when grown on oleate (114). Whilst this may be a potential way to express functional UCP2, it is not known to what degree UCP2 is expressed in these mitochondria and if growth on oleate would be practical for protein purification purposes.

It was observed that under a galactose-inducible expression system, recombinant UCP2 protein was tolerated and sustained in the FGY217 yeast strain following 22 hours galactose addition. Heterologous expression of UCP2 in wild-type (W303-1B) yeast mitochondria have suggested that the protein has a short half-life (44). The exact mechanism of UCP2 protein degradation in yeast is unknown, though in mammalian systems, evidence suggests that UCP2 degradation is mediated by the ubiquitin-proteasome pathway (45). This pathway is present in yeast (324). In the FGY217 strain, the lysosomal degradation pathway is disrupted due to deletion of the *Pep4* gene (167), though it is unclear if the ubiquitin-proteasome pathway is altered in this strain. It could be reasoned that removal of one of the proteolytic pathways in yeast may have allowed for the accumulation of intact UCP2 in FGY217 mitochondria, whereas in previous systems, such as the W303-1B, which have functional proteolytic pathways (325-327), this may not have been the case.

6.2. Chapter 4 - Key findings

Chapter 4 describes steps taken to try and purify human UCP2 protein using a bespoke purification system that was established for OaUCP1 obtained from native sources (19). Several rounds of optimisation demonstrated that whilst the S, Q, TP purification strategy was suitable for purification of untagged UCP1 protein (19, 153, 171), it proved limited for purifying untagged UCP2 protein, which could be enriched but remained contaminated with other mitochondrial carriers, such as AAC.

The use of purification tags was not explored for UCP2 as it has been shown to negatively affect UCP1 protein expression in heterologous yeast systems (215). Addition of C-terminal histidine-tags were reported to severely affect protein expression in comparison to N-terminal tags. Furthermore, subtle differences in protein expression levels were observed when 6x- or 8x-histidine-tags were engineered into the yeast-expressed UCP1 protein (215). Prior work describes UCP1 protein expression in the wild-type strain, W303-1B. This thesis describes UCP2 protein expression in the protease-deficient (FGY217) yeast strain, where heterologous UCP2 expression is tolerated. Given that two papers describe the structure of UCP1 protein purified using histidine-tagged (153) and FLAG-tagged (154) proteins, future lines of investigation could explore whether UCP2, expressed in the FGY217 strain, could be purified using purification tags. The studies in Chapter 3 demonstrated that alteration of the second amino acid from the native valine to leucine resulted in a ~4-fold

increase in UCP2 protein expression in the protease-deficient strain. If purification tags were to be added to the N-terminus, it may be worth engineering a leucine at the second amino acid position to allow for increased protein expression (231). Furthermore, protein purification by affinity chromatography, rather than the S, Q, TP method, would reduce the number of purification steps required for protein isolation, thereby reducing the chances of protein unfolding during the process. Given that the gel blot protein thermostability assay, developed in Chapter 5, reports a relatively low apparent protein melting temperatures for yeast-expressed membrane-solubilised human UCP2 at ~37-40°C (compared to ~50-53°C for UCP1 in the ligand-free condition), shorter isolation times may be particularly beneficial.

To increase the likelihood of purifying intact material, mammalian lipids could be added during purification preparation. The UCP2 preparation is supplemented with tetraoleoyl (18:1) cardiolipin, which consists of an 18-carbon fatty acyl chain, with an unsaturated double bond. Mammalian tissues are reported to be more abundant in tetralineoyl (18:2) cardiolipin species (328). Addition of extra unsaturated double bonds in cardiolipin may provide more flexibility, which may improve UCP2 protein stability. Furthermore, addition of known transport substrates to the purification preparation may also aid in purifying intact protein. Whilst micromolar concentrations of substrate was observed to destabilise mitochondrial carriers (155), millimolar concentrations of substrate was observed to induce stabilising shifts in the presence of lipids (155, 194). This approach could be utilised with proposed transport substrates, such as aspartate and malate (93) to potentially improve intact UCP2 purification.

6.3. Chapter 5 - Key findings

It was evident from the studies in Chapter 4 that human UCP2 could not be purified to sufficient homogeneity for biochemical characterisation using the CPM protein thermal shift assays. As such, Chapter 5 sought to clarify the functional properties of UCP2 using methods that did not require pure, homogenous samples. Methods taken to clarify proton transport activity of UCP2 proved challenging and could not be used to obtain an outcome. To answer the question of whether UCP2 binds nucleotides in a similar manner to that of UCP1, a novel thermostability assay, capable of probing the ligand binding properties of proteins in impure samples, was developed. The thiol-reactive reagent, PEG-Mal-2K, could be used systematically at different temperatures

as a probe to detect the folded state of the protein in detergent-solubilised mitochondrial samples and build a temperature sensitivity profile. Western blots demonstrated the appearance and disappearance of the UCP1 signal that strongly correlated with temperatures where the protein was observed to be folded and unfolded, respectively, in CPM assay tests.

The method by which the protein stability is quantified in the gel blot protein thermostability assay is similar to that of trypsin digestion experiments conducted by Eckerskorn and Klingenberg (329). These experiments demonstrate that sensitivity to trypsin can provide information on protein stability and conformation. In these experiments, it was reported that in the absence of ligand, UCP1 was more prone to trypsin cleavage, evidenced by a lower molecular weight species in Western blots. Conversely, in the presence of GTP, the amount of trypsin-cleaved UCP1 protein was reduced over time, suggesting either a change in protein conformation or stabilisation exerted by nucleotide addition (329). Similarly, the gel blot protein thermostability assay is also able to report on the protein stability through changes in protein molecular weight, which can be quantified as an apparent protein T_m, subsequently providing invaluable information on protein stability and ligand binding properties.

In the gel blot protein thermostability assay, for human UCP1 in the absence of ligand, the melting temperatures generated were consistent with reported melting temperatures gained using the CPM protein thermal shift assay. Furthermore, distinct stabilising shifts in UCP1 protein thermostability were observed in the presence of nucleotides, thereby mimicking the trends observed in the CPM assay (155), highlighting a proof-of-concept principle that the gel-based assay can detect protein stability shifts induced by ligands. Moreover, the use of the new assay demonstrates that monomeric UCP2 is inherently unstable compared to UCP1 and does not bind nucleotides in the same way as it does not induce protein stabilisation. The finding that UCP2 does not bind purine nucleotides calls into question previous literature that uses purine nucleotides to verify UCP2-dependent activity. For example, FRET experiments conducted with fluorescent nucleotides suggests that UCP2 binds in purine nucleotides in the 3-5 μM range (205), which is approximately three orders of magnitude less than what was used in the gel blot protein thermostability assay experiments. However, lack of purine nucleotide binding to UCP2 has been indicated in previous work (330), including the work by Vozza and colleagues where they show

~50% UCP2 inhibition in the presence of 10 mM purine nucleotide (93), suggesting a non-specific interaction that would corroborate observations in our assay.

6.4. Probing into protein thermostability in unpurified samples

The gel blot protein thermostability assay demonstrates that protein thermostability can be obtained for proteins in unpurified samples, which is particularly useful if protein stability is impeded by the purification process or if the protein is scarce, as is the case for UCP2 (38, 185) and many other eukaryotic membrane proteins (320). Interestingly, another method, termed ThermoBRET, has recently been developed which is also capable of determining protein thermostability in unpurified samples (331). The ThermoBRET assay utilises bioluminescence resonance energy transfer (BRET) between Nanoluciferase (Nluc) and a thiol-reactive fluorescent dye, sulfo-cyanine3 maleimide (SCM). In this method, Nluc is engineered onto the N-terminus of the protein of interest and acts as a light donor, whilst the SCM dye acts as a light acceptor. Heterogenous samples containing Nluc-tagged protein are heated in a thermal cycler in the presence of SCM. As the protein unfolds, buried cysteine residues react with SCM, which quenches the fluorophore's signal. Protein thermostability is quantified as the ratio between the light emitted by Nluc and the SCM dye, which can be fitted on a Boltzmann sigmoidal curve, the midpoint of which can provide an apparent protein T_m. Furthermore, this method was also able to observe changes in protein thermal shifts in the presence of ligands or solubilisation in different detergents (331).

Whilst this method uses a different biochemical approach to measure protein thermostability compared to the gel blot protein thermostability assay, core elements are shared between them. Such elements include: the use of a thiol-reactive probe to monitor protein unfolding, of which the output can be fitted onto Boltzmann curves that generate an apparent protein T_m. Furthermore, both the ThermoBRET assay and the gel blot protein thermostability assay have utilised the well-established CPM assay as a reference control for assay development, with both novel assays providing comparable protein T_ms from purified samples. Like the CPM assay, both methods are only effective with cysteine-containing proteins owing to the thiol-reactive nature of the maleimide-based probes (192, 331). Whilst both methods do not need to purify protein to obtain an output for protein thermostability, ThermoBRET relies on the

engineering or covalently bonding of an Nluc tag onto the protein to obtain the ratio between light emissions of the Nluc tag and SCM dye. Moreover, addition of an Nluc tag may alter protein thermostability, which may provide artefactual readouts in apparent protein T_m. In contrast, the gel blot protein thermostability assay does not require tagged or modified protein, making it a potentially versatile method in probing protein stability in a wide range of applications, as protein thermostability can be assessed if there are effective antibodies that can visualise the protein of interest in Western blots. Moreover, both thermostability assays can be used to detect protein-ligand interactions in unpurified samples through positive shifts in protein thermostability. The ThermoBRET method can be conducted in a 96-well or 384-well plate format, which makes the system ideal for drug screens. It is capable of detecting shifts in thermostability using picomolar concentrations of ligand to protein owing to bioluminescence signal enhancement of the Nluc tag the substrate furimazine (332, 333). In contrast, the gel blot protein thermostability assay is lower throughput as it is limited by the number of wells on protein gels as the method relies on Western blotting for sample detection. The work in this thesis only tests 1 mM concentration of ligand in the gel blot protein thermostability assay, as this was the concentration observed to give the greatest shift in apparent protein T_m in the CPM assay, but it would be fascinating to see what the minimal concentration of ligand would be required to detect stabilising shifts in protein-ligand interactions in the gel blot protein thermostability assay.

6.5. UCP2 is more unstable compared to UCP1

The development of the gel blot protein thermostability assay reveals that UCP2 is particularly unstable, with apparent protein T_ms observed at ~37-40°C, whereas UCP1 reported apparent T_ms at ~50-53°C. Experiments conducted in this thesis show T_ms obtained using detergent-solubilised yeast mitochondrial membrane samples, which may not necessarily reflect UCP2 protein stability *in vivo*. Comparatively, other methods have been utilised to measure detergent-solubilised, cardiolipin-supplemented carrier protein thermostability, including the CPM assay and nanoDSF, the latter of which relies on intrinsic protein fluorescence from native tryptophan residues to assess the folded state of a protein (334). Despite the different methodological approaches, the general trend across studies shows that purified mitochondrial carriers exhibit apparent T_m in the range of 50-55°C (98, 147, 153, 155). In the case of human UCP1,

similar T_m values (e.g. 52°C at pH 6.0 in the absence of ligands) have been reported across various techniques including nanoDSF (153), CPM and gel blot protein thermostability assays (see Chapter 5). This comparison highlights that the gel blot protein thermostability assay can yield protein T_ms comparable to already well-established methods, including nanoDSF, which does not rely on maleimide-based chemistry to report on protein thermostability (334). Since the gel blot protein thermostability assay relies on Western blotting to provide a readout, it would be interesting to see if blotting against other mitochondrial carriers reproduces apparent T_ms obtained from the CPM assay (147, 155, 194, 195, 219) and nanoDSF (98, 153), thereby further strengthening the application of this novel assay. The notably low T_m value obtained for UCP2 in detergent-solubilised, yet lipid-containing membrane, emphasises the highly unstable nature of this mitochondrial carrier protein. Other carrier proteins, such as the dicarboxylate carrier (DIC) and the oxoglutarate carrier (OGC), which share various transport substrates with UCP2 (93, 98), exhibit much higher apparent T_ms of 54.1°C and 51°C, respectively (98). The low protein T_m obtained for UCP2, suggests either that UCP2 may be prone unfolding even within the membrane environment, which may contribute to its apparent very short half-life of 30 minutes - 1 hour (44) or that UCP2 may interact with other proteins, as some researchers have suggested (125, 335), which may potentially stabilise UCP2 in the mitochondrial membrane.

With respect to UCP2's short half-life, Azzu and colleagues have indicated that UCP2 is likely pro-actively controlled via degradation through cytoplasmic proteasome machinery, though the exact mechanism by which this occurs is unclear (46). It has been reported that ubiquitin-proteasome system (UPS) may play a role in regulating cellular metabolism. For example, in various cancer cells it was observed that under hypoxic conditions, glutamine oxidation was reduced due to cytosolic E3 ligase-mediated proteolysis of OGDH2, a component of the α-ketoglutarate dehydrogenase complex, which is localised in the mitochondrial matrix (336), though the exact mechanism by which UPS-mediated proteolysis occurs is also unclear. Given the emerging evidence that UCP2 is a mitochondrial protein implicated in regulating cellular metabolism during nutrient stress, especially with regards to glutamine oxidation (93, 114, 119, 298), it could be argued that the proteasome is responsible for mediating UCP2 protein turnover. However, given the evidence that UCP2 is particularly unstable in mitochondrial membranes, even in the presence of

stabilising lipids such as cardiolipin (155), the UPS system may merely be acting passively, clearing only already unfolded UCP2 that is generated due to the protein's inherent instability.

This thesis shows the recombinant expression of human UCP2 protein in a yeast system. Protein produced was observed to be predominantly folded in mild, non-ionic detergents, indicative of folded material. The gel blot protein thermostability assay suggests that, although extractable from yeast membranes, UCP2 is particularly unstable, as quantified by low apparent T_ms. The physiological relevance of the mouse UCP2 NMR structure, obtained by bacterial expression and solubilisation in DPC, has been called into question by many researchers (155, 158-162). This work presented in this thesis further indicates that the elucidated UCP2 structure obtained from *E. coli*-expressed system is likely to be misfolded. Firstly, the use of a GDP analogue was used to select for folded UCP2 protein during the purification process, as it was presumed that UCP2, like UCP1, binds purine nucleotides (156). Secondly, NMR experiments were conducted at 33°C at pH 6.5 (156), which are conditions where UCP2 was observed to be unstable in 12MNG-solubilised membranes. Thirdly, the UCP2 protein structure was reported to bind GDP inside the cavity (156), as is the case for UCP1 (153, 237), which is inconsistent with results obtained with the gel blot protein thermostability assay, which observed no stabilising interaction between UCP2 and GDP.

6.6. The biochemical properties of UCP2 are distinct from UCP1

Human UCP2 has a high (59%) sequence similarity to that of human UCP1 (4), yet emerging evidence suggest that these proteins likely carry out different physiological roles (198, 293, 299, 337, 338). Since the discovery of UCP1 paralogues, such as UCP2, various studies have reported the existence of other uncoupling proteins across different branches of the evolutionary tree, including plants (339-342), amoeba (343, 344), fungi (345), parasites (346, 347), fish (348-353), birds (354-356) and mammals (4, 5, 7, 8, 357-365). Whilst most of these proposed uncoupling proteins were named based on their sequence similarity to UCP1 (4, 6-8, 341, 342, 348, 350-354, 356-358, 366, 367), some were designated as UCPs due to functional reports showing increased respiratory activity in the presence of fatty acids, which was negatively regulated by purine nucleotides (340, 343-347, 349, 362) – features commonly associated with

eutherian UCP1 (2, 3, 9, 27, 29-31, 36, 293, 364, 368). In eutherian mammals, the physiological function of UCP1 is well-established – the protein facilitates NST by enabling thermoregulation in newborns (9, 36, 362, 365). Although present throughout the animal kingdom, the role of UCP1 in non-eutherian mammals is not well-characterised.

In lower eukaryotes, oxygen consumption assays hinted the existence of UCP1-like proteins capable of enhancing respiration in the presence of fatty acids (343, 344, 369). In protozoa, such as *Acanthamoeba castellani* and *Dictyostelium discoideum*, fatty acid-induced respiratory activity was shown to be weakly regulated by GDP (344) or GDP-insensitive (343), respectively. Heterologous expression of *A. castellani* UCP (AcUCP) in a yeast system failed to show GDP-regulated, fatty acid-enhanced respiratory activity, thereby suggesting that other endogenous mitochondrial proteins present in *A. castellani*, but not *S. cerevisiae* are responsible for the previously observed uncoupling activity (370). Protein sequence comparison of AcUCP with human UCP paralogues show a 37-43% similarity in protein sequence, with HsUCP4 showing the highest similarity (370). Like HsUCP2, AcUCP exhibits residues that are highly conserved in UCP1, such as the key mitochondrial carrier features (1, 133, 138), the arginine triplet present in the substrate binding site (136, 153, 237), and the presence of hydrophobic and aromatic residues as part of the cytoplasmic gating elements (153, 237, 314) which have been reported to interact with purine nucleotides (153, 237). Whilst AcUCP has all the necessary residues for purine nucleotide binding (370), functional studies have shown that this protein weakly binds GDP (344). This observation somewhat supports the observations made in this thesis that purine nucleotides do not bind to HsUCP2 in the same manner as HsUCP1. The protein sequence for *D. discoideum* UCP remains to be elucidated, but it would be interesting to see if this UCP variant shows the same level of conservation of key UCP residues as this protein was not regulated by GDP in respiratory assays (343).

Studies into a UCP derived from *B. belcheri*, the "closest living invertebrate relative of vertebrates", shows high protein sequence similarity to HsUCP2 and HsUCP3 (330). From this study, it was concluded that BbUCP functions more like HsUCP2 than eutherian UCP1, as mitochondrial proton leak could not be induced in the presence of fatty acids and was observed to be unresponsive to GDP (330). Like AcUCP1, BbUCP has all the conserved structural features of HsUCP1 (330) that has been reported to participate in purine nucleotide binding (153, 237). Lack of GDP

inhibition in the presence of fatty acids, suggests that BbUCP does not bind purine nucleotides like that of UCP1, which aligns with the results obtained in the gel blot protein thermostability assay that show that HsUCP2 does not bind purine nucleotides as observed by a lack of stabilising shifts in protein thermostability.

Recent investigations using *Monodelphis domestica*, a marsupial model organism, indicate that MdUCP1 is likely localised to inguinal adipose tissue, which based on transcriptomic analyses, resembles beige adipose tissue properties (371). Heterologous expression of MdUCP1 in HEK293 cells indicate that this UCP1 isoform does not catalyse proton leak activity in the presence of UCP1 activators, suggesting a different physiological role for MdUCP1 (371). Comparison of protein sequences indicates that MdUCP1 shares a higher sequence identity with HsUCP2 (72%) than with HsUCP1, which shares 65% sequence identity with MdUCP1. Results obtained with *M. domestica*, suggest that modern eutherian UCP1 likely gained its thermogenic properties following divergence from marsupials (363, 372), following UCP1 localisation to BAT (371). Purification trials using a method capable of purifying untagged eutherian UCP1 proved to be unsuccessful in purifying folded, untagged MdUCP1 protein from a yeast expression system (Dr. Camila Cotrim – unpublished work). Interestingly, heterologous expression of either MdUCP1 or HsUCP2 in an AAC-deficient yeast strain resulted in predominantly unfolded protein that was not enriched for in the final sample, whereas expression of HsUCP1 in the AAC-deficient yeast strain yielded folded and functional protein (Danielle Copeman and Dr. Camila Cotrim – unpublished work). Although anecdotal, differences in recombinant protein expression and purification supports the idea that the molecular properties of marsupial UCP1 and human UCP2 are distinct from eutherian UCP1.

Phylogenetic analyses predicts that UCPs, DICs and OGCs cluster together and likely evolved from a common ancestor (63, 369, 373-376). Emerging evidence suggests that UCP2 (93, 114, 119) and UCP3 (280) function as metabolite transporters, rather than uncoupling proteins. Given the wide tissue of expression of UCP2 (38, 41, 42, 90, 105, 185) and the observation that this protein can transport various C4 metabolites (93), it is likely that UCP2, UCP3 and ancestral UCP1 proteins carried out a distinct metabolite transport function, which may have later diverged in eutherian UCP1, where it likely gained its thermogenic function after it became localised to BAT (3, 20, 371). This rationale is consistent with the work shown in thesis, in that UCP2 is less stable than UCP1 (155), and other mitochondrial carriers

(98, 141, 147, 219, 221). Furthermore, differences in the molecular properties of UCP2, support the idea that UCP2 functions differently from UCP1. Moreover, characteristic properties of UCP1, such as the ability to bind purine nucleotides (31-35, 196) and translocate protons in a fatty acid-dependent manner (27, 30, 31), is likely unique to the eutherian UCP1 variant.

Acknowledgements

Throughout my PhD journey, I've been fortunate enough to have an amazing support network and I would like to express gratitude to everyone involved. First and foremost, I would like to thank my supervisor, Dr. Paul Crichton, for giving me the chance to pursue a doctorate, for your patience and mentorship throughout my time at UEA and for providing me with such a supportive team to help me carry out my project. To that end, I would like to thank the lab team I worked alongside with and guided me through my PhD. My deepest thanks go to Danielle Copeman and Dr. Camila Cotrim, two very inspirational women whom I am constantly in awe of – their strong work ethics and kind-hearted personalities have shaped me into the researcher I am today. I am truly grateful for them and their invaluable emotional and moral support over the years. Thanks to Riccardo Cavalieri for being a friend during the PhD and beyond. You have shown me how to navigate a PhD at UEA and what post-PhD life could be like. Additionally, I'd like to thank Paul for giving me the unique opportunity to supervise and train a visiting student, Mike Gaudry, from whom I've gained a friendship as well as a wealth of (random) information. Through this collaboration it was nice to be involved in and exposed to the international nature of research, so thank you Paul for organising this experience.

Thanks to the UEA-EBEC conference gang, Josh, Ben and Alejandro, for giving me the opportunity to pick your brains about biochemistry and membrane protein related questions. Thank you to all the friends I have made in the BMRC over the years; a special thanks goes to Georgina Hurle, Bernie Breeze, Luke Griffith, Maria Ramos and Hassan Boudjelal for their constant encouragement and kind words throughout my PhD. A huge thank you to my deskmate, Sergio Llaneza Lago, for guiding me through the emotional turmoil of the final year and reassuring me there is light at the end of the tunnel post thesis writing. (A special shout-out also goes to his partner Tasos Bampalis, for the invites for dinner and any excuse to treat me to food…this did not go unnoticed!)

A massive thanks to my University of Southampton friends, firstly, my "boys and girls in the city", Tom and Georgia, for constantly getting me excited over things other than work, as well as my girls in the south, Sid and Sarah, for giving me reasons to switch off for the whole weekend by making me wander back to Southampton every

couple of months to catch up with our lives. Thank you all for keeping me grounded throughout this period of my life, the little escapes from work have done wonders for me.

Lastly, I would like to thank my family for understanding my academic endeavours. I am eternally grateful to my mum, Maribel, who has supported emotionally and financially throughout this time and helped make this pursuit a reality. Thank you to my siblings, Taz and Argel, for listening to me drone on about my work (…I hope you learnt a lot about brown fat and why we should keep the heating down).
A final special shoutout goes to my dad, Noel, for taking an interest in my work by constantly asking "Where is the protein?", his layman way of asking if I've purified UCP2 yet….and my answer to that question is: "I still don't know". But with this project, I've come to learn that that's the nature of research, I won't always get an answer to every single question I would like to know the answer to…sometimes things are just left open-ended. With that I want to say…good luck Mehmethan!

Appendices

Appendix 1 (Methods)

Appendix 1.1. Chemical, reagents and enzymes

Reagents used for the composition of growth media, including ampicillin and isopropyl ß-D-1-thiogalactopyranoside (IPTG), were purchased from Formedium (Cambridge).

FastDigest restriction enzymes were purchased through Thermo Scientific: SacI (FD1133), XbaI (FD0684), NdeI (FD0583), EcoRI (FD0274). DpnI (M0202S) and T4 ligase (R0176S) were bought from New England BioLabs. Lysozyme and Zymolyase 20T was purchased from Fisher (10076813) and AMSBIO (120491-1), respectively. Polyethylene glycol 4000 (PEG) was purchased from Alfa aesar. QIAgen kits: QIAprep Spin Miniprep kit (27104), QIAquick PCR purification kit (28104) and QIA gel extraction kit (29704) were obtained from Qiagen.

Ethidium bromide solution, sodium carbonate, 30mL Dounce glass homogeniser, enhanced chemiluminescence (ECL) kits, BCA assay protein detection kits, 6-aminocaproic acid, benzamidine hydrochloride, phenylmethylsulfonyl fluoride (PMSF) were purchased from Fisher Scientific. Protease inhibitor tablets were purchased from Roche (cat. no: 04 693 132 001).

Detergents, n-dodecyl-ß-D-maltopyranoside (DDM) and lauryl maltose neopentyl glycol (12MNG), were purchased from Anatrace (catalogue numbers: B310 and NG310 respectively). Triton X-100 (TX-100) and Tween-20 was purchased from Sigma (T9284 and 9005-64-5, respectively) and N-lauryl sarcosine sodium salt (sarkosyl) was purchased from Merck (8.14715).

Ni-NTA Superflow cartridges were obtained by Qiagen (1046323). Hydroxyapatite resin was purchased through Bio-Rad (130-0420). Vivaspin concentrators and ion-exchange spin columns, Vivapure S and Q Maxi (VS-IX20SH08 and VS-IX20QH08, respectively), were bought from Sartorius. Thiopropyl sepharose 6B (TPS) was purchased from Cytiva (T8387), thiopropyl agarose (TPA) was purchased from

Stratech (THIO-001A-CRE). Sephadex G-25 PD10 columns were obtained from GE Healthcare Life Sciences (17-0851-01).

Precision plus protein standards (161-0374), 10- and 15-well 4-15% Mini PROTEAN TGX precast gels (4561083 and 4561086, respectively), and anhydrous hydroxyapatite (130-04020) were purchased from Bio-Rad. Coomassie Blue stains, InstantBlue and ReadyBlue, were purchased from Expedeon (ISB1L) and Sigma (87-69-4), respectively. Antibodies against uncoupling protein 1 (UCP1) and a 6x-histidine tag were purchased from Invitrogen (cat. no: U6382 and MA1021315-HRP, respectively). Uncoupling protein 2 (UCP2) antibodies were obtained from Abcam (ab97931) and Millipore (144-157). Anti-rabbit-HRP conjugated antibodies were purchased from Millipore (AP132P). Custom-made antibodies against the ADP/ATP carrier (AAC) (A298) raised in chicken were obtained from the Kunji lab (MRC Mitochondrial Biology Unit, Cambridge). Anti-chicken HRP-conjugated antibodies were purchased from Sigma (cat. no: 9046). For UCP1 quantification using bacterially expressed protein, the UCP1 antibody used for immunoblots were obtained from Abcam (155117).
7-diethylamino-3-(4'-maleimidophenyl)-4-methylcoumarin (CPM) was obtained from Invitrogen (D346). Carboxyatractyloside (CATR) was purchased from Cambridge Biosciences (HY-N1502). Guanosine 5'-diphosphate (GDP) (43139-22-6); adenosine 5'-diphosphate (ADP) (A2754); aspartic acid (A6683); poly(ethylene glycol) methyl ether maleimide conjugated to either a 2 kilodalton species (PEG-Maleimide-2K) (731765) or a 5 kilodalton species (PEG-Maleimide-5K) (63187) was purchased from Sigma (A6683).

Appendix 1.2. Sequence alignment of the UCP2 constructs

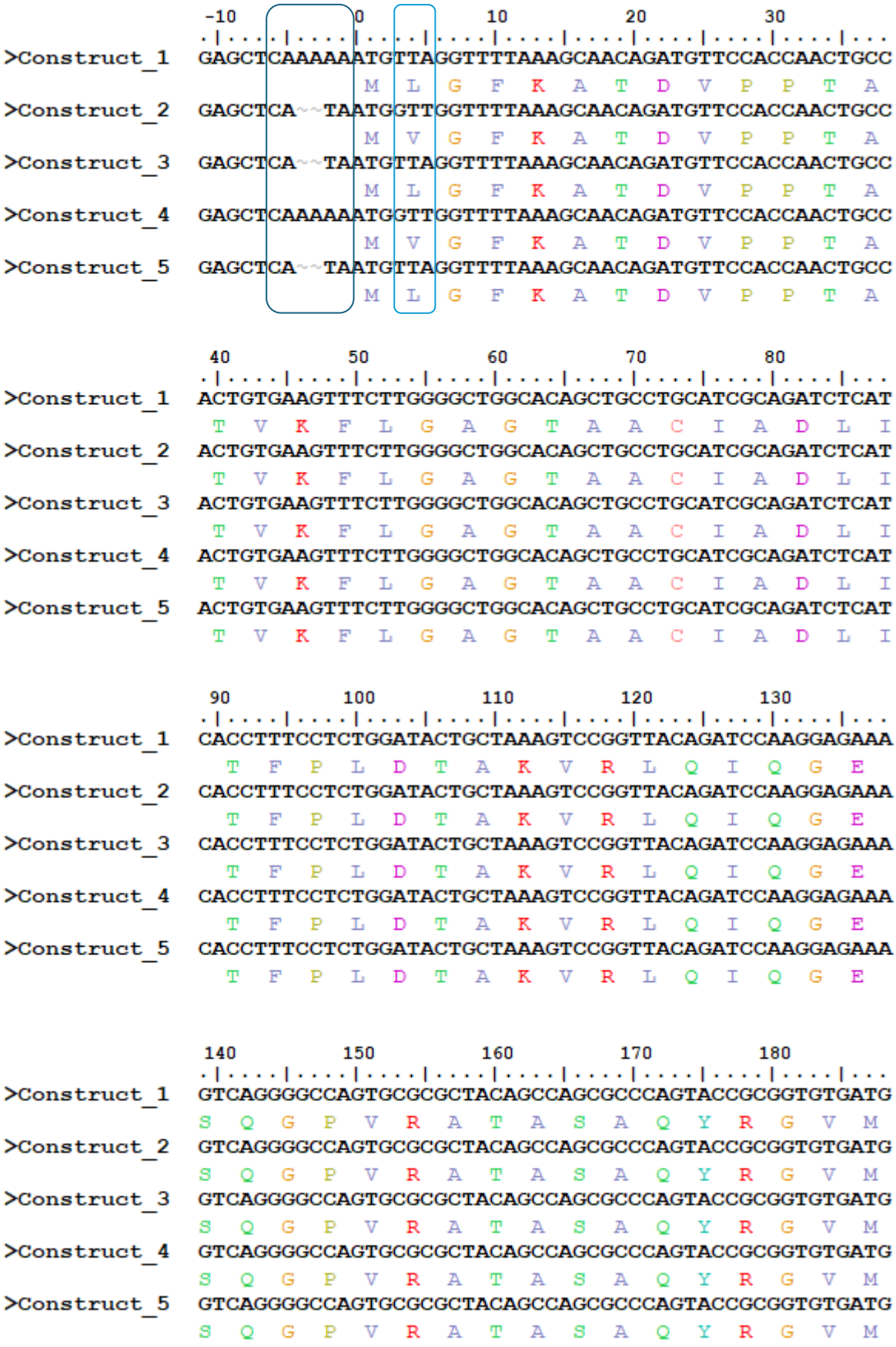

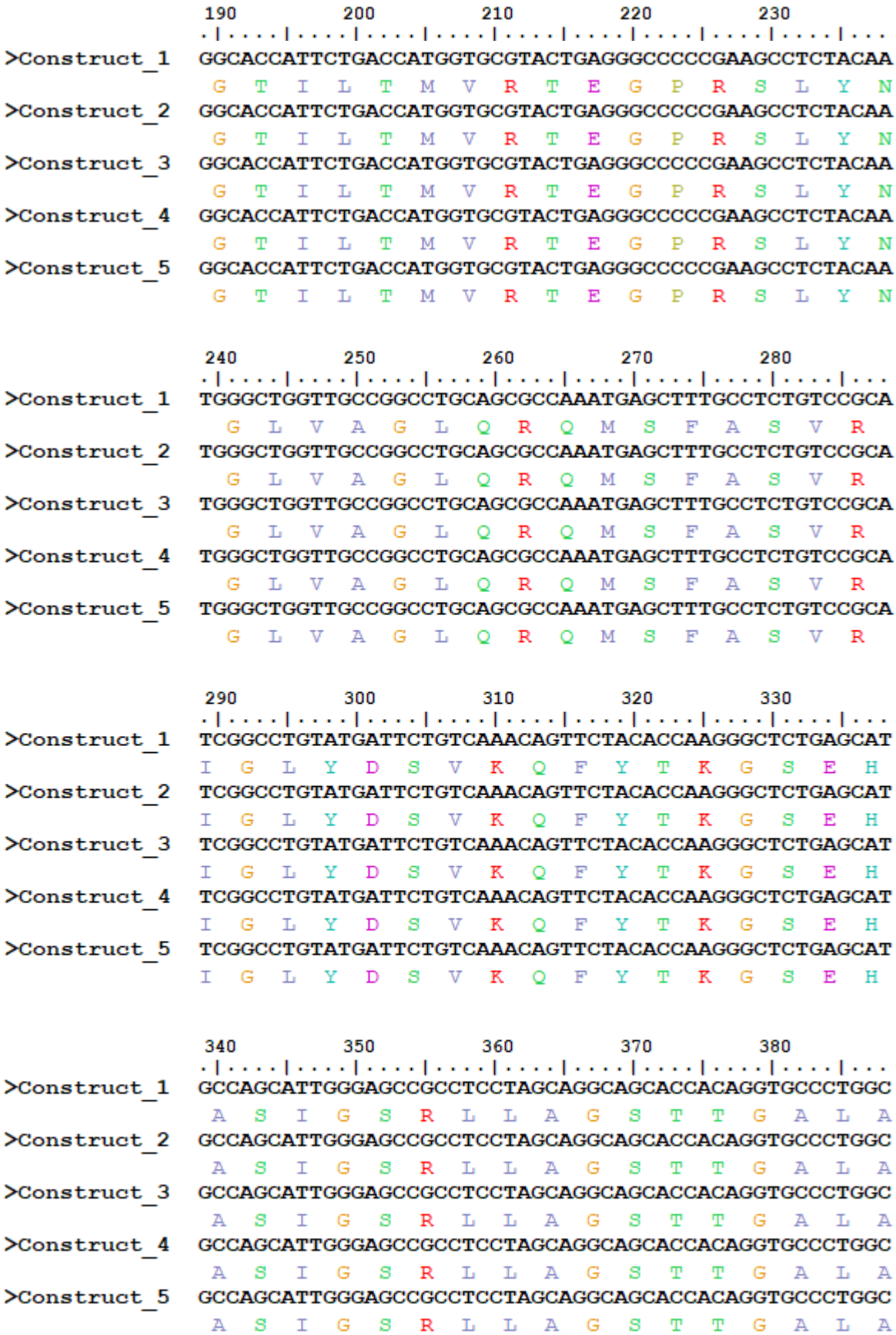
190 200 210 220 230
>Construct_1 GGCACCATTCTGACCATGGTGCGTACTGAGGGCCCCCGAAGCCTCTACAA
G T I L T M V R T E G P R S L Y N
>Construct_2 GGCACCATTCTGACCATGGTGCGTACTGAGGGCCCCCGAAGCCTCTACAA
G T I L T M V R T E G P R S L Y N
>Construct_3 GGCACCATTCTGACCATGGTGCGTACTGAGGGCCCCCGAAGCCTCTACAA
G T I L T M V R T E G P R S L Y N
>Construct_4 GGCACCATTCTGACCATGGTGCGTACTGAGGGCCCCCGAAGCCTCTACAA
G T I L T M V R T E G P R S L Y N
>Construct_5 GGCACCATTCTGACCATGGTGCGTACTGAGGGCCCCCGAAGCCTCTACAA
G T I L T M V R T E G P R S L Y N
240 250 260 270 280
>Construct_1 TGGGCTGGTTGCCGGCCTGCAGCGCCAAATGAGCTTTGCCTCTGTCCGCA
G L V A G L Q R Q M S F A S V R
>Construct_2 TGGGCTGGTTGCCGGCCTGCAGCGCCAAATGAGCTTTGCCTCTGTCCGCA
G L V A G L Q R Q M S F A S V R
>Construct_3 TGGGCTGGTTGCCGGCCTGCAGCGCCAAATGAGCTTTGCCTCTGTCCGCA
G L V A G L Q R Q M S F A S V R
>Construct_4 TGGGCTGGTTGCCGGCCTGCAGCGCCAAATGAGCTTTGCCTCTGTCCGCA
G L V A G L Q R Q M S F A S V R
>Construct_5 TGGGCTGGTTGCCGGCCTGCAGCGCCAAATGAGCTTTGCCTCTGTCCGCA
G L V A G L Q R Q M S F A S V R
290 300 310 320 330
>Construct_1 TCGGCCTGTATGATTCTGTCAAACAGTTCTACACCAAGGGCTCTGAGCAT
I G L Y D S V K Q F Y T K G S E H
>Construct_2 TCGGCCTGTATGATTCTGTCAAACAGTTCTACACCAAGGGCTCTGAGCAT
I G L Y D S V K Q F Y T K G S E H
>Construct_3 TCGGCCTGTATGATTCTGTCAAACAGTTCTACACCAAGGGCTCTGAGCAT
I G L Y D S V K Q F Y T K G S E H
>Construct_4 TCGGCCTGTATGATTCTGTCAAACAGTTCTACACCAAGGGCTCTGAGCAT
I G L Y D S V K Q F Y T K G S E H
>Construct_5 TCGGCCTGTATGATTCTGTCAAACAGTTCTACACCAAGGGCTCTGAGCAT
I G L Y D S V K Q F Y T K G S E H
340 350 360 370 380
>Construct_1 GCCAGCATTGGGAGCCGCCTCCTAGCAGGCAGCACCACAGGTGCCCTGGC
A S I G S R L L A G S T T G A L A
>Construct_2 GCCAGCATTGGGAGCCGCCTCCTAGCAGGCAGCACCACAGGTGCCCTGGC
A S I G S R L L A G S T T G A L A
>Construct_3 GCCAGCATTGGGAGCCGCCTCCTAGCAGGCAGCACCACAGGTGCCCTGGC
A S I G S R L L A G S T T G A L A
>Construct_4 GCCAGCATTGGGAGCCGCCTCCTAGCAGGCAGCACCACAGGTGCCCTGGC
A S I G S R L L A G S T T G A L A
>Construct_5 GCCAGCATTGGGAGCCGCCTCCTAGCAGGCAGCACCACAGGTGCCCTGGC
A S I G S R L L A G S T T G A L A

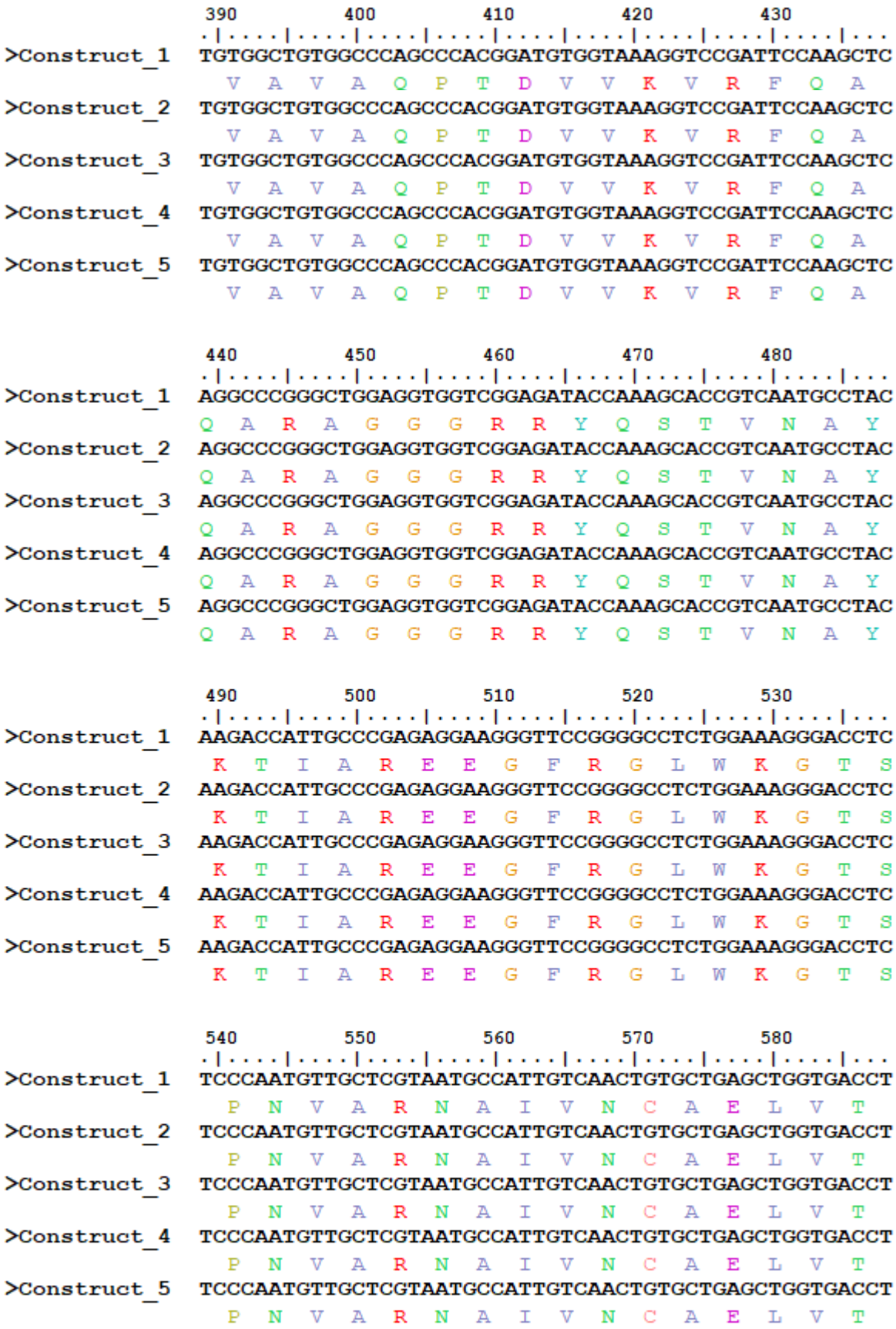
390 400 410 420 430
>Construct_1 TGTGGCTGTGGCCCAGCCCACGGATGTGGTAAAGGTCCGATTCCAAGCTC
V A V A Q P T D V V K V R F Q A
>Construct_2 TGTGGCTGTGGCCCAGCCCACGGATGTGGTAAAGGTCCGATTCCAAGCTC
V A V A Q P T D V V K V R F Q A
>Construct_3 TGTGGCTGTGGCCCAGCCCACGGATGTGGTAAAGGTCCGATTCCAAGCTC
V A V A Q P T D V V K V R F Q A
>Construct_4 TGTGGCTGTGGCCCAGCCCACGGATGTGGTAAAGGTCCGATTCCAAGCTC
V A V A Q P T D V V K V R F Q A
>Construct_5 TGTGGCTGTGGCCCAGCCCACGGATGTGGTAAAGGTCCGATTCCAAGCTC
V A V A Q P T D V V K V R F Q A
440 450 460 470 480
>Construct_1 AGGCCCGGGCTGGAGGTGGTCGGAGATACCAAAGCACCGTCAATGCCTAC
Q A R A G G G R R Y Q S T V N A Y
>Construct_2 AGGCCCGGGCTGGAGGTGGTCGGAGATACCAAAGCACCGTCAATGCCTAC
Q A R A G G G R R Y Q S T V N A Y
>Construct_3 AGGCCCGGGCTGGAGGTGGTCGGAGATACCAAAGCACCGTCAATGCCTAC
Q A R A G G G R R Y Q S T V N A Y
>Construct_4 AGGCCCGGGCTGGAGGTGGTCGGAGATACCAAAGCACCGTCAATGCCTAC
Q A R A G G G R R Y Q S T V N A Y
>Construct_5 AGGCCCGGGCTGGAGGTGGTCGGAGATACCAAAGCACCGTCAATGCCTAC
Q A R A G G G R R Y Q S T V N A Y
490 500 510 520 530
>Construct_1 AAGACCATTGCCCGAGAGGAAGGGTTCCGGGGCCTCTGGAAAGGGACCTC
K T I A R E E G F R G L W K G T S
>Construct_2 AAGACCATTGCCCGAGAGGAAGGGTTCCGGGGCCTCTGGAAAGGGACCTC
K T I A R E E G F R G L W K G T S
>Construct_3 AAGACCATTGCCCGAGAGGAAGGGTTCCGGGGCCTCTGGAAAGGGACCTC
K T I A R E E G F R G L W K G T S
>Construct_4 AAGACCATTGCCCGAGAGGAAGGGTTCCGGGGCCTCTGGAAAGGGACCTC
K T I A R E E G F R G L W K G T S
>Construct_5 AAGACCATTGCCCGAGAGGAAGGGTTCCGGGGCCTCTGGAAAGGGACCTC
K T I A R E E G F R G L W K G T S
540 550 560 570 580
>Construct_1 TCCCAATGTTGCTCGTAATGCCATTGTCAACTGTGCTGAGCTGGTGACCT
P N V A R N A I V N C A E L V T
>Construct_2 TCCCAATGTTGCTCGTAATGCCATTGTCAACTGTGCTGAGCTGGTGACCT
P N V A R N A I V N C A E L V T
>Construct_3 TCCCAATGTTGCTCGTAATGCCATTGTCAACTGTGCTGAGCTGGTGACCT
P N V A R N A I V N C A E L V T
>Construct_4 TCCCAATGTTGCTCGTAATGCCATTGTCAACTGTGCTGAGCTGGTGACCT
P N V A R N A I V N C A E L V T
>Construct_5 TCCCAATGTTGCTCGTAATGCCATTGTCAACTGTGCTGAGCTGGTGACCT
P N V A R N A I V N C A E L V T

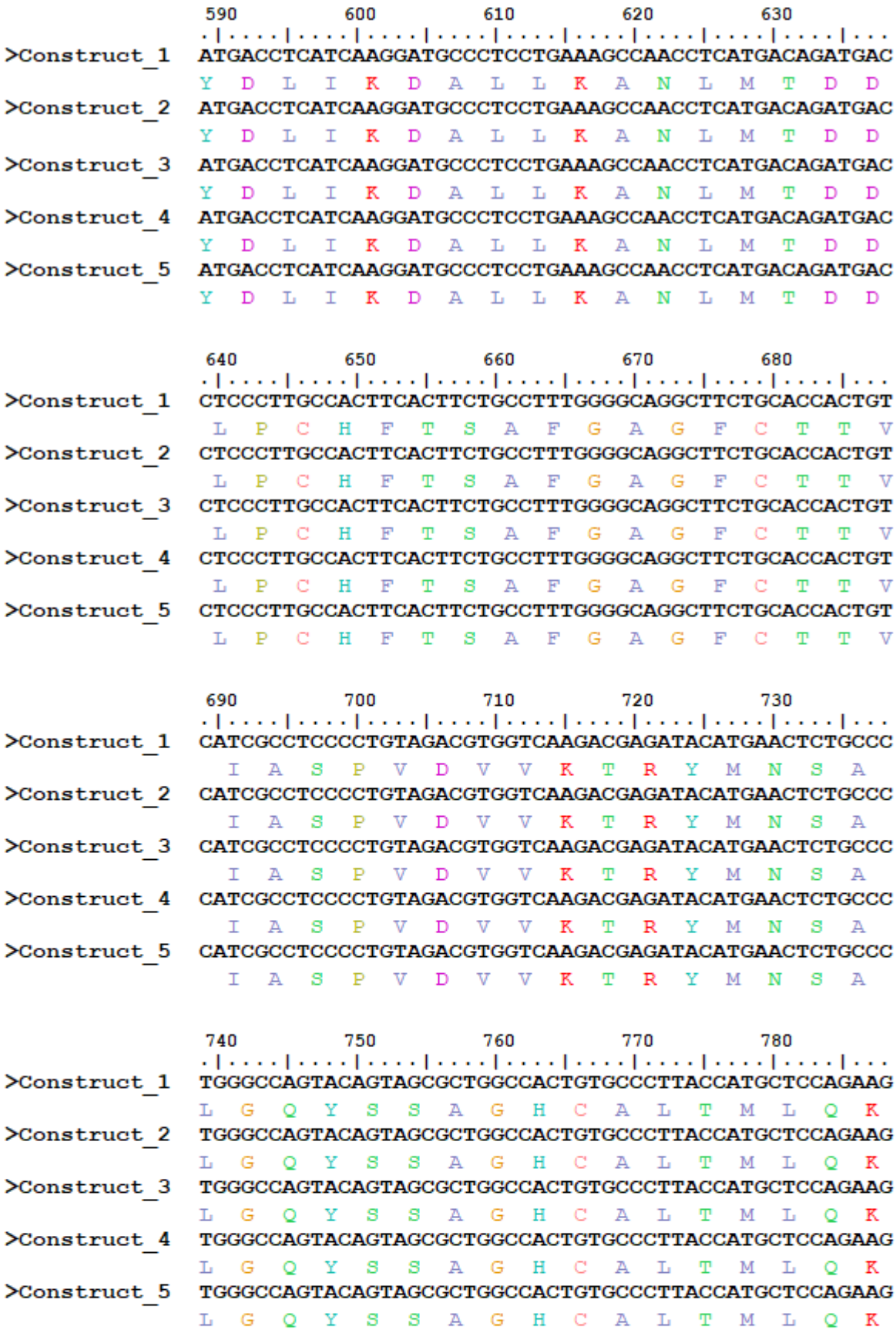
590 600 610 620 630
>Construct_1 ATGACCTCATCAAGGATGCCCTCCTGAAAGCCAACCTCATGACAGATGAC
Y D L I K D A L L K A N L M T D D
>Construct_2 ATGACCTCATCAAGGATGCCCTCCTGAAAGCCAACCTCATGACAGATGAC
Y D L I K D A L L K A N L M T D D
>Construct_3 ATGACCTCATCAAGGATGCCCTCCTGAAAGCCAACCTCATGACAGATGAC
Y D L I K D A L L K A N L M T D D
>Construct_4 ATGACCTCATCAAGGATGCCCTCCTGAAAGCCAACCTCATGACAGATGAC
Y D L I K D A L L K A N L M T D D
>Construct_5 ATGACCTCATCAAGGATGCCCTCCTGAAAGCCAACCTCATGACAGATGAC
Y D L I K D A L L K A N L M T D D
640 650 660 670 680
>Construct_1 CTCCCTTGCCACTTCACTTCTGCCTTTGGGGCAGGCTTCTGCACCACTGT
L P C H F T S A F G A G F C T T V
>Construct_2 CTCCCTTGCCACTTCACTTCTGCCTTTGGGGCAGGCTTCTGCACCACTGT
L P C H F T S A F G A G F C T T V
>Construct_3 CTCCCTTGCCACTTCACTTCTGCCTTTGGGGCAGGCTTCTGCACCACTGT
L P C H F T S A F G A G F C T T V
>Construct_4 CTCCCTTGCCACTTCACTTCTGCCTTTGGGGCAGGCTTCTGCACCACTGT
L P C H F T S A F G A G F C T T V
>Construct_5 CTCCCTTGCCACTTCACTTCTGCCTTTGGGGCAGGCTTCTGCACCACTGT
L P C H F T S A F G A G F C T T V
690 700 710 720 730
>Construct_1 CATCGCCTCCCCTGTAGACGTGGTCAAGACGAGATACATGAACTCTGCCC
I A S P V D V V K T R Y M N S A
>Construct_2 CATCGCCTCCCCTGTAGACGTGGTCAAGACGAGATACATGAACTCTGCCC
I A S P V D V V K T R Y M N S A
>Construct_3 CATCGCCTCCCCTGTAGACGTGGTCAAGACGAGATACATGAACTCTGCCC
I A S P V D V V K T R Y M N S A
>Construct_4 CATCGCCTCCCCTGTAGACGTGGTCAAGACGAGATACATGAACTCTGCCC
I A S P V D V V K T R Y M N S A
>Construct_5 CATCGCCTCCCCTGTAGACGTGGTCAAGACGAGATACATGAACTCTGCCC
I A S P V D V V K T R Y M N S A
740 750 760 770 780
>Construct_1 TGGGCCAGTACAGTAGCGCTGGCCACTGTGCCCTTACCATGCTCCAGAAG
L G Q Y S S A G H C A L T M L Q K
>Construct_2 TGGGCCAGTACAGTAGCGCTGGCCACTGTGCCCTTACCATGCTCCAGAAG
L G Q Y S S A G H C A L T M L Q K
>Construct_3 TGGGCCAGTACAGTAGCGCTGGCCACTGTGCCCTTACCATGCTCCAGAAG
L G Q Y S S A G H C A L T M L Q K
>Construct_4 TGGGCCAGTACAGTAGCGCTGGCCACTGTGCCCTTACCATGCTCCAGAAG
L G Q Y S S A G H C A L T M L Q K
>Construct_5 TGGGCCAGTACAGTAGCGCTGGCCACTGTGCCCTTACCATGCTCCAGAAG
L G Q Y S S A G H C A L T M L Q K

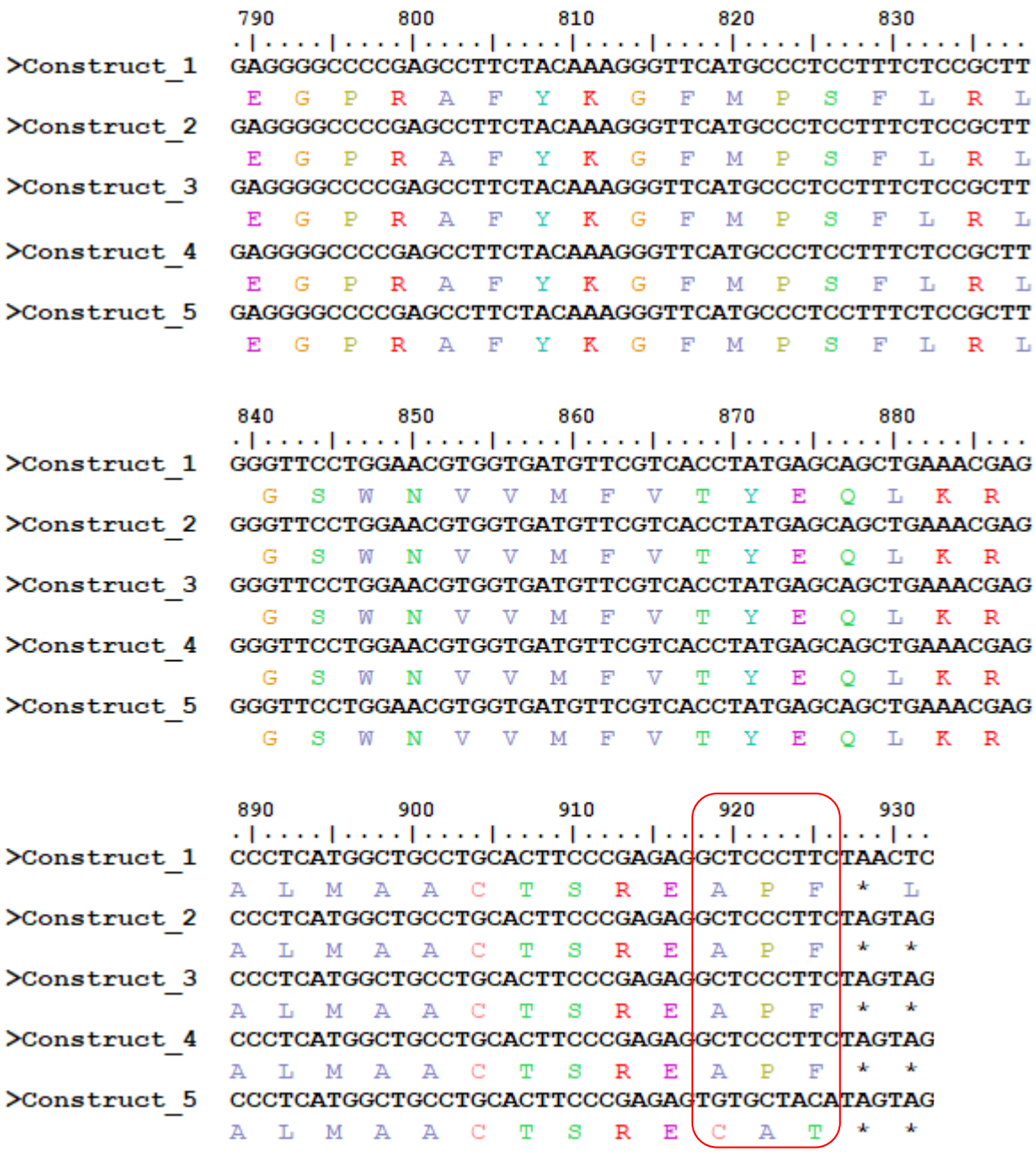

Appendix Figure 1.1: Sequence alignments of HsUCP2 constructs. *DNA and protein sequence alignments of HsUCP2 constructs, starting from the SacI restriction site and ending in the stop codons. To highlight differences in the Kozak sequences, the codon encoding for the amino acid at position 2 and alterations in the C-terminus, blue, yellow and red boxes are circled around each respective parameter. Sequences were aligned using Bioedit. Nucleotides are depicted in black, whilst amino acids displayed underneath each codon are coloured based on the ClustalX colour scheme (https://www.jalview.org/help/htmL/colourSchemes/clustal.htmL).*

Appendix 1.3. Primers designed for HsUCP2 variants

Appendix Table 1.1: Primers designed for the generation of HsUCP2 variants.

Name	DNA sequence (5'→3')	Reason for primer design
Primers designed for pYES2 vector (using construct 2 as the backbone DNA)		
Construct 3 forward	GGTACCGAGCTCATAATG*TTA*GGTTTTAAAGCAACAGATGTTCCACC	Alters the second amino acid to leucine
Construct 4 forward	GGTAGCTGAGCTC*AAAAA*ATGGTTGGTTTTAAAGCGG	Produces an adenine-rich Kozak sequence
pYES2 insert forward	TAGGGAATATTAAGCTTGGTACCGAG	To confirm gene insertion into the pYES2 vector following colony PCR
pYES2 insert reverse	TACCTTCGAAGGGCCCTCTAGA	
pYES2 seq forward	TTCAACATTTTCGGTTTGTAT	Sequencing primers for pYES2 gene inserts
pYES2 seq reverse	AACTCCTTCCTTTTCGGTTAGAG	
Primers designed for pMW172-type vector		
pMW172 SDM forward	GACCACAACGGTTTCCCTC*C*AGAAATAATTTTGTTTAAAC	Removal of an internal XbaI site in inherited pMW172 vector containing MmUCP1
pMW172 SDM reverse	GTTAAACAAAATTATTTCT*G*GAGGGAAACCGTTGTGGTC	
pMW172 His-tag forward	GAGGACATATGCATCATCATCATCATCACGAGCTCATAATGGTTGGTTTTA	Adds an NdeI restriction site to the 5'-end of the protein and a hexa-histidine-tag in the encoded protein
pMW172 His-tag reverse	TACCGGAATTCTAGACTACTAGAAGGGAGCCTCTCGGGAAGTG	Adds an EcoRI restriction site to the 3'-end of the construct
pMW172 insert forward	TAATACGACTCACTATAGGG	

pMW172 insert reverse	GCTAGTTATTGCTCAGCGG	To confirm gene insertion into the pMW172 vector following colony PCR
pMW172 seq forward	TGTGTCAGAGGTTTTCACCGTCAT	Sequencing primers for pMW172 gene inserts
pMW172 seq reverse	AGGCCCTTTCGTCTTCAAGAA	

Nucleotides that are italicised and underlined highlight changes that have been designed to incorporate changes in the pYES2 plasmid harbouring the UCP2 gene.

Appendix 1.4. Production of histidine-tagged UCP standards from bacterial inclusion bodies

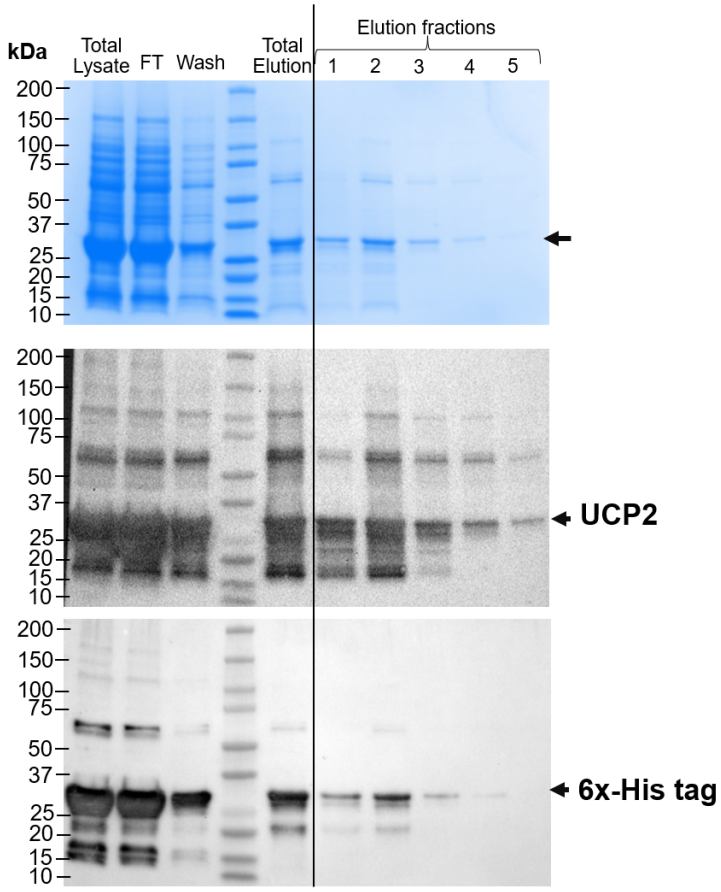

Appendix Figure 1.2: Assessment of histidine-tagged inclusion body purity. *Purification profile of histidine-tagged UCP2 inclusion bodies purified by Ni-NTA chromatography under denaturing conditions. Coomassie-stained gel (top) and Western blots of Ni-NTA purification profile, blots were probed using antibodies against UCP2 (middle) and a hexa-histidine tag (bottom). To determine protein purity, the elution fraction was taken in 2 mL aliquots and labelled according to when the samples were eluted from the cartridge; for example, elution fraction 1 would correspond to the first 2 mL eluate. Coomassie-stained gel shows that a majority of the protein is eluted after 4 mL, with highly purified UCP2 protein being eluted between 5-8 mL of elution buffer as demonstrated by a single band in the Coomassie-stained gel (top panel) and Western blots (middle panel). When visualised with hexa-histidine antibody, a majority of histidine-tagged proteins were seen to be eluted following the first 2 mL elution (bottom panel). Samples are loaded as a fraction proportional to the total sample volume. 'Total lysate' represents the inclusion body fraction isolated from bacteria following sample clarification using by centrifugation and a filtration through a 0.2 µm filter; FT represents the 'flow through'*

fraction; 'Wash' corresponds to a wash with slightly acidic pH. The 'Total Elution' refers to the 10 mL elution fraction, which is comprised of the individual 2 mL elution fractions.

Protein concentrations of purified inclusion body material were quantified using the BCA method. To verify that protein concentrations were free from urea contamination, half-logarithmic protein standards were generated to determine if the signal on Coomassie-stained gels and Western blots were proportional (see **Appendix Figure 1.3**).

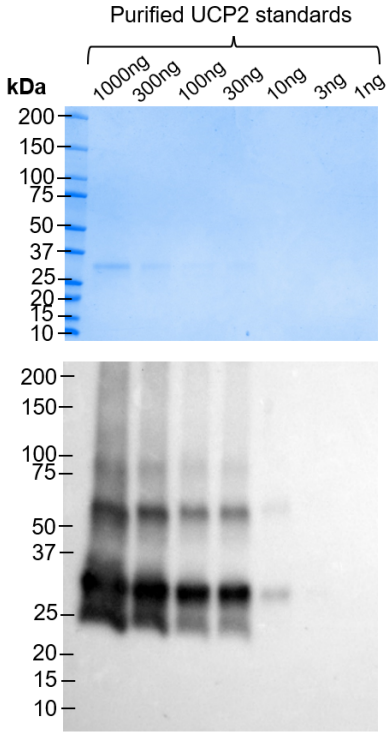

Appendix Figure 1.3: Assessment and quantification of purified histidine-tagged UCP2 protein. *Coomassie-stained gels (top) and Western blot (bottom) of histidine-tagged UCP2 protein standards loaded to give a half-logarithmic curve. Protein amounts stated above the lanes correspond to the protein loaded on the gel. The Coomassie-stained gel shows a single molecular weight band (top panel), consistent with the size of histidine-tagged UCP2, which is verified by Western blots (bottom panel). Coomassie-stained gel illustrates that there is a gradual decrease in protein concentration as a function of protein loaded onto the gel; thereby validating that the protein concentration obtained following Ni-NTA purification and subsequent urea removal. At concentrations where protein is undetectable in (ReadyBlue) Coomassie-stained gels (<30 ng protein/lane), histidine-tagged UCP2 protein was visualised by Western blot using the Millipore 144-157 UCP2 antibody.*

It was crucial to load saturating amounts of protein for Coomassie-staining to assess UCP2 protein purity. However, high protein loads saturated signals in Western blots, made it difficult to create linear standard curves for the interpolation of UCP2 protein expression in our recombinant system. It was therefore essential to optimise the Western blot procedure to ensure that the detection of the UCP2 standard curve was not immediately saturating; hence, different combinations of primary and secondary antibodies were trialled to determine which combination gave the most linear trend following densitometric analysis (see **Appendix Figure 1.4**).

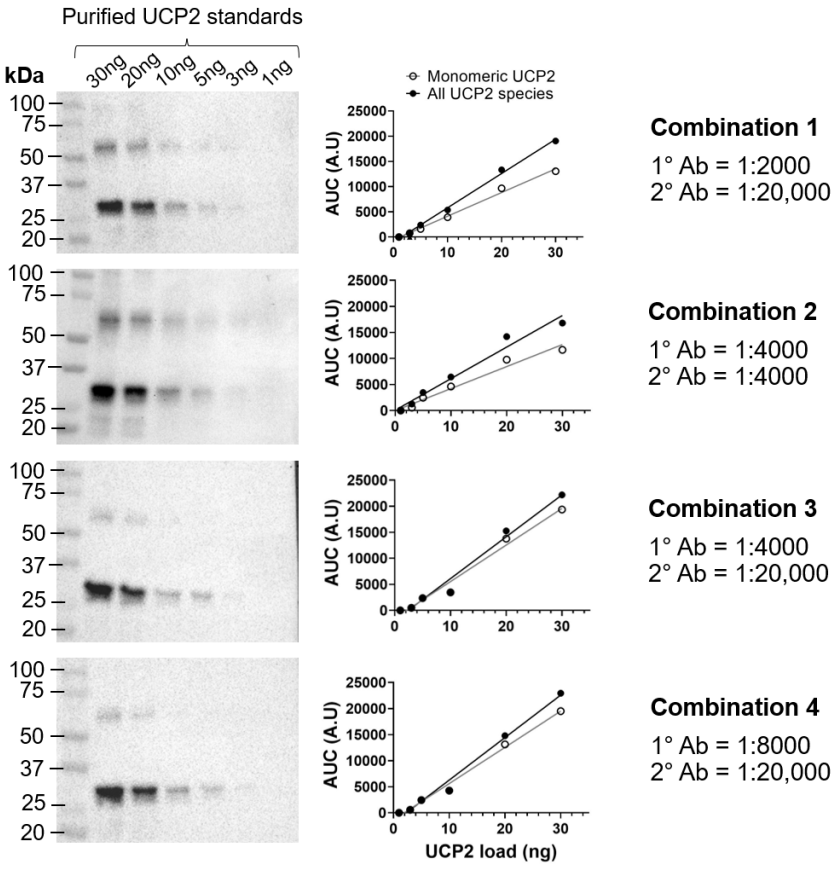

Appendix Figure 1.4: Titration of UCP2 antibodies for optimal Western blot analysis. *Western blots of a UCP2 standard curve (30-1 ng) using different combinations of antibodies (denoted on the right). Linear standard curves produced following densitometric analysis of corresponding Western blots. All blots are visualised following 8 minutes exposure using the ChemiDoc XRS+ system. At high primary antibody concentrations, dimeric species could be observed at the high end of the standard curve.*

Appendix Table 1.2: Primary and secondary antibody dilutions.

Combination	Primary antibody titration	Secondary antibody titration	R^2 value	
			Monomeric UCP2	All UCP2 species
1	1 in 2000	1 in 20000	0.993	0.997
2	1 in 4000	1 in 4000	0.982	0.983
3	1 in 4000	1 in 20000	0.986	0.970
4	1 in 8000	1 in 20000	0.982	0.983

Primary antibody refers to the anti-UCP2 Millipore (144-157) antibody; secondary antibody refers to a goat anti-rabbit HRP-conjugated antibody by Millipore (AP123P). UCP2 standard curves from ***Appendix Figure 1.4*** *were plotted using densitometry values obtained following incubation with different antibody combinations (as described in second and third columns), for both monomeric (33 kDa) and all UCP2 protein species (all signals). Little difference is observed in terms of linear curve fitting, as evidenced by calculated R^2 values, hence combination 4 (1 in 8000 primary antibody incubation, followed by 1 in 20,000 secondary antibody) was utilised in subsequent Western blots.*

Appendix 2 (Chapter 3)

Appendix 2.1. Results from preliminary UCP2 expression trials

Appendix Table 2.1: Cell growth of yeast cells transformed with HsUCP2 construct.

Yeast strain	Optical density (OD_{600nm})				
	Selective lactate starter culture	YPL growth culture			
		Pre-induction (0h)	4h	6h	8h
W303-1B	0.95	0.05	-	-	-
FGY217	3.60	1.65	3.30	4.30	5.15

OD_{600} values taken from preliminary protein expression trials conducted with W303-1B and FGY217 cells transformed with HsUCP2 (construct 2). Expression was conducted based on UCP1 expression protocols (177, 178), whereby single colonies were inoculated into selective lactate media supplemented with 0.1% (w/v) glucose prior to inoculation into 50 mL YPL media. Following 16/17 hours growth in YPL, cultures are induced with 1% (v/v) galactose (0 hrs) and following 4-, 6- and 8-hours protein expression. OD_{600} values of selective lactate starter cultures were taken immediately prior to inoculation into 50 mL YPL growth media. OD_{600} readings are representative of cell growth prior to induction (0h) and following 4-, 6- and 8-hours galactose addition. Since W303-1B cells struggled to grow in selective pre-culture following overnight growth on YPL, these cells were not taken forward for further expression trials.

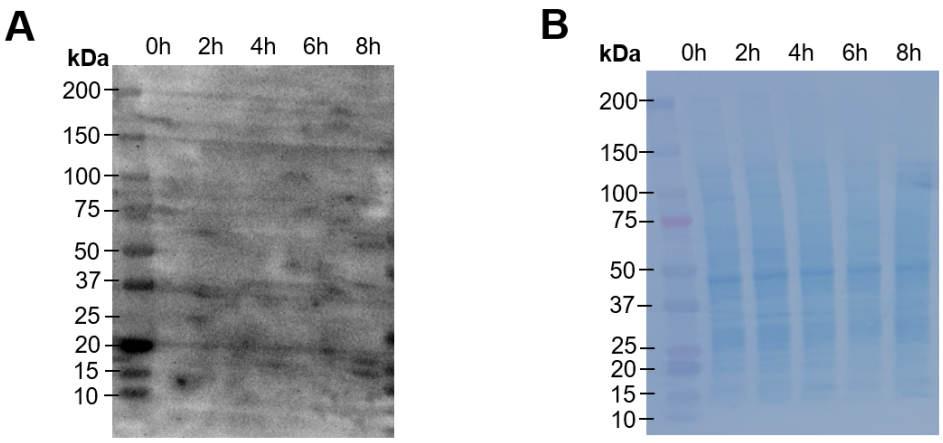

Appendix Figure 2.1: Determination of recombinant UCP2 protein expression in yeast system. *A) Representative Western blot of a human uncoupling protein 2 expression trial, probed with the anti-UCP2 probe provided by Abcam (ab97931) and the corresponding blot stained with Coomassie Blue stain to visualise total proteins following transfer and immunoblot visualisation (B). Samples were taken prior to induction with 1% galactose (0h), and 2-, 4-, 6- and 8-hours following induction; times above blots indicate sample collection following galactose induction. The Western blot image highlights the inefficiency of the Abcam antibody in detecting UCP2 protein in our expression system. To exclude the notion that the lack of signal in Western blots could be attributed to inefficient protein transfer from the SDS-PAGE gel onto the PVDF membrane, the blot was irreversibly stained with Coomassie Blue stain, subsequently showing whole protein detection on the blot.*

Appendix 2.2. Initial UCP2 solubilisation tests

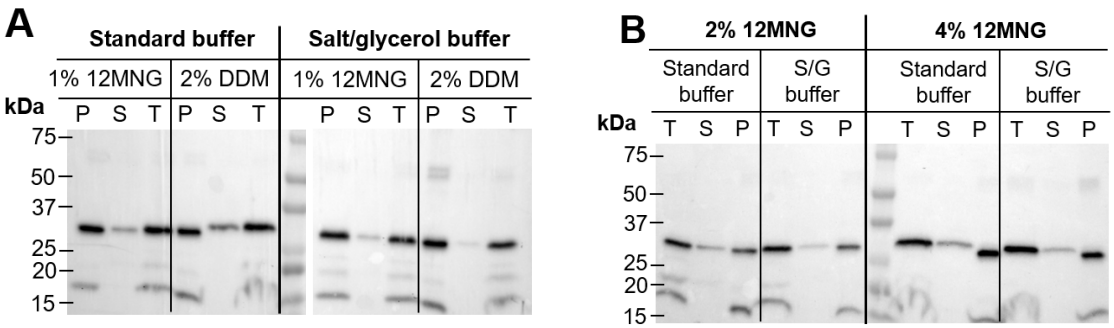

Appendix Figure 2.2: Investigating UCP2 solubility under different solubilisation conditions. *A) Western blots of (construct 3-expressed) UCP2 solubilisation fractions, following treatment with mild, non-ionic detergents, 12MNG and DDM. B) Western blots of (construct 3-expressed) UCP2 solubilisation fractions treated with 4% detergent with samples mixtures solubilised in different buffers. Samples were resuspended either in 'standard buffer' (50 mM Tris HCl (pH 8.0), 0.65 M D-sorbitol) or 'salt/glycerol buffer' (100 mM Tris HCl (pH 8.0), 10% (v/v) glycerol, 150 mM NaCl supplemented with a protease inhibitor tablet) as indicated above lanes ('salt/glycerol buffer' is abbreviated to 'S/G buffer' in B). Samples were loaded proportional to the total volume and labelled as: T - total protein; S – solubilised supernatant; P – insoluble pellet.*

Appendix 2.3. Large-scale protein expression trials

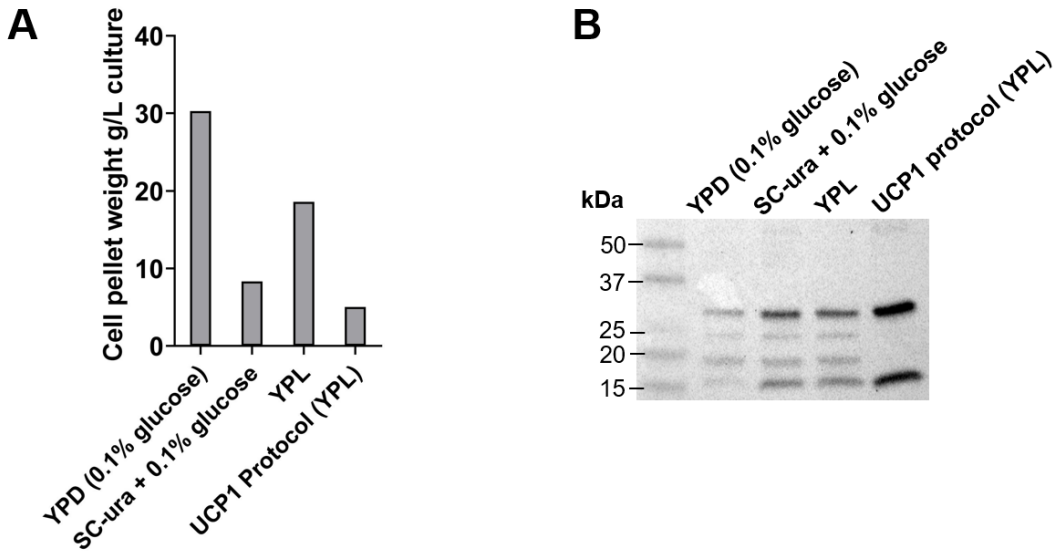

Appendix Figure 2.3: Preliminary large-scale expression trial using the Drew protocol with 2% glucose starter cultures. *A) Cell pellet weights obtained per litre of culture following 22 hours protein expression. B) Western blots quantifying UCP2 expression following 22 hours induction; 10 µg yeast mitochondrial membranes were loaded onto each lane, with membranes isolated from cells grown using the UCP1 protocol loaded for comparison ('UCP1 protocol (YPL)' lane).*

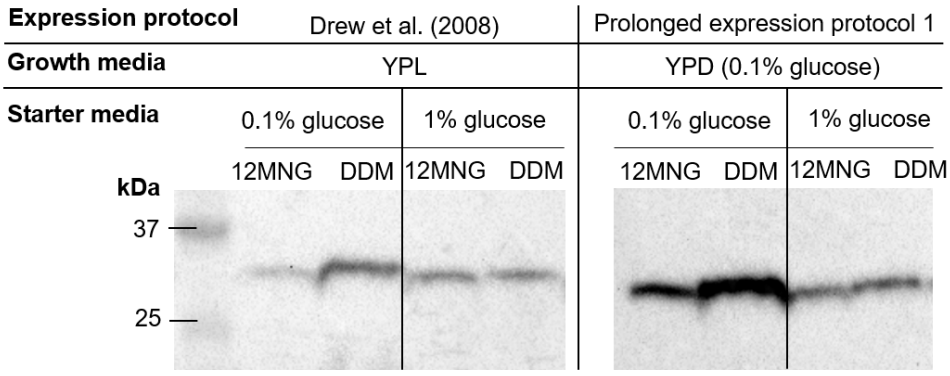

Appendix Figure 2.4: Testing UCP2 solubility using membranes derived from large-scale expression trials. *Solubilisation screens were conducted with membranes isolated from cells that demonstrated optimal growth and UCP2 expression. Western blots show solubilised supernatant fractions obtained from cells grown either on YPL growth media using the Drew protocol (left) or in YPD (0.1% glucose) growth media using prolonged expression protocol 1 (right), with glucose concentration used in the starter culture shown above. Membranes are solubilised in either 4% 12MNG or 4% DDM as stated above lanes, with samples fractionally loaded onto the gel.*

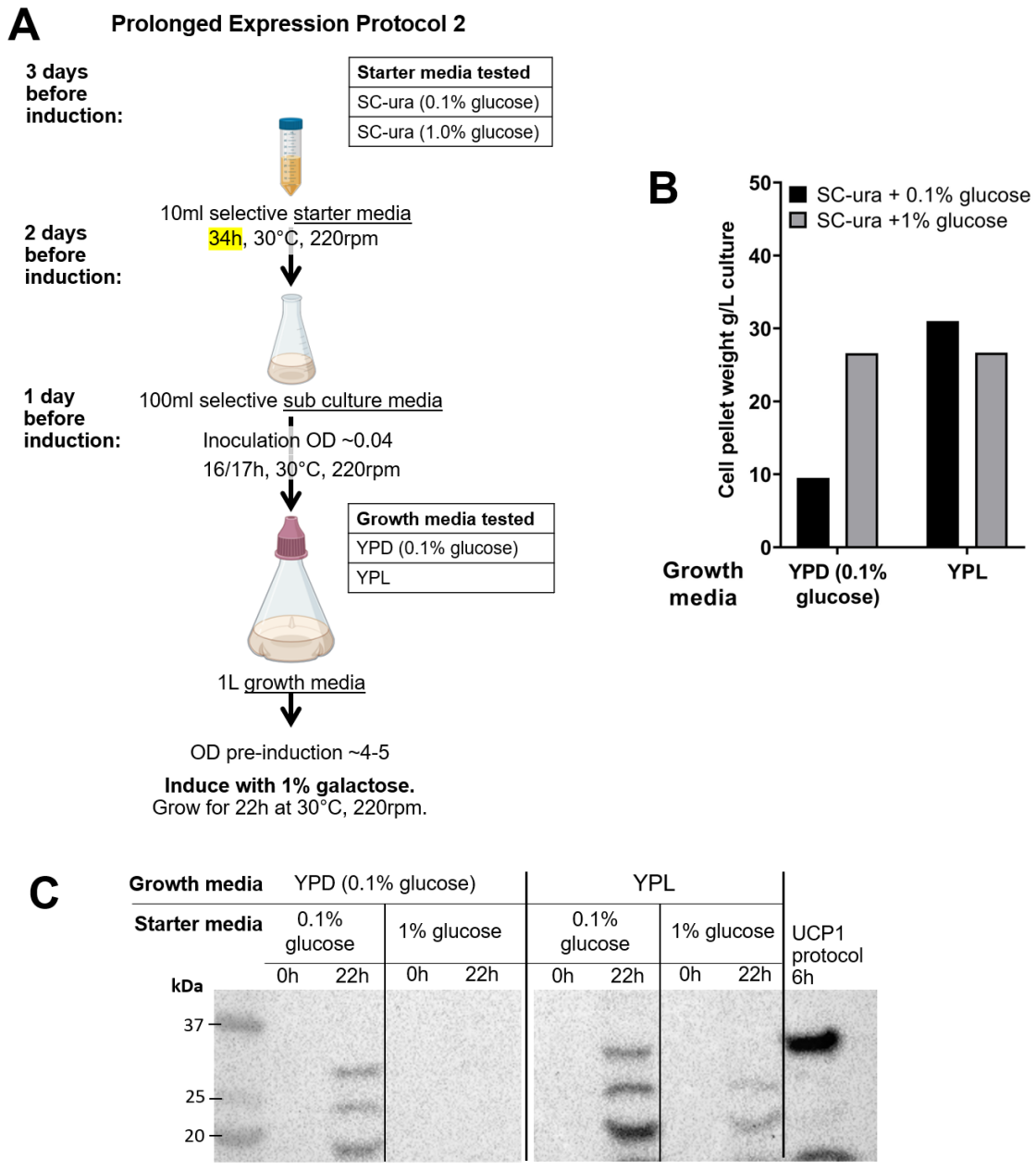

Appendix Figure 2.5: Large-scale expression trial of cells grown using a variation of "Prolonged expression protocol 1". *A) Schematic of large-scale expression protocol using a variation of the "Prolonged expression protocol 1", the key difference being prolonged incubation (~34 hours) in the 100 mL selective starter culture rather than overnight (16-22 hours) growth, prior to inoculation into 1 L growth media. B) FGY217 cell growth determined by cell pellet weights obtained per litre of culture following 22 hours protein expression. Cells are propagated in selective media (SC-ura) containing either 0.1% (w/v) glucose (black bars) or 1% (w/v) glucose (grey bars), before further cultivation either in 1 L YPD (0.1% (w/v) glucose) or YPL growth media. C) Western blot quantifying UCP2 expression following 22 hours induction; in each lane*

10 µg yeast mitochondrial membranes were loaded, with membranes isolated from cells grown using the UCP1 protocol loaded for comparison ('UCP1 protocol 6h' lane).

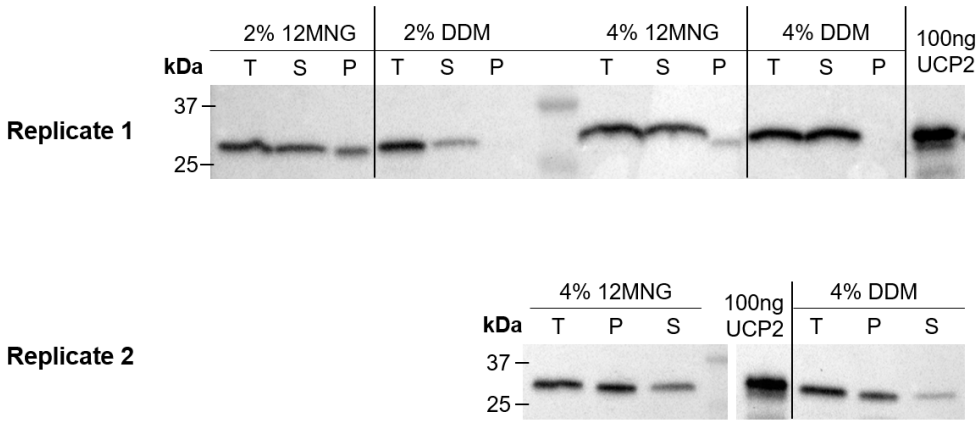

Appendix Figure 2.6: Inconsistencies in small-scale (150 µl) solubilisation screens. *Western blots of fractions obtained from small-scale (150 µl) solubilisation screens. Membranes were isolated from cells grown in 0.75% (w/v) glucose from two independent tests, as indicated. Membranes were solubilised in 2% (w/v) or 4% (w/v) detergent as indicated above lanes. 100 ng purified UCP2 inclusion bodies are used as a control between blots. Samples are loaded as a fraction of the total volume and are denoted as T – total proteins; S – solubilised supernatant; P – insoluble pellet.*

Appendix 3 (Chapter 4)

Appendix 3.1. Results from UCP2 binding trials

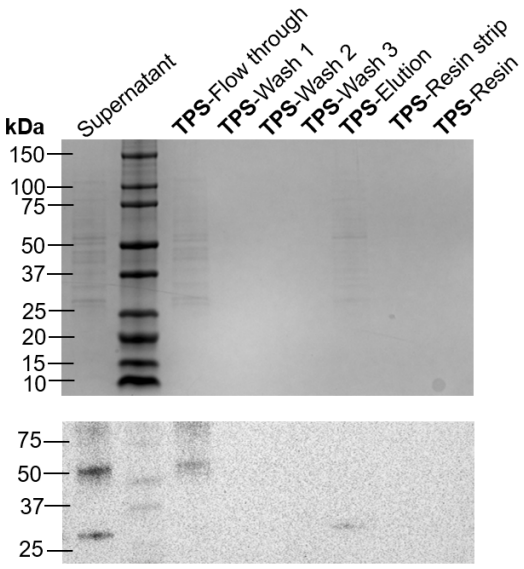

Appendix Figure 3.1: Solubilised fraction binding to TPS resin. *Coomassie-stained gel (top) and Western blot (bottom) of fractions taken from the TPS binding trial. The folded supernatant fraction was incubated with thiol-reactive (TPS) resin for an hour, prior to flow through and three sequential washes with TPS wash buffer (50 mM Tris HCl (pH 8.0), 150 mM NaCl, 1 mM EDTA), followed by elution with 150 mM DTT. The resin was resuspended in distilled water ("TPS-Resin"), and then stripped with 1% (v/v) SDS to elute any strongly bound proteins ("TPS-Resin strip"). Samples are loaded as a proportion of the total volume; the "TPS-Flow through" fraction is representative of the flow through fraction followed by a 20 mL chase with TPS wash buffer.*

Appendix 3.2. Results from S+Q TP purification trials

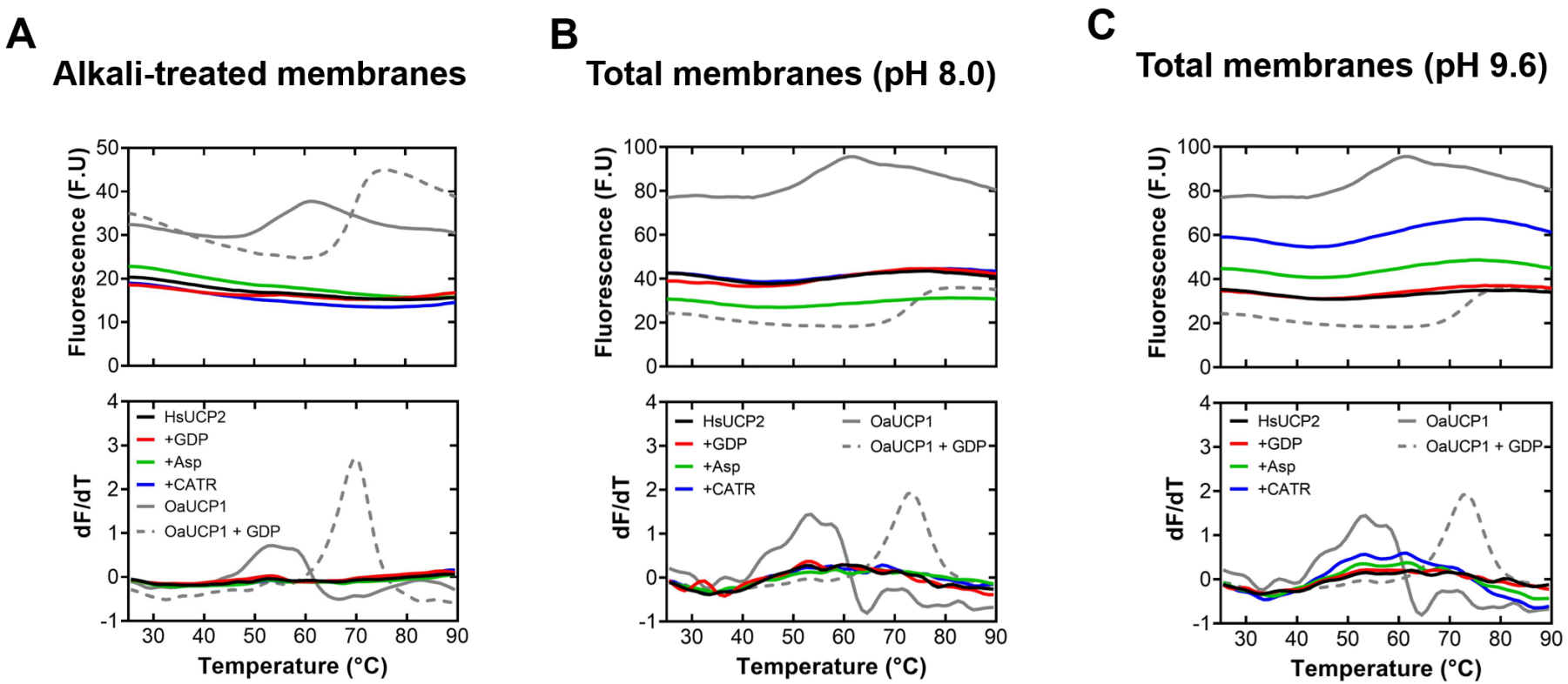

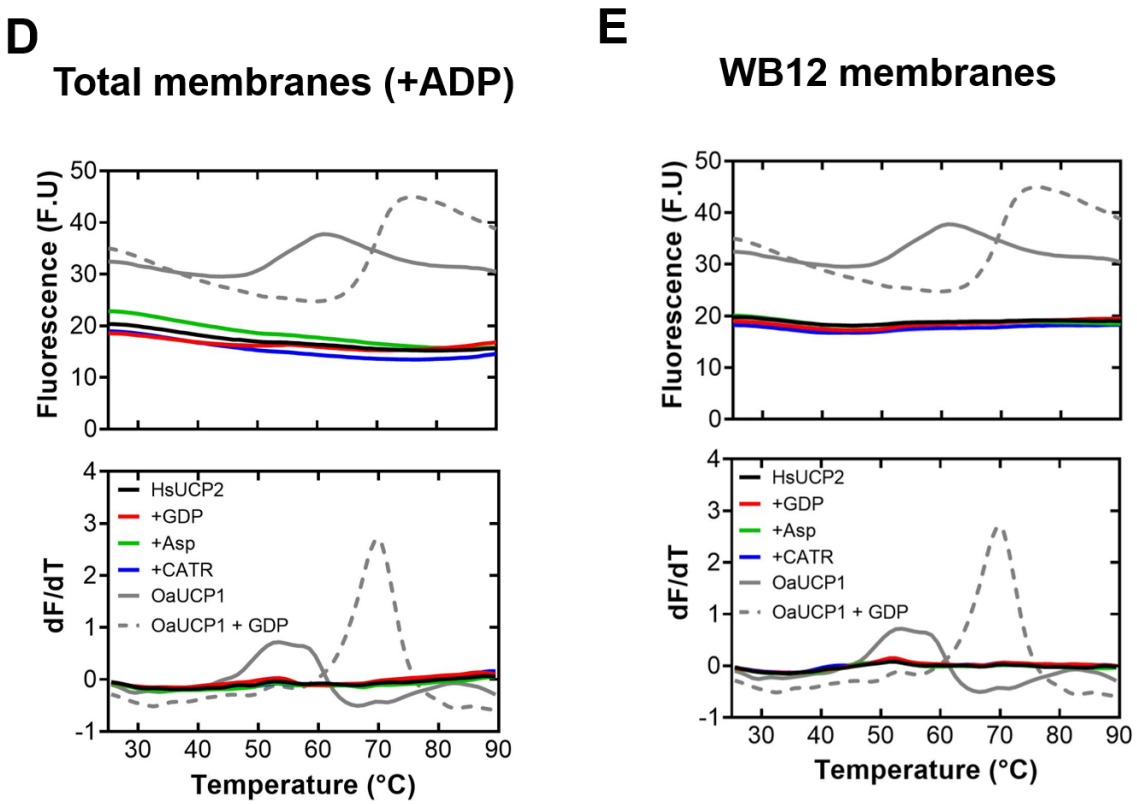

Appendix Figure 3.2: CPM thermostability assays of purified samples following HsUCP2 purification trials, conducted with purified native OaUCP1 as a control. *Fluorescence (top) and first derivative (dF/dT) (bottom) traces of CPM assays conducted with native OaUCP1 and HsUCP2. HsUCP2 samples were obtained from purifications from different conditions – enriched, alkali-treated membranes (A); under mild conditions with the ion exchange part conducted at pH 8.0 (B) or pH 9.6 (C); mild conditions with cell lysates treated with 1 mM ADP during mitochondrial membrane isolation (D) and UCP2 derived from WB12 mitochondrial membranes (E). In all experiments, 2 µg of purified protein sample was used per run.*

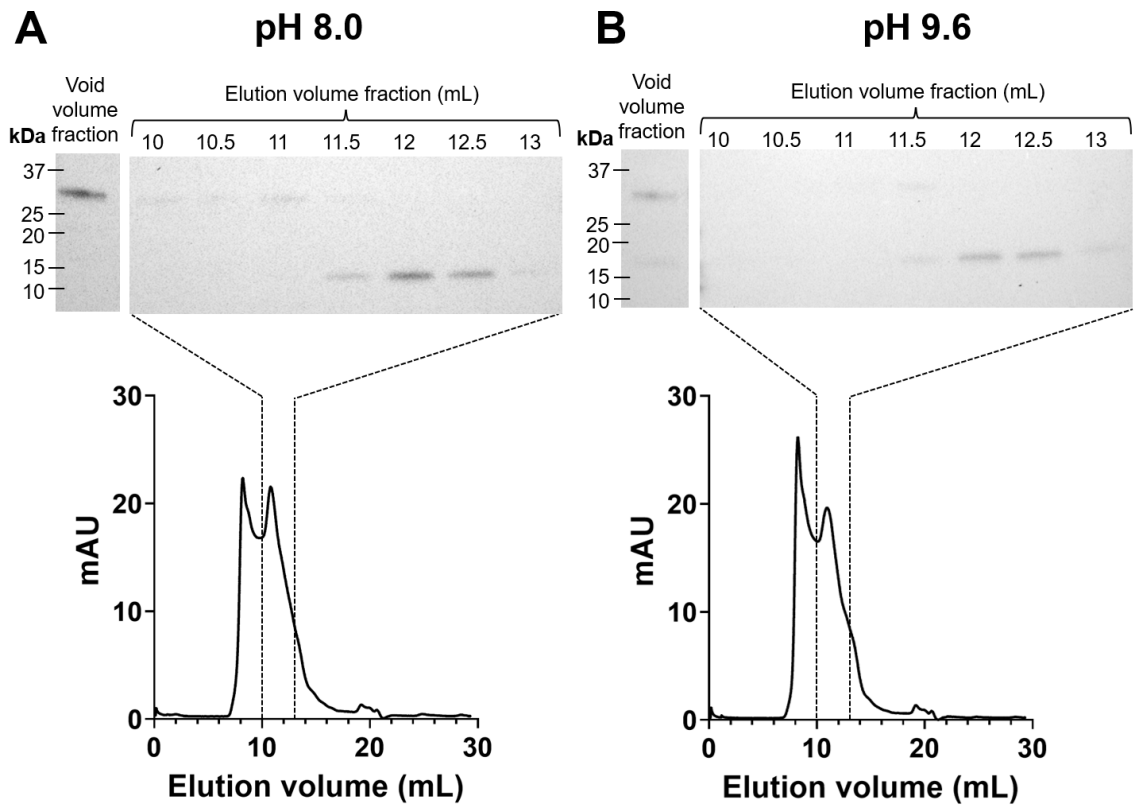

Appendix Figure 3.3: Chromatograms of unconcentrated samples from S+Q TPA purifications in mild alkali pH. *A-B) Chromatograms (bottom panels) of size exclusion runs using unconcentrated eluates from post PD10 samples from S+Q TPS purifications, with samples resuspended in 20 mM Tris HCl (pH 8.0) (A) or 20 mM piperazine (pH 9.6) (B). Western blots (top panel) taken from corresponding SEC runs; lanes are labelled to match the fractions taken; the void peak was taken at 9 mL elution volume. Samples are loaded in proportion to the fraction volume collected by the AKTA.*

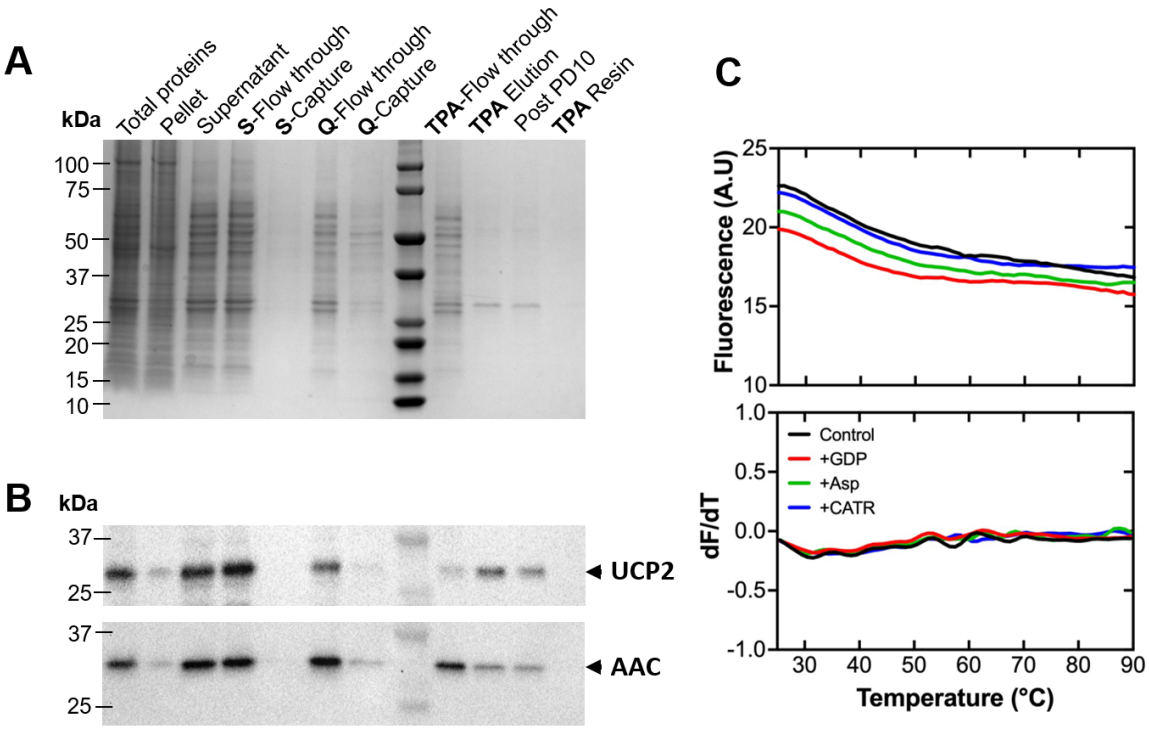

Appendix Figure 3.4: S+Q TPA purification using membranes pre-treated with ADP. *Coomassie-stained gel (A) and Western blots (B) monitoring HsUCP2 and ScAAC protein in S+Q TPA purification of total, ultracentrifuged membranes. Crude membranes underwent large-scale membrane isolation in the presence of 1 mM ADP to destabilise yeast AAC protein. Gel samples are loaded as a fraction proportional to the sample volume. C) Fluorescence (top) and derivative (bottom) traces from CPM thermostability assay runs using the final purified sample from the corresponding S+Q TPA purification. CPM assays were conducted with 2 µg of purified protein in the absence or presence of 1 mM CATR, 1 mM GDP and 1 mM aspartate to detect AAC- and UCP2-dependent thermal shifts, respectively. Native OaUCP1 was used as a control (see* ***Appendix Figure 3.2D*** *for trace with OaUCP1).*

Appendix 3.3. Results relating to HsUCP2 construct 5

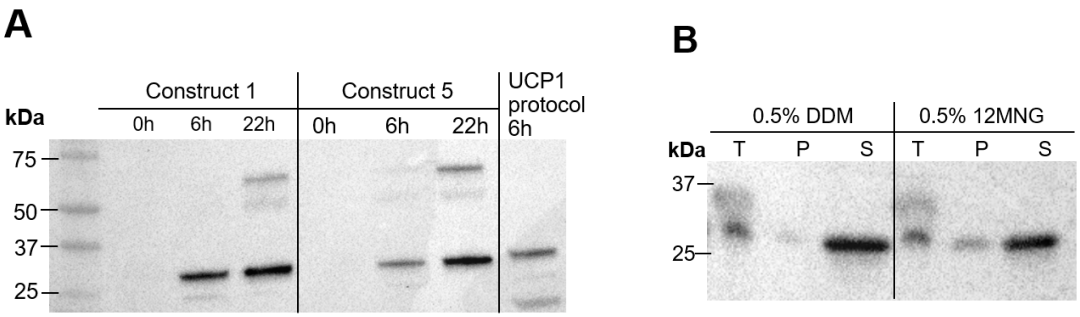

Appendix Figure 3.5: Expression and solubilisation tests of the construct 5 (HsUCP2 variant with a UCP1-like C-terminus). *A) Small-scale (50 mL) expression trial of construct 5, grown and expressed as outlined in "Prolonged expression protocol 3" (see* ***Chapter 3*** *for details). Cells transformed with construct 1 was used as a control for protein expression. Western blot analysis shows that construct 5 produces similar levels of protein to that of construct 1. UCP2 protein produced as outlined in the UCP1 expression protocol were loaded as a control ('UCP1 protocol 6h' lane). In each lane, 10 µg mitochondrial membranes were loaded onto the gels. B) Preparative solubilisation test fractions show that a large portion of the construct 5 variant can be solubilised in the presence of mild, non-ionic detergent, consistent with previous preparative solubilisation trials (see* ***Figure 3.10*** *and* ***Figure 4.1****). Samples are loaded onto the gel as a proportion of the total sample.*

Appendix 3.4. Results from WB12 expression trials

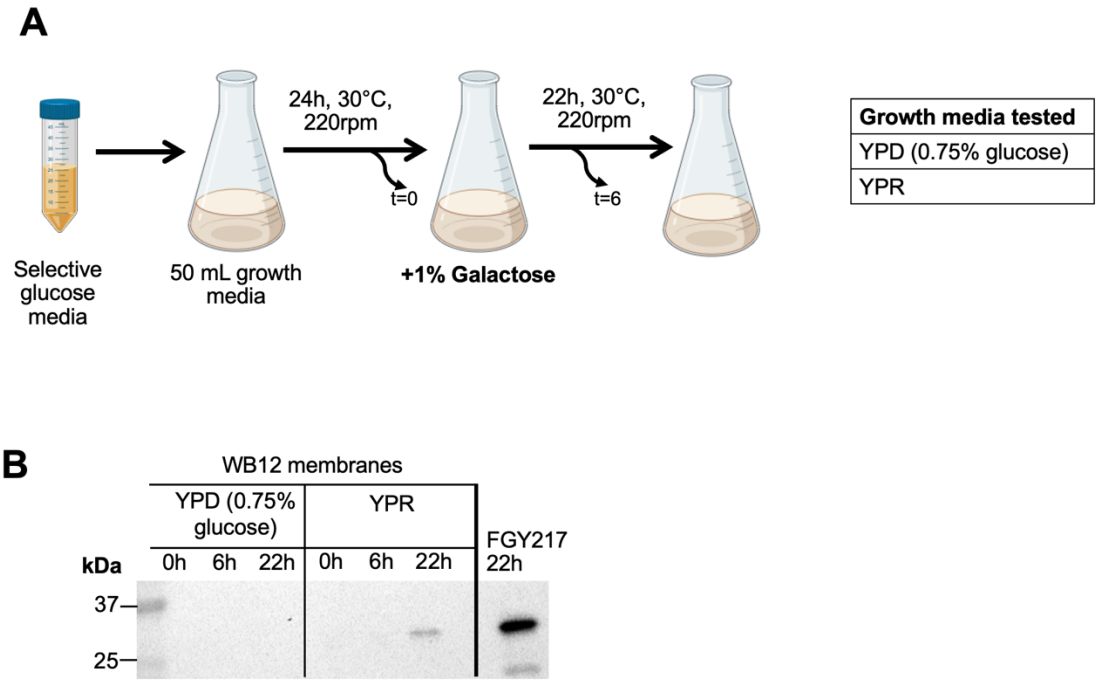

Appendix Figure 3.6: Small-scale WB12 expression screen of HsUCP2 protein following prolonged expression protocol 3 (as outlined in Chapter 3). *A) Schematic of small-scale (50 mL) WB12 expression screen following "Prolonged expression protocol 3" with some adaptations. Cells are initially propagated in selective glucose starter culture, before 24-hour growth in 50 mL growth media supplemented with either 0.75% glucose or 2% raffinose (YPR), followed by 22-hour induction with 1% galactose. B) Western blot of isolated mitochondria samples obtained from WB12 UCP2 expression trial, following induction with galactose (0h); times indicated above lanes represent time cells were harvested following galactose addition. FGY217-derived membranes were loaded to compare protein expression levels ('FGY217 22h' lane). 10 µg mitochondrial membranes loaded onto the gel.*

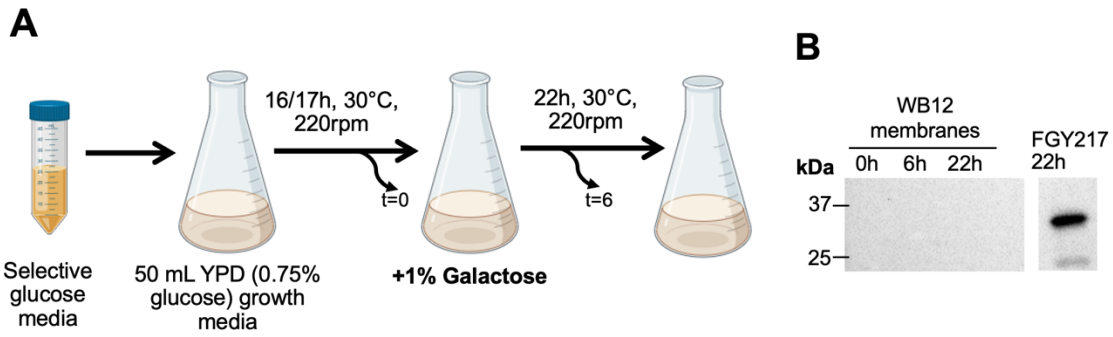

Appendix Figure 3.7: Small-scale WB12 expression screen of HsUCP2 protein following an adapted UCP1 expression protocol. *A) Schematic of small-scale WB12 expression screen following adapted UCP1 expression protocols (177, 178). Single colonies are propagated overnight in 10 mL selective glucose media before inoculation into 50 mL YPD media (0.75% glucose) media for 16/17 hours. Protein expression was induced with 1% galactose for 22 hours. B) Western blot of isolated mitochondria from WB12 expression trial as outlined above; times above lanes are representative of time after galactose addition (0h). FGY217-derived membranes were loaded for protein expression comparison. 10 µg mitochondrial membranes loaded onto the gel.*

Appendix Table 3.1: Table summarising purified protein yields from UCP2 S+Q TP purifications.

Purification Condition	**[Protein] (mg/mL)**	**Total protein yield (mg)**	**Amount of membranes used for purification (mg)**	**Protein purified per mg membrane (%)**
Standard UCP1 purification as described by (19)	0.38	0.190	320 mg alkali-washed membranes (760 mg total untreated membranes)	0.06 (0.03)
Buffer-exchange by ultracentrifugation (pH 9.6). Ion exchange conducted at pH 9.6	1.24	3.250	375 mg total untreated membranes	0.87
Buffer-exchange by ultracentrifugation (pH 8.0). Ion exchange conducted at pH 8.0	1.30	3.090	375 mg total untreated membranes	0.82
Pre-treatment with ADP* (pH 8.0) *during preceding membrane isolation step	0.68	1.700	250 mg total membranes (pre-treated with 1 mM ADP in preceding large-scale membrane isolation step)	0.68
WB12-derived membranes	0.61	1.525	193 mg total untreated (WB12) membranes	0.79

Appendix 4 (Chapter 5)

Appendix 4.1. Liposomal reconstitution of purified UCP2

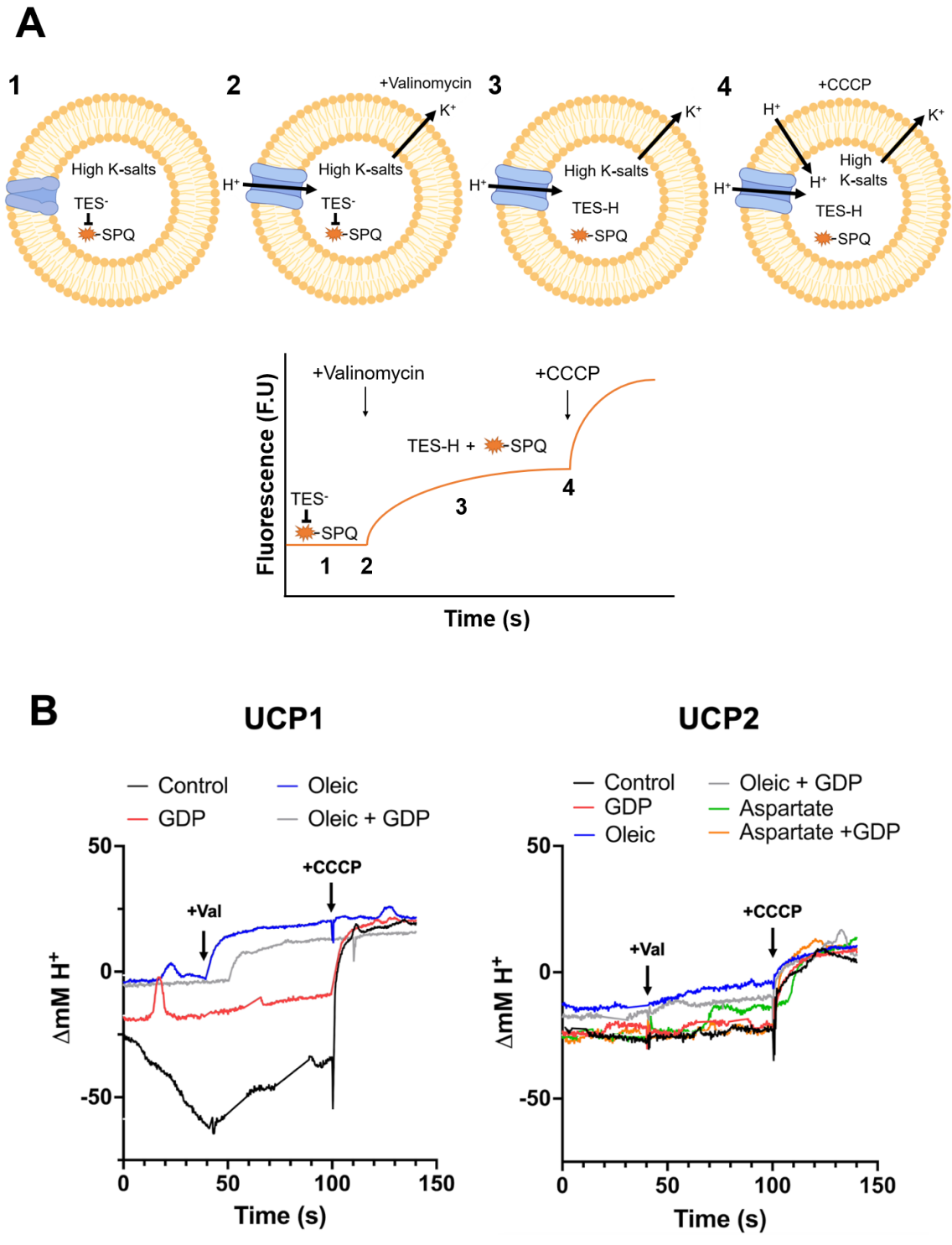

Appendix Figure 4.1: SPQ flux assays, principles and representative traces. *A) Schematic of SPQ flux assay as described by Orosz and Garlid (1992) (191). Formed liposomes reconstituted with either UCP1 or UCP2 purified samples are encapsulated with SPQ dye that is quenched in the presence of the TES⁻ anion (top panel), represented by low fluorescence*

in experimental traces (bottom panel) (step 1). Upon addition of the potassium ionophore, valinomycin, a membrane potential is generated due to differences in potassium concentration in and out of the liposomes. The membrane potential generated following valinomycin addition provides a route for UCP-meditated proton transport into the liposomes, which is shown by an increase in fluorescence in traces as protons interact with the TES^- anion, consequently removing the quenching effect exerted on SPQ (step 2). Charge transfer continues and reaches a steady state (step 3). Addition of the protonphore, CCCP, allows for continuous proton cycling across the liposomal membrane, revealing the total proton transport capacity of the system, which is illustrated by a steep increase in fluorescence (step 4). B) Normalised traces of HsUCP1 and HsUCP2 liposomes, in the absence or presence of various ligands as indicated.

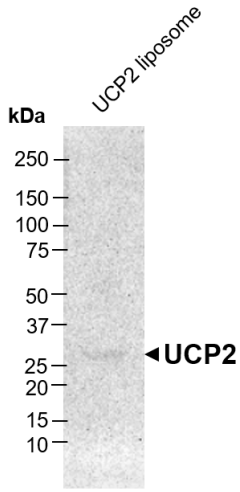

Appendix Figure 4.2: Western blot showing HsUCP2 liposome fraction without purified inclusion body standards.

Appendix 4.2. Oxygen consumption assays

Appendix Table 4.1: Summary table showing RCR values for HsUCP1 and HsUCP2 mitochondria.

Experiment	Replicate	UCP1		UCP2	
		Uninduced	Induced	Uninduced	Induced
1	1	1.1	1.5	2.1	1.4
	2	2.3	1.6	1.8	1.7
	3	1.4	1.4	1.9	1.7
2	1	1.3	2.0	2.1	1.9
	2		2.3	1.9	1.6
Average RCR:		1.5	1.8	2.0	1.7
S.E.M:		0.31	0.16	0.06	0.09
p-value:		0.46		0.02	
Significance?		ns		*	

*RCR values were calculated by dividing the oxygen consumption rate obtained in the uncoupled state (i.e. in the presence of NADH and FCCP), by the rate obtained in state 2 respiration (i.e. with NADH alone). Error is presented as S.E.M. Statistical analysis between uninduced and induced mitochondria was conducted using t-tests, *p<0.05.*

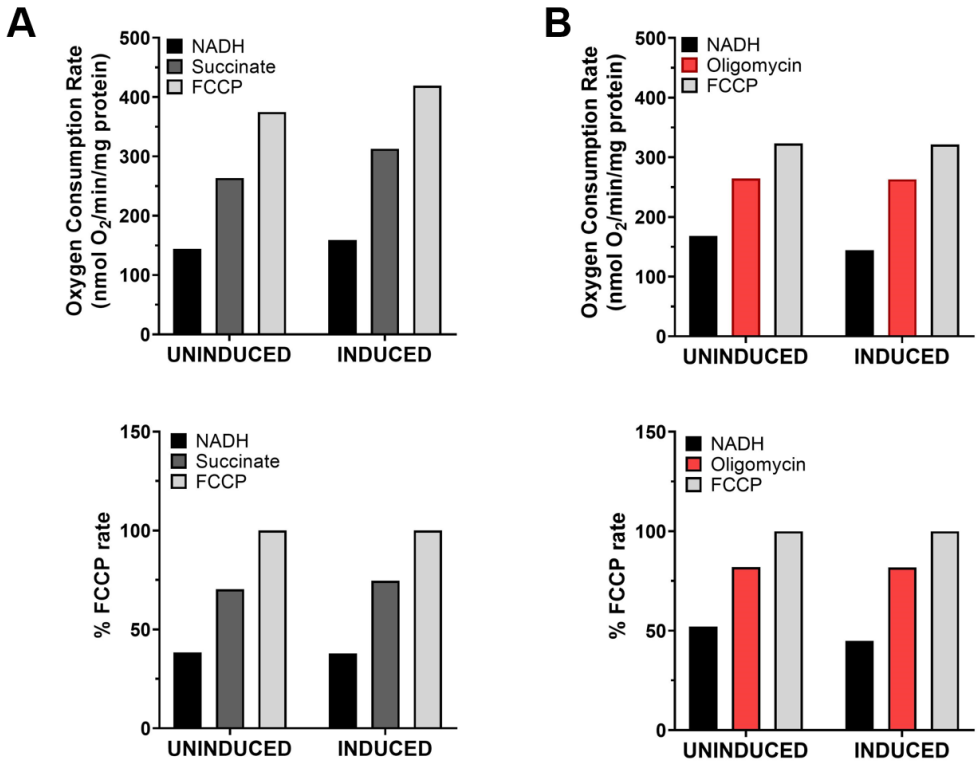

Appendix Figure 4.3: Differences in rates for induced and uninduced mitochondria. *Oxygen consumption rates of mitochondria either devoid (uninduced) or containing (induced) HsUCP1 protein. Rates are normalised to 0.5 mg/mL protein (top panel) and to the FCCP-uncoupled rate (bottom panel). A) Addition of two substrates (3 mM NADH, followed by 1 mM succinate) were tested to determine if there were limitations in proton transport in the respiratory chain. B) Addition of oligomycin (1 µg/mL) was tested to determine potential proton leak activity by ATP synthase. In all experiments, 1 mM FCCP was added to determine the maximal rate of proton leak of the mitochondria. Graphs are representative of one repeat.*

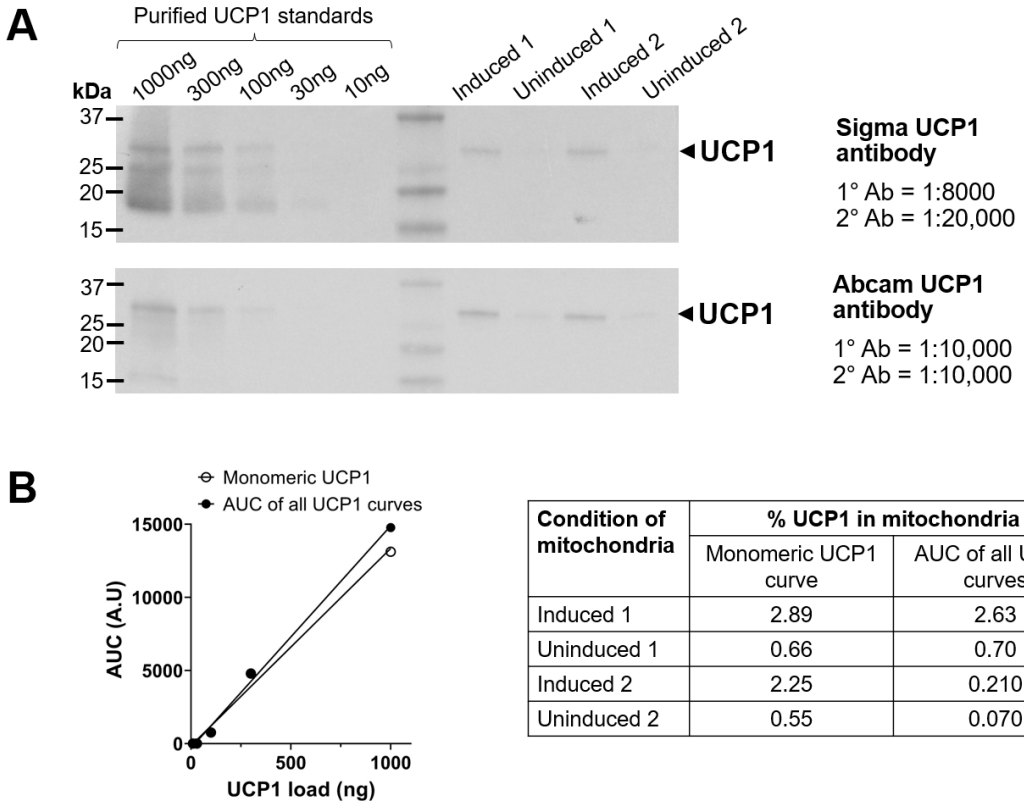

Condition of mitochondria	% UCP1 in mitochondria	
	Monomeric UCP1 curve	AUC of all UCP1 curves
Induced 1	2.89	2.63
Uninduced 1	0.66	0.70
Induced 2	2.25	0.210
Uninduced 2	0.55	0.070

Appendix Figure 4.4: Quantification of HsUCP1 in induced and uninduced mitochondria. *A) Western blots quantifying human UCP1 expression in yeast mitochondria using purified bacterial inclusion bodies as protein standards. UCP1 protein was probed using either the Sigma UCP1 (U6382) (top panel) or the Abcam (155117) antibody (bottom panel) at the antibody dilutions stated. B) The Western blot probed with the Abcam 155117 antibody was used for UCP1 quantification. The signal obtained was interpolated against a UCP1 standard curve. UCP1 content was calculated as a percentage of mitochondrial protein (see table for values).*

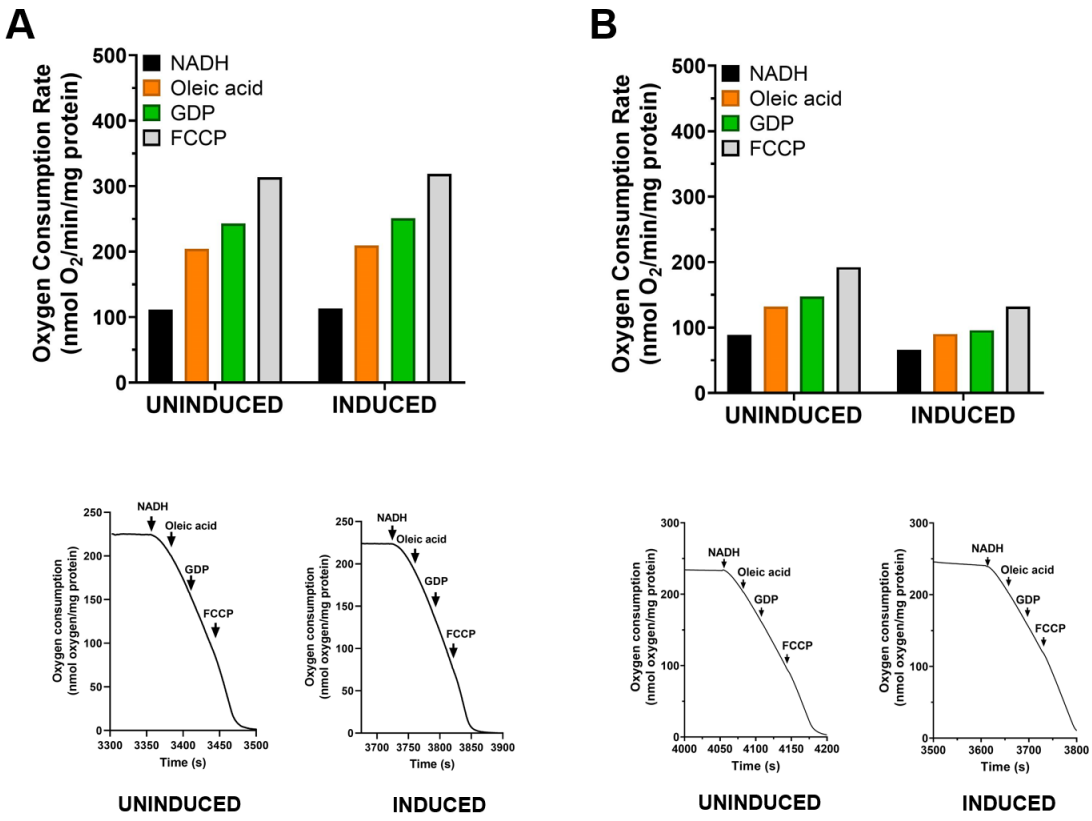

Appendix Figure 4.5: Oxygen consumption rates of UCP1- and UCP2-containing mitochondria (top panel), with corresponding traces (bottom panel). *Oxygen consumption rates of mitochondria, containing HsUCP1 (A) or HsUCP2 (B) protein. Rates are normalised to 0.5 mg/mL protein. For all experiments, mitochondria were energised with 3 mM NADH to induce state 2 respiration, prior to addition of 6 μM oleic acid to induce UCP1-mediated uncoupling activity. 100 μM GDP was added to inhibit UCP1-mediated proton leak and 1 mM FCCP was added to allow for maximal uncoupling activity. Graphs are representative of one experiment, with the corresponding traces shown below.*

Appendix 4.3. CPM assay results

Appendix Table 4.2: Triplicate values for apparent protein T_ms HsUCP1 CPM assay experiments in the presence of ADP

Condition	[ADP] (µM)	Apparent T_m (°C)				S.E.M	Adjusted p value	Signi-ficant?
		Repeat 1	Repeat 2	Repeat 3	Mean			
pH 6.0	0 (No ligand)	46.5	50.3	50.5	49.1	1.30		
	0.1	47.8	50.5	51.0	49.8	0.99	>0.9999	ns
	1	50.7	53.5	55.5	53.2	1.39	0.5718	ns
	10	60.5	61.3	63.5	61.8	0.90	<0.0001	***
	100	65.7	68.0	68.0	67.2	0.77	<0.0001	***
	1000	68.2	70.8	72.5	70.5	1.26	<0.0001	***
pH 7.5	0 (No ligand)	43.2	46.0	50	46.4	1.97		
	0.1	42.8	46.5	47.8	45.7	1.50	0.9978	ns
	1	43.7	47.3	49.8	46.9	1.77	0.9994	ns
	10	45.3	49.5	50.3	48.4	1.55	0.8244	ns
	100	49.0	52.0	52.2	51.1	1.03	0.0785	ns
	1000	63.0	47.3	63.0	63.0	0.00	<0.0001	***

Appendix Table 4.3: Triplicate values for apparent protein T_ms HsUCP1 CPM assay experiments in the presence of GDP

Condition	[GDP] (μM)	Apparent T_m (°C)				S.E.M	Adjusted p value	Signi-ficant?
		Repeat 1	Repeat 2	Repeat 3	Mean			
pH 6.0	0 (No ligand)	48.5	50.5	50.0	49.7	0.60		
	0.1	50.0	51.3	50.5	50.6	0.38	>0.9999	ns
	1	51.5	53.2	52.5	52.4	0.49	0.0794	ns
	10	57.7	61.0	60.5	59.7	1.03	<0.0001	***
	100	62.0	65.5	65.0	64.2	1.10	<0.0001	***
	1000	67.0	69.3	68.0	68.1	0.67	<0.0001	***
pH 7.5	45.3	49.5	47.7	47.5	45.3	1.22		
	47.0	48.8	47.7	47.8	47.0	0.52	>0.9999	ns
	48.0	49.5	48.5	48.7	48.0	0.44	0.9772	ns
	49.7	51.0	50.2	50.3	49.7	0.38	0.5259	ns
	51.2	52.5	52.3	52.0	51.2	0.40	0.0965	ns
	60.2	59.7	60.8	60.2	60.2	0.32	<0.0001	***

*Apparent protein T_ms obtained from CPM assay experiments conducted in 20 mM bis-Tris (pH 6.0) or 20 mM HEPES (pH 7.5) + 0.1% 12MNG in the absence and presence of ADP or GDP. Value in red is excluded from calculations to obtain the average apparent melting temperature. Error is calculated as S.E.M. Statistical analysis was conducted using one-way ANOVA, * p<0.05, **p<0.01, ***p<0.001. Refer to* ***Figure 5.2*** *for graph.*

Appendix 4.4. Gel blot protein thermostability assay development

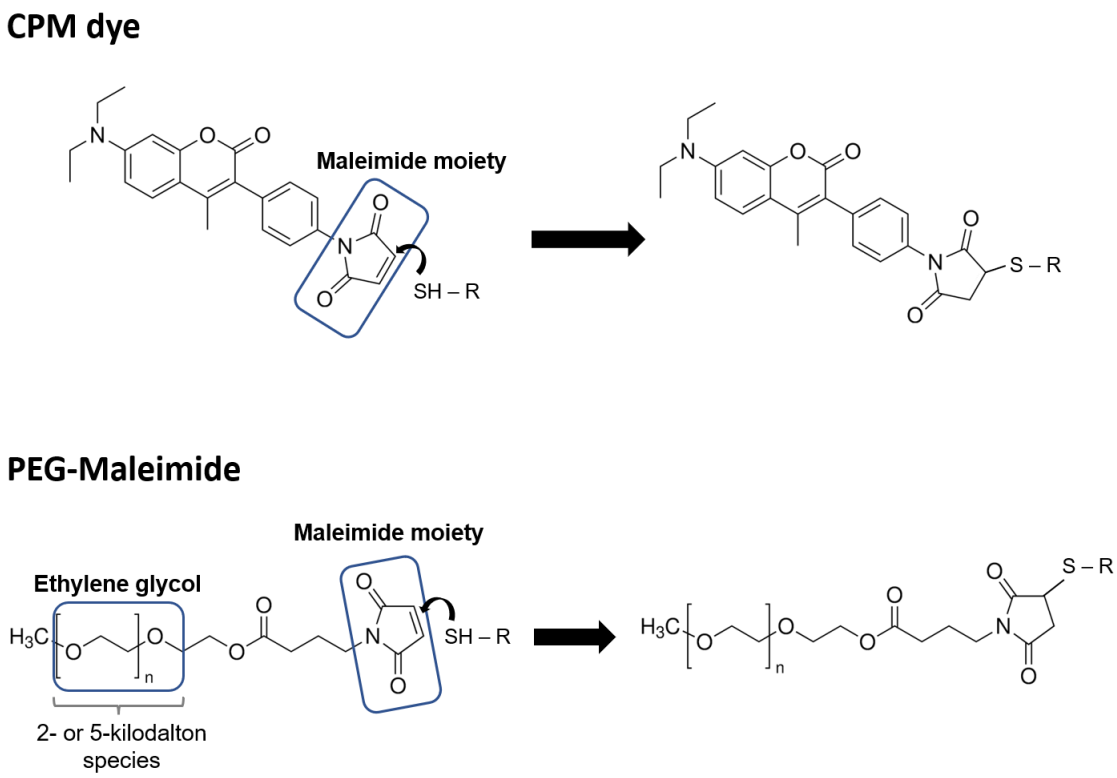

Appendix Figure 4.6: Structures of CPM and PEG-Mal-2K and reaction of maleimide moiety with the sulfhydryl moiety in the cysteine side chain.

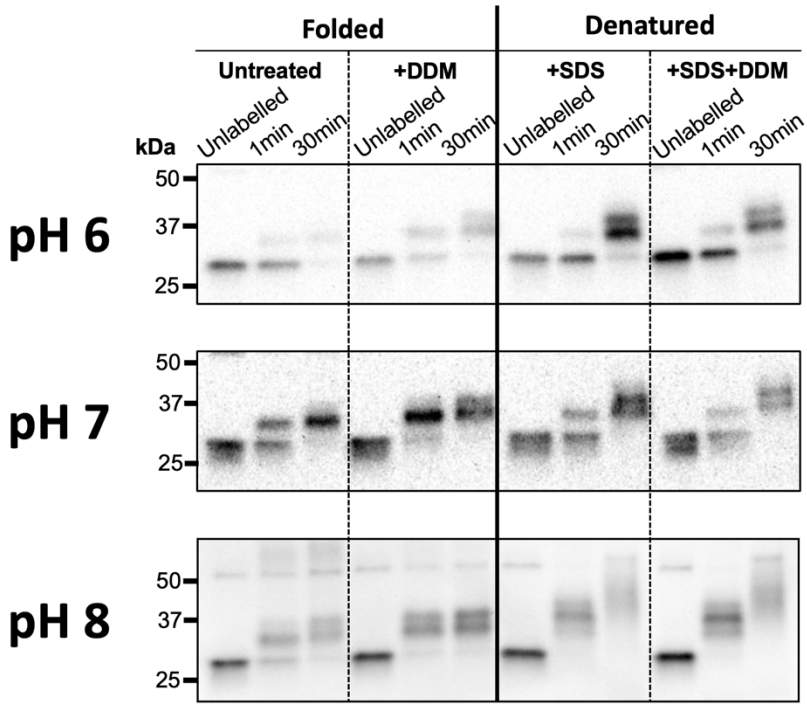

Appendix Figure 4.7: pH sensitivity of PEG-Mal-2K. *Western blots of UCP1-containing mitochondrial membranes reacted with PEG-Mal-2K under native (folded) and SDS-unfolded conditions. Under folded conditions, mitochondria were either "untreated" or solubilised with 0.1% DDM, whereas in denatured conditions, samples were treated with 1% SDS in the absence or presence of DDM. Experiments were conducted on ice at pH 6.0, pH 7.0, and pH 8.0 as indicated; times above the lanes represent the incubation time with PEG-Mal-2K, with the "Unlabelled" lane representative of samples devoid of PEG-Mal-2K. ~3.3 µg of isolated mitochondria was loaded into each lane. Images displayed are unprocessed chemiluminescent images.*

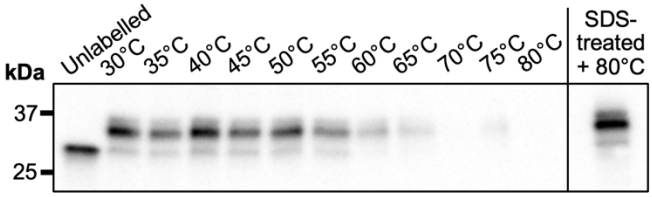

Appendix Figure 4.8: Differences in PEG-Mal-2K labelled signals between thermally and chemically denatured proteins. *Western blot of preliminary UCP1 gel blot protein thermostability assay conducted at 30°C to 80°C in the presence of PEG-Mal-2K, with mitochondria solubilised in the presence of 0.1% DDM. The final lane, "SDS-treated + 80°C" are representative of samples pre-treated with 1% SDS prior to incubation with PEG-Mal-2K and then heat treated at 80°C. Temperatures tested are indicated above lanes; the "Unlabelled" lane does not contain PEG-Mal-2K and was kept at 4°C. Each lane is loaded ~3.3 µg of isolated mitochondria.*

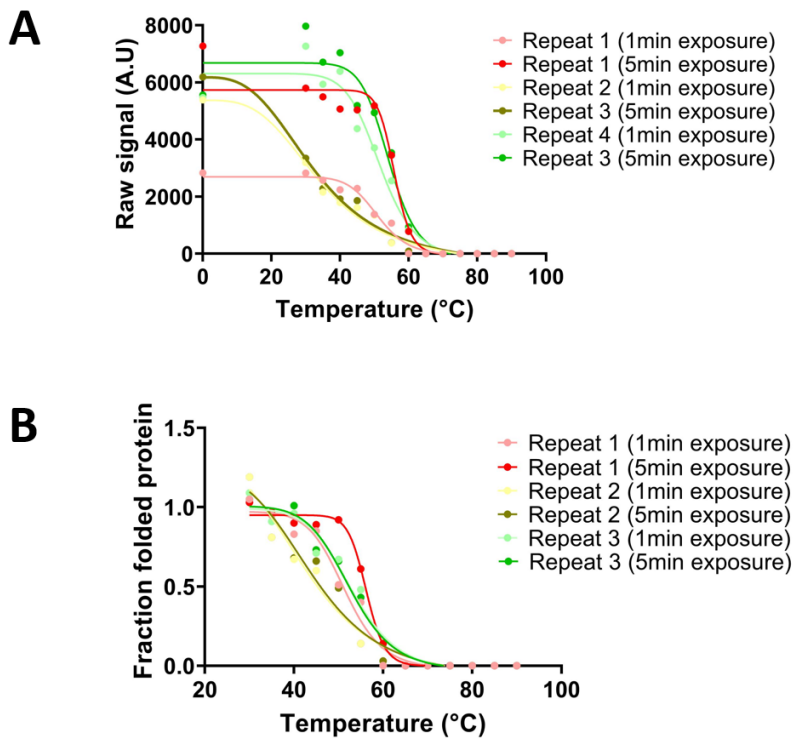

Appendix Figure 4.9: Modelling densitometric signals from UCP1 gel blot protein thermostability profiles with inverted Boltzmann sigmoidal curves (A) and following normalisation to track relative change (B). *Data points are obtained following densitometry analysis of UCP1 gel blot protein thermostability assay experiments conducted at pH 6.0 in the absence of ligand, with inverted Boltzmann sigmoidal curves fitted to generate an apparent protein T_m. A) Graphs showing raw arbitrary units obtained from densitometry analyses, plotted as a function of temperature. Variation in raw chemiluminescent signals between blots resulted in differences in calculated protein T_ms (see* ***Appendix Table 4.4****), hence a form of normalisation between blots was required. Densitometric data was normalised to the average signal obtained from the first two lanes containing PEG-Mal-2K, as these fractions represents folded protein as samples are incubated at temperatures that would be considered thermostable. B) Graphs plotted using normalised data as described. For both plots, 3 repeats are shown with densitometry values from different 1-minute and 5-minute exposure times plotted.*

Appendix Table 4.4: Apparent protein T_ms obtained from inverted Boltzmann sigmoidal curves.

Repeat	Blot exposure time (min)	Apparent melting temperature (°C)	
		Densitometry data	Normalised data
1	1	51.04	51.44
	5	55.81	56.22
2	1	34.49	42.23
	5	33.08	43.78
3	1	51.68	52.97
	5	54.22	52.54

Melting temperatures are estimated from densitometry data before and after normalisation to give the fractional change in signal associated with the temperature change. Tests both include 1- and 5-minute blot exposure times. Thermostability experiments were conducted with HsUCP1-containing DDM-solubilised mitochondria in the absence of ligand at pH 6.0.

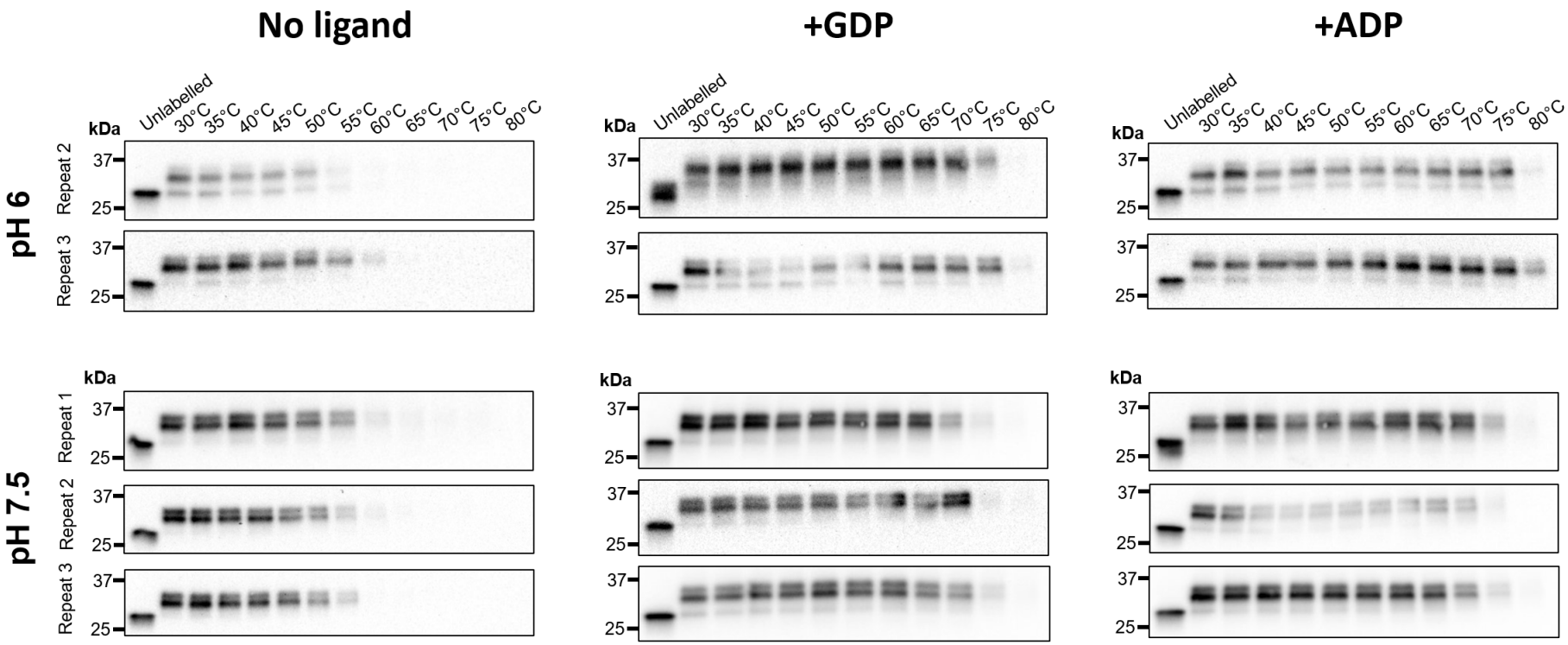

Appendix Figure 4.10: Western blot replicates of gel blot protein thermostability assay for HsUCP1 samples. *Chemiluminescent images of replicate blots obtained from the gel blot protein thermostability shift assay obtained using 0.1% DDM-solubilised HsUCP1-containing mitochondrial membrane samples, in the absence or presence of 1 mM GDP or 1 mM ADP, as indicated. Experiments were conducted at pH 6.0 or pH 7.5. Lanes represent the incubation temperature of the samples, with the "Unlabelled" lane representative of samples incubated at 4°C in the absence of PEG-Mal-2K; ~3.3 µg of isolated mitochondria was loaded into each lane. Images displayed are unprocessed chemiluminescent images. Densitometric analysis was conducted on all blots to produce thermal denaturation curves, from which an apparent T_m could be obtained (refer to* ***Figure 5.8****).*

Appendix Table 4.5: Apparent T_ms obtained from gel blot protein thermostability assay from HsUCP1 samples.

pH	Condition	Apparent T_ms (°C)				S.E.M	p value	Signifi-cant?
		Repeat 1	Repeat 2	Repeat 3	Mean			
pH 6.0	No ligand	56.22	43.78	52.54	51.0	3.80		
	+GDP	73.26	73.27	73.97	73.5	0.23	0.0036	**
	+ADP	79.41	79.84	75.97	78.4	1.21	0.0021	**
pH 7.5	No ligand	53.01	52.46	52.98	52.8	0.17		
	+GDP	69.00	69.11	71.06	69.7	0.68	<0.0001	***
	+ADP	74.20	79.29	69.89	74.5	2.72	0.0014	**

*Apparent protein T_ms of 0.1% DDM detergent-solubilised HsUCP1 mitochondrial membrane samples, obtained from three independent gel blot protein thermostability assay experiments in the absence or presence of 1 mM ADP or 1 mM GDP. Error shown as the S.E.M shown, statistical analysis performed using a Student's t-test (*p<0.05, **p<0.005, ***p<0.001). Refer to* ***Figure 5.8B*** *for graph.*

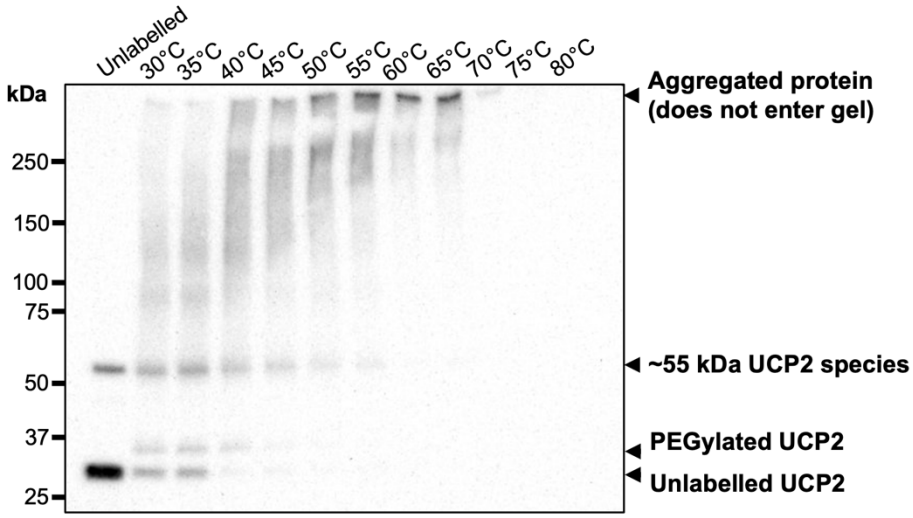

Appendix Figure 4.11: Initial results obtained for HsUCP2 gel blot protein thermostability assay. *Chemiluminescent image of an initial attempt applying UCP2 samples with the gel blot protein thermostability assay using conditions tested for UCP1. Experiments were conducted at pH 6.0 with DDM-solubilised samples incubated between 30°C to 80°C; with temperatures tested indicated above lanes. The "Unlabelled" lane, which*

is devoid of PEG-Mal-2K, represents the total protein fraction and was kept at 4°C. Each lane is loaded ~3.3 µg of isolated mitochondria.

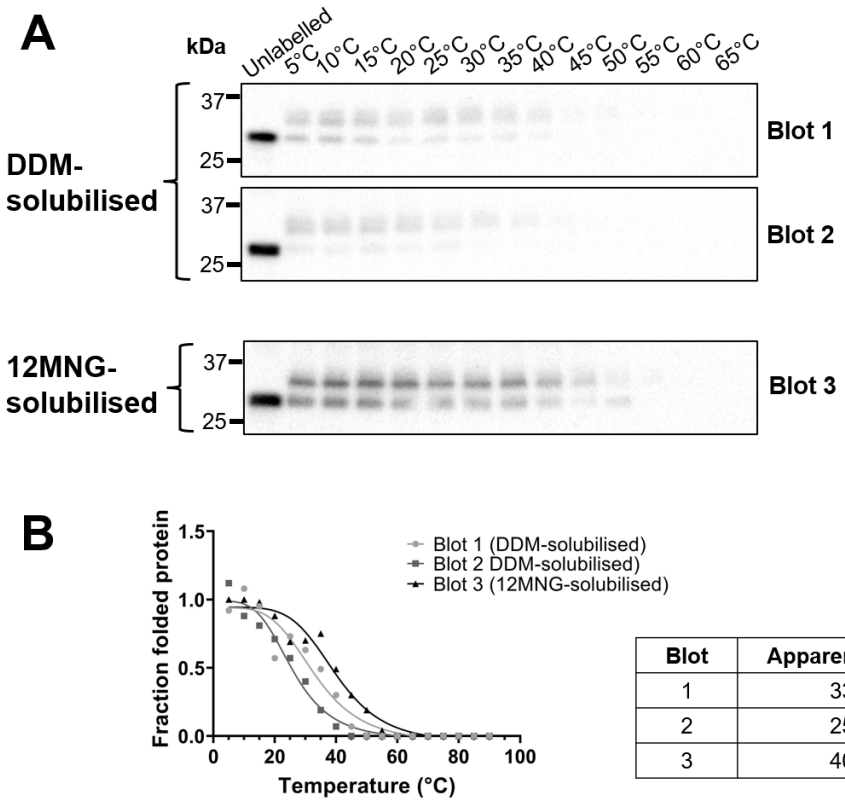

Blot	Apparent Tm (°C)
1	33.29
2	25.99
3	40.17

Appendix Figure 4.12: Differences in UCP2 signal obtained in the presence of DDM and 12MNG. *A) Western blots of UCP2 gel blot protein thermostability assay experiments conducted at 5°C to 65°C, with mitochondria solubilised in the presence of 0.1% DDM or 0.1% 12MNG as indicated. Temperatures tested are indicated above lanes; the "Unlabelled" lane does not contain PEG-Mal-2K and was kept at 4°C. Each lane is loaded with ~3.3 µg of isolated mitochondria. B) Inverted Boltzmann sigmoidal curves of normalised densitometry data (left panel), from DDM- and 12MNG-solubilised blots; apparent protein T_ms are summarised in the table.*

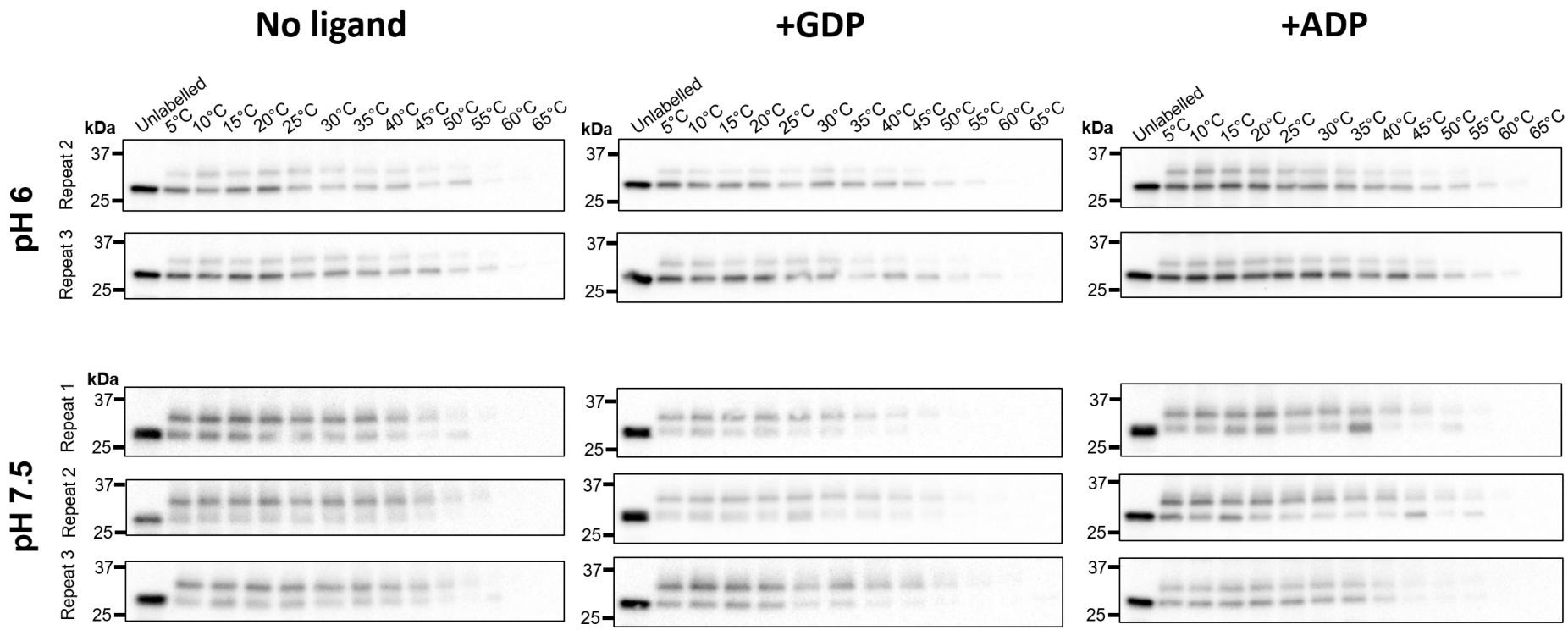

Appendix Figure 4.13: Western blots of gel blot protein thermostability assay for HsUCP2 samples. *Chemiluminescent images of replicate blots obtained from the gel blot protein thermostability assay obtained using 0.1% 12MNG-solubilised HsUCP2-containing mitochondrial membrane samples, in the absence or presence of 1 mM GDP or 1 mM ADP, as indicated. Experiments were conducted at pH 6.0 or pH 7.5. Lanes represent the incubation temperature of the samples, with the "Unlabelled" lane representative of samples incubated at 4°C in the absence of PEG-Mal-2K; ~3.3 µg of isolated mitochondria was loaded into each lane. Images displayed are unprocessed chemiluminescent images. Densitometric analysis was conducted on all blots to produce thermal denaturation curves, from which an apparent T_m could be obtained (refer to* ***Figure 5.8****).*

Appendix Table 4.6: Apparent T_ms obtained from gel blot protein thermostability assay from HsUCP2 samples.

pH	Condition	Apparent T_ms (°C)				S.E.M	p value	Signifi-cant?
		Repeat 1	Repeat 2	Repeat 3	Mean			
pH 6.0	No ligand	36.38	35.58	39.97	37.3	1.35		
	+GDP	36.26	40.47	29.88	35.6	3.08	0.626	ns
	+ADP	35.39	35.88	46.75	39.3	3.72	0.162	ns
pH 7.5	No ligand	40.17	46.17	35.02	40.5	3.24		
	+GDP	32.99	37.80	31.09	34.0	1.99	0.634	ns
	+ADP	41.44	37.01	37.64	38.7	1.38	0.643	ns

Apparent protein T_ms of 0.1% 12MNG detergent-solubilised HsUCP2 mitochondrial membrane samples, obtained from three independent gel blot protein thermostability assay experiments in the absence or presence of 1 mM ADP or 1 mM GDP. Error shown as the S.E.M shown, statistical analysis performed using a Student's t-test. Refer to ***Figure 5.8B*** *for graph.*

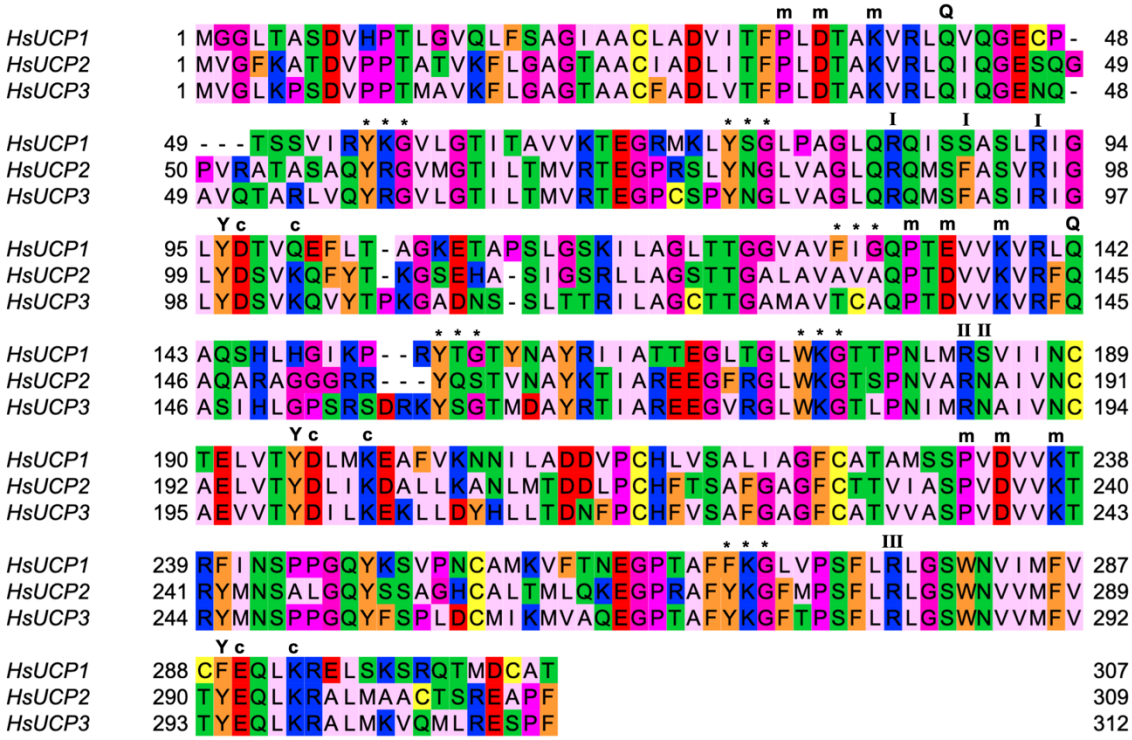

Appendix Figure 4.14: Sequence alignment of human UCP1, UCP2 and UCP3. *Multiple sequence alignment of human UCP1, UCP2 and UCP3, aligned using MUSCLE sequence alignment in Jalview. Residues are coloured based on their physiochemical properties: positively charged residues are in blue; negatively charged residues in red; polar amino acids are shown in green; hydrophobic amino acids in pink; aromatic residues are in orange; helix-breakers (glycine and proline) are depicted in magenta and cysteine is shown in yellow. Mitochondrial carrier structural features are annotated above the sequences: 'm' denotes key residues of the matrix salt-bridge network, with the Q brace depicted as 'Q'; 'c' represents charged residues of the cytoplasmic salt-bridge network, with the Y brace shown as 'Y'. Residues that interact with cardiolipin headgroups are shown as an asterisk (*). Residues of the substrate binding site are illustrated as 'I', 'II' and 'III', representing contact points on helix 2, 4 and 6, respectively, as outlined by Robinson and Kunji (2006) (136).*

References

1. Kunji ERS. The role and structure of mitochondrial carriers. Febs Lett. 2004;564(3):239-44.
2. Nedergaard J, Golozoubova V, Matthias A, Asadi A, Jacobsson A, Cannon B. UCP1: the only protein able to mediate adaptive non-shivering thermogenesis and metabolic inefficiency. Bba-Bioenergetics. 2001;1504(1):82-106.
3. Cannon B, Hedin A, Nedergaard J. Exclusive occurrence of thermogenin antigen in brown adipose tissue. Febs Lett. 1982;150(1):129-32.
4. Fleury C, Neverova M, Collins S, Raimbault S, Champigny O, LeviMeyrueis C, et al. Uncoupling protein-2: A novel gene linked to obesity and hyperinsulinemia. Nat Genet. 1997;15(3):269-72.
5. Boss O, Samec S, Paoloni-Giacobino A, Rossier C, Dulloo A, Seydoux J, et al. Uncoupling protein-3: a new member of the mitochondrial carrier family with tissue-specific expression. Febs Lett. 1997;408(1):39-42.
6. Vidal-Puig A, Solanes G, Grujic D, Flier JS, Lowell BB. UCP3: an uncoupling protein homologue expressed preferentially and abundantly in skeletal muscle and brown adipose tissue. Biochem Bioph Res Co. 1997;235(1):79-82.
7. Mao W, Yu XX, Zhong A, Li W, Brush J, Sherwood SW, et al. UCP4, a novel brain-specific mitochondrial protein that reduces membrane potential in mammalian cells. Febs Lett. 1999;443(3):326-30.
8. Sanchis D, Fleury C, Chomiki N, Goubern M, Huang Q, Neverova M, et al. BMCP1, a novel mitochondrial carrier with high expression in the central nervous system of humans and rodents, and respiration uncoupling activity in recombinant yeast. J Biol Chem. 1998;273(51):34611-5.
9. Golozoubova V, Hohtola E, Matthias A, Jacobsson A, Cannon B, Nedergaard J. Only UCP1 can mediate adaptive nonshivering thermogenesis in the cold. FASEB J. 2001;15(9):2048-+.
10. Matthias A, Ohlson KBE, Fredriksson JM, Jacobsson A, Nedergaard J, Cannon B. Thermogenic responses in brown fat cells are fully UCP1-dependent - UCP2 or UCP3 do not substitute for UCP1 in adrenergically or fatty acid-induced thermogenesis. J Biol Chem. 2000;275(33):25073-81.
11. Mailloux RJ, Harper ME. Uncoupling proteins and the control of mitochondrial reactive oxygen species production. Free Radic Bio Med. 2011;51(6):1106-15.
12. Boss O, Hagen T, Lowell BB. Uncoupling proteins 2 and 3: Potential regulators of mitochondrial energy metabolism. Diabetes. 2000;49(2):143-56.
13. Dulloo AG, Samec S. Uncoupling proteins: their roles in adaptive thermogenesis and substrate metabolism reconsidered. B J Nutr. 2001;86(2):123-39.
14. Bell CG, Walley AJ, Froguel P. The genetics of human obesity. Nat Rev Genet. 2005;6(3):221-34.
15. Andrews ZB, Diano S, Horvath TL. Mitochondrial uncoupling proteins in the CNS: in support of function and survival. Nat Rev Neurosci. 2005;6(11):829-40.
16. Robbins D, Zhao YF. New aspects of mitochondrial Uncoupling Proteins (UCPs) and their roles in tumorigenesis. Int J Mol Sci. 2011;12(8):5285-93.
17. Ricquier D, Gervais C, Kader JC, Hemon P. Partial purification by guanosine-5'-diphosphate--agarose affinity chromatography of the 32,000 molecular weight polypeptide from mitochondria of brown adipose tissue. Febs Lett. 1979;101(1):35-8.
18. Ricquier D, Kader J-C. Mitochondrial protein alteration in active brown fat: A sodium dodecyl sulfate-polyacrylamide gel electrophoretic study. Biochem Biophys Res Commun. 1976;73(3):577-83.

19. Lee Y, Willers C, Kunji ERS, Crichton PG. Uncoupling protein 1 binds one nucleotide per monomer and is stabilized by tightly bound cardiolipin. Proc Natl Acad Sci U S A. 2015;112(22):6973-8.
20. Frontini A, Rousset S, Cassard-Doulcier AM, Zingaretti C, Ricquier D, Cinti S. Thymus uncoupling protein 1 is exclusive to typical brown adipocytes and is not found in thymocytes. J Histochem Cytochem. 2007;55(2):183-9.
21. Klingenberg M, Winkler E. The reconstituted isolated uncoupling protein is a membrane potential driven H+ translocator. EMBO J. 1985;4(12):3087-92.
22. Klingenspor M. Cold-induced recruitment of brown adipose tissue thermogenesis. Exp Physiol. 2003;88(1):141-8.
23. Oelkrug R, Polymeropoulos ET, Jastroch M. Brown adipose tissue: physiological function and evolutionary significance. J Comp Physiol B. 2015;185(6):587-606.
24. van der Lans AA, Hoeks J, Brans B, Vijgen GH, Visser MG, Vosselman MJ, et al. Cold acclimation recruits human brown fat and increases nonshivering thermogenesis. Journal of Clinical Investigation. 2013;123(8):3395-403.
25. Heaton JM. The distribution of brown adipose tissue in the human. J Anat. 1972;112(Pt 1):35-9.
26. Cypess AM, Lehman S, Williams G, Tal I, Rodman D, Goldfine AB, et al. Identification and importance of brown adipose tissue in adult humans. N Engl J Med. 2009;360(15):1509-17.
27. Locke RM, Rial E, Scott ID, Nicholls DG. Fatty acids as acute regulators of the proton conductance of hamster brown-fat mitochondria. Eur J Biochem. 1982;129(2):373-80.
28. Winkler E, Klingenberg M. Effect of fatty acids on H+ transport activity of the reconstituted uncoupling protein. J Biol Chem. 1994;269(4):2508-15.
29. Nicholls DG. Hamster brown-adipose-tissue mitochondria. The control of respiration and the proton electrochemical potential gradient by possible physiological effectors of the proton conductance of the inner membrane. Eur J Biochem. 1974;49(3):573-83.
30. Rial E, Poustie A, Nicholls DG. Brown-adipose-tissue mitochondria: the regulation of the 32000-Mr uncoupling protein by fatty acids and purine nucleotides. Eur J Biochem. 1983;137(1-2):197-203.
31. Locke RM, Rial E, Nicholls DG. The acute regulation of mitochondrial proton conductance in cells and mitochondria from the brown fat of cold-adapted and warm-adapted guinea pigs. Eur J Biochem. 1982;129(2):381-7.
32. Nedergaard J, Cannon B. [3H]GDP binding and thermogenin amount in brown adipose tissue mitochondria from cold-exposed rats. Am J Physiol. 1985;248(3):C365-C71.
33. Klingenberg M. Nucleotide binding to uncoupling protein - Mechanism of control by protonation. Biochemistry-Us. 1988;27(2):781-91.
34. Garlid KD, Orosz DE, Modriansky M, Vassanelli S, Jezek P. On the mechanism of fatty acid-induced proton transport by mitochondrial uncoupling protein. J Biol Chem. 1996;271(5):2615-20.
35. Shabalina IG, Jacobsson A, Cannon B, Nedergaard J. Native UCP1 displays simple competitive kinetics between the regulators purine nucleotides and fatty acids. J Biol Chem. 2004;279(37):38236-48.
36. Cannon B, Nedergaard J. Brown adipose tissue: function and physiological significance. Physiol Rev. 2004;84(1):277-359.
37. Crichton PG, Lee Y, Kunji ERS. The molecular features of uncoupling protein 1 support a conventional mitochondrial carrier-like mechanism. Biochimie. 2017;134:35-50.
38. Pecqueur C, Alves-Guerra MC, Gelly C, Levi-Meyrueis C, Couplan E, Collins S, et al. Uncoupling protein 2, in vivo distribution, induction upon oxidative stress, and evidence for translational regulation. J Biol Chem. 2001;276(12):8705-12.
39. Zhang CY, Baffy G, Perret P, Krauss S, Peroni O, Grujic D, et al. Uncoupling protein-2 negatively regulates insulin secretion and is a major link between obesity, β cell dysfunction, and type 2 diabetes. Cell. 2001;105(6):745-55.

40. Azzu V, Affourtit C, Breen EP, Parker N, Brand MD. Dynamic regulation of uncoupling protein 2 content in INS-1E insulinoma cells. Bba-Bioenergetics. 2008;1777(10):1378-83.
41. Rousset S, Emre Y, Join-Lambert O, Hurtaud C, Ricquier D, Cassard-Doulcier AM. The uncoupling protein 2 modulates the cytokine balance in innate immunity. Cytokine. 2006;35(3-4):135-42.
42. Rupprecht A, Brauer AU, Smorodchenko A, Goyn J, Hilse KE, Shabalina IG, et al. Quantification of Uncoupling Protein 2 Reveals Its Main Expression in Immune Cells and Selective Up-Regulation during T-Cell Proliferation. Plos One. 2012;7(8).
43. Puigserver P, Herron D, Gianotti M, Palou A, Cannon B, Nedergaard J. Induction and degradation of the uncoupling protein thermogenin in brown adipocytes in vitro and in vivo. Evidence for a rapidly degradable pool. Biochem J. 1992;284 (Pt 2)(Pt 2):393-8.
44. Rousset S, Mozo J, Dujardin G, Emre Y, Masscheleyn S, Ricquier D, et al. UCP2 is a mitochondrial transporter with an unusual very short half-life. Febs Lett. 2007;581(3):479-82.
45. Azzu V, Brand MD. Degradation of an intramitochondrial protein by the cytosolic proteasome. J Cell Sci. 2010;123(Pt 4):578-85.
46. Azzu V, Jastroch M, Divakaruni AS, Brand MD. The regulation and turnover of mitochondrial uncoupling proteins. Biochim Biophys Acta. 2010;1797(6-7):785-91.
47. Pecqueur C, Vacher D, Miroux B. Expression and purification of the mitochondrial uncoupling proteins: a comparative study between Escherichia coli and Saccharomyces cerevisiae. Biochem Soc Trans. 1999;27(6):888-93.
48. Rial E, Gonzalez-Barroso M, Fleury C, Iturrizaga S, Sanchis D, Jimenez-Jimenez J, et al. Retinoids activate proton transport by the uncoupling proteins UCP1 and UCP2. EMBO J. 1999;18(21):5827-33.
49. Echtay KS, Brand MD. Coenzyme Q induces GDP-sensitive proton conductance in kidney mitochondria. Biochem Soc Trans. 2001;29(Pt 6):763-8.
50. Echtay KS, Esteves TC, Pakay JL, Jekabsons MB, Lambert AJ, Portero-Otin M, et al. A signalling role for 4-hydroxy-2-nonenal in regulation of mitochondrial uncoupling. EMBO J. 2003;22(16):4103-10.
51. Fink BD, Hong YS, Mathahs MM, Scholz TD, Dillon JS, Sivitz WI. UCP2-dependent proton leak in isolated mammalian mitochondria. J Biol Chem. 2002;277(6):3918-25.
52. Echtay KS, Murphy MP, Smith RAJ, Talbot DA, Brand MD. Superoxide activates mitochondrial uncoupling protein 2 from the matrix side - Studies using targeted antioxidants. J Biol Chem. 2002;277(49):47129-35.
53. Echtay KS, Roussel D, St-Pierre J, Jekabsons MB, Cadenas S, Stuart JA, et al. Superoxide activates mitochondrial uncoupling proteins. Nature. 2002;415(6867):96-9.
54. Harper JA, Stuart JA, Jekabsons MB, Roussel D, Brindle KM, Dickinson K, et al. Artifactual uncoupling by uncoupling protein 3 in yeast mitochondria at the concentrations found in mouse and rat skeletal-muscle mitochondria. Biochem J. 2002;361(Pt 1):49-56.
55. Stuart JA, Harper JA, Brindle KM, Jekabsons MB, Brand MD. A mitochondrial uncoupling artifact can be caused by expression of uncoupling protein 1 in yeast. Biochem J. 2001;356:779-89.
56. Stuart JA, Harper JA, Brindle KM, Jekabsons MB, Brand MD. Physiological levels of mammalian uncoupling protein 2 do not uncouple yeast mitochondria. J Biol Chem. 2001;276(21):18633-9.
57. Jaburek M, Varecha M, Gimeno RE, Dembski M, Jezek P, Zhang M, et al. Transport function and regulation of mitochondrial uncoupling proteins 2 and 3. J Biol Chem. 1999;274(37):26003-7.
58. Zackova M, Jezek P. Reconstitution of novel mitochondrial uncoupling proteins UCP2 and UCP3. Bioscience Reports. 2002;22(1):33-46.

59. Jaburek M, Jezek P, Garlid KD. Coenzyme Q is not an obligatory cofactor of UCP2- and UCP3-catalyzed proton transport. Biophys J. 2002;82(1):109A-10A.
60. Zácková M, Skobisová E, Urbánková E, Jezek P. Activating ω-6 polyunsaturated fatty acids and inhibitory purine nucleotides are high affinity Ligands for novel mitochondrial uncoupling proteins UCP2 and UCP3. J Biol Chem. 2003;278(23):20761-9.
61. Jaburek M, Miyamoto S, Di Mascio P, Garlid KD, Jezek P. Hydroperoxy fatty acid cycling mediated by mitochondrial uncoupling protein UCP2. J Biol Chem. 2004;279(51):53097-102.
62. Bienengraeber M, Echtay KS, Klingenberg M. H+ transport by uncoupling protein (UCP-1) Is dependent on a histidine pair, absent in UCP-2 and UCP-3. Biochemistry-Us. 1998;37(1):3-8.
63. Jimenez-Jimenez J, Zardoya R, Ledesma A, Garcia de Lacoba M, Zaragoza P, Mar Gonzalez-Barroso M, et al. Evolutionarily distinct residues in the uncoupling protein UCP1 are essential for its characteristic basal proton conductance. J Mol Biol. 2006;359(4):1010-22.
64. Gaudry MJ. Comparative analysis of the thermogenic protein UCP1 across the mammalian phylogeny. The Wenner-Gren Institute Stockholm University; 2023.
65. Echtay KS, Winkler E, Frischmuth K, Klingenberg M. Uncoupling proteins 2 and 3 are highly active H(+) transporters and highly nucleotide sensitive when activated by coenzyme Q (ubiquinone). Proc Natl Acad Sci U S A. 2001;98(4):1416-21.
66. Echtay KS, Winkler E, Klingenberg M. Coenzyme Q is an obligatory cofactor for uncoupling protein function. Nature. 2000;408(6812):609-13.
67. Echtay KS, Brand MD. Coenzyme Q induces GDP-sensitive proton conductance in kidney mitochondria. Biochem Soc T. 2001;29:763-8.
68. Echtay KS, Roussel D, St-Pierre J, Jekabsons MB, Cadenas S, Stuart JA, et al. Superoxide activates mitochondrial uncoupling proteins. Nature. 2002;415(6867):96-9.
69. Murphy MP, Echtay KS, Blaikie FH, Asin-Cayuela J, Cocheme HM, Green K, et al. Superoxide activates uncoupling proteins by generating carbon-centered radicals and initiating lipid peroxidation: studies using a mitochondria-targeted spin trap derived from alpha-phenyl-N-tert-butylnitrone. J Biol Chem. 2003;278(49):48534-45.
70. Jabůrek M, Garlid KD. Reconstitution of Recombinant Uncoupling Proteins: UCP1, -2, AND -3 HAVE SIMILAR AFFINITIES FOR ATP AND ARE UNAFFECTED BY COENZYME Q 10*. J Biol Chem. 2003;278(28):25825-31.
71. Esteves TC, Echtay KS, Jonassen T, Clarke CF, Brand MD. Ubiquinone is not required for proton conductance by uncoupling protein 1 in yeast mitochondria. Biochem J. 2004;379:309-15.
72. Skulachev VP. Role of uncoupled and non-coupled oxidations in maintenance of safely low levels of oxygen and its one-electron reductants. Q Rev Biophys. 1996;29(2):169-202.
73. Brand MD, Affourtit C, Esteves TC, Green K, Lambert AJ, Miwa S, et al. Mitochondrial superoxide: Production, biological effects, and activation of uncoupling proteins. Free Radic Bio Med. 2004;37(6):755-67.
74. Murphy MP, Echtay KS, Blaikie FH, Asin-Cayuela J, Cochemé HM, Green K, et al. Superoxide activates uncoupling proteins by generating carbon-centered radicals and initiating lipid peroxidation -: Studies using a mitochondria-targeted spin trap derived from α-phenyl-N-tert-butylnitrone. J Biol Chem. 2003;278(49):48534-45.
75. Tomas P, Jimenez-Jimenez J, Zaragoza P, Vuligonda V, Chandraratna RAS, Rial E. Activation by retinoids of the uncoupling protein UCP1. Bba-Bioenergetics. 2004;1658(1-2):157-64.
76. Benedetti A, Comporti M, Esterbauer H. Identification of 4-hydroxynonenal as a cytotoxic product originating from the peroxidation of liver microsomal lipids. Biochim Biophys Acta. 1980;620(2):281-96.

77. Esterbauer H, Schaur RJ, Zollner H. Chemistry and biochemistry of 4-hydroxynonenal, malonaldehyde and related aldehydes. Free Radic Biol Med. 1991;11(1):81-128.
78. Uchida K. 4-Hydroxy-2-nonenal: a product and mediator of oxidative stress. Prog Lipid Res. 2003;42(4):318-43.
79. Malingriaux EA, Rupprecht A, Gille L, Jovanovic O, Jezek P, Jaburek M, et al. Fatty acids are key in 4-hydroxy-2-nonenal-mediated activation of uncoupling proteins 1 and 2. Plos One. 2013;8(10):e77786.
80. Fedorenko A, Lishko PV, Kirichok Y. Mechanism of Fatty-Acid-Dependent UCP1 Uncoupling in Brown Fat Mitochondria. Cell. 2012;151(2):400-13.
81. Couplan E, Gonzalez-Barroso MD, Alves-Guerra MC, Ricquier D, Goubern M, Bouillaud F. No evidence for a basal, retinoic, or superoxide-induced uncoupling activity of the uncoupling protein 2 present in spleen or lung mitochondria. J Biol Chem. 2002;277(29):26268-75.
82. Shabalina IG, Petrovic N, Kramarova TV, Hoeks J, Cannon B, Nedergaard J. UCP1 and defense against oxidative stress. 4-Hydroxy-2-nonenal effects on brown fat mitochondria are uncoupling protein 1-independent. J Biol Chem. 2006;281(20):13882-93.
83. Parker N, Vidal-Puig A, Brand MD. Stimulation of mitochondrial proton conductance by hydroxynonenal requires a high membrane potential. Biosci Rep. 2008;28(2):83-8.
84. Murphy KM, Weaver C, Janeway C. Janeway's immunobiology. 9th edition ed. New York: Garland Science New York; 2017.
85. Kizaki T, Suzuki K, Hitomi Y, Taniguchi N, Saitoh D, Watanabe K, et al. Uncoupling protein 2 plays an important role in nitric oxide production of lipopolysaccharide-stimulated macrophages. Proc Natl Acad Sci U S A. 2002;99(14):9392-7.
86. Arsenijevic D, Onuma H, Pecqueur C, Raimbault S, Manning BS, Miroux B, et al. Disruption of the uncoupling protein-2 gene in mice reveals a role in immunity and reactive oxygen species production. Nat Genet. 2000;26(4):435-9.
87. Basu Ball W, Kar S, Mukherjee M, Chande AG, Mukhopadhyaya R, Das PK. Uncoupling protein 2 negatively regulates mitochondrial reactive oxygen species generation and induces phosphatase-mediated anti-inflammatory response in experimental visceral leishmaniasis. J Immunol. 2011;187(3):1322-32.
88. Victor VM, Rocha M, De la Fuente M. Immune cells: free radicals and antioxidants in sepsis. International Immunopharmacology. 2004;4(3):327-47.
89. Emre Y, Hurtaud C, Karaca M, Nubel T, Zavala F, Ricquier D. Role of uncoupling protein UCP2 in cell-mediated immunity: how macrophage-mediated insulitis is accelerated in a model of autoimmune diabetes. Proc Natl Acad Sci U S A. 2007;104(48):19085-90.
90. Krauss S, Zhang CY, Scorrano L, Dalgaard LT, St-Pierre J, Grey ST, et al. Superoxide-mediated activation of uncoupling protein 2 causes pancreatic beta cell dysfunction. J Clin Invest. 2003;112(12):1831-42.
91. Zhang CY, Krauss S, Scorrano L, St Pierre J, Grey S, Lowell B. Superoxide and UCP2 - A novel pathway causing hyperglycemia-induced B-cell dysfunction. Diabetes. 2003;52:A380-A1.
92. Affourtit C, Brand MD. Activity of uncoupling protein-2 in pancreatic beta cells. Bba-Bioenergetics. 2008;1777:S76-S7.
93. Vozza A, Parisi G, De Leonardis F, Lasorsa FM, Castegna A, Amorese D, et al. UCP2 transports C4 metabolites out of mitochondria, regulating glucose and glutamine oxidation. Proc Natl Acad Sci U S A. 2014;111(3):960-5.
94. Carretero MV, Torres L, Latasa U, García-Trevijano ER, Prieto J, Mato JM, et al. Transformed but not normal hepatocytes express UCP2. Febs Lett. 1998;439(1-2):55-8.
95. Hurtaud C, Gelly C, Chen Z, Lévi-Meyrueis C, Bouillaud F. Glutamine stimulates translation of uncoupling protein 2mRNA. Cell Mol Life Sci. 2007;64(14):1853-60.
96. Johnson RN, Chappell JB. The transport of inorganic phosphate by the mitochondrial dicarboxylate carrier. Biochem J. 1973;134(3):769-74.

97. Kakhniashvili D, Mayor JA, Gremse DA, Xu Y, Kaplan RS. Identification of a novel gene encoding the yeast mitochondrial dicarboxylate transport protein via overexpression, purification, and characterization of its protein product. J Biol Chem. 1997;272(7):4516-21.
98. Cimadamore-Werthein C, King MS, Lacabanne D, Pyrihova E, Jaiquel Baron S, Kunji ER. Human mitochondrial carriers of the SLC25 family function as monomers exchanging substrates with a ping-pong kinetic mechanism. EMBO J. 2024;43(16):3450-65.
99. Pyrihová E, King MS, King AC, Toleco MR, van der Giezen M, Kunji ERS. A mitochondrial carrier transports glycolytic intermediates to link cytosolic and mitochondrial glycolysis in the human gut parasite Blastocystis. Elife. 2024;13:RP94187.
100. Polonsky KS, Semenkovich CF. The pancreatic β cell heats up:: UCP2 and insulin secretion in diabetes. Cell. 2001;105(6):705-7.
101. Pecqueur C, Alves-Guerra C, Ricquier D, Bouillaud F. UCP2, A Metabolic Sensor Coupling Glucose Oxidation to Mitochondrial Metabolism? IUBMB Life. 2009;61(7):762-7.
102. Emre Y, Nübel T. Uncoupling protein UCP2: When mitochondrial activity meets immunity. Febs Lett. 2010;584(8):1437-42.
103. Diano S, Horvath TL. Mitochondrial uncoupling protein 2 (UCP2) in glucose and lipid metabolism. Trends Mol Med. 2012;18(1):52-8.
104. Hall JE, Guyton AC. Guyton and Hall textbook of medical physiology. Philadelphia, PA: Saunders Elsevier Philadelphia, PA; 2011. Available from: http://www.clinicalkey.com/dura/browse/bookChapter/3-s2.0-C20090602506.
105. Zhang CY, Baffy G, Perret P, Krauss S, Peroni O, Grujic D, et al. Uncoupling protein-2 negatively regulates insulin secretion and is a major link between obesity, beta cell dysfunction, and type 2 diabetes. Cell. 2001;105(6):745-55.
106. Krauss S, Zhang CY, Scorrano L, Dalgaard LT, St-Pierre J, Grey ST, et al. Superoxide-mediated activation of uncoupling protein 2 causes pancreatic β cell dysfunction. Journal of Clinical Investigation. 2003;112(12):1831-42.
107. Drel VR, Mashtalir N, Ilnytska O, Shin J, Li F, Lyzogubov VV, et al. The leptin-deficient (ob/ob) mouse: a new animal model of peripheral neuropathy of type 2 diabetes and obesity. Diabetes. 2006;55(12):3335-43.
108. Galetti S, Sarre A, Perreten H, Produit-Zengaffinen N, Muzzin P, Assimacopoulos-Jeannet F. Fatty acids do not activate UCP2 in pancreatic beta cells: comparison with UCP1. Pflug Arch Eur J Phy. 2009;457(4):931-40.
109. De Souza CT, Araujo EP, Stoppiglia LF, Pauli JR, Ropelle E, Rocco SA, et al. Inhibition of UCP2 expression reverses diet-induced diabetes mellitus by effects on both insulin secretion and action. FASEB J. 2007;21(4):1153-63.
110. Nicholls DG, Ferguson SJ. Bioenergetics. 4th ed: Elsevier Ltd.; 2013.
111. Derdak Z, Mark NM, Beldi G, Robson SC, Wands JR, Baffy G. The mitochondrial uncoupling protein-2 promotes chemoresistance in cancer cells. Cancer Res. 2008;68(8):2813-9.
112. Li W, Nichols K, Nathan CA, Zhao Y. Mitochondrial uncoupling protein 2 is up-regulated in human head and neck, skin, pancreatic, and prostate tumors. Cancer Biomark. 2013;13(5):377-83.
113. Pons DG, Nadal-Serrano M, Torrens-Mas M, Valle A, Oliver J, Roca P. UCP2 inhibition sensitizes breast cancer cells to therapeutic agents by increasing oxidative stress. Free Radic Biol Med. 2015;86:67-77.
114. Raho S, Capobianco L, Malivindi R, Vozza A, Piazzolla C, De Leonardis F, et al. KRAS-regulated glutamine metabolism requires UCP2-mediated aspartate transport to support pancreatic cancer growth. Nat Metab. 2020;2(12).
115. Cheng WC, Tsui YC, Ragusa S, Koelzer VH, Mina M, Franco F, et al. Uncoupling protein 2 reprograms the tumor microenvironment to support the anti-tumor immune cycle. Nat Immunol. 2019;20(2):206-17.

116. Aguilar E, Esteves P, Sancerni T, Lenoir V, Aparicio T, Bouillaud F, et al. UCP2 Deficiency Increases Colon Tumorigenesis by Promoting Lipid Synthesis and Depleting NADPH for Antioxidant Defenses. Cell Rep. 2019;28(9):2306-+.
117. Esteves P, Pecqueur C, Ransy C, Esnous C, Lenoir V, Bouillaud F, et al. Mitochondrial retrograde signaling mediated by UCP2 inhibits cancer cell proliferation and tumorigenesis. Cancer Res. 2014;74(14):3971-82.
118. Esteves P, Pecqueur C, Alves-Guerra MC. UCP2 induces metabolic reprogramming to inhibit proliferation of cancer cells. Mol Cell Oncol. 2015;2(1):e975024.
119. Sancerni T, Renoult O, Luby A, Caradeuc C, Lenoir V, Croyal M, et al. UCP2 silencing restrains leukemia cell proliferation through glutamine metabolic remodeling. Front Immunol. 2022;13:960226.
120. Bystry RS, Aluvihare V, Welch KA, Kallikourdis M, Betz AG. B cells and professional APCs recruit regulatory T cells via CCL4. Nat Immunol. 2001;2(12):1126-32.
121. Borish LC, Steinke JW. 2. Cytokines and chemokines. Journal of Allergy and Clinical Immunology. 2003;111(2 Suppl):S460-75.
122. Mombaerts P, Iacomini J, Johnson RS, Herrup K, Tonegawa S, Papaioannou VE. RAG-1-deficient mice have no mature B and T lymphocytes. Cell. 1992;68(5):869-77.
123. Hildner K, Edelson BT, Purtha WE, Diamond M, Matsushita H, Kohyama M, et al. Batf3 deficiency reveals a critical role for CD8alpha+ dendritic cells in cytotoxic T cell immunity. Science. 2008;322(5904):1097-100.
124. Parang B, Barrett CW, Williams CS. AOM/DSS Model of Colitis-Associated Cancer. Methods Mol Biol. 2016;1422:297-307.
125. Schiffer TA, Lof L, Gallini R, Kamali-Moghaddam M, Carlstrom M, Palm F. Mitochondrial Respiration-Dependent ANT2-UCP2 Interaction. Front Physiol. 2022;13:866590.
126. Son J, Lyssiotis CA, Ying H, Wang X, Hua S, Ligorio M, et al. Glutamine supports pancreatic cancer growth through a KRAS-regulated metabolic pathway. Nature. 2013;496(7443):101-5.
127. Yoo HC, Park SJ, Nam M, Kang J, Kim K, Yeo JH, et al. A Variant of SLC1A5 Is a Mitochondrial Glutamine Transporter for Metabolic Reprogramming in Cancer Cells. Cell Metabolism. 2020;31(2):267-83 e12.
128. Hanahan D, Weinberg RA. Hallmarks of cancer: the next generation. Cell. 2011;144(5):646-74.
129. Aquila H, Link TA, Klingenberg M. The uncoupling protein from brown fat mitochondria is related to the mitochondrial ADP/ATP carrier. Analysis of sequence homologies and of folding of the protein in the membrane. EMBO J. 1985;4(9):2369-76.
130. Runswick MJ, Powell SJ, Nyren P, Walker JE. Sequence of the bovine mitochondrial phosphate carrier protein: structural relationship to ADP/ATP translocase and the brown fat mitochondria uncoupling protein. EMBO J. 1987;6(5):1367-73.
131. Runswick MJ, Walker JE, Bisaccia F, Iacobazzi V, Palmieri F. Sequence of the bovine 2-oxoglutarate/malate carrier protein: structural relationship to other mitochondrial transport proteins. Biochemistry-Us. 1990;29(50):11033-40.
132. Bisaccia F, De Palma A, Palmieri F. Identification and purification of the aspartate/glutamate carrier from bovine heart mitochondria. Biochim Biophys Acta. 1992;1106(2):291-6.
133. Walker JE. The mitochondrial transporter family. Curr Opin Struc Biol. 1992;2(4):519-26.
134. Pebay-Peyroula E, Dahout-Gonzalez C, Kahn R, Trezeguet V, Lauquin GJM, Brandolin R. Structure of mitochondrial ADP/ATP carrier in complex with carboxyatractyloside. Nature. 2003;426(6962):39-44.
135. Dehez F, Pebay-Peyroula E, Chipot C. Binding of ADP in the mitochondrial ADP/ATP carrier is driven by an electrostatic funnel. J Am Chem Soc. 2008;130(38):12725-33.
136. Robinson AJ, Kunji ER. Mitochondrial carriers in the cytoplasmic state have a common substrate binding site. Proc Natl Acad Sci U S A. 2006;103(8):2617-22.

137. Pebay-Peyroula E, Dahout-Gonzalez C, Kahn R, Trezeguet V, Lauquin GJ, Brandolin G. Structure of mitochondrial ADP/ATP carrier in complex with carboxyatractyloside. Nature. 2003;426(6962):39-44.
138. Ruprecht JJ, Kunji ERS. The SLC25 Mitochondrial Carrier Family: Structure and Mechanism. Trends Biochem Sci. 2020;45(3):244-58.
139. Robinson AJ, Overy C, Kunji ERS. The mechanism of transport by mitochondrial carriers based on analysis of symmetry. Proc Natl Acad Sci U S A. 2008;105(46):17766-71.
140. Ruprecht JJ, Hellawell AM, Harding M, Crichton PG, Mccoy AJ, Kunji ERS. Structures of yeast mitochondrial ADP/ATP carriers support a domain-based alternating-access transport mechanism. Proc Natl Acad Sci U S A. 2014;111(4):E426-E34.
141. Ruprecht JJ, King MS, Zogg T, Aleksandrova AA, Pardon E, Crichton PG, et al. The Molecular Mechanism of Transport by the Mitochondrial ADP/ATP Carrier. Cell. 2019;176(3):435-47 e15.
142. Claypool SM. Cardiolipin, a critical determinant of mitochondrial carrier protein assembly and function. Biochim Biophys Acta. 2009;1788(10):2059-68.
143. Klingenberg M. Cardiolipin and mitochondrial carriers. Biochim Biophys Acta. 2009;1788(10):2048-58.
144. Kramer R, Klingenberg M. Enhancement of reconstituted ADP,ATP exchange activity by phosphatidylethanolamine and by anionic phospholipids. Febs Lett. 1980;119(2):257-60.
145. Ruprecht JJ, Hellawell AM, Harding M, Crichton PG, McCoy AJ, Kunji ER. Structures of yeast mitochondrial ADP/ATP carriers support a domain-based alternating-access transport mechanism. Proc Natl Acad Sci U S A. 2014;111(4):E426-34.
146. Nury H, Dahout-Gonzalez C, Trezeguet V, Lauquin G, Brandolin G, Pebay-Peyroula E. Structural basis for lipid-mediated interactions between mitochondrial ADP/ATP carrier monomers. Febs Lett. 2005;579(27):6031-6.
147. King MS, Kerr M, Crichton PG, Springett R, Kunji ERS. Formation of a cytoplasmic salt bridge network in the matrix state is a fundamental step in the transport mechanism of the mitochondrial ADP/ATP carrier. Biochim Biophys Acta. 2016;1857(1):14-22.
148. Kunji ER, Robinson AJ. The conserved substrate binding site of mitochondrial carriers. Biochim Biophys Acta. 2006;1757(9-10):1237-48.
149. Springett R, King MS, Crichton PG, Kunji ERS. Modelling the free energy profile of the mitochondrial ADP/ATP carrier. Bba-Bioenergetics. 2017;1858(11):906-14.
150. Ruprecht JJ, Kunji ER. Structural changes in the transport cycle of the mitochondrial ADP/ATP carrier. Curr Opin Struct Biol. 2019;57:135-44.
151. Cimadamore-Werthein C, Jaiquel Baron S, King MS, Springett R, Kunji ER. Human mitochondrial ADP/ATP carrier SLC25A4 operates with a ping-pong kinetic mechanism. EMBO Rep. 2023;24(8):e57127.
152. Mavridou V, King MS, Tavoulari S, Ruprecht JJ, Palmer SM, Kunji ERS. Substrate binding in the mitochondrial ADP/ATP carrier is a step-wise process guiding the structural changes in the transport cycle. Nat Commun. 2022;13(1).
153. Jones SA, Gogoi P, Ruprecht JJ, King MS, Lee Y, Zogg T, et al. Structural basis of purine nucleotide inhibition of human uncoupling protein 1. Sci Adv. 2023;9(22):eadh4251.
154. Kang YL, Chen L. Structural basis for the binding of DNP and purine nucleotides onto UCP1. Nature. 2023;620(7972):226-+.
155. Crichton PG, Lee Y, Ruprecht JJ, Cerson E, Thangaratnarajah C, King MS, et al. Trends in thermostability provide information on the nature of substrate, inhibitor, and lipid interactions with mitochondrial carriers. J Biol Chem. 2015;290(13):8206-17.
156. Berardi MJ, Shih WM, Harrison SC, Chou JJ. Mitochondrial uncoupling protein 2 structure determined by NMR molecular fragment searching. Nature. 2011;476(7358):109-13.
157. Berardi MJ, Chou JJ. Fatty acid flippase activity of UCP2 is essential for its proton transport in mitochondria. Cell Metab. 2014;20(3):541-52.

158. Kurauskas V, Hessel A, Ma P, Lunetti P, Weinhaupl K, Imbert L, et al. How Detergent Impacts Membrane Proteins: Atomic-Level Views of Mitochondrial Carriers in Dodecylphosphocholine. J Phys Chem Lett. 2018;9(5):933-8.
159. Chipot C, Dehez F, Schnell JR, Zitzmann N, Pebay-Peyroula E, Catoire LJ, et al. Perturbations of Native Membrane Protein Structure in Alkyl Phosphocholine Detergents: A Critical Assessment of NMR and Biophysical Studies. Chem Rev. 2018;118(7):3559-607.
160. Dehez F, Schanda P, King MS, Kunji ERS, Chipot C. Mitochondrial ADP/ATP Carrier in Dodecylphosphocholine Binds Cardiolipins with Non-native Affinity. Biophys J. 2017;113(11):2311-5.
161. King MS, Crichton PG, Ruprecht JJ, Kunji ERS. Concerns with yeast mitochondrial ADP/ATP carrier's integrity in DPC (vol 25, pg 747, 2018). Nat Struct Mol Biol. 2018;25(10):988-.
162. Piel MS, Masscheleyn S, Bouillaud F, Moncoq K, Miroux B. Structural models of mitochondrial uncoupling proteins obtained in DPC micelles are not functionally relevant. Febs J. 2021;288(9):3024-33.
163. Zoonens M, Comer J, Masscheleyn S, Pebay-Peyroula E, Chipot C, Miroux B, et al. Dangerous Liaisons between Detergents and Membrane Proteins. The Case of Mitochondrial Uncoupling Protein 2. J Am Chem Soc. 2013;135(40):15174-82.
164. Ruzicka M, Skobisová E, Dlasková A, Santorova J, Smolková K, Spacek T, et al. Recruitment of mitochondrial uncoupling protein UCP2 after lipopolysaccharide induction. Int J Biochem Cell Biol. 2005;37(4):809-21.
165. Miroux B, Walker JE. Over-production of proteins in Escherichia coli: mutant hosts that allow synthesis of some membrane proteins and globular proteins at high levels. J Mol Biol. 1996;260(3):289-98.
166. Kota J, Gilstring CF, Ljungdahl PO. Membrane chaperone Shr3 assists in folding amino acid permeases preventing precocious ERAD. J Cell Biol. 2007;176(5):617-28.
167. Ammerer G, Hunter CP, Rothman JH, Saari GC, Valls LA, Stevens TH. PEP4 gene of Saccharomyces cerevisiae encodes proteinase A, a vacuolar enzyme required for processing of vacuolar precursors. Mol Cell Biol. 1986;6(7):2490-9.
168. Hashimoto M, Shinohara Y, Majima E, Hatanaka T, Yamazaki N, Terada H. Expression of the bovine heart mitochondrial ADP/ATP carrier in yeast mitochondria: significantly enhanced expression by replacement of the N-terminal region of the bovine carrier by the corresponding regions of the yeast carriers. Biochim Biophys Acta. 1999;1409(3):113-24.
169. Tang XR, Nakata Y, Li HO, Zhang MD, Gao H, Fujita A, et al. The Optimization of Preparations of Competent Cells for Transformation of Escherichia-Coli. Nucleic Acids Res. 1994;22(14):2857-8.
170. Invitrogen. pYES2 User Manual: Invitrogen; 2008 [Invitrogen pYES2 expression vector].
171. Cavalieri R. The interaction of mitochondrial Uncoupling Protein-1 with regulatory ligands: University of East Anglia; 2021.
172. Way M, Pope B, Gooch J, Hawkins M, Weeds AG. Identification of a region in segment 1 of gelsolin critical for actin binding. EMBO J. 1990;9(12):4103-9.
173. Studier FW, Rosenberg AH, Dunn JJ, Dubendorff JW. Use of T7 RNA polymerase to direct expression of cloned genes. Methods Enzymol. 1990;185:60-89.
174. Nelson M, Mcclelland M. Use of DNA methyltransferase/endonuclease enzyme combinations for megabase mapping of chromosomes. Method Enzymol. 1992;216:279-303.
175. Gietz RD, Woods RA. Transformation of yeast by lithium acetate/single-stranded carrier DNA/polyethylene glycol method. Guide to Yeast Genetics and Molecular and Cell Biology, Pt B. 2002;350:87-96.
176. Sorensen K, Brodbeck U. A Sensitive Protein Assay-Method Using Micro-Titer Plates. Experientia. 1986;42(2):161-2.

177. Arechaga I, Raimbault S, Prieto S, Levi-Meyrueis C, Zaragoza P, Miroux B, et al. Cysteine residues are not essential for uncoupling protein function. Biochem J. 1993;296 (Pt 3)(Pt 3):693-700.
178. Echtay KS, Bienengraeber M, Klingenberg M. Mutagenesis of the uncoupling protein of brown adipose tissue. Neutralization of E190 largely abolishes pH control of nucleotide binding. Biochemistry-Us. 1997;36(27):8253-60.
179. Lin CS, Klingenberg M. Isolation of the uncoupling protein from brown adipose tissue mitochondria. Febs Lett. 1980;113(2):299-303.
180. Fujiki Y, Hubbard AL, Fowler S, Lazarow PB. Isolation of Intracellular Membranes by Means of Sodium-Carbonate Treatment - Application to Endoplasmic-Reticulum. J Cell Biol. 1982;93(1):97-102.
181. Echtay KS, Liu Q, Caskey T, Winkler E, Frischmuth K, Bienengraber M, et al. Regulation of UCP3 by nucleotides is different from regulation of UCP1. Febs Lett. 1999;450(1-2):8-12.
182. Bio-Rad. Image Acquistion for Western Blotting 2023 [Available from: https://www.bio-rad.com/en-uk/applications-technologies/image-acquisition-for-western-blotting?ID=PQEEQORA83CC.
183. Towbin H, Staehelin T, Gordon J. Electrophoretic transfer of proteins from polyacrylamide gels to nitrocellulose sheets: procedure and some applications. Proc Natl Acad Sci U S A. 1979;76(9):4350-4.
184. Rai S, Arasteh M, Jefferson M, Pearson T, Wang YX, Zhang WJ, et al. The ATG5-binding and coiled coil domains of ATG16L1 maintain autophagy and tissue homeostasis in mice independently of the WD domain required for LC3-associated phagocytosis. Autophagy. 2019;15(4):599-612.
185. Azzu V, Affourtit C, Breen EP, Parker N, Brand MD. Dynamic regulation of uncoupling protein 2 content in INS-1E insulinoma cells. Biochim Biophys Acta. 2008;1777(10):1378-83.
186. Izawa T, Unger A-K. Isolation of Mitochondria from Saccharomyces cerevisiae. In: Mokranjac D, Perocchi F, editors. Mitochondria: Practical Protocols. New York, NY: Springer New York; 2017. p. 33-42.
187. Serrano R, Martín H, Casamayor A, Ariño J. Signaling alkaline pH stress in the yeast *Saccharomyces cerevisiae* through the Wsc1 cell surface sensor and the Slt2 MAPK pathway. J Biol Chem. 2006;281(52):39785-95.
188. Klis FM, Mol P, Hellingwerf K, Brul S. Dynamics of cell wall structure in Saccharomyces cerevisiae. Fems Microbiol Rev. 2002;26(3):239-56.
189. Yin QY, de Groot PWJ, Dekker HL, de Jong L, Klis FM, de Koster CG. Comprehensive proteomic analysis of Saccharomyces cerevisiae cell walls. J Biol Chem. 2005;280(21):20894-901.
190. Ovalle R, Lim ST, Holder B, Jue CK, Moore CW, Lipke PN. A spheroplast rate assay for determination of cell wall integrity in yeast. Yeast. 1998;14(13):1159-66.
191. Orosz DE, Garlid KD. The Ci-Sensitive Fluorescent Indicator, Spq, Responds to Buffer Anions and Provides a Sensitive Assay for H+ Transport in Liposomes. FASEB J. 1992;6(1):A311-A.
192. Alexandrov AI, Mileni M, Chien EYT, Hanson MA, Stevens RC. Microscale fluorescent thermal stability assay for membrane proteins. Structure. 2008;16(3):351-9.
193. Sippel TO. New Fluorochromes for Thiols - Maleimide and Iodoacetamide Derivatives of a 3-Phenylcoumarin Fluorophore. J Histochem Cytochem. 1981;29(2):314-6.
194. Majd H, King MS, Palmer SM, Smith AC, Elbourne LDH, Paulsen IT, et al. Screening of candidate substrates and coupling ions of transporters by thermostability shift assays. Elife. 2018;7.
195. Jaiquel Baron S, King MS, Kunji ERS, Schirris TJJ. Characterization of drug-induced human mitochondrial ADP/ATP carrier inhibition. Theranostics. 2021;11(11):5077-91.

196. Niesen FH, Berglund H, Vedadi M. The use of differential scanning fluorimetry to detect ligand interactions that promote protein stability. Nat Protoc. 2007;2(9):2212-21.
197. Beam AM-R, A. Beyond IC50s: Towards Robust Statistical Methods for in vitro Association Studies. J Pharmacogenomics Pharmcoproteomics. 2014;5(1).
198. Nedergaard J, Cannon B. The 'novel' 'uncoupling' proteins UCP2 and UCP3: what do they really do? Pros and cons for suggested functions. Exp Physiol. 2003;88(1):65-84.
199. Riccio P, Aquila H, Klingenberg M. Purification of the carboxy-atractylate binding protein from mitochondria. Febs Lett. 1975;56(1):133-8.
200. Lin CS, Klingenberg M. Characteristics of the Isolated Purine Nucleotide Binding-Protein from Brown Fat Mitochondria. Biochemistry-Us. 1982;21(12):2950-6.
201. Wagner S, Bader ML, Drew D, de Gier JW. Rationalizing membrane protein overexpression. Trends in Biotechnology. 2006;24(8):364-71.
202. Terpe K. Overview of bacterial expression systems for heterologous protein production: from molecular and biochemical fundamentals to commercial systems. Appl Microbiol Biotechnol. 2006;72(2):211-22.
203. Fiermonte G, Walker JE, Palmieri F. Abundant bacterial expression and reconstitution of an intrinsic membrane-transport protein from bovine mitochondria. Biochem J. 1993;294:293-9.
204. Jekabsons MB, Echtay KS, Arechaga I, Brand MD. Molecular properties of purified human uncoupling protein 2 refolded from bacterial inclusion bodies. J Bioenerg Biomembr. 2003;35(5):409-18.
205. Jekabsons MB, Echtay KS, Brand MD. Nucleotide binding to human uncoupling protein-2 refolded from bacterial inclusion bodies. Biochem J. 2002;366:565-71.
206. Beck V, Jaburek M, Demina T, Rupprecht A, Porter RK, Jezek P, et al. Polyunsaturated fatty acids activate human uncoupling proteins 1 and 2 in planar lipid bilayers. FASEB J. 2007;21(4):1137-44.
207. Palmieri F, Indiveri C, Bisaccia F, Iacobazzi V. Mitochondrial metabolite carrier proteins: Purification, reconstitution, and transport studies. Method Enzymol. 1995;260:349-69.
208. Palmieri L, Palmieri F, Runswick MJ, Walker JE. Identification by bacterial expression and functional reconstitution of the yeast genomic sequence encoding the mitochondrial dicarboxylate carrier protein. Febs Lett. 1996;399(3):299-302.
209. Palmieri L, Pardo B, Lasorsa FM, del Arco A, Kobayashi K, Iijima M, et al. Citrin and aralar1 are Ca(2+)-stimulated aspartate/glutamate transporters in mitochondria. EMBO J. 2001;20(18):5060-9.
210. Palmieri L, Runswick MJ, Fiermonte G, Walker JE, Palmieri F. Yeast mitochondrial carriers: Bacterial expression, biochemical identification and metabolic significance. J Bioenerg Biomembr. 2000;32(1):67-77.
211. King MS, Boes C, Kunji ERS. Chapter Four - Membrane Protein Expression in Lactococcus lactis. In: Shukla AK, editor. Membrane Proteins—Production and Functional Characterization. 5562015. p. 77-97.
212. Kunji ERS, Slotboom DJ, Poolman B. Lactococcus lactis as host for overproduction of functional membrane proteins. Biochim Biophys Acta. 2003;1610(1):97-108.
213. Monné M, Chan KW, Slotboom DJ, Kunji ERS. Functional expression of eukaryotic membrane proteins in Lactococcus lactis. Protein Sci. 2005;14(12):3048-56.
214. Majd H, King MS, Smith AC, Kunji ERS. Pathogenic mutations of the human mitochondrial citrate carrier SLC25A1 lead to impaired citrate export required for lipid, dolichol, ubiquinone and sterol synthesis. Bba-Bioenergetics. 2018;1859(1):1-7.
215. Williams LS. Over-expression, Purification and Stabilisation of the Mitochondrial Uncoupling Protein. Medical Research Council Mitochondrial Biology Unit: University of Cambridge; 2010.
216. Haferkamp I, Linka N. Functional expression and characterisation of membrane transport proteins. Plant Biol. 2012;14(5):675-90.

217. Routledge SJ, Mikaliunaite L, Patel A, Clare M, Cartwright SP, Bawa Z, et al. The synthesis of recombinant membrane proteins in yeast for structural studies. Methods. 2016;95:26-37.
218. Carlesso A, Delgado R, Isant OR, Uwangue O, Valli D, Bill RM, et al. Yeast as a tool for membrane protein production and structure determination. Fems Yeast Res. 2022;22(1).
219. Harborne SPD, King MS, Crichton PG, Kunji ERS. Calcium regulation of the human mitochondrial ATP-Mg/Pi carrier SLC25A24 uses a locking pin mechanism. Sci Rep-Uk. 2017;7.
220. Tavoulari S, Thangaratnarajah C, Mavrido V, Harbor ME, Martinou JC, Kunji ERS. The yeast mitochondrial pyruvate carrier is a hetero-dimer in its functional state. EMBO J. 2019;38(10).
221. Tavoulari S, Schirris TJJ, Mavridou V, Thangaratnarajah C, King MS, Jones DTD, et al. Key features of inhibitor binding to the human mitochondrial pyruvate carrier hetero-dimer. Mol Metab. 2022;60.
222. de Tilques MD, Tribouillard-Tanvier D, Tétaud E, Testet E, di Rago JP, Lasserre JP. Overexpression of mitochondrial oxodicarboxylate carrier (ODC1) preserves oxidative phosphorylation in a yeast model of Barth syndrome. Dis Model Mech. 2017;10(4):439-50.
223. Bathgate B, Freebairn EM, Greenland AJ, Reid GA. Functional expression of the rat brown adipose tissue uncoupling protein in Saccharomyces cerevisiae. Mol Microbiol. 1992;6(3):363-70.
224. Cunningham O, McElligott AM, Carroll AM, Breen E, Reguenga C, Oliveira ME, et al. Selective detection of UCP 3 expression in skeletal muscle: effect of thyroid status and temperature acclimation. Biochim Biophys Acta. 2003;1604(3):170-9.
225. Heidkaemper D, Winkler E, Muller V, Frischmuth K, Liu Q, Caskey T, et al. The bulk of UCP3 expressed in yeast cells is incompetent for a nucleotide regulated H+ transport. Febs Lett. 2000;480(2-3):265-70.
226. Hamilton R, Watanabe CK, Deboer HA. Compilation and comparison of the sequence context around the AUG startcodons in Saccharomyces cerevisiae mRNAs. Nucleic Acids Res. 1987;15(8):3581-93.
227. Dvir S, Velten L, Sharon E, Zeevi D, Carey LB, Weinberger A, et al. Deciphering the rules by which 5 '-UTR sequences affect protein expression in yeast. Proc Natl Acad Sci U S A. 2013;110(30):E2792-E801.
228. Drew D, Newstead S, Sonoda Y, Kim H, von Heijne G, Iwata S. GFP-based optimization scheme for the overexpression and purification of eukaryotic membrane proteins in Saccharomyces cerevisiae. Nat Protoc. 2008;3(5):784-98.
229. Abcam. Anti-UCP2 antibody (ab97931) 2023 [Webpage for a UCP2 antibody from Abcam (97931)]. Available from: https://www.abcam.com/products/primary-antibodies/ucp2-antibody-ab97931.html.
230. Millipore M. Anti-Uncoupling Protein-2 (UCP-2) (144-157) Rabbit pAb 2023 [Webpage for Merck Millipore anti-UCP2 antibody (144-57)]. Available from: https://www.merckmillipore.com/GB/en/product/Anti-Uncoupling-Protein-2-UCP-2-144-157-Rabbit-pAb,EMD_BIO-662047?ReferrerURL=https%3A%2F%2Fwww.google.com%2F.
231. Nashed S, El Barbry H, Benchouaia M, Dijoux-Marechal A, Delaveau T, Ruiz-Gutierrez N, et al. Functional mapping of N-terminal residues in the yeast proteome uncovers novel determinants for mitochondrial protein import. Plos Genet. 2023;19(8).
232. Riccio P, Aquila H, Klingenberg M. Solubilization of the carboxy-atractylate binding protein from mitochondria. Febs Lett. 1975;56(1):129-32.
233. Chae PS, Rasmussen SGF, Rana RR, Gotfryd K, Chandra R, Goren MA, et al. Maltose-neopentyl glycol (MNG) amphiphiles for solubilization, stabilization and crystallization of membrane proteins. Nat Methods. 2010;7(12):1003-U90.

234. Saouros S, Cecchetti C, Jones A, Cameron AD, Byrne B. Strategies for successful isolation of a eukaryotic transporter. Protein Expr Purif. 2020;166:105522.
235. Chung IJ, Grba DN, Wright JJ, Hirst J. Making the leap from structure to mechanism: are the open states of mammalian complex I identified by cryoEM resting states or catalytic intermediates? Curr Opin Struct Biol. 2022;77.
236. Grba DN, Chung IJ, Bridges HR, Agip ANA, Hirst J. Investigation of hydrated channels and proton pathways in a high-resolution cryo-EM structure of mammalian complex I. Sci Adv. 2023;9(31).
237. Kang Y, Chen L. Structural basis for the binding of DNP and purine nucleotides onto UCP1. Nature. 2023;620(7972):226-31.
238. Horuk R, Colby TJ, Darbonne WC, Schall TJ, Neote K. The human erythrocyte inflammatory peptide (chemokine) receptor. Biochemical characterization, solubilization, and development of a binding assay for the soluble receptor. Biochemistry-Us. 1993;32(22):5733-8.
239. Staudinger R, Bandres JC. Solubilization of the chemokine receptor CXCR4. Biochem Biophys Res Commun. 2000;274(1):153-6.
240. Sherman F. Getting started with yeast. Guide to Yeast Genetics and Molecular and Cell Biology, Pt B. 2002;350:3-41.
241. Freigassner M, Pichler H, Glieder A. Tuning microbial hosts for membrane protein production. Microb Cell Fact. 2009;8.
242. West RW, Yocum RR, Ptashne M. Saccharomyces cerevisiae GAL1-GAL10 divergent promoter region: location and function of the upstream activating sequence UASG. Molecular and Cellular Biology. 1984;4(11):2467-78.
243. Johnston M, Flick JS, Pexton T. Multiple mechanisms provide rapid and stringent glucose repression of GAL gene expression in Saccharomyces cerevisiae. Mol Cell Biol. 1994;14(6):3834-41.
244. Roop JI, Chang KC, Brem RB. Polygenic evolution of a sugar specialization trade-off in yeast. Nature. 2016;530(7590):336-+.
245. Kissova I, Salin B, Schaeffer J, Bhatia S, Manon S, Camougrand N. Selective and non-selective autophagic degradation of mitochondria in yeast. Autophagy. 2007;3(4):329-36.
246. Carmona-Gutierrez D, Bauer MA, Ring J, Knauer H, Eisenberg T, Buttner S, et al. The propeptide of yeast cathepsin D inhibits programmed necrosis. Cell Death Dis. 2011;2(5):e161.
247. Starheim KK, Gevaert K, Arnesen T. Protein N-terminal acetyltransferases: when the start matters. Trends Biochem Sci. 2012;37(4):152-61.
248. Hammen PK, Heard TS, Waltner M, Weiner H. The loss in hydrophobic surface area resulting from a Leu to Val mutation at the N-terminus of the aldehyde dehydrogenase presequence prevents import of the protein into mitochondria. Protein Sci. 1999;8(4):890-6.
249. Adachi A, Koizumi M, Ohsumi Y. Autophagy induction under carbon starvation conditions is negatively regulated by carbon catabolite repression. J Biol Chem. 2017;292(48):19905-18.
250. Teichert U, Mechler B, Muller H, Wolf DH. Lysosomal (vacuolar) proteinases of yeast are essential catalysts for protein degradation, differentiation, and cell survival. J Biol Chem. 1989;264(27):16037-45.
251. Bouillaud F, Arechaga I, Petit PX, Raimbault S, Levi-Meyrueis C, Casteilla L, et al. A sequence related to a DNA recognition element is essential for the inhibition by nucleotides of proton transport through the mitochondrial uncoupling protein. EMBO J. 1994;13(8):1990-7.
252. Escalante-Chong R, Savir Y, Carroll SM, Ingraham JB, Wang J, Marx CJ, et al. Galactose metabolic genes in yeast respond to a ratio of galactose and glucose. Proc Natl Acad Sci U S A. 2015;112(5):1636-41.

253. Wang J, Atolia E, Hua B, Savir Y, Escalante-Chong R, Springer M. Natural Variation in Preparation for Nutrient Depletion Reveals a Cost-Benefit Tradeoff. Plos Biol. 2015;13(1).
254. Klingenberg M, Riccio P, Aquila H. Isolation of Adp, Atp Carrier as Carboxyatractylate-Protein Complex from Mitochondria. Biochim Biophys Acta. 1978;503(2):193-210.
255. Echtay KS, Bienengraeber M, Klingenberg M. Role of intrahelical arginine residues in functional properties of uncoupling protein (UCP1). Biochemistry-Us. 2001;40(17):5243-8.
256. Echtay KS, Bienengraeber M, Winkler E, Klingenberg M. In the uncoupling protein (UCP-1) His-214 is involved in the regulation of purine nucleoside triphosphate but not diphosphate binding. J Biol Chem. 1998;273(38):24368-74.
257. Echtay KS, Winkler E, Bienengraeber M, Klingenberg M. Site-directed mutagenesis identifies residues in uncoupling protein (UCP1) involved in three different functions. Biochemistry-Us. 2000;39(12):3311-7.
258. Cytiva. Protein Purification Methods - Chromatography principles 2023 [Available from: https://www.cytivalifesciences.com/en/us/solutions/protein-research/knowledge-center/protein-purification-methods/chromatography-principles.
259. Hedin LE, Illergård K, Elofsson A. An Introduction to Membrane Proteins. J Proteome Res. 2011;10(8):3324-31.
260. Henderson PJF. 8.12 Membrane Proteins for Secondary Active Transport and their Molecular Mechanisms. In: Egelman EH, editor. Comprehensive Biophysics. Amsterdam: Elsevier; 2012. p. 265-88.
261. Alberts B, Johnson A, Lewis J, Morgan D, Raff MC, Roberts K, et al. Molecular biology of the cell. Sixth edition ed. New York, NY: Garland Science, Taylor and Francis Group New York, NY; 2015. p. 565-96.
262. Luckey M. Membrane Structural Biology: With Biochemical and Biophysical Foundations: Cambridge University Press; 2014.
263. Rothnie AJ. Detergent-Free Membrane Protein Purification. In: Mus-Veteau I, editor. Heterologous Expression of Membrane Proteins: Methods and Protocols. New York, NY: Springer New York; 2016. p. 261-7.
264. Gulati S, Jamshad M, Knowles TJ, Morrison KA, Downing R, Cant N, et al. Detergent-free purification of ABC (ATP-binding-cassette) transporters. Biochem J. 2014;461:269-78.
265. Kopf AH, Dörr JM, Koorengevel MC, Antoniciello F, Jahn H, Killian JA. Factors influencing the solubilization of membrane proteins from membranes by styrene-maleic acid copolymers. Bba-Biomembranes. 2020;1862(2).
266. Pollock NL, Lloyd J, Montinaro C, Rai M, Dafforn TR. Conformational trapping of an ABC transporter in polymer lipid nanoparticles. Biochem J. 2022;479(2):145-59.
267. Swainsbury DJK, Scheidelaar S, van Grondelle R, Killian JA, Jones MR. Bacterial Reaction Centers Purified with Styrene Maleic Acid Copolymer Retain Native Membrane Functional Properties and Display Enhanced Stability. Angew Chem Int Edit. 2014;53(44):11803-7.
268. Ritchie TK, Grinkova YV, Bayburt TH, Denisov IG, Zolnerciks JK, Atkins WM, et al. Reconstitution of Membrane Proteins in Phospholipid Bilayer Nanodiscs. Methods in Enzymology; Liposomes, Pt F. 2009;464:211-31.
269. Denisov IG, Sligar SG. Cytochromes P450 in Nanodiscs. Bba-Proteins Proteom. 2011;1814(1):223-9.
270. Denisov IG, Sligar SG. Nanodiscs for structural and functional studies of membrane proteins. Nat Struct Mol Biol. 2016;23(6):481-6.
271. Lin S-H, Guidotti G. Chapter 35 Purification of Membrane Proteins. In: Burgess RR, Deutscher MP, editors. Method Enzymol. 463: Academic Press; 2009. p. 619-29.
272. Peng SS, Deng MD, Grund AD, Rosson RA. Purification and characterization of a membrane-bound linoleic acid isomerase from Clostridium sporogenes. Enzyme Microb Technol. 2007;40(4):831-9.

273. Fujii R, Kita M, Iinuma Y, Oka N, Takaesu Y, Taira T, et al. Isolation and purification of the major photosynthetic antenna, fucoxanthin-Chl a/c protein, from cultured discoid germilings of the brown Alga, Cladosiphon okamuranus TOKIDA (Okinawa Mozuku). Photosynth Res. 2012;111(1-2):157-63.
274. Pedro AQ, Pereira P, Bonifácio MJ, Queiroz JA, Passarinha LA. Purification of Membrane-Bound Catechol-O-Methyltransferase by Arginine-Affinity Chromatography. Chromatographia. 2015;78(21-22):1339-48.
275. Taylor RM, Burritt JB, Foubert TR, Snodgrass MA, Stone KC, Baniulis D, et al. Single-step immunoaffinity purification and characterization of dodecylmaltoside-solubilized human neutrophil flavocytochrome b. Bba-Biomembranes. 2003;1612(1):65-75.
276. Tiselius A, Hjerten S, Levin O. Protein Chromatography on Calcium Phosphate Columns. Arch Biochem Biophys. 1956;65(1):132-55.
277. Purdy KJ, Embley TM, Takii S, Nedwell DB. Rapid extraction of DNA and rRNA from sediments by a novel hydroxyapatite spin-column method. Appl Environ Microb. 1996;62(10):3905-7.
278. Gorbunoff MJ. Protein Chromatography on Hydroxyapatite Columns. Method Enzymol. 1990;182:329-39.
279. Fiermonte G, Dolce V, Palmieri F. Expression in Escherichia coli, functional characterization, and tissue distribution of isoforms A and B of the phosphate carrier from bovine mitochondria. J Biol Chem. 1998;273(35):22782-7.
280. De Leonardis F, Ahmed A, Vozza A, Capobianco L, Riley CL, Barile SN, et al. Human mitochondrial uncoupling protein 3 functions as a metabolite transporter. Febs Lett. 2024;598(3):338-46.
281. Yamamoto S, Nakanishi K, Matsuno R. Ion-Exchange Chromatography of Proteins: Taylor & Francis; 1988.
282. Kunji ERS. 8.9 Structural and Mechanistic Aspects of Mitochondrial Transport Proteins. In: Egelman EH, editor. Comprehensive Biophysics. Amsterdam: Elsevier; 2012. p. 174-205.
283. Støve SI, Flydal MI, Hausvik E, Underhaug J, Martinez A. Chapter 15 - Differential scanning fluorimetry in the screening and validation of pharmacological chaperones for soluble and membrane proteins. In: Pey AL, editor. Protein Homeostasis Diseases: Academic Press; 2020. p. 329-41.
284. Cavalieri R, Hazebroek MK, Cotrim CA, Lee Y, Kunji ERS, Jastroch M, et al. Activating ligands of Uncoupling protein 1 identified by rapid membrane protein thermostability shift analysis. Mol Metab. 2022;62.
285. Ayers FC, Warner GL, Smith KL, Lawrence DA. Fluorometric Quantitation of Cellular and Nonprotein Thiols. Anal Biochem. 1986;154(1):186-93.
286. Fiore C, Trezeguet V, Le Saux A, Roux P, Schwimmer C, Dianoux AC, et al. The mitochondrial ADP/ATP carrier: Structural, physiological and pathological aspects. Biochimie. 1998;80(2):137-50.
287. Skulj S, Brkljaca Z, Kreiter J, Pohl EE, Vazdar M. Molecular Dynamics Simulations of Mitochondrial Uncoupling Protein 2. Int J Mol Sci. 2021;22(3).
288. Cytiva. Thiopropyl Sepharose 6B 2023 [Product details of 'Thiopropyl Sepharose 6B' resin]. Available from: https://www.cytivalifesciences.com/en/us/shop/chromatography/resins/affinity-specific-groups/thiopropyl-sepharose-6b-p-00897.
289. Ma J, Xu Y, Wang Y, Li J, Liu L, Si W, et al. Piperazine-Coumarin based fluorescence probe with enhanced brightness and solubility for bio-thiol detection and esophageal carcinoma diagnosis. Bioorg Chem. 2021;116:105391.
290. Bamber L, Harding M, Butler PJ, Kunji ER. Yeast mitochondrial ADP/ATP carriers are monomeric in detergents. Proc Natl Acad Sci U S A. 2006;103(44):16224-9.

291. Carlson M, Osmond BC, Neigeborn L, Botstein D. A Suppressor of Snf1 Mutations Causes Constitutive High-Level Invertase Synthesis in Yeast. Genetics. 1984;107(1):19-32.
292. Stuart JA, Cadenas S, Jekabsons MB, Roussel D, Brand MD. Mitochondrial proton leak and the uncoupling protein 1 homologues. Bba-Bioenergetics. 2001;1504(1):144-58.
293. Nicholls DG. Mitochondrial proton leaks and uncoupling proteins. Bba-Bioenergetics. 2021;1862(7):148428.
294. Modriansky M, Garlid KD. Arginines, but not lysines, found in the membrane spanning regions of uncoupling protein are essential for nucleotide inhibition. Biophys J. 1996;70(2):Wp191-Wp.
295. Shabalina IG, Petrovic N, de Jong JMA, Kalinovich AV, Cannon B, Nedergaard J. UCP1 in brite/beige adipose tissue mitochondria is functionally thermogenic. Cell Rep. 2013;5(5):1196-203.
296. Brand MD, Esteves TC. Physiological functions of the mitochondrial uncoupling proteins UCP2 and UCP3. Cell Metab. 2005;2(2):85-93.
297. Esteves TC, Parker N, Brand MD. Synergy of fatty acid and reactive alkenal activation of proton conductance through uncoupling protein 1 in mitochondria. Biochem J. 2006;395(3):619-28.
298. Segalés J, Sánchez-Martín C, Pujol-Morcillo A, Martín-Ruiz M, de Los Santos P, Lobato-Alonso D, et al. Role of UCP2 in the Energy Metabolism of the Cancer Cell Line A549. Int J Mol Sci. 2023;24(9).
299. Bouillaud F, Alves-Guerra MC, Ricquier D. UCPs, at the interface between bioenergetics and metabolism. Biochim Biophys Acta. 2016;1863(10):2443-56.
300. Chomiki N, Voss JC, Warden CH. Structure-function relationships in UCP1, UCP2 and chimeras: EPR analysis and retinoic acid activation of UCP2. Eur J Biochem. 2001;268(4):903-13.
301. Friederich-Persson M, Aslam S, Nordquist L, Welch WJ, Wilcox CS, Palm F. Acute knockdown of uncoupling protein-2 increases uncoupling via the adenine nucleotide transporter and decreases oxidative stress in diabetic kidneys. Plos One. 2012;7(7).
302. Suski JM, Schönfeld P, Bonora M, Shabalina I, Pinton P, Wieckowski MR. Guanosine diphosphate exerts a lower effect on superoxide release from mitochondrial matrix in the brains of uncoupling protein-2 knockout mice: New evidence for a putative novel function of uncoupling proteins as superoxide anion transporters. Biochem Biophys Res Commun. 2012;428(2):234-8.
303. Luttik MAH, Overkamp KM, Kötter P, de Vries S, van Dijken JP, Pronk JT. The Saccharomyces cerevisiae NDE1 and NDE2 genes encode separate mitochondrial NADH dehydrogenases catalyzing the oxidation of cytosolic NADH. J Biol Chem. 1998;273(38):24529-34.
304. Baron SJ, King MS, Kunji ERS, Schirris TJJ. Characterization of drug-induced human mitochondrial ADP/ATP carrier inhibition. Theranostics. 2021;11(11):5077-91.
305. Shabalina IG, Ost M, Petrovic N, Vrbacky M, Nedergaard J, Cannon B. Uncoupling protein-1 is not leaky. Biochim Biophys Acta. 2010;1797(6-7):773-84.
306. Klingenberg M. Nucleotide binding to uncoupling protein. Mechanism of control by protonation. Biochemistry-Us. 1988;27(2):781-91.
307. Huang SG, Klingenberg M. Two-stage nucleotide binding mechanism and its implications to H+ transport inhibition of the uncoupling protein from brown adipose tissue mitochondrial. Biochemistry-Us. 1996;35(24):7846-54.
308. Winkler E, Wachter E, Klingenberg M. Identification of the pH sensor for nucleotide binding in the uncoupling protein from brown adipose tissue. Biochemistry-Us. 1997;36(1):148-55.
309. Nair DP, Podgórski M, Chatani S, Gong T, Xi W, Fenoli CR, et al. The Thiol-Michael Addition Click Reaction: A Powerful and Widely Used Tool in Materials Chemistry. Chem Mater. 2014;26(1):724-44.

310. Ravasco JMJM, Faustino H, Trindade A, Gois PMP. Bioconjugation with Maleimides: A Useful Tool for Chemical Biology. Chem-Eur J. 2019;25(1):43-59.
311. Hermanson GT. Chapter 3 - The Reactions of Bioconjugation. In: Hermanson GT, editor. Bioconjugate Techniques (Third Edition). Boston: Academic Press; 2013. p. 229-58.
312. ABP Biosciences L. ECL Western blot Reagent 2023 [Available from: https://www.abpbio.com/product/ecl-western-blot/.
313. Bio-Rad. Image Acquisition for Western Blotting 2023 [Available from: https://www.bio-rad.com/en-uk/applications-technologies/image-acquisition-for-western-blotting?ID=PQEEQORA83CC.
314. Gagelin A, Largeau C, Masscheleyn S, Piel MS, Calderón-Mora D, Bouillaud F, et al. Molecular determinants of inhibition of UCP1-mediated respiratory uncoupling. Nat Commun. 2023;14(1).
315. Voet D, Voet JG. Biochemistry. 4th ed. Hoboken, NJ: John Wiley and Sons Hoboken, NJ; 2011.
316. Kasko AM. Degradable Poly(ethylene glycol) Hydrogels for 2D and 3D Cell Culture Sigma Aldrich2023 [Available from: https://www.sigmaaldrich.com/GB/en/technical-documents/technical-article/materials-science-and-engineering/tissue-engineering/degradable-polyethylene-glycol-hydrogels.
317. Cho YS. Genipin, an Inhibitor of UCP2 as a Promising New Anticancer Agent: A Review of the Literature. Int J Mol Sci. 2022;23(10).
318. Rial E, Rodríguez-Sánchez L, Aller P, Guisado A, González-Barroso MM, Gallardo-Vara E, et al. Development of chromanes as novel inhibitors of the uncoupling proteins. Chemistry & Biology. 2011;18(2):264-74.
319. Milić D, Veprintsev DB. Large-scale production and protein engineering of G protein-coupled receptors for structural studies. Front Pharmacol. 2015;6:66.
320. Thomas JA, Tate CG. Quality Control in Eukaryotic Membrane Protein Overproduction. J Mol Biol. 2014;426(24):4139-54.
321. Sali A, Blundell TL. Comparative Protein Modeling by Satisfaction of Spatial Restraints. J Mol Biol. 1993;234(3):779-815.
322. Fiser A, Do RKG, Sali A. Modeling of loops in protein structures. Protein Sci. 2000;9(9):1753-73.
323. Ko J, Park HY, Heo L, Seok C. GalaxyWEB server for protein structure prediction and refinement. Nucleic Acids Res. 2012;40(W1):W294-W7.
324. Finley D, Ulrich HD, Sommer T, Kaiser P. The ubiquitin-proteasome system of Saccharomyces cerevisiae. Genetics. 2012;192(2):319-60.
325. Horak J, Wolf DH. Catabolite inactivation of the galactose transporter in the yeast Saccharomyces cerevisiae: ubiquitination, endocytosis, and degradation in the vacuole. J Bacteriol. 1997;179(5):1541-9.
326. Pereira C, Chaves S, Alves S, Salin B, Camougrand N, Manon S, et al. Mitochondrial degradation in acetic acid-induced yeast apoptosis: the role of Pep4 and the ADP/ATP carrier. Mol Microbiol. 2010;76(6):1398-410.
327. Hofmann L, Saunier R, Cossard R, Esposito M, Rinaldi T, Delahodde A. A nonproteolytic proteasome activity controls organelle fission in yeast. J Cell Sci. 2009;122(Pt 20):3673-83.
328. Schlame M, Ren M, Xu Y, Greenberg ML, Haller I. Molecular symmetry in mitochondrial cardiolipins. Chem Phys Lipids. 2005;138(1):38-49.
329. Eckerskorn C, Klingenberg M. In the uncoupling protein from brown adipose tissue the C-terminus protrudes to the c-side of the membrane as shown by tryptic cleavage. Febs Lett. 1987;226(1):166-70.
330. Chen K, Sun G, Lv Z, Wang C, Jiang X, Li D, et al. Molecular cloning of amphioxus uncoupling protein and assessment of its uncoupling activity using a yeast heterologous expression system. Biochem Biophys Res Commun. 2010;400(4):701-6.

331. Hoare BL, Tippett DN, Kaur A, Cullum SA, Miljuš T, Koers EJ, et al. ThermoBRET: A Ligand-Engagement Nanoscale Thermostability Assay Applied to GPCRs. ChemBioChem. 2024;25(2):e202300459.
332. Gaspar N, Walker JR, Zambito G, Marella-Panth K, Lowik C, Kirkland TA, et al. Evaluation of NanoLuc substrates for bioluminescence imaging of transferred cells in mice. J Photochem Photobiol B. 2021;216:112128.
333. Hoare BL, Tippett DN, Kaur A, Cullum SA, Miljuš T, Koers EJ, et al. ThermoBRET: a ligand-engagement nanoscale thermostability assay applied to GPCRs. bioRxiv. 2023:2020.08.05.237982.
334. Alexander CG, Wanner R, Johnson CM, Breitsprecher D, Winter G, Duhr S, et al. Novel microscale approaches for easy, rapid determination of protein stability in academic and commercial settings. Bba-Proteins Proteom. 2014;1844(12):2241-50.
335. Gottschalk B, Koshenov Z, Waldeck-Weiermair M, Radulovic S, Oflaz FE, Hirtl M, et al. MICU1 controls spatial membrane potential gradients and guides Ca(2+) fluxes within mitochondrial substructures. Commun Biol. 2022;5(1):649.
336. Sun RC, Denko NC. Hypoxic regulation of glutamine metabolism through HIF1 and SIAH2 supports lipid synthesis that is necessary for tumor growth. Cell Metab. 2014;19(2):285-92.
337. Rial E, Gonzalez-Barroso MM. Physiological regulation of the transport activity in the uncoupling proteins UCP1 and UCP2. Biochim Biophys Acta. 2001;1504(1):70-81.
338. Giralt M, Villarroya F. Mitochondrial Uncoupling and the Regulation of Glucose Homeostasis. Curr Diabetes Rev. 2017;13(4):386-94.
339. Hourton-Cabassa C, Rita Matos A, Zachowski A, Moreau F. The plant uncoupling protein homologues: a new family of energy-dissipating proteins in plant mitochondria. Plant Physiology and Biochemistry. 2004;42(4):283-90.
340. Vercesi AE, Martins lS, Silva MAP, Leite HMF, Cuccovia IM, Chaimovich H. PUMPing plants. Nature. 1995;375(6526):24-.
341. Maia IG, Benedetti CE, Leite A, Turcinelli SR, Vercesi AE, Arruda P. AtPUMP: an Arabidopsis gene encoding a plant uncoupling mitochondrial protein. Febs Lett. 1998;429(3):403-6.
342. Watanabe A, Nakazono M, Tsutsumi N, Hirai A. AtUCP2: a Novel Isoform of the Mitochondrial Uncoupling Protein of Arabidopsis thaliana. Plant and Cell Physiology. 1999;40(11):1160-6.
343. Jarmuszkiewicz W, Behrendt M, Navet R, Sluse FE. Uncoupling protein and alternative oxidase of Dictyostelium discoideum: occurrence, properties and protein expression during vegetative life and starvation-induced early development. Febs Lett. 2002;532(3):459-64.
344. Jarmuszkiewicz W, Sluse-Goffart CM, Hryniewiecka L, Sluse FE. Identification and characterization of a protozoan uncoupling protein in Acanthamoeba castellanii. J Biol Chem. 1999;274(33):23198-202.
345. Jarmuszkiewicz W, Milani G, Fortes F, Schreiber AZ, Sluse FE, Vercesi AE. First evidence and characterization of an uncoupling protein in fungi kingdom: CpUCP of Candida parapsilosis. Febs Lett. 2000;467(2):145-9.
346. Uyemura SA, Luo S, Moreno SN, Docampo R. Oxidative phosphorylation, Ca(2+) transport, and fatty acid-induced uncoupling in malaria parasites mitochondria. J Biol Chem. 2000;275(13):9709-15.
347. Uyemura SA, Luo S, Vieira M, Moreno SN, Docampo R. Oxidative phosphorylation and rotenone-insensitive malate- and NADH-quinone oxidoreductases in Plasmodium yoelii yoelii mitochondria in situ. J Biol Chem. 2004;279(1):385-93.
348. Bermejo-Nogales A, Calduch-Giner JA, Pérez-Sánchez J. Tissue-specific gene expression and functional regulation of uncoupling protein 2 (UCP2) by hypoxia and nutrient availability in gilthead sea bream (Sparus aurata): implications on the physiological significance of UCP1–3 variants. Fish Physiol Biochem. 2014;40(3):751-62.

349. Jastroch M, Buckingham JA, Helwig M, Klingenspor M, Brand MD. Functional characterisation of UCP1 in the common carp: uncoupling activity in liver mitochondria and cold-induced expression in the brain. J Comp Physiol B. 2007;177(7):743-52.
350. Jastroch M, Wuertz S, Kloas W, Klingenspor M. Uncoupling protein 1 in fish uncovers an ancient evolutionary history of mammalian nonshivering thermogenesis. Physiol Genomics. 2005;22(2):150-6.
351. Stuart JA, Harper JA, Brindle KM, Brand MD. Uncoupling protein 2 from carp and zebrafish, ectothermic vertebrates. Biochim Biophys Acta. 1999;1413(1):50-4.
352. Tine M, Kuhl H, Jastroch M, Reinhardt R. Genomic characterization of the European sea bass Dicentrarchus labrax reveals the presence of a novel uncoupling protein (UCP) gene family member in the teleost fish lineage. BMC Evol Biol. 2012;12:62.
353. Wen ZY, Liang XF, He S, Li L, Shen D, Tao YX. Molecular cloning and tissue expression of uncoupling protein 1, 2 and 3 genes in Chinese perch (Siniperca chuatsi). Comparative Biochemistry and Physiology B. 2015;185:24-33.
354. Raimbault S, Dridi S, Denjean F, Lachuer J, Couplan E, Bouillaud F, et al. An uncoupling protein homologue putatively involved in facultative muscle thermogenesis in birds. Biochem J. 2001;353(Pt 3):441-4.
355. Talbot DA, Duchamp C, Rey B, Hanuise N, Rouanet JL, Sibille B, et al. Uncoupling protein and ATP/ADP carrier increase mitochondrial proton conductance after cold adaptation of king penguins. J Physiol. 2004;558(Pt 1):123-35.
356. Vianna CR, Hagen T, Zhang CY, Bachman E, Boss O, Gereben B, et al. Cloning and functional characterization of an uncoupling protein homolog in hummingbirds. Physiological Genomics. 2001;5(3):137-45.
357. Bouillaud F, Raimbault S, Ricquier D. The gene for rat uncoupling protein: Complete sequence, structure of primary transcript and evolutionary relationship between exons. Biochem Biophys Res Commun. 1988;157(2):783-92.
358. Bouillaud F, Ricquier D, Thibault J, Weissenbach J. Molecular approach to thermogenesis in brown adipose tissue: cDNA cloning of the mitochondrial uncoupling protein. Proc Natl Acad Sci U S A. 1985;82(2):445-8.
359. Ricquier D, Lin C, Klingenberg M. Isolation of the Gdp Binding-Protein from Brown Adipose-Tissue Mitochondria of Several Animals and Amino-Acid-Composition Study in Rat. Biochem Biophys Res Commun. 1982;106(2):582-9.
360. Boyer BB, Barnes BM, Lowell BB, Grujic D. Differential regulation of uncoupling protein gene homologues in multiple tissues of hibernating ground squirrels. Am J Physiol. 1998;275(4):R1232-8.
361. Jastroch M, Withers KW, Taudien S, Frappell PB, Helwig M, Fromme T, et al. Marsupial uncoupling protein 1 sheds light on the evolution of mammalian nonshivering thermogenesis. Physiological Genomics. 2008;32(2):161-9.
362. Oelkrug R, Goetze N, Exner C, Lee Y, Ganjam GK, Kutschke M, et al. Brown fat in a protoendothermic mammal fuels eutherian evolution. Nat Commun. 2013;4:2140.
363. Polymeropoulos ET, Jastroch M, Frappell PB. Absence of adaptive nonshivering thermogenesis in a marsupial, the fat-tailed dunnart (Sminthopsis crassicaudata). J Comp Physiol B. 2012;182(3):393-401.
364. Sundin U, Moore G, Nedergaard J, Cannon B. Thermogenin amount and activity in hamster brown fat mitochondria: effect of cold acclimation. Am J Physiol. 1987;252(5):R822-R32.
365. Génin F, Nibbelink M, Galand M, Perret M, Ambid L. Brown fat and nonshivering thermogenesis in the gray mouse lemur (Microcebus murinus). Am J Physiol Regul Integr Comp Physiol. 2003;284(3):R811-8.
366. Bouillaud F, Villarroya F, Hentz E, Raimbault S, Cassard AM, Ricquier D. Detection of brown adipose tissue uncoupling protein mRNA in adult patients by a human genomic probe. Clin Sci. 1988;75(1):21-7.

367. Jastroch M, Withers KW, Taudien S, Frappell PB, Helwig M, Fromme T, et al. Marsupial uncoupling protein 1 sheds light on the evolution of mammalian nonshivering thermogenesis. Physiol Genomics. 2008;32(2):161-9.
368. Rial E, Nicholls DG. The regulation of the proton conductance of brown fat mitochondria. Identification of functional and non-functional nucleotide-binding sites. Febs Lett. 1983;161(2):284-8.
369. Luevano-Martinez LA, Moyano E, de Lacoba MG, Rial E, Uribe-Carvajal S. Identification of the mitochondrial carrier that provides Yarrowia lipolytica with a fatty acid-induced and nucleotide-sensitive uncoupling protein-like activity. Biochim Biophys Acta. 2010;1797(1):81-8.
370. Antos-Krzeminska N, Kicinska A, Nowak W, Jarmuszkiewicz W. Acanthamoeba castellanii Uncoupling Protein: A Complete Sequence, Activity, and Role in Response to Oxidative Stress. Int J Mol Sci. 2023;24(15):12501.
371. Keipert S, Gaudry MJ, Kutschke M, Keuper M, Dela Rosa MAS, Cheng Y, et al. Two-stage evolution of mammalian adipose tissue thermogenesis. Science. 2024;384(6700):1111-7.
372. Jastroch M, Polymeropoulos ET, Gaudry MJ. Pros and cons for the evidence of adaptive non-shivering thermogenesis in marsupials. J Comp Physiol B. 2021;191(6):1085-95.
373. Gaudry MJ, Jastroch M. Molecular evolution of uncoupling proteins and implications for brain function. Neurosci Lett. 2019;696:140-5.
374. Ledesma A, de Lacoba MG, Rial E. The mitochondrial uncoupling proteins. Genome Biol. 2002;3(12):REVIEWS3015.
375. Ricquier D, Bouillaud F. The uncoupling protein homologues: UCP1, UCP2, UCP3, StUCP and AtUCP. Biochem J. 2000;345 Pt 2(Pt 2):161-79.
376. Antos-Krzeminska N, Kicinska A, Nowak W, Jarmuszkiewicz W. Acanthamoeba castellanii Uncoupling Protein: A Complete Sequence, Activity, and Role in Response to Oxidative Stress. Int J Mol Sci. 2023;24(15).
377. Klingenberg M. Nucleotide-Binding Protein from Brown Fat Mitochondria. H-S Z Physiol Chem. 1982;363(9):915-.